PHARMACOKINETIC EVALUATION AND MODELING OF CLINICALLY SIGNIFICANT DRUG METABOLITES

EDITED BY: Constantin Mircioiu, Momir Mikov, Victor A. Voicu, Adrian Nicolescu and Valentina Anuta

PUBLISHED IN: Frontiers in Pharmacology

frontiers Research Topics

ISSN 1664-8714
ISBN 978-2-88971-043-0
DOI 10.3389/978-2-88971-043-0

About Frontiers

Frontiers is more than just an open-access publisher of scholarly articles: it is a pioneering approach to the world of academia, radically improving the way scholarly research is managed. The grand vision of Frontiers is a world where all people have an equal opportunity to seek, share and generate knowledge. Frontiers provides immediate and permanent online open access to all its publications, but this alone is not enough to realize our grand goals.

Frontiers Journal Series

The Frontiers Journal Series is a multi-tier and interdisciplinary set of open-access, online journals, promising a paradigm shift from the current review, selection and dissemination processes in academic publishing. All Frontiers journals are driven by researchers for researchers; therefore, they constitute a service to the scholarly community. At the same time, the Frontiers Journal Series operates on a revolutionary invention, the tiered publishing system, initially addressing specific communities of scholars, and gradually climbing up to broader public understanding, thus serving the interests of the lay society, too.

Dedication to Quality

Each Frontiers article is a landmark of the highest quality, thanks to genuinely collaborative interactions between authors and review editors, who include some of the world's best academicians. Research must be certified by peers before entering a stream of knowledge that may eventually reach the public - and shape society; therefore, Frontiers only applies the most rigorous and unbiased reviews.
Frontiers revolutionizes research publishing by freely delivering the most outstanding research, evaluated with no bias from both the academic and social point of view. By applying the most advanced information technologies, Frontiers is catapulting scholarly publishing into a new generation.

What are Frontiers Research Topics?

Frontiers Research Topics are very popular trademarks of the Frontiers Journals Series: they are collections of at least ten articles, all centered on a particular subject. With their unique mix of varied contributions from Original Research to Review Articles, Frontiers Research Topics unify the most influential researchers, the latest key findings and historical advances in a hot research area! Find out more on how to host your own Frontiers Research Topic or contribute to one as an author by contacting the Frontiers Editorial Office: frontiersin.org/about/contact

PHARMACOKINETIC EVALUATION AND MODELING OF CLINICALLY SIGNIFICANT DRUG METABOLITES

Topic Editors:
Constantin Mircioiu, Carol Davila University of Medicine and Pharmacy, Romania
Momir Mikov, University of Novi Sad, Serbia
Victor A. Voicu, Carol Davila University of Medicine and Pharmacy, Romania
Adrian Nicolescu, Queen's University, Canada
Valentina Anuta, Carol Davila University of Medicine and Pharmacy, Romania

Citation: Mircioiu, C., Mikov, M., Voicu, V. A., Nicolescu, A., Anuta, V., eds. (2021). Pharmacokinetic Evaluation and Modeling of Clinically Significant Drug Metabolites. Lausanne: Frontiers Media SA. doi: 10.3389/978-2-88971-043-0

Table of Contents

frontiers in Pharmacology

EDITORIAL
published: 20 May 2021
doi: 10.3389/fphar.2021.693922

Editorial: Pharmacokinetic Evaluation and Modeling of Clinically Significant Drug Metabolites

Constantin Mircioiu[1], Valentina Anuta[1], Momir Mikov[2], Adrian Nicolescu[3] and Victor A. Voicu[1]*

[1]Faculty of Pharmacy, "Carol Davila" University of Medicine and Pharmacy, Bucharest, Romania, [2]Faculty of Medicine, University of Novi Sad, Novi Sad, Serbia, [3]Department of Medicine, Queen's University, Kingston, ON, Canada

Keywords: IVIVC, metabolites, biorelevant dissolution testing, first pass metabolism, pharmacokinetics

Editorial on the Research Topic

Pharmacokinetic Evaluation and Modeling of Clinically Significant Drug Metabolites

Pharmacokinetic evaluations and modeling in order to correlate in vitro drug dissolution kinetics with their in vivo release and absorption kinetics, estimated from the deconvolution of their pharmacokinetic data, is known as IVIVC. IVIVC is a main tool in the development of new drug formulations, and is required by regulators in the case of extended-release drugs, following well-established procedures that have subsequently been tried in applications for immediate-release medicinal products (Emami, 2010; Cardot and Davit, 2012). Additionally, successful IVIVCs allow subsequent waivers of in vivo studies for bioequivalence (Karalis et al., 2010).

In most cases, applications of such correlations for immediate release lipophilic drugs encounter difficulties due to slow and incomplete dissolution from dosage forms, extensive metabolism, distribution in deep compartments, and enterohepatic circulation (Chrenova et al., 2010).

Recently, an alternative IVIVC method for such drugs has been proposed: the correlation between the dissolution kinetics of parent drugs *in vitro* and the plasma kinetics of their metabolites (Mircioiu et al., 2019), mainly due to the fact that metabolites have a simpler pharmacokinetic model (Marchidanu et al., 2013). On the other hand, the performance of IVIC is dependent on the results of in vitro dissolution methods. It is necessary to model the release kinetics and establish the most biorelevant method (Cardot and Davit, 2012; Preda et al., 2012; Paolino et al., 2019).

The use of metabolites PK in the evaluation of bioequivalence is also a challenge. There are critical situations that cannot be solved without an evaluation of the metabolites if: 1) the parent drug levels in plasma are too low to allow accurate analytical measurements, 2) the parent drug is unstable in the biological matrix, 3) the parent drug is an inactive prodrug, 4) the formation of the metabolite occurs rapidly, or 5) the metabolite significantly contributes to the overall net activity.

In the frame of this research topic, contributions have been received concerning:—Development of biorelevant in vitro dissolution tests

- Modeling of the PK of metabolites.
- Use of PK of metabolites in the evaluation of bioequivalence—time scaling for IVIVC.
- Drug-drug pharmacokinetic interactions.

Li et al. studied the influence of danhong injection, a mixture of Salvia miltiorrhiza and Carthamus tinctorius, on the PK of acetylsalicylic acid (ASA), using an analysis based on 5,183 clinical cases by determining the PK and disposition profile of salicylic acid (SA), the primary

OPEN ACCESS

Edited and reviewed by:
Jaime Kapitulnik, Hebrew University of Jerusalem, Israel

****Correspondence:***
Valentina Anuta
vali_anuta@yahoo.com

Specialty section:
This article was submitted to Drug Metabolism and Transport, a section of the journal Frontiers in Pharmacology

Received: *12 April 2021*
Accepted: *07 May 2021*
Published: *20 May 2021*

Citation:
Mircioiu C, Anuta V, Mikov M, Nicolescu A and Voicu VA (2021) Editorial: Pharmacokinetic Evaluation and Modeling of Clinically Significant Drug Metabolites. Front. Pharmacol. 12:693922. doi: 10.3389/fphar.2021.693922

metabolite of ASA in rats. The maximum plasma concentration of SA increased significantly, by a factor of 1.37, while renal excretion of SA significantly decreased by 32.54%.

Huang et al. determined the toxicology and PK of simvastatin in cerebrospinal fluid after intradiscal injection in rabbits.

Gao et al. studied the in vitro metabolic stability and in vivo oral bioavailability of a novel compound, YL-IPA08. It was determined how metabolic disposition by microsomal P450 enzymes in the liver and intestine limited its bioavailability and further affected brain penetration to the target. An extensive first-pass effect was found in the gut (35%) and liver (17%). Therapeutic human plasma concentrations were predicted to be 27.2 ng/ml.

Li et al. studied HY-021068, which is under development as an anti-platelet agent. Plasma concentrations of HY-021068 and its effects on the platelet aggregation rate were determined. A one-compartment model with saturable Michaelis-Menten elimination was fitted to the pharmacokinetic data of HY-021068.

You et al. have shown that nicotinamide mononucleotide (NMN), a key precursory metabolite of NAD+, is able to elevate the cellular level of NAD+ and ameliorate various age-related diseases in mice and beagles.

Liu et al. studied the disposition of formononetin via the sulfonation pathway.

The expression-activity correlation was performed to identify the contributions of sulfotransferase to formononetin metabolism. Human embryonic kidney cells catalyzed formononetin formation of a monosulfate metabolite. Sulfate formation of formononetin in the cell lysate followed Michaelis-Menten kinetics.

Rizea-Savu et al. developed an analytical method for the determination of alverine, in combination with the metabolites 4-hydroxy alverine, N-desethyl alverine, and 4-hydroxy alverine glucuronide, in human plasma. The PK were determined in an open label, non-comparative study of Spasmonal® Forte. It was found that the parent compound, alverine, is subject to high PK variability, the metabolic process most susceptible to outlying performance is hydroxylation to the active metabolite 4-hydroxy alverine. Another observation was that alverine accounts for only 3% of alverine-related moieties in circulation, whereas total 4-hydroxy alverine accounts for 94%.

Shleghm et al. developed a method for estimating the in vivo release of amiodarone from the PK of its active metabolite, desethylamiodarone, and correlation with its in vitro release. The correlation of the in vitro dissolution and estimated in vivo dissolution of amiodarone was based on a model proposed by the authors that considers that amiodarone has a slow dissolution, rapid absorption, and rapid metabolism and, before returning to the blood from other compartments, its PK is determined mainly by the kinetics of release in the intestine from the pharmaceutical formulation. Under these conditions, the rate of apparition of desethylamiodarone in the blood was found to be a metric of the release of amiodarone in the intestinal fluid.

Yang et al. developed a novel intravenous formulation for general anesthesia by encapsulating isoflurane molecules into an emulsion. A clinical study demonstraed that the bioequivalence of emulsified and non-emulsified isofluarane; the safety and anesthesia effectiveness were also similar.

Ghiciuc et al. demonstrated that the low solubility and high permeability of amiodarone is the limiting step for its bioavailability, therefore, new formulations are needed that improve the solubility of amiodarone, either to increase its oral bioavailability or to reduce its toxic effects. A study on the acute toxicity of amiodarone using new complexes with cyclodextrin demonstrated that including amiodarone in cyclodextrin does not lead to increased toxicity.

AUTHOR CONTRIBUTIONS

All authors listed have made a substantial, direct, and intellectual contribution to the work and approved it for publication.

REFERENCES

Cardot, J.-M., and Davit, B. M. (2012). In Vitro-In Vivo Correlations: Tricks and Traps. *Aaps J.* 14 (3), 491–499. doi:10.1208/s12248-012-9359-0

Chrenova, J., Durisova, M., Mircioui, C., and Dedik, L. (2010). Effect of Gastric Emptying and Entero-Hepatic Circulation on Bioequivalence Assessment of Ranitidine. *Methods Find Exp. Clin. Pharmacol.* 32 (6), 413–419. doi:10.1358/mf.2010.32.6.1472184

Emami, J. (2010). Comparative In Vitro and In Vivo Evaluation of Three Tablet Formulations of Amiodarone in Healthy Subjects. *Daru* 18 (3), 193–199.

Karalis, V., Magklara, E., Shah, V. P., and MacHeras, P. (2010). From Drug Delivery Systems to Drug Release, Dissolution, IVIVC, BCS, BDDCS, Bioequivalence and Biowaivers. *Pharm. Res.* 27 (9), 2018–2029. doi:10.1007/s11095-010-0220-9

Marchidanu, D., Raducanu, N., Miron, D. S., Radulescu, F. S. R., Anuța, V., Mircioiu, I., et al. (2013). Comparative Pharmacokinetics of Rifampicin and 25-desacetyl Rifampicin in Healthy Volunteers after Single Oral Dose Administration. *Farmacia* 61 (2), 398–410.

Mircioiu, C., Anuta, V., Mircioiu, I., Nicolescu, A., and Fotaki, N. (2019). In Vitro-In Vivo Correlations Based on In Vitro Dissolution of Parent Drug Diltiazem and Pharmacokinetics of its Metabolite. *Pharmaceutics* 11 (7), 344. doi:10.3390/pharmaceutics11070344

Paolino, D., Tudose, A., Celia, C., Di Marzio, L., Cilurzo, F., and Mircioiu, C. (2019). Mathematical Models as Tools to Predict the Release Kinetic of Fluorescein from Lyotropic Colloidal Liquid Crystals. *Materials* 12 (5), 693. doi:10.3390/ma12050693

Preda, I. A., Mircioiu, I., Mircioiu, C., Corlan, G., Pahomi, G., Prasacu, I., et al. (2012). Research Concerning the Development of a Biorelevant Dissolution Test for Formulations Containing Norfloxacin. I. Modelling of In Vitro Release Kinetics. *Farmacia* 60 (5), 675–687.

Conflict of Interest: The authors declare that the research was conducted in the absence of any commercial or financial relationships that could be construed as a potential conflict of interest.

frontiers in Pharmacology

ORIGINAL RESEARCH
published: 02 October 2020
doi: 10.3389/fphar.2020.577012

Characteristic and Mechanism of Drug-Herb Interaction Between Acetylsalicylic Acid and Danhong Injection Mediated by Organic Anion Transporters

Jianping Li[1,2], *Jingbo Lu*[1,2], *Yin Peng*[1,2], *Xuejun Xu*[1,2], *Chenkai Chen*[1,2], *Ming Gao*[3], *Ling Lin*[3], *Jianming Guo*[1,2*] *and Jinao Duan*[1,2*]

[1] Jiangsu Collaborative Innovation Center of Chinese Medicinal Resources Industrialization, Nanjing University of Chinese Medicine, Nanjing, China, [2] Jiangsu Key Laboratory for High Technology Research of TCM Formulae, Nanjing University of Chinese Medicine, Nanjing, China, [3] Pharmaceutical Department, East Region Military Command General Hospital, Nanjing, China

OPEN ACCESS

Edited by:
Constantin Mircioiu,
Carol Davila University of Medicine and Pharmacy, Romania

Reviewed by:
Yurong Lai,
Gilead, United States
Stanislav Yanev,
Bulgarian Academy of Sciences (BAS), Bulgaria

***Correspondence:**
Jianming Guo
njuguo@njucm.edu.cn
Jinao Duan
dja@njucm.edu.cn

Specialty section:
This article was submitted to Drug Metabolism and Transport, a section of the journal Frontiers in Pharmacology

Received: 28 June 2020
Accepted: 10 September 2020
Published: 02 October 2020

Citation:
Li J, Lu J, Peng Y, Xu X, Chen C, Gao M, Lin L, Guo J and Duan J (2020) Characteristic and Mechanism of Drug-Herb Interaction Between Acetylsalicylic Acid and Danhong Injection Mediated by Organic Anion Transporters. Front. Pharmacol. 11:577012. doi: 10.3389/fphar.2020.577012

The mixture of *Salvia miltiorrhiza* and *Carthamus tinctorius* (Danhong injection, DHI) is widely prescribed in China for the treatment of cardiovascular and cerebrovascular diseases. In most cases, DHI is used in combination with acetylsalicylic acid (aspirin, ASA). However, the interaction between DHI and ASA remains largely undefined. The purpose of this study is to explore the interaction profile and mechanism between DHI and ASA. The frequency of drug combination of DHI and ASA was analyzed based on 5,183 clinical cases. The interaction characteristics were evaluated by analyzing the pharmacokinetics and disposition profile of salicylic acid (SA, the primary metabolite of ASA) in rats. The interaction mechanisms were explored through evaluating the hydrolysis of ASA regulated by ASA esterase, the tubular secretion of SA mediated by influx and efflux transporters, and the tubular reabsorption of SA regulated by urinary acidity-alkalinity. The inhibitory potential of DHI on organic anion transporters (OATs) was further verified in aristolochic acid I (AAI) induced nephropathy. Clinical cases analysis showed that DHI and ASA were used in combination with high frequency of 70.73%. In drug combination of DHI and ASA, the maximum plasma concentration of SA was significantly increased by 1.37 times, while the renal excretion of SA was significantly decreased by 32.54%. The mechanism study showed that DHI significantly inhibited the transport function, gene transcription and protein expression of OATs. In OATs mediated AAI nephropathy, DHI significantly reduced the renal accumulation of AAI by 55.27%, and alleviated renal damage such as glomerulus swelling, tubular blockage and lymphocyte filtration. In drug combination of DHI and ASA, DHI increased the plasma concentration of SA not through enhancing the hydrolysis of ASA, and the tubular reabsorption of SA was not significantly affected. Inhibition of tubular secretion of SA mediated by OATs might be the reason that contributes to the decrease of SA renal excretion.

Keywords: organic anion transporter, drug interaction, acetylsalicylic acid (aspirin), Danhong injection, salicylic acid, aristolochic acid

INTRODUCTION

Drug-drug interaction (DDI) refers to the pharmacokinetics and pharmacodynamics characteristics alteration of one drug induced by the presence of other drugs. Unanticipated DDIs are suggested to be the major causes of uncontrollable efficacy and safety issues associated with prescription drugs. For example, probenecid, one of the mostly recognized inhibitors of organic anion transporters (OATs), would delay the OATs mediated tubular secretion of penicillin and thus enhance the antibacterial effect of penicillin (Robbins et al., 2012). Conversely, mibefradil, a calcium channel blocker, has been withdrawn from the market because of its potent inhibitory effect on cytochrome P450 that leads to severe clinical risks of rhabdomyolysis during its concurrent treatment with simvastatin (Schmassmann-Suhijar et al., 1998). Therefore, it is important to understand the profile and mechanism of DDIs in order to ensure the drug safety and efficacy.

Acetylsalicylic acid (aspirin, ASA) is a representative antiplatelet drug and is widely prescribed to prevent first-time cardiovascular disease in high-risk patients at low daily doses. ASA could also be used as a classic analgesic and anti-inflammatory agent at higher daily doses. Danhong injection (DHI) is the aqueous extract of two Chinese medicines, the radix and rhizome of *Salvia miltiorrhiza Bunge* (Labiatae) and the dry flower of *Carthamus tinctorius L.* (Asteraceae). DHI is widely prescribed in China for the treatments of cardiovascular and cerebrovascular disease such as myocardial infarction and cerebral thrombosis. Salvianolic acids such as lithospermic acid (LA), protocatechuic aldehyde (PA), salvianolic acid A (SaA), salvianolic acid B (SaB), rosmarinic acid (RA), tanshinol (DSS), and caffeic acid (CA) are primary components of DHI (Liu et al., 2013; Li et al., 2016a).

DHI and ASA were widely used in combination in clinic for the treatment of cerebral infarction and coronary heart diseases (Du et al., 2011), it is important to determine whether there is an herb-drug interaction between DHI and ASA, and whether this interaction potential would influence the drug efficacy and safety. Our previous studies have revealed the herb-drug interaction between DHI and ASA by metabolomics strategy and multivariate statistical analysis (Li et al., 2016b), and have suggested that DHI could alleviate ASA-induced gastric mucosal damage during drug combination of DHI and ASA (Li et al., 2016a). The present study aimed to evaluate the herb-drug interaction profile between DHI and ASA by pharmacokinetics analysis, and to explore the mechanisms of potential interactions.

MATERIALS AND METHODS

Materials and Animals

ASA (purity ≥ 99%) was purchased from Aladdin Chemistry Co., Ltd. (Shanghai, China). Standards of salicylic acid (SA), SaA, SaB, RA, DSS, PA, CA, and LA (HPLC ≥ 98%) were purchased from Chinese Materials Research Center (Nanjing, China). Aristolochic acid (AAI), estrone sulfate (ES), para-aminohippurate (PAH), and probenecid (purity ≥ 99%) were purchased from Sigma-Aldrich Co. LLC. (St. Louis, USA). Liver microsome of male Sprague-Dawley (SD) rat was purchased from Research Institute for Liver Disease Co., Ltd. (Shanghai, China). Transgenic HEK293 cell lines stably overexpressing human *OAT1* (Cat. No. GM1003) and *OAT3* (Cat. No. GM1004) were supplied by GenoMembrane Lo. Ltd. (Yokahama, Janpan).

DHI was provided by Buchang Pharma Co., Ltd., China (Shandong, China; Lot Number: 15081038). Chromatographic fingerprint of DHI was established by UHPLC-PDA-QTOF/MS analysis (**Figure S1**). Seven peaks were identified as SaA, SaB, RA, DSS, PA, CA, and LA by comparing retention time, UV spectrum and MS fragment with corresponding standards (**Figure S2**). SaA, SaB, RA, DSS, PA, CA, and LA are primary components of DHI, and the concentrations of SaA, SaB, RA, DSS, PA, CA, and LA in DHI were 41.73 ± 1.83, 410.42 ± 4.91, 21.40 ± 0.32, 173.98 ± 5.34, 24.37 ± 0.41, 1.03 ± 0.01, and 1.17 ± 0.02 μg/ml, respectively.

Specific Pathogen Free (SPF) male SD rats weighting 350–400 g and male C57BL/6 mice weighting 25–30 g were purchased from Vital River Laboratory Animal Technology Co. Ltd. (Beijing, China; License Number: SCXK (Jing) 2012-0001). All animals were kept in the Drug Safety Evaluation Center of Nanjing University of Chinese Medicine (Nanjing, China). Experiments conducted on animals were approved by the Animal Ethics Committee of Nanjing University of Chinese Medicine, and performed in compliance with the Guide for the Care and Use of Laboratory Animals.

Analysis of Clinical Cases

Clinical cases of DHI in Nanjing General Hospital of People's Liberation Army from July 2012 to July 2017 were collected, and the cases with missing information such as medication time, administration dosage and combination drugs were excluded. The drugs that used in combination with DHI were placed in order according to their number of cases. The time interval between DHI and the drug that most commonly used in combination with DHI (i.e. ASA) was further analyzed. The results obtained from clinical case analysis were prepared for the further experiment design of herb-drug interaction between DHI and ASA that conducted on rats.

Experimental Design of Drug-Herb Interaction Between DHI and ASA

Twelve male SD rats weighting 350–400 g were randomly divided into two groups, rats in Group ASA were administrated with ASA solution (10.41 mg/kg) intragastrically; rats in Group DHI-ASA were injected with DHI (4.16 ml/kg) through caudal vein immediately after the administration of ASA solution (10.41 mg/kg). All rats were administrated daily at scheduled time (9:00–10:00 a.m.) for 14 consecutive days (**Figure 1C**). In this study, a total of two cohorts of animal experiment were performed, one cohort was for the evaluation of pharmacokinetic profile of SA, and the other was for the assays of renal excretion of SA, pH value of urine, gene transcription, and protein expression of OATs.

Blood was sampled from retrobulbar venous plexus of each rat at different time points (1, 5, 15, 30, 45 min, 1, 1.5, 2, 4, 6, 9, 12, and 24 h after the last administration). The blood volume of each collection was 0.3 ml, and the blood was placed in a PE tube containing 33 μl of sodium citrate solution (3.8%, w/v). During the process of blood sampling, physiological saline was injected intraperitoneally every two hours to maintain the circulating blood volume of rats (Diehl et al., 2001). The blood samples were centrifuged at 13,000 rpm/min for 10 min to collect plasma. An aliquot of 100 μl plasma was pipetted into a new PE tube, and mixed with 100 μl of internal standard solution (diphenhydramine, 0.71 μg/ml) and 200 μl of methanol thoroughly. The mixture was centrifuged (13,000 rpm/min, 10 min) to obtain the supernatant for determination of SA concentration by UHPLC-MS/MS analysis.

Determination of Inhibition Potential of DHI on the Activity of ASA Esterase

To determine the effect of DHI on the activity of plasma ASA esterase *in vivo*, twelve male SD rats weighting 350–400 g were randomly divided into two groups, rats in Group CTL were supplied with food and water regularly; rats in Group DHI were injected with DHI (4.16 ml/kg) through caudal vein daily for 14 consecutive days. On the 15th day, blood was sampled from the retrobulbar venous plexus of each rat, and mixed with sodium citrate solution (3.8%, w/v) to obtain plasma. An aliquot of 100 μl plasma were pipetted into a new PE tube, and mixed with 10 μl of ASA hydrochloride solution (100 mM) and 890 μl of Tris buffer (pH 7.4) thoroughly. The mixture was incubated at 37°C in a water bath for 20 min. Then an aliquot of 100 μl reaction solution was mixed with an equal volume of internal standard solution (diphenhydramine, 0.71 μg/ml) thoroughly to stop the reaction and to precipitate the protein. The mixture was centrifuged at 13,000 rpm/min for 10 min to obtain the supernatant for determination of SA concentration by UHPLC-MS/MS. One unit of ASA esterase activity (U) was defined as the production of 1 μmol of SA in a reaction system with the substrate concentration of 1 mM, pH of 7.4 and temperature of 37°C per minute and per milliliter of plasma. Furthermore, to clarify the relationship between the plasma concentration of DHI and the inhibition effect on ASA esterase, rats in Group DHI were injected with DHI (4.16 ml/kg) through caudal vein after the first blood collection, and plasma was sampled at different time points (1, 15, and 60 min after the single injection of DHI) for determination of the activity of ASA esterase.

To determine the effect of DHI on the activity of plasma ASA esterase *in vitro*, a total of 1.8 ml fresh blank plasma of male SD rat was divided into 18 aliquots. The aliquots were randomly divided into three groups as follows (n = 6): Group CTL, no DHI was added to the reaction system; Group DHI-1, 10 μl of DHI was added to the system and the final concentration of DHI was 100-fold dilution of the original DHI; Group DHI-2, 100 μl of DHI was added to the incubation system and the final concentration of DHI was 10-fold dilution of the original DHI. Furthermore, to determine the effect of DHI on the activity of ASA esterase in liver microsome, a total of 450 μl of blank liver microsome of male SD rat was divided into three group as that in the assay of plasma ASA esterase (five aliquots of 30 μl in each group, n = 5). The activity of ASA esterase in plasma and liver microsomes was determined according to the method detailed above *in vivo* study.

Determination of SA Renal Excretion and Urinary pH Value

Rats were housed in metabolism cages immediately after the last administration, and urine samples of each rat were collected on ice at different time periods (0–5, 5–10, and 10–24 h). The urine samples were centrifuged at 3,000 rpm/min for 10 min to precipitate impurities, and the urinary pH value was detected by pH meter. Meanwhile, an aliquot of 400 μl supernatant was mixed with 100 μl of methanol thoroughly to precipitate some protein, and the final supernatant was obtained for the determination of SA concentration by UHPLC-MS/MS analysis.

Determination of the Effect of DHI on Gene Transcription and Protein Expression of OATs

Rats were sacrificed after the last administration, and kidneys of each rat were sampled for qPCR and Western blot analysis to evaluate the gene expression and protein levels of OAT1, OAT2, and OAT3, respectively. The primer sequences of *rOAT1*, *rOAT2*, and *rOAT3* were detailed in **Table 1**.

Human embryonic kidney 293 wild type cell lines (HEK293) were seeded at the density of 5×10^5 cell/well in six-well plates, and cultured for 24 h in a humidified incubator (37°C, 5% CO_2). The spent culture medium was removed, and 2 ml of fresh medium containing DHI (1000, 500, 100, 50, and 20-fold dilution of DHI) or salvianolic acids (SaA, SaB, RA, DSS, PA, CA, and LA; 50 μM) was added to each well (n = 6). Finally, the cells were lysed with RNA lysis buffer after the incubation for 24 h, and the total RNA was collected for qPCR analysis. The primer sequences of *hOAT1*, *hOAT2*, and *hOAT3* were detailed in **Table 1**.

Determination of the Effect of DHI on Transport Function of OATs

Transgenic HEK293 cell lines stably overexpressing OAT1 and OAT3 were cultured in high glucose DMEM containing 10% of fetal bovine serum, 1% of penicillin-streptomycin and 0.5 mg/ml of geneticin. The cells were seeded at the density of 1×10^6 cell/

TABLE 1 | Primer sequences of rat OATs (*rOAT1*, *rOAT2*, and *rOAT3*) and human OATs (*hOAT1*, *hOAT2*, and *hOAT3*).

Primer	Sequence (5'-3')
rOAT1	**(S)** TCAACTGCATGACACTAAATGTG; **(AS)** AGCCTTCCTGAGGAGGAGTA
rOAT2	**(S)** ATCATTGTGCTCCCACTGGAG; **(AS)** CTCCACACGACCCTGGGTTA
rOAT3	**(S)** CAGCATCTCGGGCATTTCTC; **(AS)** TACCCACCAGGACAACAAGG
hOAT1	**(S)** GCCTTCTTCATCTACTCCTGG; **(AS)** CCCGGAGTACCTCCATACT
hOAT2	**(S)** CCTCCAAGCTGCTGGTCTAC; **(AS)** CAGGTAGGCAGTGGTGAAGG
hOAT3	**(S)** GCTGAGCTGCCCTACTACAG; **(AS)** CGAGAAGGTCATGGCACTGG

well in 24-well plates, and transport experiments were performed when the cell density reached 80–90%. Spent culture medium was removed and cells were washed with pre-warmed HEPES buffer (50 mM of HEPES, 250 mM of NaCl, 9.6 mM of KCl, 11.2 mM of D-(+)-glucose, 2.4 mM of $CaCl_2$, 2.4 mM of KH_2PO4, and 2.4 mM of MgSO4; pH 7.4). Then the wash buffer was discarded and 0.25 ml of fresh HEPES buffer containing DHI and substrates was added to each well. There were eight concentrations of DHI prepared through diluting the original DHI by 2×10^4, 1×10^4, 2×10^3, 1×10^3, 500, 100, 20, and 10 times with physiological saline, respectively. The substrates of OAT1 and OAT3 were PAH (20 μM) and ES (20 μM), respectively. The transport system of positive control (PC) consisted of substrates and probenecid (20 μM), probenecid was a recognized inhibitor of both OAT1 and OAT3, while that blank control (CTL) containing only the substrates. Immediately after the incubation of 10 min, the cells were washed with pre-cooled HEPES buffer for three times, and then lysed with 0.15 ml of NaOH solution (1M) per well for 30 min at room temperature (25°C). When the cells were completely lysed, an equal amount of HCl solution (1M) was added to neutralize the lysate. An aliquot of the lysate was sampled to determine the protein concentration by Pierce® BCA protein assay kit (ThermoFisher Scientific, Cat. No. 23225), and the remaining lysate was used to determine the concentration of PAH (Liu et al., 2012) and ES (Corona et al., 2010) by UHPLC-MS/MS. The uptake rates of OAT1 and OAT3 were calculated according to the concentrations of PAH and ES in lysate, respectively, which detailed as follows: Uptake rate (pmol/mg/min) = Substrate concentration/(Protein concentration × Incubation time).

Experimental Design of Drug Interaction Between DHI and AAI

Twenty-four male SD rats weighting 350–400 g were randomly divided into two groups as follows (n = 12): rats in Group AAI were injected with physiological saline (4.16 ml/kg) through caudal vein 30 min before intraperitoneal injection of AAI (10 mg/kg); rats in Group AAI-DHI were injected with DHI (4.16 ml/kg) through caudal vein 30 min before intraperitoneal injection of AAI (10 mg/kg). The rate of caudal vein injection was controlled at about 1 ml/min. After the single administration of AAI and/or DHI, half of the rats in each group were sacrificed and kidneys were sampled for AAI quantification by UHPLC-MS/MS. The other half of the rats were used for blood collection at different time points (15, 30, 45, 60, 90, and 120 min after the injection of AAI), and the plasma samples were prepared for determination of AAI concentration by UHPLC-MS/MS.

Twenty-four male C57BL/6 mice weighting 25–30 g were randomly divided into three groups as follows (n = 8): mice in Group CTL were supplied with food and water regularly; mice in Group AAI were injected with AAI solution (10 mg/kg) intraperitoneally; mice in Group AAI-DHI were injected with DHI (6.01 ml/kg) through caudal vein 30 min before intraperitoneal injection of AAI (10 mg/kg). All mice were administrated daily at scheduled time (9:00–10:00 a.m.) for seven consecutive days. On the 8^{th} day, plasma was sampled from abdominal aorta of each mouse for the detection of creatinine level, and kidneys were collected and fixed in 10% of formalin buffer for hematoxylin-eosin staining (HE).

Statistical Analysis

All data were expressed as means ± S.E.M. Differences among groups were analyzed by one-way ANOVA test. Statistical significant difference was set as $P<0.05$, and very significant difference was set as $P<0.01$.

RESULTS

DHI Was Used in Combination With ASA With High Frequency in Clinic

A total of 5,183 clinical cases of DHI in Nanjing General Hospital of People's Liberation Army from July 2012 to July 2017 were collected, and the analysis results revealed that 473 kinds of drugs might be used in combination with DHI for the treatment of cerebrovascular and cardiovascular diseases such as cerebral infarction and coronary heart disease. Among the 473 kinds of drugs, ASA was the drug that most commonly used in combination with DHI, and the frequency of drug combination was 70.73% (**Figure 1A**), which was in accordance with the conclusion reported in previous studies (Du et al., 2011). Top ten drugs that commonly used in combination with DHI were ASA, clopidogrel, oxiracetam injection, atorvastatin calcium, mecobalamin injection and tablet, rosuvastatin calcium, heparin sodium injection, lidocaine injection, fasudil injection, and phenobarbital injection.

The Pharmacokinetics Profile of SA Was Influenced During Drug Combination of DHI and ASA

In the drug combination of DHI and ASA, the plasma concentration of SA was significantly increased at different time points (**Figure 1D**). The area under concentration-time curve (AUC_{0-t}) and the maximum plasma concentration of SA (C_{max}) was 2.57 and 2.37 times than that in single administration of ASA, respectively (**Figure 1D**; $P<0.01$).

In this herb-drug interaction experiment that performed on rats, DHI and ASA were administrated simultaneously, because as for 44.71% of the patients, the time interval between the use of DHI and ASA was counted to be zero according to the results of clinical case analysis (**Figure 1B**). The administration dose of DHI and ASA were designed based on the clinical conclusion reported previously (Chen et al., 2011), and the daily doses of DHI (4.16 ml/kg) and ASA (10.41 mg/kg) were equivalent to a 60 kg person taking 40 ml of DHI and 100 mg of ASA daily.

DHI Increased the Plasma Concentration of SA Not Through Enhancing ASA Esterase Activity

The activity of plasma ASA esterase was significantly inhibited by 9.01% when rats were treated with DHI for 14 consecutive days (**Figure 2A**; $P < 0.05$), and the inhibition effect of DHI was fading

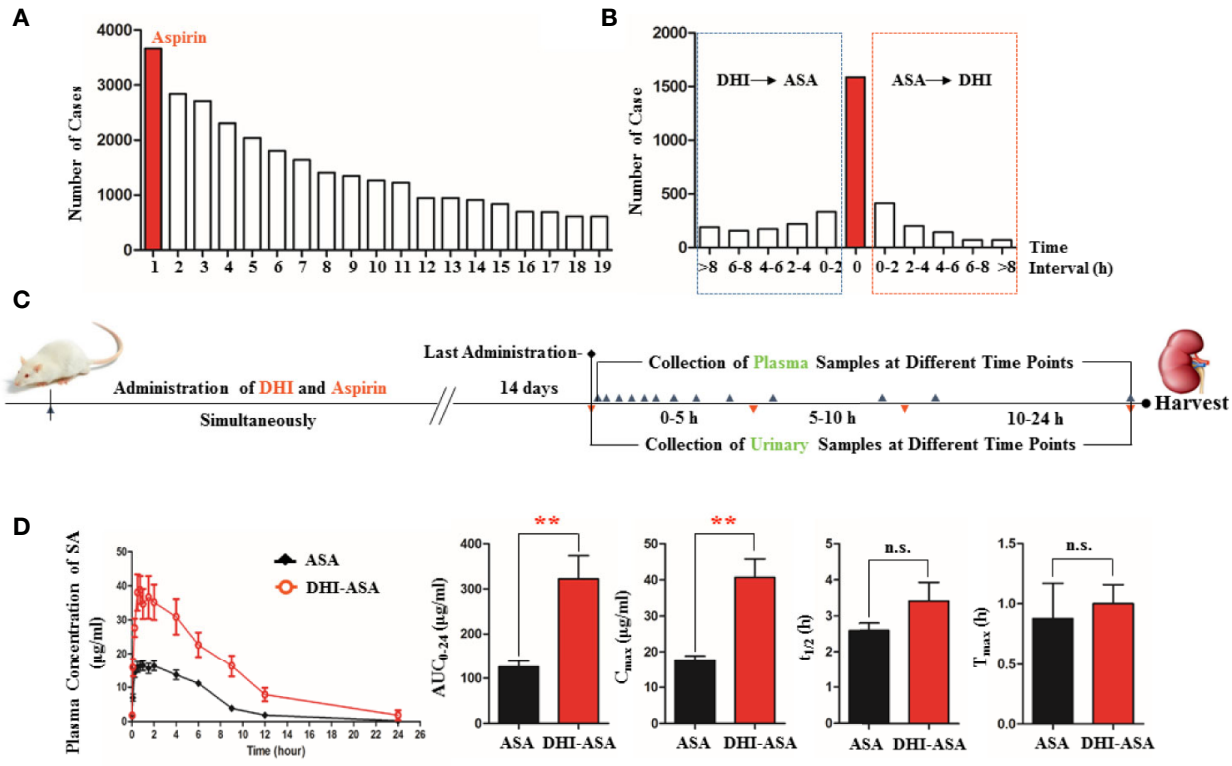

FIGURE 1 | Altered pharmacokinetics profile of SA during drug combination of DHI and ASA. **(A)** Drugs that commonly used in combination with DHI in clinic (1. ASA, 2. Clopidogrel, 3. Oxiracetam injection, 4. Atorvastatin calcium, 5. Mecobalamin injection and tablet, 6. Rosuvastatin calcium, 7. Heparin sodium injection, 8. Lidocaine injection, 9. Fasudil injection, 10. Phenobarbital injection, 11. Amlodipine, 12. Troxerutin injection, 13. Vitamin B1, 14. Edaravone injection, 15. Alprostadil injection, 16. Pantoprazole injection, 17. Potassium chloride sustained-release tablet, 18. Butylphthalide soft capsule, 19. Vitamin B6); **(B)** Time interval of drug combination of DHI and ASA in clinic; **(C)** Experimental design of herb-drug interaction between DHI and ASA conducted on rats; **(D)** Pharmacokinetic profile and parameters of SA. $^{**}P < 0.01$.

when the plasma concentration of DHI was decreasing with time (**Figure 2B**; $P < 0.05$). Furthermore, the inhibitory effect of DHI on ASA esterase was confirmed *in vitro* study, as the activity of ASA esterase in plasma and liver microsome was significantly inhibited by DHI in a concentration dependent manner (**Figures 2C, D**, $P < 0.05$).

Renal Excretion of SA Was Decreased During Drug Combination of DHI and ASA

When ASA was used in combination with DHI, the content of SA excreted in urine in the first five hours was significantly reduced by 44.44% from 2.43 ± 0.49 to 1.35 ± 0.20 mg (**Figure 3A**; $P < 0.05$). As to the accumulative urinary excretion of SA in 0–24 h, the content of SA was significantly decreased by 32.54% from 2.95 ± 0.45 to 1.99 ± 0.45 mg (**Figure 3B**; $P < 0.01$).

The Tubular Reabsorption of SA Was Not Affected During Drug Combination of DHI and ASA

A slight decrease of urinary pH value by 0.08 was observed during drug combination of DHI and ASA as compared with single administration of ASA (**Figure 4A**). The proportion of ionized SA was further calculated based on the equation 4 (**Figure 4C**), which was obtained according to the acid-base proton theory (Equations 1 and 2) and the Henderson-Hasselbalch formula (Equation 3). The results showed that the SA was almost totally ionized in urine regardless of whether ASA was used alone or used in combination with DHI (**Figure 4B**), and thus the portion of SA reabsorbed by renal tubular is tiny.

Gene Transcription and Protein Expression of OATs Were Down-Regulated by DHI

The gene transcription and protein expression of OAT1 in kidney were significantly down-regulated during drug combination of DHI and ASA as compared to single administration of ASA (**Figures 5**, **S4**; $P < 0.05$). The inhibitory effect of DHI on OATs was further confirmed *in vitro* study, as the gene expression of *OAT1*, *OAT2*, and *OAT3* were significantly inhibited by DHI in HEK293 wild type cells (**Figure 6A**; $P < 0.01$).

To identify the components that contribute to the inhibitory potency of DHI, the effects of seven salvianolic acids on OATs gene expression were further analyzed. Salvianolic acids including SaA, SaB, RA, DSS, PA, CA, and LA are main

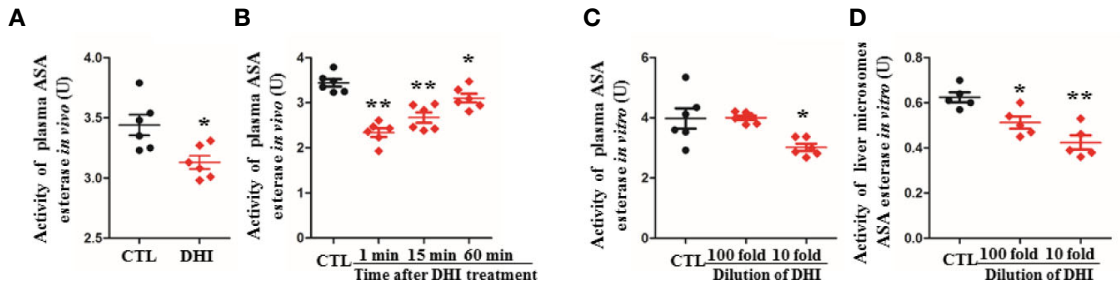

FIGURE 2 | Inhibition potential of DHI on ASA esterase activity. **(A)** Activity of plasma ASA esterase *in vivo* when rats were treated with DHI for 14 consecutive days; **(B)** Activity of plasma ASA esterase *in vivo* at different time points (1, 5, and 60 min after DHI treatment); **(C)** Activity of plasma ASA esterase *in vitro*; **(D)** Activity of liver microsome ASA esterase *in vitro*. $^{*}P < 0.05$, $^{**}P < 0.01$.

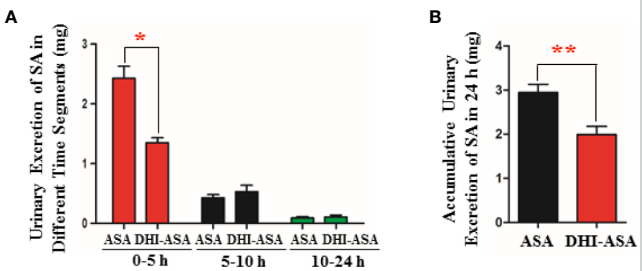

FIGURE 3 | Decreased renal excretion of SA during drug combination of DHI and ASA. **(A)** Content of SA excreted in urine in different time segments; **(B)** Accumulative content of SA excreted in urine in 24 h. $^{*}P < 0.05$, $^{**}P < 0.01$.

bioactive components of DHI (Liu et al., 2013). The results showed that SaA, RA, and SaB significantly down-regulated the gene expression of *OAT1* by 75.21, 75.63, and 65.80%, respectively; SaA, RA, SaB, LA, CA, PA, and DSS significantly down-regulated the gene expression of *OAT2* by 61.79, 81.48, 57.66, 70.00, 73.66, 53.94, and 52.67%, and down-regulated the gene expression of *OAT3* by 98.02, 98.30, 97.27, 88.70, 66.95, 69.58, and 66.90%, respectively (**Figure 6B**; $P < 0.01$).

Transport Function of OATs Was Inhibited by DHI

DHI significantly inhibited the uptake of PAH by OAT1 and ES by OAT3 in transgenic HEK293 cells overexpressing *OAT1* and *OAT3*. The higher concentration of DHI, the stronger inhibitory effect on OAT transport function (**Figure 7**; $P < 0.01$). As to transport function of OAT1, even if the 1,000-fold dilution of DHI decreased the uptake of PAH by 70.35% from 208.00 to 61.67 pmol/mg/min (**Figure 7A**; $P < 0.01$). The inhibitory effect of DHI at high concentration (100, 20, and 10-fold dilution of DHI) was equivalent to that of positive control (probenecid, 20 μM). The inhibitory effect of DHI on transport function of OAT3 (IC50: 0.116% of DHI; 95% CI: 0.0991–0.137%; **Figure 7B**) was suggested to be stronger than that of OAT1 (IC50: 0.759% of DHI; 95% CI: 0.645–0.895%).

DHI Inhibited OATs-Mediated AAI Transportation and Alleviated AAI Nephropathy

When AAI was used in combination with DHI in rats, the AAI content in kidney was significantly decreased from 11.96 to 5.35 ng/mg (**Figure 8A**; $P < 0.05$). Accordingly, DHI significantly increased the plasma concentration of AAI at different time

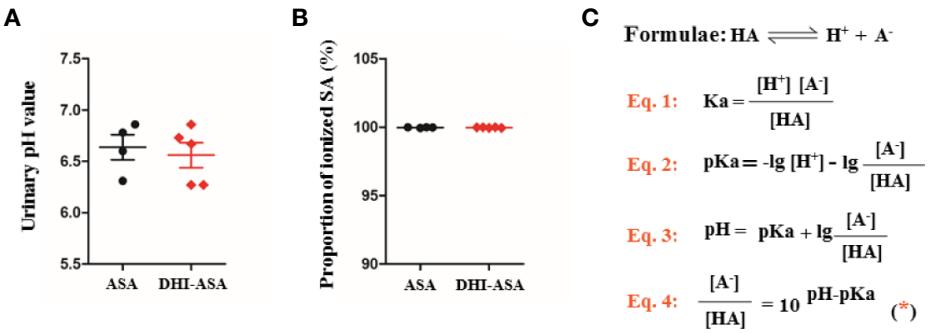

FIGURE 4 | Tubular reabsorption of SA was not affected during drug combination of DHI and ASA; **(A)** pH value of urine; **(B)** Proportion of ionized SA; **(C)** Equations for calculating the proportion of ionized SA.

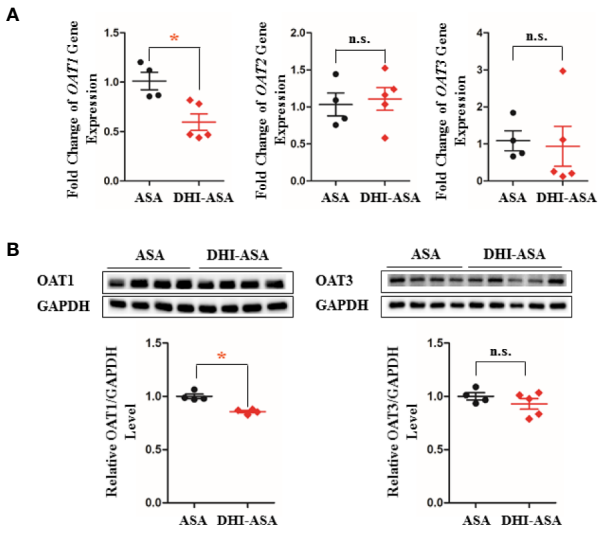

FIGURE 5 | Inhibitory effect of DHI on OATs *in vivo*. **(A)** Gene transcription of OATs; **(B)** Protein expression of OATs during drug combination of DHI and ASA. *$P < 0.05$.

points, and the maximum concentration of AAI was increased from 34.54 to 43.51 μg/ml (**Figure 8B**; $P < 0.05$).

The renal damage induced by AAI in mice was mainly characterized as increased creatinine level (**Figure 8C**; $P < 0.05$), glomerulus swelling, tubular blockage, and lymphocyte infiltration (**Figure 8D**). When AAI was used in combination with DHI, the plasma level of creatinine was significantly decreased from 26.0 to 23.12 μmol/l (**Figure 8C**; $P < 0.05$). Furthermore, the glomerulus swelling and lymphocyte filtration were significantly alleviated, and the total damage score was reduced from 1.8 to 1.4 (**Figures 8D, E**; $P < 0.05$).

DISCUSSION

Glomerular filtration, tubular secretion and reabsorption are primary processes of renal excretion of SA (**Figure 9**). The SA in blood circulation enters the glomerulus through afferent arteriole, and the unbound SA is directly filtered into the Bowman's capsule. The SA bound with albumin would be flowed into peritubular capillaries and transported from plasma into proximal tubular cells by OATs which are located in the basolateral membrane of proximal tubular cells. Then SA in the proximal tubular cells would be excreted into the lumen of tubule by efflux transporters such as multidrug resistance protein 4 (MRP4; Mattiello et al., 2011), multi drug resistance transporter 1 (MDR1; Polachek et al., 2010), and mono carboxylate transporter 1 (MCT1; Tamai et al., 1999), which are located in the apical membrane of proximal tubule cells. The molecular form of SA in the urine would be reabsorbed back into peritubular capillaries, while the SA in ionic form would be excreted with urine (Weiner et al., 1959; Miners, 1989).

In drug combination of DHI and ASA, the renal excretion of SA was significantly decreased, which might be caused by the alteration of SA excretion through glomerular filtration, tubular secretion or tubular reabsorption. Our results suggested that the tubular reabsorption of SA was not affected during drug combination of DHI and ASA. According to the consensus of ion trapping, the tubular reabsorption of SA is primarily regulated by the acidity-alkalinity of urine (Proudfoot et al.,

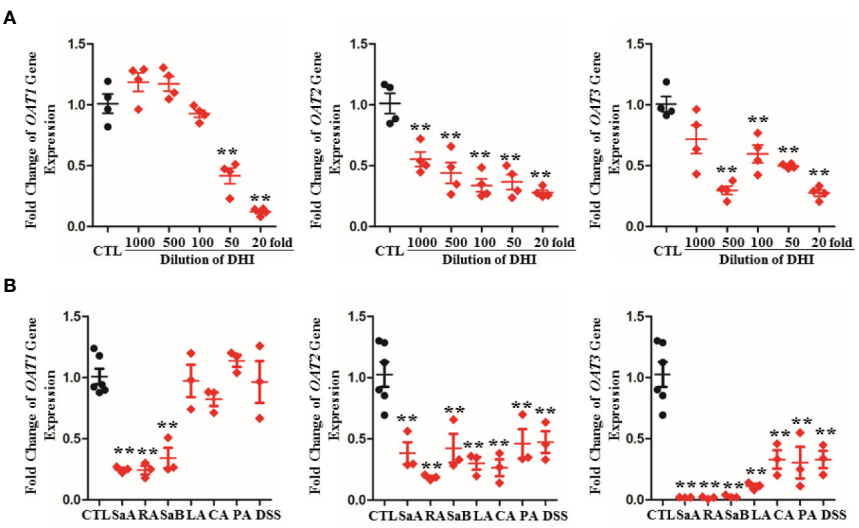

FIGURE 6 | Inhibitory effect of DHI and salvianolic acids on OATs in HEK293 wild type cell lines. **(A)** Down-regulation of gene expression of *OAT1*, *OAT2*, and *OAT3* by DHI; **(B)** Down-regulation of gene expression of *OAT1*, *OAT2*, and *OAT3* by main salvianolic acids in DHI (salvianolic acid A, SaA; rosmarinic acid, RA; salvianolic acid B, SaB; lithospermic acid, LA; caffeic acid, CA; protocatechuic aldehyde, PA; Tanshinol, DSS). **$P < 0.01$.

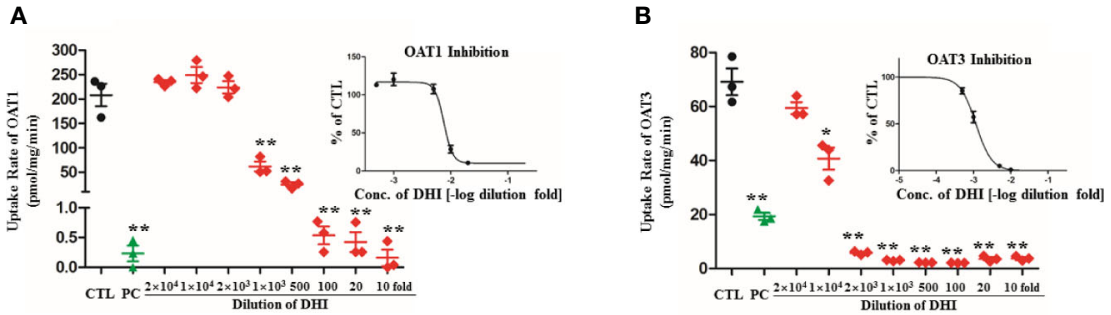

FIGURE 7 | Inhibitory effect of DHI on transport function of OATs in transgenic HEK293 cells overexpressing *OAT1* and *OAT3*. **(A)** Uptake rate of PAH by OAT1; **(B)** Uptake rate of ES by OAT3. $^{**}P < 0.01$.

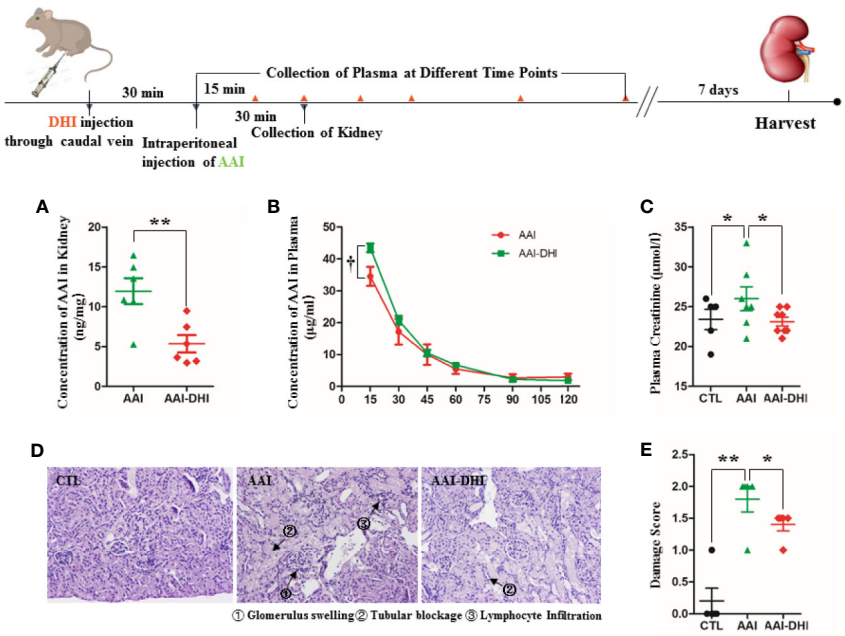

FIGURE 8 | DHI decreased the renal accumulation of aristolochic acid I (AAI) and alleviated the renal damage induced by AAI. **(A)** Concentration of AAI in kidney; **(B)** Concentration of AAI in plasma; **(C)** Plasma concentration of creatinine; **(D)** Histological analysis of renal damage (HE staining, original magnification × 400); **(E)** Renal damage score. $^{*}P < 0.05$, $^{**}P < 0.01$.

2003). Because SA is weakly ionized in physiological fluids, and only the unionized SA with high fat solubility can be absorbed through the tubule epithelium and the capillary endothelium. Our data showed a slight decrease of urinary pH value when DHI was used in combination with ASA. However, SA was almost totally ionized in urine regardless of whether ASA was used alone or used in combination with DHI. Therefore, the portion of SA reabsorbed by renal tubular is tiny.

Salvianolic acids in DHI are considered as strong ligands of albumin, and the binding ability to human serum albumin of salvianolic acids are stronger than sodium salicylate (Zhu et al., 2017). It is possible that the SA bound with albumin in blood circulation might be squeezed down by salvianolic acids, and the proportion of SA directly excreted by glomerular filtration might be consequently increased. Our data showed that the renal excretion of SA was significantly decreased during drug combination of DHI and ASA, which suggested that the alteration of SA excretion by glomerular filtration might not be the main contributor.

OATs are suggested to be central to the renal tubular secretion of SA (**Figure 9**; Bow et al., 2006; Emami Riedmaeir et al., 2012; Nigam et al., 2015). OATs belong to the solute carrier 22 subfamily (SLC22) of major facilitator superfamily (MFS), and are generally considered as influx transporters that facilitate the movement of substrates

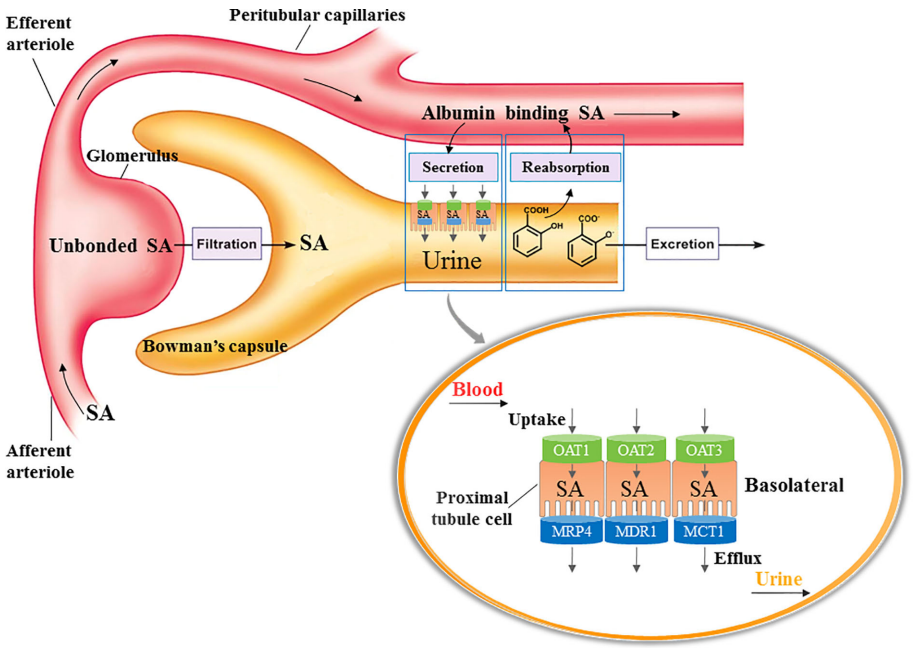

FIGURE 9 | Process of SA excretion in kidney. Glomerular filtration, tubular secretion and reabsorption are primary processes of renal excretion of SA. The SA in blood circulation enters the glomerulus through afferent arteriole, and the unbound SA is directly filtered into the Bowman's capsule. The SA bound with albumin would be flowed into peritubular capillaries and transported from plasma into proximal tubular cells by OATs which are located in the basolateral membrane of proximal tubular cells. Then SA in the proximal tubular cells would be excreted into the lumen of tubule by efflux transporters such as multidrug resistance protein 4 (MRP4), multi drug resistance transporter 1 (MDR1), and mono carboxylate transporter 1 (MCT1), which are located in the apical membrane of proximal tubule cells. The molecular form of SA in the urine would be reabsorbed back into peritubular capillaries, while the SA in ionic form would be excreted with urine.

from blood circulation into the renal tubular epithelial cells (Nigam et al., 2015). OATs are currently recognized as the most important membrane transporters and have been demonstrated to be the important mediator of many DDIs (Emami Riedmaeir et al., 2012). Our results showed that the gene transcription, protein expression, and transport function of OATs were significantly down-regulated by DHI, which might consequently induce the decrease of SA renal excretion during drug combination of DHI and ASA. However, the limitation was that the molecular biotechnology applied in this section such as western blot was not sensitive enough to reveal the small change of OATs, and the methods with better sensitivity and reliability such as targeted quantitative proteomics, as well as application of probe substrates would be applied to confirm the effect of DHI on OATs in our future study. Efflux transporters located in the apical membrane of proximal tubule cells are also critical in renal tubular secretion of SA, because MRP4, MDR, and MCT1 facilitate the transportation of SA from proximal tubule cells to tubule lumen. However, our results showed that no significant changes of gene transcription of *MRP4*, *MDR1*, or *MCT1* were observed in drug combination of DHI and ASA (**Figure S3**; **Table S1**).

OATs play a key role in the pathogenesis of AAI nephropathy, previous studies have confirmed that the transportation of AAI from blood circulation to proximal tubular cells by OAT1 and OAT3 is the initial cause of renal damage induced by AAI (Bakhiya et al., 2009; Xue et al., 2011), and the acute tubular injuries induced by AAI can be alleviated by probenecid, an inhibitor of OATs (Baudoux et al., 2012). In order to confirm the inhibitory effect of DHI on OATs *in vivo*, we further studied whether DHI could inhibit OATs-mediated AAI transportation into kidney and alleviate AAI induced nephropathy. Our results showed that DHI significantly reduced the renal accumulation of AAI, and alleviated renal damage such as glomerulus swelling, tubular blockage and lymphocyte filtration.

ASA esterase (Enzyme Commission number: 3.1.1.55) is the general term of a kind of hydrolase that acts on the ester bond to hydrolyze ASA, which is also known as acetylsalicylic deacetylase (Braunschweig Enzyme Database, BRENDA). The hydrolysis process of ASA to SA is principally determined by ASA esterase activity in addition to the weak role of simple hydrolysis. Therefore, the production of SA released from ASA is primarily determined by ASA esterase activity (White et al., 2005). In drug combination of DHI and ASA, the plasma concentration of SA was significantly increased. It is possible that the increase of SA plasma concentration was caused by the enhanced activity of ASA esterase. However, our results suggested that the activity of ASA esterase was significantly inhibited by DHI, and the alteration of ASA esterase activity might not be the reason that contribute to the increase of SA concentration.

In this study, hydrolysis of ASA regulated by ASA esterase, tubular secretion of SA mediated by influx and efflux transporters, and tubular reabsorption of SA regulated by urinary acidity-alkalinity were included in the mechanism study of herb-drug interaction between DHI and ASA. However, there are still other possible mechanisms that have not been reported. For example, in blood circulation, a portion of SA remains the prototype, and the other portion of SA is metabolized to salicyluric acid, gentisic acid, salicyl acyl glucuronide, salicyl phenolic glucuronide, salicyluric acid phenolic glucuronide and gentisuric acid by cytochrome P450, acyl-CoA N-acyltransferase or uridine 5'-diphosphoglucuronosyltransferases (Li et al., 2017). Each metabolite should undergo a complete and independent process of renal excretion. For example, salicyluric acid is also excreted mainly by glomerular filtration, tubular secretion and absorption (Cox et al., 1989). The results regarding the influence of drug combination on renal excretion of other metabolites such as salicyluric acid, gentisic acid, salicyl phenolic glucuronide and salicyluric acid phenolic glucuronide would be presented in our another manuscript. Furthermore, SA can be metabolized to 2,3-dihydroxybenzoic acid by direct hydroxyl radical attack, and the plasma level of 2,3-dihydroxybenzoate is suggested to be powerful biomarker of oxidative stress in chronic complications (Ghiselli et al., 1992). This is a new insight of herb-drug interaction between DHI and ASA, which would be included in our future study.

CONCLUSION

ASA and DHI were widely used in combination in clinic for the treatment of cardiovascular and cerebrovascular diseases. The drug-herb interaction between ASA and DHI was characterized by increased plasma concentration of SA, and decreased renal excretion of SA. The inhibitory effect of DHI on the gene transcription, protein expression and transport function of OATs might be the reason that contribute to the decrease of SA renal excretion.

DATA AVAILABILITY STATEMENT

The original contributions presented in the study are included in the article/supplementary material; further inquiries can be directed to the corresponding authors.

ETHICS STATEMENT

The experiments on rats were approved by the Animal Ethics Committee of Nanjing University of Chinese medicine, and performed in compliance with the Guide for the Care and Use of Laboratory Animals.

AUTHOR CONTRIBUTIONS

JPL, JG, and JD designed research. JPL, JBL, YP, XX, and CC performed research. MG and LL analyzed clinical cases. JPL wrote the paper. All authors contributed to the article and approved the submitted version.

FUNDING

This work was supported by the National Natural Science Foundation of China (Grant numbers 81803795); Natural Science Foundation of Jiangsu Province of China (Grant number BK20180823); and Natural Science Foundation of the Jiangsu Higher Education Institutions of China (Grant number 18KJB360003).

SUPPLEMENTARY MATERIAL

The Supplementary Material for this article can be found online at: https://www.frontiersin.org/articles/10.3389/fphar.2020.577012/full#supplementary-material

REFERENCES

Bakhiya, N., Arlt, V. M., Bahn, A., Burckhardt, G., Phillips, D. H., and Glatt, H. (2009). Molecular evidence for an involvement of organic anion transporters (OATs) in aristolochic acid nephropathy. *Toxicol* 264, 74–79. doi: 10.1016/j.tox.2009.07.014

Baudoux, T. E., Pozdzik, A. A., Arlt, V. M., De Prez, E. G., Antoine, M. H., Quellard, N., et al. (2012). Probenecid prevents acute tubular necrosis in a mouse model of aristolochic acid nephropathy. *Kidney Int.* 82, 1105–1113. doi: 10.1038/ki.2012.264

Bow, D. A., Perry, J. L., Simon, J. D., and Pritchard, J. B. (2006). The impact of plasma protein binding on the renal transport of organic anions. *J. Pharmacol. Exp. Ther.* 316, 349–355. doi: 10.1124/jpet.105.093070

Chen, Q., Yi, D. H., Xie, Y. M., Yang, W., Yang, W., Yang, W., et al. (2011). Analysis of clinical use of Danhong injection based on hospital information system. *Zhongguo Zhong Yao Za Zhi* 36, 2817–2820. doi: 10.4268/cjcmm20112016

Corona, G., Elia, C., Casetta, B., Da Ponte, A., Del Pup, L., Ottavian, E., et al. (2010). Liquid chromatography tandem mass spectrometry assay for fast and sensitive quantification of estrone-sulfate. *Clin. Chim. Acta* 411, 574–580. doi: 10.1016/j.cca.2010.01.019

Cox, P. G., Moons, W. M., Russel, F. G., and Ginneken, C. A. (1989). Renal handling of salicyluric acid in the isolated perfused rat kidney: evidence for accumulation in tubular cells. *J. Pharmacol. Exp. Ther.* 251, 750–755.

Diehl, K. H., Hull, R., Morton, D., Pfister, R., Rabemampianina, Y., Smith, D., et al. (2001). A good practice guide to the administration of substances and removal of blood, including routes and volumes. *J. Appl. Toxicol.* 21, 15–23. doi: 10.1002/jat.727

Du, J., Yang, W., Yi, D. H., Xie, Y. M., Yang, W., Yang, W., et al. (2011). Analysis of using Danhong injection to treatment coronary heart disease patient's medicines based on real world HIS database. *Zhongguo Zhong Yao Za Zhi* 36, 2821–2824. doi: 10.4268/cjcmm20112017

Emami Riedmaier, A., Nies, A. T., Schaeffeler, E., and Schwab, M. (2012). Organic anion transporters and their implications in pharmacotherapy. *Pharmacol. Rev.* 64, 421–449. doi: 10.1124/pr.111.004614

Ghiselli, A., Laurenti, O., Mattia, G. D., Maiani, G., and Ferro-Luzzi, A. (1992). Salicylate hydroxylation as an early marker of in vivo oxidative stress in diabetic patients. *Free Radic. Biol. Med.* 13, 621–626. doi: 10.1016/0891-5849(92)90036-g

Li, J. P., Guo, J. M., Hua, Y. Q., Zhu, K. Y., Tang, Y. P., Zhao, B. C., et al. (2016a). The mixture of Salvia miltiorrhiza-Carthamus tinctorius (Danhong injection) alleviates low-dose aspirin induced gastric mucosal damage in rats. *Phytomedicine* 23, 662–671. doi: 10.1016/j.phymed.2016.03.006

Li, J. P., Guo, J. M., Shang, E. X., Zhu, Z. H., Zhu, K. Y., Li, S. J., et al. (2016b). A metabolomics strategy to explore urinary biomarkers and metabolicpathways for assessment of interaction between Danhong injection and low-dose aspirin during their synergistic treatment. *J. Chromatogr. B.* 1026, 168–175. doi: 10.1016/j.jchromb.2015.07.045

Li, J. P., Guo, J. M., Shang, E. X., Zhu, Z. H., Liu, Y., Zhao, B. C., et al. (2017). Quantitative determination of five metabolites of aspirin by UHPLC-MS/MS coupled with enzymatic reaction and its application to evaluate the effects of aspirin dosage on the metabolic profile. *J. Pharm. Biomed. Anal.* 138, 109–117. doi: 10.1016/j.jpba.2016.12.038

Liu, T., Meng, Q., Wang, C., Liu, Q., Guo, X., Sun, H., et al. (2012). Changes in expression of renal Oat1, Oat3 and Mrp2 in cisplatin-induced acute renal failure after treatment of JBP485 in rats. *Toxicol. Appl. Pharmacol.* 264, 423–430. doi: 10.1016/j.taap.2012.08.019

Liu, X., Wu, Z., Yang, K., Ding, H., and Wu, Y. (2013). Quantitative analysis combined with chromatographic fingerprint for comprehensive evaluation of Danhong injection using HPLC-DAD. *J. Pharm. Biomed. Anal.* 76, 70–74. doi: 10.1016/j.jpba.2012.12.013

Mattiello, T., Guerriero, R., Lotti, L. V., Trifiro, E., Felli, M. P., Barbarulo, A., et al. (2011). Aspirin extrusion from human platelets through multidrug resistance protein-4-mediated transport: Evidence of a reduced drug action in patients after coronary artery bypass grafting. *J. Am. Coll. Cardiol.* 58, 752–761. doi: 10.1016/j.jacc.2011.03.049

Miners, J. O. (1989). Drug interactions involving aspirin (acetylsalicylic acid) and salicylic acid. *Clin. Pharmacokinet.* 17, 327–344. doi: 10.2165/00003088-198917050-00003

Nigam, S. K., Bush, K. T., Martovetsky, G., Ahn, S. Y., Liu, H. C., Richard, E., et al. (2015). The organic anion transporter (OAT) family: a systems biology perspective. *Physiol. Rev.* 95, 83–123. doi: 10.1152/physrev.00025.2013

Polachek, H., Holcberg, G., Polachek, J., Rubin, M., Feinshtein, V., Sheiner, E., et al. (2010). Carrier-mediated uptake of levofloxacin by bewo cells, a human trophoblast cell line. *Arch. Gynecol. Obstet.* 281, 833–838. doi: 10.1007/s00404-009-1177-y

Proudfoot, A. T., Krenzelok, E. P., Brent, J., and Vale, J. A. (2003). Does urine alkalinization increase salicylate elimination? If so, why? *Toxicol. Rev.* 22, 129–136. doi: 10.2165/00139709-200322030-00001

Robbins, N., Koch, S. E., Tranter, M., and Rubinstein, J. (2012). The history and future of probenecid. *Cardiovasc. Toxicol.* 12, 1–9. doi: 10.1007/s12012-011-9145-8

Schmassmann-Suhijar, D., Bullingham, R., Gasser, R., Schmutz, J., and Haefeli, W. E. (1998). Rhabdomyolysis due to interaction of simvastatin with mibefradil. *Lancet* 351, 1929–1930. doi: 10.1016/S0140-6736(05)78613-X

Tamai, I., Sai, Y., Ono, A., Kido, Y., Yabuuchi, H., Takanaga, H., et al. (1999). Immunohistochemical and functional characterization of ph-dependent intestinal absorption of weak organic acids by the monocarboxylic acid transporter mct1. *J. Pharm. Pharmacol.* 51, 1113–1121. doi: 10.1211/0022357991776804

Weiner, I. M., Washington, J. A., and Mudge, G. H. (1959). Studies on the renal excretion of salicylate in the dog. *Bull. Johns Hopkins Hosp.* 105, 284–297.

White, S., Calver, B. L., Newsway, V., Wade, R., Patel, S., Bayer, A., et al. (2005). Enzymes of drug metabolism during delirium. *Age Ageing* 34, 603–608. doi: 10.1093/ageing/afi189

Xue, X., Gong, L. K., Maeda, K., Luan, Y., Qi, X. M., Sugiyama, Y., et al. (2011). Critical role of organic anion transporters 1 and 3 in kidney accumulation and toxicity of aristolochic acid I. *Mol. Pharm.* 8, 2183–2192. doi: 10.1021/mp100418u

Zhu, J. F., Yi, X. J., Huang, P., Chen, S. Q., and Wu, Y. J. (2017). Drug-protein binding of Danhong injection and the potentialinfluence of drug combination with aspirin: Insight by ultrafiltration LC-MS and molecular modeling. *J. Pharm. Biomed. Anal.* 134, 100–107. doi: 10.1016/j.jpba.2016.11.028

Conflict of Interest: The authors declare that the research was conducted in the absence of any commercial or financial relationships that could be construed as a potential conflict of interest.

frontiers in Pharmacology

ORIGINAL RESEARCH
published: 27 November 2020
doi: 10.3389/fphar.2020.588127

Comparable Intestinal and Hepatic First-Pass Effect of YL-IPA08 on the Bioavailability and Effective Brain Exposure, a Rapid Anti-PTSD and Anti-Depression Compound

*You Gao, Chunmiao Yang, Lingchao Wang, Yanan Xiang, Wenpeng Zhang, Yunfeng Li and Xiaomei Zhuang**

State Key Laboratory of Toxicology and Medical Countermeasures, Beijing Institute of Pharmacology and Toxicology, Beijing, China

OPEN ACCESS

Edited by:
Victor A. Voicu, Carol Davila University of Medicine and Pharmacy, Romania

Reviewed by:
Stanislav Yanev, Bulgarian Academy of Sciences (BAS), Bulgaria
Zhihao Liu, United States Department of Agriculture, United States

***Correspondence:**
Xiaomei Zhuang
xiaomeizhuang@163.com

Specialty section:
This article was submitted to Drug Metabolism and Transport, a section of the journal Frontiers in Pharmacology

Received: *28 July 2020*
Accepted: *26 October 2020*
Published: *27 November 2020*

Citation:
Gao Y, Yang C, Wang L, Xiang Y, Zhang W, Li Y and Zhuang X (2020) Comparable Intestinal and Hepatic First-Pass Effect of YL-IPA08 on the Bioavailability and Effective Brain Exposure, a Rapid Anti-PTSD and Anti-Depression Compound. Front. Pharmacol. 11:588127. doi: 10.3389/fphar.2020.588127

YL-IPA08, exerting rapid antidepressant-like and anxiolytic-like effects on behaviors by translocator protein (TSPO) mediation, is a novel compound that has been discovered and developed at our institute. Fit-for-purpose pharmacokinetic properties is urgently needed to be discovered as early as possible for a new compound. YL-IPA08 exhibited low bioavailability (~6%) during the preliminary pharmacokinetics study in rats after oral administration. Our aim was to determine how metabolic disposition by microsomal P450 enzymes in liver and intestine limited YL-IPA08's bioavailability and further affected brain penetration to the target. Studies of *in vitro* metabolic stability and permeability combined with *in vivo* oral bioavailability, panel CYP inhibitor co-administration via different routes, and double cannulation rats were conducted to elucidate the intestinal and hepatic first-pass effect of YL-IPA08 on bioavailability. Unbound brain-to-plasma ratio ($K_{p,uu}$) in rats was determined at steady state. Results indicated that P450-mediated elimination appeared to be important for its extensive first-pass effect with comparative contribution of gut (35%) and liver (17%), and no significant species difference was observed. The unbound concentration of YL-IPA08 in rat brain (6.5 pg/ml) was estimated based on $K_{p,uu}$ (0.18) and was slightly higher than *in vitro* TSPO-binding activity (4.9 pg/ml). Based on the onset efficacy of YL-IPA08 toward TPSO in brain and $K_{p,uu}$, therapeutic human plasma concentration was predicted to be ~27.2 ng/ml would easily be reached even with unfavorable bioavailability.

Keywords: YL-IPA08, pharmacokinetics, bioavailability, hepatic metabolism, intestinal metabolism, brain exposure, *in vitro-in vivo* extrapolation

INTRODUCTION

Major depressive disorder (MDD) is a chronic and debilitating disorder with high rates of medical and psychiatric co-morbidity. Translocator protein (TSPO, 18 kDa) has drawn growing attention in the pathophysiology of stress-response and stress-related disorders (Rupprecht et al., 2009; Pinna, 2010). YL-IPA08, upon binding to TSPO, stimulates the *de novo* synthesis of neurosteroids, which

potentiates the $GABA_A$ receptor function and, consequently, conducts its antidepressant- and anxiolytic-like effects (Zhang et al., 2017).

Oral bioavailability and target exposure related to the pharmacological efficacy of orally administered drugs is a key aspect of new drug development (Obach, 2001; Li et al., 2019). However, YL-IPA08 exhibited low bioavailability (~6%) during the preliminary pharmacokinetics (PK) study in rats after oral intake. It is well recognized that a drug with low oral bioavailability can be impacted by multiple factors including absorption barrier, intestinal and hepatic metabolism before going into systemic circulation (Fan et al., 2019). Both CYP and UGT enzymes are major drug metabolizing enzymes in gut and liver that facilitate the elimination of xenobiotics. Although the liver contains higher amount of CYPs and UGTs, the small intestine is usually exposed to higher concentration of xenobiotics. Thus, both liver and intestine play important roles in bioavailability (Ohno and Nakajin, 2009; Court et al., 2012; Karlsson et al., 2013). Several studies have demonstrated the relative importance of intestinal metabolism to low bioavailability, and the situations were substrate-dependent (Cubitt et al., 2009; Fan et al., 2019).

To address the roles of the liver and intestine in YL-IPA08 first-pass metabolism, gastrointestinal absorption and hepatic and gut first-pass metabolism of YL-IPA08 were evaluated to understand of the causes of low bioavailability. Then, the antidepressant-like efficacy achieved in rat models were taken to explore the effective brain exposure of YL-IPA08 under the same oral dose regiment combined with *in vitro* TSPO-binding assessment. Liver microsomes and intestinal microsomes of rat and human were firstly used to conduct *in vitro* stability of YL-IPA08 in the presence of NADPH and UDPGA as cofactors to identify the major enzymes and metabolic organs responsible for the first-pass elimination. In the view of rat model is commonly used in pharmacokinetic studies (Zeng et al., 2019), rat pharmacokinetic studies were conducted using ABT as CYP inhibitor to knock out the function of hepatic CYPs or hepatic and intestinal CYPs via different routes (Strelevitz et al., 2006). In addition, a rat model with double cannulation of portal and jugular veins (Murakam et al., 2003) was used to testify the contribution of hepatic metabolism. As a central nervous system (CNS) drug, CNS penetration assessment was performed in rat under steady-state to obtain the brain/plasma partition. $K_{p,uu}$ was calculated by correction of unbound fractions of YL-IPA08 in plasma and brain. Brain exposure of YL-IPA08 was estimated in the case of limited systemic exposure. Based on the current results, we attempt to elucidate the disposition characters of YL-IPA08 associated with its efficacy and explore the potential of clinical application based on our mechanistic understanding.

MATERIALS AND METHODS

Chemical and Reagents

YL-IPA08 and AC-5216 internal standard (IS) (**Figure 1**) were supplied by chemical synthesis laboratory of our Institute (Beijing, China) with purity greater than 99%. Midazolam (MDZ), 1′-OH-MDZ, phenacetin, acetaminophen, diclofenac, S-mephenytoin, 4-OH-diclofenac, 4-OH-mephenytoin, bupropion, OH-bupropion, amodiaquine, N-desethylamodiaquine, dextromethorphan, dextrorphan, atenolol, propranolol, and digoxin were all purchased from Sigma-Aldrich (St. Louis, MO). Human liver microsomes (pool of 50, mixed gender), male rat liver microsomes (pool of 495), human intestinal microsomes (pool of 15, mixed gender) and male rat intestinal microsomes (pool of 100) were purchased from XENOTECH (Lenexa, KS). NADPH was purchased from Roche Life Science (Basel-Stadt, Switzerland). Other reagents were of HPLC grade or better.

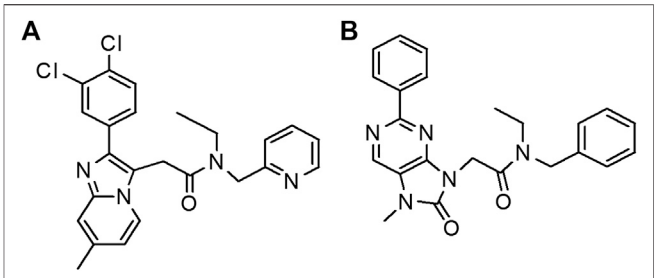

FIGURE 1 | Chemical structural of YL-IPA08 **(A)** and AC-5216 (IS) **(B)**.

In Vitro Study

NADPH- and UDPGA-Dependent Hepatic Clearance in Liver and Intestinal Microsomes of Rat and Human

Pilot *in vitro* metabolic stability experiments were conducted to identify the incubation conditions to capture the linear elimination of YL-IPA08 including concentration of YL-IPA08, protein concentration of microsomes, and stop times. The CYP-mediated hepatic and intestinal metabolic stability test was performed in incubations containing YL-IPA08 (1 μM, dissolved in saline) in pooled rat or human liver and intestinal microsomes (0.2 mg/ml protein) in 100 mM of potassium phosphate buffer with 3 mM of $MgCl_2$, pH 7.4. The mixture was pre-incubated at 37°C for 5 min. The reaction was started with the addition of NADPH (with final concentration of 1 mM). For UGT-mediated metabolic clearance assays, alamethicin at final concentration of 50 μg/mg protein, 1 μM of YL-IPA08 and rat or human liver and intestinal microsomes in 100 mM of potassium phosphate buffer (pH 7.4) were mixed on ice for 15 min. The mixture was then pre-incubated at 37°C for 5 min. The reaction was started with the addition of UDPGA (2.5 mM). Aliquots of the incubation were removed at different time points in the duration of 60 min after dosing of cofactors (NADPH or UDPGA) and diluted with 6× volume of chilled acetonitrile containing internal standard to stop the reactions. After centrifugation at 13,000 g for 10 min, the supernatant was collected and stored at −20°C until LC-MS/MS analysis. Negative control without NADPH and positive control with cocktailed probe compounds (phenacetin, diclofenac, S-mephenytoin, bupropion, amodiaquine, dextromethorphan, and midazolam) in liver microsomes and midazolam in intestinal microsomes were conducted simultaneously.

Transcellular Transport Experiment With Caco-2 Cells

Caco-2 cell lines were cultured (ATCC, Manassas, VA, United States) as described previously (Liu et al., 2014). Briefly, the cells were cultured at 37°C in 5% CO_2 at 90% humidity in DMEM high glucose medium containing 20% fetal bovine serum, 1% nonessential amino acids, 100 U/ml penicillin and 1% streptomycin. For the efflux studies, the cells were seeded onto polyethylene terephthalate Millicell® cell culture inserts (0.4 μm pore size, 6.5 mm diameter, Millipore Corporation, Billerica, MA, United States) at a density of 1.7×10^5 cells/ml. The culture medium was refreshed on the day after seeding, after which it was refreshed every other day and on the day before the transport experiment. The cells were cultured for 20–22 days after seeding and then evaluated by measuring the transepithelial electrical resistance (TEER) (Millicell ERS®, Millipore Corporation) before experiments. Batches of Caco-2 cells were certified by measuring the TEER values and the apparent permeability coefficient (P_{app}) of control compounds: atenolol (10 μM, low permeability), propranolol (10 μM, high permeability), and P-gp substrate digoxin (10 μM). Transepithelial permeability studies for YL-IPA08 (10 μM) were conducted from apical to basolateral side (A-B) and basolateral to apical side (B-A) for 120 min 0.2% BSA was included in the receiver solution to avoid nonspecific binding. At 60, 90, and 120 min, half volume of solution from receiver side was withdrawn, and same volume of HBSS was immediately added. Obtained samples were precipitated by adding 4× volumes of acetonitrile containing IS and centrifuged. The supernatants were stored in −20°C until further analysis by LC-MS/MS.

Blood/Plasma Partitional Ratio

The blood/plasma partitional ratio ($R_{b/p}$) in rat and human blood was measured *in vitro* using fresh pooled blood including heparin. Whole blood was preincubated at 37°C in a water bath, and spiked with YL-IPA08 at 1 μM. The blood samples were incubated at 37°C for 1 h. After incubation, aliquots of 25 μl spiked whole blood were removed, and the remaining blood was centrifuged at 2,000 × g for 10 min, after which 25 μl aliquots of plasma were removed. Obtained blood and plasma samples were spiked with same volume of blank plasma or blood, respectively, and then immediately precipitated by adding 4× volumes of acetonitrile containing IS to get the same matrix. The concentrations of YL-IPA08 in blood and plasma were determined by LC-MS/MS.

Protein Binding in Different Biomatrices

The fraction of unbound YL-IPA08 in plasma and liver microsomes of rat and human, and brain homogenates of rat were determined utilizing Rapid Equilibrium Dialysis method (Waters et al., 2008). Rat brain homogenate was harvested in 4-fold volume (w/v) of PBS (pH 7.4). YL-IPA08 were spiked into fresh plasma, rat brain homogenate, liver microsomes (0.2 mg/ml protein) at concentration of 1 μM, and then dialyzed against biomatrices on a shaker at 37°C for 4 h. To avoid the high non-specific binding of YL-IPA08, 0.01% Tween 80 was added in the incubation mixture. At the end of the incubation, protein was precipitated with acetonitrile (containing IS) and analyzed by LC-MS/MS. Phenacetin, quinidine, and warfarin were selected as positive control for the protein binding test.

In Vivo Study

Male SD rats (200–240 g) were obtained from Beijing Vital River Laboratory Animal Technology Co., Ltd. Animals were housed in a temperature- and humidity-controlled room with a 12 h light/dark cycle. They were fasted 12 h before the experiments and had ad libitum access to water. The animal experiments were conducted in the Beijing Center for Drug Safety Evaluation and according to a protocol (IACUC-DWZX-2020-691) approved by the Institutional Animal Care and Use Committee of the Center, which followed the guidelines of the Association for Assessment and Accreditation of Laboratory Animal Care International (AAALAC).

Bioavailability Study

Male rats (n = 6) were administered YL-IPA08 by oral gavage at 1, 3 and 10 mg/kg or i.v. injection at 0.3 mg/kg. Blood samples were collected before and after dosing at 0.033 (i.v. dosing only), 0.083, 0.25, 0.5, 1, 2, 4, 6, 8,12 and 24 h. Blood sample (no more than 100 μl) was collected from the jugular vein into tubes containing heparin on ice and centrifuged within 1 h of collection. Plasma was harvested and stored at −20°C for bioanalysis.

Surgical Procedure for Portal and Jugular Vein Double Cannulation and the Pharmacokinetic Study With the Same Parameters as Normal Rats After p.o.

The surgical procedure for portal vein catheter insertion was performed according to reference (Matsuda et al., 2012). Male SD rats (250–280 g) were purchased from Beijing Vital River Laboratory Animal Technology Co., Ltd. (Beijing, China). Rats were anesthetized with 2% pentobarbital sodium (0.2–0.3 mg/100 g) intraperitoneally dosed. Cannulation into the jugular vein was performed by the method of Murakami reported (Murakami et al., 2003) with minor modification. Briefly, an incision of ~0.5 cm near right clavicle was made and the jugular vein was exposed. Next, this vein was cannulated with ~12.5 cm of silicone gel tubing (0.6 mm I.D. × 0.9 mm O.D., Skillsmodel Inc., Beijing, China). The other side of the tubing was passed through the back skin. 2.5 cm midline incision was made in the abdominal cavity close to ensiform process and the portal vein was detached. To prevent bleeding, the portal vein was ligated temporarily as the catheter was inserted. The silicone tubing (22 cm, 0.6 mm I.D. × 0.9 mm O.D., Skillsmodel Inc., Beijing, China) was inserted immediately and fixed by a purse-string suture on the portal vein. The time to reperfusion was about 1 min after intercepted blood flow. In addition, a catheter with trumpet-shaped opening was used to prevent the catheter from slipping out of the vessel and minimize the effect on blood flow. Another end of the catheter was passed subcutaneously to the skin close to the scapula.

Male rats (n = 5), after recovery from successful double cannulation, were administered YL-IPA08 by oral gavage at 1 mg/kg. Blood samples were collected at 0, 0.083, 0.25, 0.5, 1,

2, 4, 6, 8 and 12 h. Blood (approximately 100 µl) was collected from the jugular and portal veins into tubes containing heparin on ice and centrifuged within 1 h of collection. Plasma was harvested and stored at −20°C for bioanalysis.

Intestinal and Hepatic Availability of YL-IPA08 Using ABT Block the CYP Metabolism

ABT was used to differentiate the gastrointestinal and hepatic first-pass elimination of YL-IPA08 by conducting four groups of rat *in vivo* experiments (n = 6 per group). YL-IPA08 was formulated in saline and dosed p.o. (1 mg/kg) or i.v. (0.1 mg/kg or 0.5 mg/kg) in rats pretreated for 1 h with ABT i.v. (50 mg/kg in saline, 5 ml/kg) or 15 h with ABT p.o. (100 mg/kg in saline, 10 ml/kg). Blood was collected from the jugular vein at 0.033 (i.v. dosing only), 0.083, 0.25, 0.5, 1, 2, 4, 6, 8, 12, and 24 h postdosing. Blood samples were immediately transferred into tubes containing heparin, and plasma was obtained following centrifugation at 2,000 g for 10 min at 4°C. The plasma samples were stored at −20°C until analysis.

Brain Distribution Under Steady State

Rats (n = 3) was i.v. injected YL-IPA08 at loading dose of 0.28 mg/kg, then continuous i.v. infusion at the speed of 0.22 mg/h lasted for 1 h via tail vein. Jugular vein blood samples were collected at 30, 40, 50, and 60 min of i.v. infusion to verify attainment of steady state. Immediately after collecting the last blood sample (60 min), rats were terminally anesthetized and brain tissues were harvested, weighted and frozen at −80°C until analysis. Brain samples were homogenized with 4× fold volume of cold buffer. The homogenates were precipitated with acetonitrile (containing IS) and analyzed.

Bioanalysis Methods

On the day of bioanalysis, all *in vitro* and *in vivo* samples were precipitated with acetonitrile (containing IS) and analyzed by LC-MS/MS. Separation was performed using a C18 column (3.0 mm × 50 mm, 2.6 µm, Phenomenex). The mobile phase consisted of water containing 5 mM ammonium acetate (A) and acetonitrile containing 5 mM ammonium acetate (B). Separation was achieved with a 3.5-min run time with the following gradient program: initial conditions of 40% B held for 0.3 min followed by an increase to 95% B over 2.0 min, hold at 95% B for 0.5 min, and return to 40% B over 1 min. The flow rate is 0.7 ml/min. Analyte detection was achieved with an AB Sciex API 5000 Triple quadrupole mass spectrometer operated in positive ion mode with multiple reaction monitoring (MRM). The precursor and product ions transition for YL-IPA08 and internal standard were 453.195/317.100 and 402.389/227.5.

Data Analysis

The *in vitro* $t_{1/2}$ in liver microsomal incubation was calculated from the semi-log plot of percentage remaining vs. incubation time and intrinsic clearance (Cl_{int}, ml/min/mg protein) was calculated as **Eq. 1**:

$$CL_{int} = \frac{0.693}{in\ vitro\ t_{1/2}} \times \frac{volume\ of\ incubation\ (\mu l)}{amount\ of\ microsomal\ protein\ in\ incubation\ (mg)} \quad (1)$$

(Suzuki et al., 2003).

Apparent permeability was obtained according to the equation $P_{app} = (dQ/dt)/(A \times C_0)$, where dQ/dt is the mass transport rate (determined from the slope of the amount transported vs. time plot), A is the surface area of the monolayer, and C_0 is the initial concentration of YL-IPA08 in the donor chamber (Suzuki et al., 2003). The efflux ratio was calculated for each study using the following equation: endoplasmic reticulum (ER) = $P_{app(B-A)}/P_{app(A-B)}$, where $P_{app(B-A)}$ and $P_{app(A-B)}$ represent apparent drug permeability in the B to A and A to B direction, respectively. An efflux ratio greater than 2 indicates net efflux.

The unbound fraction of YL-IPA08 in plasma or liver microsomes ($f_{u,x}$) was calculated as shown in **Eq. 2**, and unbound fraction in the tissue homogenate ($f_{u,b}$) was calculated according to **Eq. 3**.

$$f_{u,x} = Conc_{buffer\ chamber} \Big/ Conc_{plasma/liver\ microsomes\ chamber} \quad (2)$$

$$f_{u,b} = Conc_{buffer\ chamber} \Big/ Conc_{brain\ homogenate\ chamber} \quad (3)$$

The measured unbound fractions would be higher when a tissue is homogenized and diluted in buffer, the unbound fractions in an undiluted tissues ($f_{u,brain}$) were calculated using **Eq. 4** (Kalvass and Maurer, 2002).

$$Undiluted\ f_{u,brain} = \frac{1/D}{\left(\left(1/f_{u,brain\ homogenate}\right) - 1\right) + 1/D} \quad (4)$$

Where D represents the fold of dilution factor in brain homogenates. The free fraction of plasma and undiluted tissue is used in tissue-to-plasma exposure ratio calculation.

Pharmacokinetic parameters were calculated by the noncompartmental method using WinNonlin 7.0 (Pharsight, CA). The area under the plasma concentration time curve (AUC) from time 0 to the last time point with a measurable concentration (AUC_{0-t}) was calculated by trapezoidal method. Bioavailability (%F) was calculated as the ratio of the mean dose-normalized AUC values for oral and intravenous dosed groups [$F_{p.o.} = AUC_{p.o.} \times Dose_{i.v.} \times 100/(AUC_{i.v.} \times Dose_{p.o.})$]. *In vivo* plasma clearance and volume of distribution were archived from the pharmacokinetic study via i.v. injection.

F_aF_g was calculated using mass balance method and rat portal blood flow (Q_{pv}) of 32 ml/min/kg, where $R_{b/p}$ is used to convert plasma concentrations to blood concentrations.

$$F_aF_g = Q_{pv} \times R_{b/p} \times \left(AUC_{po,\mathrm{portal}} - AUC_{po,\mathrm{jugular}}\right) \Big/ Dose \quad (5)$$

(Matsuda et al., 2012)

Liver and gut extraction ratios in ABT treatment were calculated using the following formula:

$$F_h = (1 - E_h) \times 100;\ E_h = Cl_h \Big/ Q_h;\ F_g = F \Big/ F_h \times 100;\ E_g = 100 - F_g;\ Q_h = 85\ ml \Big/ min \Big/ kg$$

(Kajbaf et al., 2013)

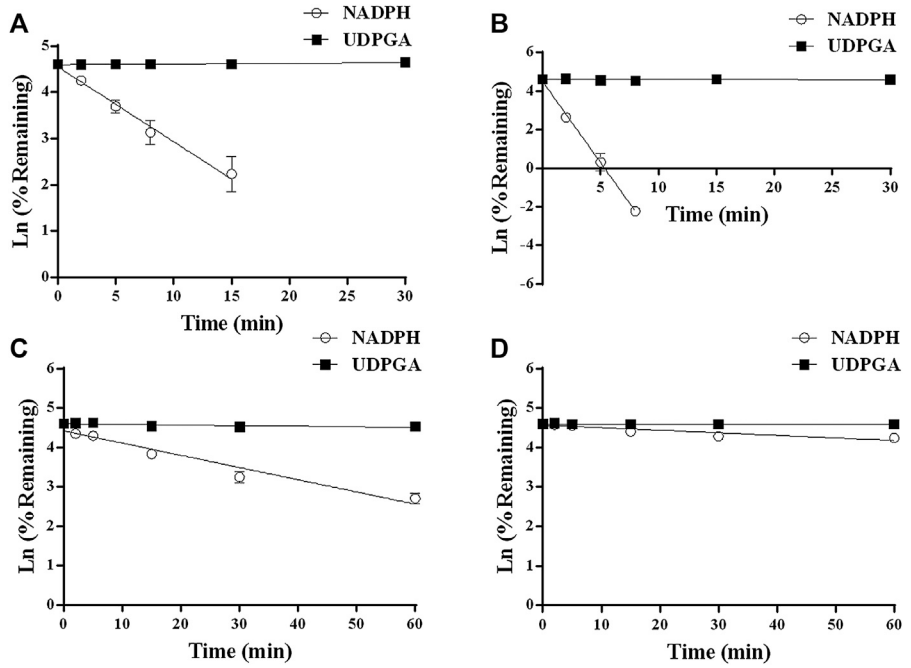

FIGURE 2 | Comparison of P450 and UGT depletion profiles of YL-IPA08 in HLM **(A)**, RLM **(B)**, HIM **(C)**, and RIM **(D)**. Open circle represents P450 metabolism, closed square represents glucuronidation (n = 3).

RESULTS

LC-MS/MS Methodology

The quantification of YL-IPA08 in rat plasma was fully validated, and *in vitro* samples were particularly validated by selectivity, precision, and stability. The calibration curves of YL-IPA08 in rat plasma and *in vitro* incubates ranged in the concentrations of 0.5–500 ng/ml and 1–1,000 nM, respectively. The intra-day precision and inter-day precision (error from the true value) were less than 15% at QC concentrations (full methodology validation results were presented in **Supplementary Tables S1–S3**).

In vitro Metabolic Elimination of YL-IPA08

YL-IPA08 was discovered to be eliminated in liver microsomes and intestinal microsomes of rat and human to different extents in the presence of CYPs (NADPH) and/or UGTs (UDPGA) co-factors. The disappearance of YL-IPA08 at various time points are presented in **Figure 2**. The intrinsic clearances (**Table 1**) were calculated based on data presented in **Figure 2**. The amounts of YL-IPA08 remained stable during the 60-mininute incubation in the presence of UDPGA in RLM, RIM, HLM and HIM, which indicated that glucuronidation of YL-IPA08 cannot take place both in liver and in gut. The depletions of YL-IPA08 were very rapid in the presence of NADPH in RLM and HLM, with the CYP-mediated intrinsic clearances of 1.13 ± 0.02 and 2.36 ± 0.03 ml/min/mg protein, respectively. If those intrinsic clearance values were normalized by respective CYP contents in rat and human, the results would be 2.76 ± 0.05 and 3.47 ± 0.04 ml/min/nmol CYP protein, respectively. However, in the intestine, the CYP-mediated intrinsic clearances in HIM and RIM were 0.20 ± 0.03 and 0.053 ± 0.02 ml/min/mg protein, respectively. Although statistical significance was observed in the intrinsic clearances between rat and human liver microsomes, the major contributions of hepatic metabolizing enzymes were almost identical. As for the contributions of intestine, the differences between rat and human were remarkable. The main reason for the difference may be the metabolic activity of intestinal microsomes. The eliminations of cocktailed probe compounds in HLM and RLM were well accepted by the literature to verify the model. Midazolam clearances in HIM and RIM were identical to the indicators provided by the vendor.

TABLE 1 | *In vitro* metabolic clearance YL-IPA08 in liver and intestinal microsomes of rats and humans in the presence of NADPH (n = 3).

Species	$t_{1/2}$ (min)	Cl_{int} (ml/min/mg protein)	Cl_{int} (ml/min/nmol CYP protein)
HLM	3.06 ± 0.04[a]	1.13 ± 0.02[a]	2.76 ± 0.05[a]
RLM	1.47 ± 0.02	2.36 ± 0.03	3.47 ± 0.04
HIM	17.31 ± 2.24	0.20 ± 0.03[b]	—
RIM	76.12 ± 39.56	0.053 ± 0.02	—

[a]p<0.01 compared with results from RLM.
[b]p<0.01 compared with results from RIM.

Bidirectional Transport of YL-IPA08 Across Caco-2 Cells

As shown in **Table 2**, transcellular transport of YL-IPA08 across Caco-2 cells showed high permeability similar to positive control propranolol. P-gp activity was confirmed by the transcellular

transport of digoxin with a flux ratio of 6.25. The basal-to-apical permeability of YL-IPA08 was comparable to apical-to-basal permeability, with a flux ratio of 0.66, suggesting the transportation through gut wall is mainly passive penetration. Furthermore, combined with the high aqueous solubility and high permeability, YL-IPA08 belongs to BCS class I compound.

Blood/Plasma Partitioning and Unbound Fractions in Biomatrices

The mean blood/plasma partitioning ($R_{b/P}$) of YL-IPA08 in human and rat whole blood were 1.58 ± 0.06 and 1.12 ± 0.08, respectively. The individual protein binding in rat plasma is 58.48 ± 2.26, 78.08 ± 4.49, and 99.67 ± 0.08% for phenacetin, quinidine, and warfarin, respectively, which is well accepted by the literature to verify the model. Protein bindings of YL-IPA08 in biomatrices were presented in **Table 3**. Plasma Protein binding is almost 99% bound. Unbound fractions of YL-IPA08 were generated according to the protein bindings. $R_{b/p}$ and unbound fractions are important parameters to perform theoretical translations between *in vitro* and *in vivo* systems.

In Vivo Pharmacokinetic Behaviors

Pharmacokinetic profiles of YL-IPA08 were archived in rats via i.v. and p.o. dosing (**Figure 3**). As shown in **Table 4**, YL-IPA08 exhibited short half-life and high clearance *in vivo*, which agreed with *in vitro* results. After oral dosing, the plasma exposures of YL-IPA08 were proportionate within the dose range of 1–10 mg/kg, possessing a low bioavailability of ~6%.

The Effect of ABT on YL-IPA08 Pharmacokinetics

As shown in **Figure 4**, combination administration with ABT significantly elevated the YL-IPA08 plasma concentrations. The pharmacokinetic parameters are presented in **Table 5**. After pretreated with ABT through i.v. injection and oral gavage, systemic clearance of YL-IPA08 reduced by about 75 and 80%, with dramatic increased oral bio-availabilities of ~20 and ~70%, respectively. Hepatic and gut extraction ratios in different route of ABT treatment groups were elucidated and shown in **Table 6**. ABT pretreated via i.v. injection or oral gavage, resulted in either hepatic metabolism inhibition or both gut and hepatic metabolism inhibition. Under such conditions, gut and liver have similar contributions to the low bioavailability of YL-IPA08. The extraction ratios of gut and liver were 65 and 83%, respectively, when gut and hepatic metabolism worked normally, while the corresponding extraction ratios were 16 and 17%, respectively, after the majority of the CYP enzymes were inactivated, excepted for the weak inactivation toward CYP2C9 (Linder, et al., 2009).

Pharmacokinetics of YL-IPA08 in Double Cannulated Rats

Figure 5 showed the concentration-time profiles of YL-IPA08 in portal and jugular venous plasma after oral administration of YL-IPA08 in double cannulated rats at a dose of 1 mg/kg. The plasma concentrations in portal veins is slightly higher than those in the jugular vein. No observed difference in clearance kinetics indicated the metabolic clearance in gut and liver is almost equal. The AUC values of YL-IPA08 were 441 ± 93 and 339 ± 93 h·ng/ml in portal and jugular venous plasma, respectively. $F_a F_g$ value was 22% after calculating with **Eq. 5** using the plasma AUC corrected by $R_{b/p}$.

TABLE 2 | Transcellular transport of YL-IPA08 in Caco-2 cell line (n = 3).

Compound	P_{app} (× 10–^{6} cm/s)		Efflux ratio
	A→B	B→A	
Atenolol	0.10 ± 0.06	0.12 ± 0.11	1.21
Propranolol	4.35 ± 2.06	2.78 ± 0.09	0.63
Digoxin	0.45 ± 0.17	2.63 ± 0.7	6.25
YL-IPA08	3.99 ± 1.46	2.63 ± 0.43	0.66

TABLE 3 | Protein bindings (%) and unbound fractions of YL-IPA08 in different sorts of biomatrices (n = 3).

Biomatrices	Protein biding (%)	Unbound fraction
Rat plasma	99.40 ± 0.01	0.006
Human plasma	99.90 ± 0.02	0.001
HLM (0.2 mg/ml)	55.26 ± 0.68	0.447
RLM (0.2 mg/ml)	57.14 ± 2.92	0.428
Rat brain homogenate	99.51 ± 0.01	0.0049

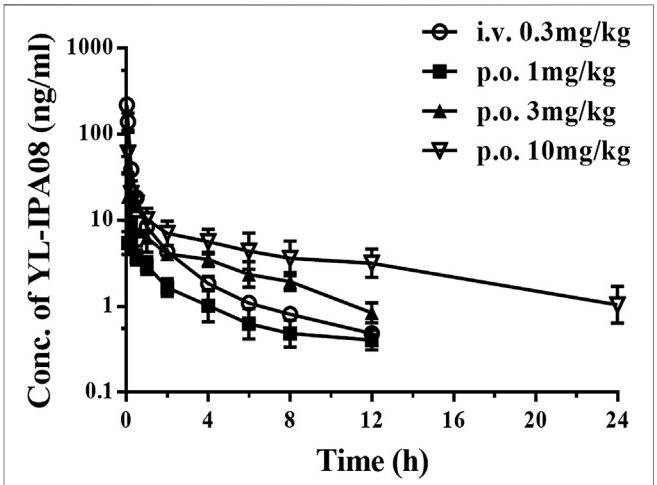

FIGURE 3 | Plasma concentration-time profiles of YL-IPA08 after intravenous (0.3 mg/kg) and oral administration of different doses (1, 3, 10 mg/kg) of YL-IPA08 in rats. Error bars represent the standard deviation of the mean concentration (n = 6).

Unbound Concentration of YL-IPA08 in Brain Connects With Its Pharmacological Effect

Unbound fractions of YL-IPA08 in rat plasma and brain homogenate were 0.6 and 0.49%, respectively. K_p value of brain to plasma in rats was obtained under steady state to reach brain equilibrium in a transient dosing regimen. Then,

TABLE 4 | Pharmacokinetic parameters of YL-IPA08 in rats after intravenous and oral administration (n = 6).

Parameters (unit)	i.v. (mg/kg)	p.o. (mg/kg)		
	0.3	1	3	10
$t_{1/2}$ (h)	1.13 ± 0.07	1.66 ± 0.68	2.47 ± 1.54	2.31 ± 1.32
T_{max} (h)	—	0.05 ± 0.03	0.15 ± 0.17	0.15 ± 0.17
C_{max} (ng/ml)	—	5.99 ± 1.36	19.17 ± 16.35	60.9 ± 44.87
$AUC_{(0-t)}$ (h·ng/ml)	70.56 ± 12.15	12.49 ± 3.88	36.85 ± 9.57	103.52 ± 29.45
$AUC_{(0-\infty)}$ (h·ng/ml)	71.35 ± 12.29	13.56 ± 4.37	39.87 ± 9.81	106.85 ± 30.19
$MRT_{(0-t)}$ (h)	1.36 ± 0.11	3.35 ± 1.27	4.61 ± 1.49	7.73 ± 2.79
V_z (l/kg)	6.98 ± 0.74	—	—	—
Cl (ml/min/kg)	71.72 ± 11.47	—	—	—
F (%)	—	—	5.59	—

$K_{p,uu}$ achieved 0.18. The unbound concentration of YL-IPA08 in brain can be estimated based on the plasma concentrations after rats receiving different dosages of YL-IPA08 via oral dosing (**Table 4**). For example, the unbound concentration of 6.5 pg/g in brain can be achieved after 1 mg/kg oral dosing. According to *in vitro* TPSO-binding activity reported by Zhang et al. (2017), YL-IPA08 showed a high affinity for TSPO (IC_{50} of 0.23 nM) in the crude mitochondrial fraction prepared from rat cerebellum, homogenized in 10 volumes of ice-cold HS buffer. The unbound concentration in the incubates was obtained with 0.0108 nM (e.g., 4.9 pg/ml) by correcting the binding fraction of 10-volume brain homogenate (0.047). Thus, it is rational that marked acute antidepressant-like effects were observed in forced swim rats at the dosage of 1, 3, and 10 mg/kg (Zhang et al., 2017).

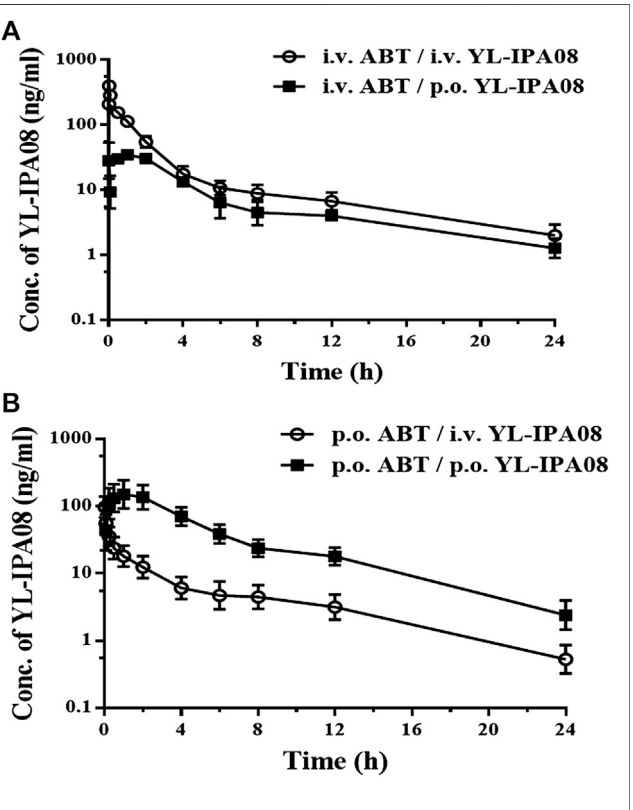

FIGURE 4 | Plasma concentration-time profiles of YL-IPA08 after intravenous (0.1 mg/kg or 0.5 mg/kg) and oral administration (1 mg/kg) of YL-IPA08 combined with ABT pretreatment via intravenous (50 mg/kg) and oral dosing (100 mg/kg) in rats. Error bars represent the standard deviation of the mean concentration (n = 6). **(A)** i.v. 50 mg/kg ABT/i.v. 0.5 mg/kg YL-IPA08 & i.v. 50 mg/kg ABT/p.o. 1 mg/kg YL-IPA08; **B:** p.o. 100 mg/kg ABT/ i.v. 0.1 mg/kg YL-IPA08 & p.o. 100 mg/kg ABT/p.o. 1 mg/kg YL-IPA08.

DISCUSSION

YL-IPA08, eliciting rapid anti-PTSD-like effects upon binding to TSPO, is a promising new drug with a novel CNS target and mechanism. The pharmacokinetic behavior, especially the CNS exposure, is closely associated with its pharmacology. In a series of rat behavior models, YL-IPA08 (1–10 mg/kg) produced significant antidepressant-like and anxiolytic-like effects (Zhang et al., 2017) following oral dosing. Thus, the pharmacokinetic study was performed in rats at the same dose regiment first. The liner PK behaviors of YL-IPA08 were observed after orally administrated with 1, 3, 10 mg/kg (**Table 4**; **Figure 3**). YL-IPA08 was absorbed rapidly and exposures were dose dependent with proportionate increasing of C_{max} and AUC. However, the bioavailability is pretty low (~6%) by comparing the AUC obtained following i.v. dosing. It is clear that the fraction of dose absorbed (F_a), fraction of absorbed dose escaping first-pass clearance in the gut wall (F_g) and fraction escaping liver first-pass clearance (F_h) are three major determinants toward oral bioavailability (*F*) (Darwich, et al., 2010; Nakanishi and Tamai, 2015).

Since identification of F_a, F_g and F_h is of importance to mechanistic understanding the systemic exposure, the related efficacy, and the potent drug-drug interactions, a number of *in vivo* and *in vitro* models have been developed to elucidate F_a, F_g and F_h. As for *in vitro* methods, liver microsomes, S9 or hepatocytes are all well accepted for the generation of hepatic clearance and F_h via *in vitro-in vivo* extrapolation (IVIVE) (Houston and Carlile, 1998). Furthermore, functionally mature enterocytes mainly express CYPs and UGTs. Among UGT isoforms, UGT1A8 and UGT1A10 show gut-specific expression patterns (Kaminsky and Zhang, 2003; Court et al., 2012). However, the achievement of intestinal clearance and (F_g) from intestinal

TABLE 5 | Pharmacokinetic parameters of YL-IPA08 in rats after intravenous and oral combination with ABT (n = 6).

Parameters (unit)	p.o. ABT		i.v. ABT	
	p.o. YL-IPA08 (1 mg/kg)	i.v. YL-IPA08 (0.1 mg/kg)	p.o. YL-IPA08 (1 mg/kg)	i.v. YL-IPA08 (0.5 mg/kg)
$t_{1/2}$ (h)	—	1.19 ± 0.12	—	1.46 ± 0.14
T_{max} (h)	1.4 ± 1.32	—	0.87 ± 0.68	—
C_{max} (ng/ml)	176.20 ± 88.52	—	41.79 ± 42.04	—
$AUC_{(0-t)}$ (h·ng/ml)	867.62 ± 184.51	124.75 ± 46.86	184.77 ± 147.68	471.89 ± 64.28
$AUC_{(0-\infty)}$ (h·ng/ml)	876.48 ± 183.33	125.70 ± 46.62	187.88 ± 145.72	476.21 ± 65.78
$MRT_{(0-t)}$ (h)	5.51 ± 1.25	5.45 ± 0.66	8.37 ± 3.67	3.82 ± 0.32
Vz (l/kg)	—	1.54 ± 0.49	—	2.24 ± 0.28
Cl (ml/min/kg)	—	14.98 ± 4.78	—	17.81 ± 2.74
F (%)	—	69.69	—	19.73

TABLE 6 | Oral bioavailability and estimated hepatic and gastrointestinal extraction values for YL-IPA08 using ABT blocking metabolism (n = 6).

Treatment	$F_{p.o.}$ (%)	F_h (%)	F_g (%)	E_g (%)	E_h (%)
No ABT	6	17	35	65	83
ABT i.v.	20	80	25	75	20
ABT p.o.	70	83	84	16	17

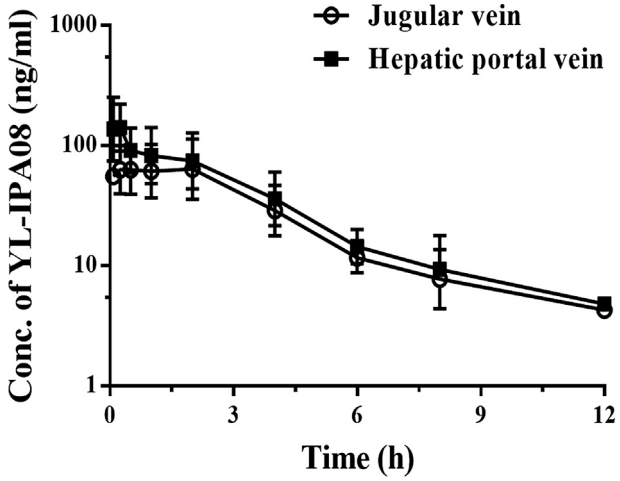

FIGURE 5 | Jugular vein and portal vein plasma concentrations of YL-IPA08 after oral administration (1 mg/kg) in double cannulated rats. Error bars represent the standard deviation of the mean concentration (n = 5).

microsomes is limited by a lack of consensus on the appropriate scaling factors and a low availability of high-quality tissue. In the present study, *in vitro* metabolic stability of YL-IPA08 was performed in liver microsomes and intestinal microsomes of rat and human in the presence of NADPH and UDPGA to identify the metabolizing enzyme, organ, and species difference. 1 μM of YL-IPA08 was incubated in liver microsomes due to the K_m values (1–3 μM) had been obtained in pilot enzyme kinetic study. The results indicated that CYP-mediated intrinsic clearances in HLM and RLM were very rapid. UGT is not involved in the depletion of YL-IPA08. Although the CYP-mediated elimination in HIM and RIM were also observed, with great difference of enzyme expression level between liver and gut, the contribution of intestinal metabolism to the oral bioavailability is hard to define. Especially, as for the RIM stability study, the significantly minimal turnover rate was mainly due to lack of normal activity. *In vitro* results from rat and human regents provided an evidence that metabolic characters of YL-IPA08 had no obvious species difference between rat and human. The contributions of hepatic and intestinal metabolism of YL-IPA08 were further investigated in *in vivo* models.

Portal vein and jugular vein double cannulation rat and ABT pretreated via different routes to inhibit CYP functions of rats were available models to differentiate liver and gut contribution to first-pass effect. In rats, administration of the panel CYP inhibitor ABT via the intravenous route (which inhibits only hepatic CYP enzymes) and the oral route (which inhibits both intestinal and hepatic CYP enzymes) can be used to assess the relative roles of the intestine and liver in the first-pass metabolism (Strelevitz et al., 2006). Double cannulation rats are also useful for separately assessing intestinal and hepatic first-pass effects (Murakam et al., 2003). This method, in which the animal is not restricted or under anesthesia, allows us to obtain reliable measurement of individual first pass effects in the intestine and liver. In the current study, we compared the two models simultaneously. After pretreated with ABT through i.v. injection and oral gavage according to recommended dosages, oral bio-availabilities elevated from 6 to ~20% and then to ~70%. Under the assumption of 100% absorption, hepatic and gut extraction ratios of YL-IPA08 were calculated to be 65 and 83%, respectively, indicating the contributions of liver and intestine to the first-pass effect are similar. In double cannulation rat model, F_aF_g value was 22%, which also indicated that if F_a is 100%, extraction of gut metabolism is 78%. This outcome is very close to the ABT inhibition study. However, at the same dose (1 mg/kg) via oral administration, the plasma concentrations from jugular vein in double cannulation rats were higher than the normal rats (**Figures 3**, **5**). The difference may be explained that the surgery altered the physiological and hematological conditions to some extent.

Apart from metabolism of intestine and liver, absorption fraction (F_a) can also affect oral bioavailability. Aqueous solubility, permeability and efflux potential of YL-IPA08 are determine factors. YL-IPA08 employed high solubility. In the present study, Caco-2 cell model was utilized to evaluate the permeability across gut wall. $P_{appA\text{-}B}$ and $P_{appB\text{-}A}$ values of YL-IPA08 was 3.99×10^{-6}

and 2.63 × 10^{-6} cm/s along with reasonable quality controls, suggesting that concentration gradient-driven passive transport cannot limit the oral bioavailability of YL-IPA08. Additionally, minimal parent recovery in feces with well less than 1% (0.004%, data not shown) in mass balance study in rats via oral administration also reflected complete absorption of YL-IPA08.

As a CNS targeted drug, BBB penetration assessment is an extra consideration to connect pharmacology. Definitive $K_{p,uu}$ is a well-recognized parameter to estimate brain espouse. $K_{p,uu}$ consists of two concepts, a) free (unbound) drug concentration at the site of action leads to pharmacological activity, and b) the free drug concentration at steady state is the same across any bio-membrane. Typically, $K_{p,uu}$ is obtained from the unbound AUC of brain and of plasma. Owing to the rapid metabolism of YL-IPA08 in gut and liver, steady state is hard to be maintained following a single dosing. In the current study, efforts were made to rapidly obtain steady-state via i.v. loading dosage combined with i.v. infusion. By using this model, dosing and sample collection is completed only in three rats after steady-state was verified by continuous measuring plasma concentrations (data not shown).

$K_{p,uu}$ in the current investigation is critical to link the PD of *in vitro* and *in vivo* results (see the result part). What is more important is that $K_{p,uu}$ is often preserved across species (Di et al., 2013). Human $K_{p,uu}$ can be estimated using that of rat ($K_{p,uu,\text{human}} \approx K_{p,uu,\text{rat}}$). Thus, unbound drug concentration in human brain can be calculated by using the rat $K_{p,uu,\ \text{rat}}$ times the human unbound plasma concentration [$C_{b,u,\text{human}} \approx K_{p,uu,\text{rat}} \times C_{p,u,\text{human}}$]. At the current stage, if $C_{b,u,\text{human}}$ (4.9 pg/ml) was set as the *in vitro* TPSO-binding activity concentration for the onset efficacy, therapeutic human plasma concentration would be around 27.2 ng/ml according to the calculation. Additionally, no significant species difference between rat and human in gut and liver metabolism was observed in the current study, which will be an important information for the projection to human and first in-human study.

Finally, with gut and liver confirmed as the equal contribution clearance pathway of YL-IPA08, CYP3A is the major metabolizing enzyme involved. The Med ID and pharmacokinetic drug interactions of YL-IPA08 deserve further investigation.

CONCLUSION

Although YL-IPA08 has shown potential antidepressant effect in *in vitro* binding assessment and *in vivo* animal model, great challenge still exists in its clinical therapy in patients, due to uncertain target exposure of the CNS agent. In this study, our result indicated P450-mediated elimination appeared to be important for its extensive first-pass effect with comparative contribution of gut and liver and no species difference was observed. Then, efforts were made to achieve the brain distribution at steady-state. Therapeutic human plasma concentration was predicted in advance with confidence.

DATA AVAILABILITY STATEMENT

The raw data supporting the conclusions of this article will be made available by the authors, without undue reservation, to any qualified researcher.

ETHICS STATEMENT

The animal study was reviewed and approved by Beijing Center for Drug Safety Evaluation. Written informed consent was obtained from the owners for the participation of their animals in this study.

AUTHOR CONTRIBUTIONS

YG, CY, CW, and YX conducted the experiments. YG analyzed the data. YL provided YL-IPA08. XZ and WZ conceived the research. XZ contributed reagents, wrote the manuscript, is responsible for the corresponding. All authors contributed to the article and approved the submitted version.

FUNDING

This work was financially supported by Chinese Major Scientific and Technological Special Project of China (2018ZX09304017).

SUPPLEMENTARY MATERIAL

The Supplementary Material for this article can be found online at: https://www.frontiersin.org/articles/10.3389/fphar.2020.588127/full#supplementary-material

REFERENCES

Court, M. H., Zhang, X., Ding, X., Yee, K. K., Hesse, L. M., and Finel, M. (2012). Quantitative distribution of mRNAs encoding the 19 human UDP-glucuronosyltransferase enzymes in 26 adult and 3 fetal tissues. *Xenobiotica* 42, 266–277. doi:10.3109/00498254.2011.618954

Cubitt, H. E., Houston, J. B., and Galetin, A. (2009). Relative importance of intestinal and hepatic glucuronidation-impact on the prediction of drug clearance. *Pharm. Res. (N. Y.)* 26, 1073–1083. doi:10.1007/s11095-008-9823-9

Darwich, A. S., Neuhoff, S., Jamei, M., and Rostami-Hodjegan, A. (2010). Interplay of metabolism and transport in determining oral drug absorption and gut wall metabolism: a simulation assessment using the "advanced dissolution, absorption, metabolism (ADAM)" model. *Curr. Drug Metabol.* 11 (9), 716–729. doi:10.2174/138920010794328913

Di, L., Rong, H., and Feng, B. (2013). Demystifying brain penetration in central nervous system drug discovery. *J. Med. Chem.* 56, 2–12. doi:10.1021/jm301297f

Fan, X., Li, H., Ding, X., and Zhang, Q. Y. (2019). Contributions of hepatic and intestinal metabolism to the disposition of niclosamide, a repurposed drug with poor bioavailability. *Drug Metab. Dispos.* 7, 756–763. doi:10.1124/dmd.119.086678

Houston, J. B. and Carlile, D. J. (1998). Prediction of hepatic clearance from microsomes, hepatocytes, and liver slices. *Drug Metab. Dispos.* 31, 140–144. doi:10.3109/03602539709002237

Kajbaf, M., Ricci, R., Zambon, S., and Fontana, S. (2013). Contribution of rat intestinal metabolism to the xenobiotics clearance. *Eur. J. Drug Metab. Pharmacokinet.* 38, 33–41. doi:10.1007/s13318-012-0098-5

Kalvass, J. C. and Maurer, T. S. (2002). Influence of nonspecific brain and plasma binding on CNS exposure: implications for rational drug discovery. *Biopharm. Drug Metab Dispos.* 23 (8), 327–338. doi:10.1002/bdd.325

Kaminsky, L. S. and Zhang, Q. Y. (2003). The small intestine as a xenobiotic-metabolizing organ. *Drug Metab. Dispos.* 31, 1520–1525. doi:10.1124/dmd.31.12.1520

Karlsson, F. H., Bouchene, S., Hilgendorf, C., Dolgos, H., and Peters, S. A. (2013). Utility of in vitro systems and preclinical data for the prediction of human intestinal first-pass metabolism during drug discovery and preclinical development. *Drug Metab. Dispos.* 41, 2033–2046. doi:10.1124/dmd.113.051664

Li, Z., Zhang, Y., Gao, Y., Xiang, Y., Zhang, W., Lu, C., et al. (2019). Atipamezole is a promising non-discriminative inhibitor against pan-CYP450 including diclofenac 49-hydroxylation: a comparison with ABT for drug ADME optimization and mechanism study. *Eur. J. Pharmaceut. Sci.* 130, 156–165. doi:10.1016/j.ejps.2019.01.010

Linder, C., Renaud, N., and Hutzler, J. (2009). Is 1-aminobenzotriazole an appropriate *in vitro* tool as a nonspecific cytochrome P450 inactivator? *Drug Metab. Dispos.* 37, 10–13. doi:10.1124/dmd.108.024075

Liu, F., Zhuang, X., Yang, C., Li, Z., Xiong, S., Zhang, Z., et al. (2014). Characterization of preclinical *in vitro* and *in vivo* ADME properties and prediction of human PK using a physiologically based pharmacokinetic model for YQA-14, a new dopamine D3 receptor antagonist candidate for treatment of drug addiction. *Biopharm. Drug Metab Dispos.* 35, 296–307. doi:10.1002/bdd.1897

Matsuda, Y., Konno, Y., Satsukawa, M., Kobayashi, T., Takimoto, Y., Morisaki, K, et al. (2012). Assessment of intestinal availability of various drugs in the oral absorption process using portal vein-cannulated rats. *Drug Metab. Dispos.* 40, 2231–2238. doi:10.1124/dmd.112.048223

Murakami, T., Nakanishi, M., Yoshimori, T., Okamura, N., Norikura, R., and Mizojiri, K. (2003). Separate assessment of intestinal and hepatic first-pass effect using a rat model with double cannulation of the portal and jugular veins. *Drug Metabol. Pharmacokinet.* 18 (4), 252–260. doi:10.2133/dmpk.18.252

Nakanishi, T. and Tamai, I. (2015). Interaction of drug or food with drug transporters in intestine and liver. *Curr. Drug Metabol.* 16 (9), 753–764. doi:10.2174/1389200216091512011135 37

Obach, R. S. (2001). The prediction of human clearance from hepatic microsomal metabolism data. *Curr Opin Drug Devel.* 4 (1), 36–44.

Ohno, S. and Nakajin, S. (2009). Determination of mRNA expression of human UDP-glucuronosyltransferases and application for localization in various human tissues by real-time reverse transcriptase-polymerase chain reaction. *Drug Metab. Dispos.* 37, 32–40. doi:10.1124/dmd.108.023598

Pinna, G. (2010). In a mouse model relevant for post-traumatic stress disorder, selective brain steroidogenic stimulants (SBSS) improve behavioral deficits by normalizing allopregnanolone biosynthesis. *Behav. Pharmacol.* 21, 438–450. doi:10.1097/FBP.0b013e32833d8ba0

Rupprecht, R., Rammes, G., Eser, D., Baghai, T. C., Schule, C., Kucher, K., et al. (2009). Translocator protein (18 kD) as target for anxiolytics without benzodiazepine-like side effects. *Science* 325, 490–493. doi:10.1126/science.1175055

Strelevitz, T. J., Foti, R. S., and Fisher, M. B. (2006). *In vivo* use of the P450 inactivator 1-aminobenzotriazole in the rat: varied dosing route to elucidate gut and liver contributions to first-pass and systemic clearance. *J. Pharmaceut. Sci.* 95, 1334–1341. doi:10.1002/jps.20538

Suzuki, A., Iida, I., Hirota, M., Akimoto, M., Higuchi, S., Suwa, T., et al. (2003). CYP isoforms involved in the metabolism of clarithromycin *in vitro*: comparison between the identification from disappearance rate and that from formation rate of metabolites. *Drug Metabol. Pharmacokinet.* 18, 104–113. doi:10.2133/dmpk.18.104

Waters, N. J., Jones, R., Williams, G., and Sohal, B. (2008). Validation of a rapid equilibrium dialysis approach for the measurement of plasma protein binding. *J. Pharm. Sci.* 97, 4586–4595. doi:10.1002/jps.21317

Zeng, X., Su, W., Zheng, Y., He, Y., He, Y., Rao, H., et al. (2019). Pharmacokinetics, tissue distribution, metabolism, and execration of naringin in aged rats. *Front. Pharmacol.* 10, 34. doi:10.3389/fphar.2019.00034

Zhang, L. M., Wang, Y. L., Liu, Y. Q., Xue, R., Zhang, Y. Z., Yang, R. F., et al. (2017). Antidepressant-like effects of YL-IPA08, a potent ligand for the translocator protein (18 kDa) in chronically stressed rats. *Neuropharmacology* 113, 567–575. doi:10.1016/j.neuropharm.2016.11.004

Conflict of Interest: The authors declare that the research was conducted in the absence of any commercial or financial relationships that could be construed as a potential conflict of interest.

frontiers in Pharmacology

ORIGINAL RESEARCH
published: 30 November 2020
doi: 10.3389/fphar.2020.588286

Semi-Mechanistic Modeling of HY-021068 Based on Irreversible Inhibition of Thromboxane Synthetase

Ping Li[1†], Jie Huang[2†], Donghao Geng[1], Peihua Liu[1], Zhaoxing Chu[1], Jianjun Zou[3], Guoping Yang[2]* and Li Liu[1]**

[1]Center of Pharmacokinetics and Metabolism, School of Pharmacy, China Pharmaceutical University, Nanjing, China, [2]Center of Clinical Pharmacology, The Third Xiangya Hospital of Central South University, Changsha, China, [3]Department of Clinical Pharmacology, Nanjing First Hospital, Nanjing Medical University, Nanjing, China

OPEN ACCESS

Edited by:
Constantin Mircioiu,
Carol Davila University of Medicine and Pharmacy, Romania

Reviewed by:
Fusun Fusun,
Middlesex Community College, United States
John M. Rimoldi,
University of Mississippi, United States
Valentina Anuta,
Carol Davila University of Medicine and Pharmacy, Romania

***Correspondence:**
Jianjun Zou
zoujianjun100@126.com
Guoping Yang
ygp9880@163.com
Li Liu
liulee@cpu.edu.cn

†These authors have contributed equally to this work.

Specialty section:
This article was submitted to Drug Metabolism and Transport, a section of the journal Frontiers in Pharmacology

Received: 28 July 2020
Accepted: 13 October 2020
Published: 30 November 2020

Citation:
Li P, Huang J, Geng D, Liu P, Chu Z, Zou J, Yang G and Liu L (2020) Semi-Mechanistic Modeling of HY-021068 Based on Irreversible Inhibition of Thromboxane Synthetase. Front. Pharmacol. 11:588286. doi: 10.3389/fphar.2020.588286

Background: HY-021068 [4-(2-(1H-imidazol-1-yl) ethoxy)-3-methoxybenzoate], developed by Hefei Industrial Pharmaceutical Institute Co., Ltd. (Anhui, China), is a potential thromboxane synthetase inhibitor under development as an anti-platelet agent for the treatment of stroke. A semi-mechanistic pharmacokinetic/pharmacodynamic (PK/PD) model was developed to characterize the PK of HY-021068 and its platelet aggregation inhibitory effect in beagle dogs.

Method: Beagle dogs received single oral administration of 2.5 mg/kg HY-021068 or consecutively oral administration of 5 mg/kg HY-021068 once daily for 7 days. The plasma concentration of HY-021068 and the platelet aggregation rate (PAR) were determined by liquid chromatography tandem-mass spectrometry (LC-MS/MS) assay and a photometric method, respectively. The PK/PD data was sequentially fitted by Phoenix NLME. The PK/PD parameters of HY-021068 in beagle dogs were estimated by 2.5 and 5 mg/kg dosing on the 1st day, and then used to simulate the PAR of HY-021068 on the 7th day after 5 mg/kg dosing daily.

Result: A one-compartment model with saturable Michaelis-Menten elimination was best fitted to the PK of HY-021068. A mechanistic PD model based on irreversible inhibition of thromboxane synthetase was constructed to describe the relationship between plasma concentration of HY-021068 and PAR. Diagnostic plots showed no obvious bias. Visual predictive check confirmed the stability and reliability of the model. Most of PK/PD observed data on the 7th day after 5 mg/kg dosing fell in the 90% prediction interval.

Conclusion: We established a semi-mechanistic PK/PD model for characterizing the PK of HY-021068 and its anti-platelet effect in beagle dogs. The model can be used to predict the concentration and PAR under different dosage regimen of HY-021068, and might be served as a reference for dose design in the future clinical studies.

Keywords: pharmacokinetic/pharmacodynamic model, platelet aggregation rate, HY-021068, pharmacokinetic, thromboxane A_2

INTRODUCTION

Stroke is the most common cause of mortality worldwide and is the second leading cause of long-term disability (Sila and Schoenberg, 2011; Alkagiet et al., 2018). Arachidonic acid (AA) is metabolized to TXA_2 by cyclooxygenase (Cox) and thromboxane synthase (TXS). TXA_2 is a potent platelet aggregation activator, which contributes to an increase in cytosolic Ca^{++} concentration, further activating calmodulin-dependent myosin light chain phosphorylation and diacylglycerol-dependent cytosolic pleckstrin phosphorylation to induce platelet aggregation (Cho et al., 2011). Anti-platelet drug, such as aspirin, indomethacin, and triflusal, can reduce TXA_2 formation by inhibiting the activity of COX or TXS, which have a protective effect against cerebral infarction (Mayr and Jilma, 2006; Murdoch and Plosker., 2006; Shin et al., 2018).

HY-021068 (4-(2-(1H-imidazol-1-yl) ethoxy)-3-methoxybenzic acid) (**Figure 1**) is a promising Class I new drug as an anti-platelet agent under phase I clinical trial developed by Hefei Industrial Pharmaceutical Institute Co., Ltd. (Anhui, China), which is an analog of Dazoxiben (a TXS inhibitor) (Vittorio et al., 1984). It showed protective effect on focal cerebral ischemia and reperfusion injury through inhibiting platelet aggregation. Previous study (Zhou et al., 2014; Yang et al., 2015) indicated that HY-021068 treatment could improve performance in neurological deficit and the Y-maze test as well as reduce the infarct volume in ischemia-reperfusion rats induced by middle cerebral artery occlusion. Incubation of HY-021068 (3×10^{-5} and 10^{-5} M) significantly reduced TXB_2 (stable metabolite of TXA_2) formation in rat brain microvascular endothelial cells after hypoxia/reoxygenation treatment (Zhou et al., 2014). HY-021068 can inhibit platelet aggregation induced by adenosine 5′-diphosphate or U46619 in a dose-dependent manner *in vivo* and *in vitro* (Yang et al., 2015). The results indicated that the anti-platelet aggregation effect of HY-021068 was strongly correlated with the inhibition of TXA_2 formation. AA was widely used as platelet agonists (Pyo et al., 2007; Andrioli et al., 2015; Olivier et al., 2016) in the platelet aggregation test. For example, AA-stimulated platelet aggregation was used to evaluate the anti-platelet activity of aspirin (Temperilli et al., 2015) and YS-49, YS-51 (Pyo et al., 2007). Therefore, AA was selected as a platelet aggregation stimulator to evaluate the anti-platelet aggregation activity of HY-021068 in our study.

Pharmacokinetic/pharmacodynamic (PK/PD) model has been widely applied in preclinical and clinical drug research (Liu et al., 2011; Yun et al., 2014; Li et al., 2016). PK/PD model is established by a series of equations to quantify the behavior and action of the drug *in vivo*. A well-constructed PK/PD model can help people better understand the time-course of drug efficacy and provide reference for future experiments and trials.

Platelet aggregation rate (PAR) is widely used for assaying platelet function (Mckenzie et al., 1999) and has been the pharmacodynamic indicator of many PK/PD models for anticoagulants (Yun et al., 2014; Jiang et al., 2016). The PK/PD studies of antiplatelet drugs via modeling have been reported previously (Woo et al., 2002; Hochlolzer et al., 2005; Lee et al., 2012; Ruzov et al., 2015). However, none of them share the same mechanism with HY-021068. To quantitatively assess the PK/PD properties of HY-021068 based on its inhibitory effect of TXS, we established the semi-mechanistic PK/PD model to mathematically describe the relationship between the PK of HY-021068 and the PAR.

METHOD

Reagents and Materials

HY-021068 (purity 99.68%) was provided by Hefei Industrial Pharmaceutical Institute Co., Ltd. (Anhui, China). Terazosin internal standard (IS) was purchased from National Institutes for Food and Drug Control (Beijing, China). Aspirin enteric-coated tablets were purchased from CSPC Pharmaceutical Co., Ltd. Methanol and acetonitrile of high-performance liquid chromatography (HPLC) grade were obtained from Merck (Darmstadt, Germany). All the other reagents were analytical grade. Water was purified using a Milli-Q Ultrapure Water System (Millipore, Bedford, MA, United States).

Animals

Twenty-four adult beagle dogs (12 male and 12 female, weighing 8–10 kg) were purchased from Yizheng an Li Mao Biotechnology Co., Ltd. They were housed in an environmentally controlled room temperature and humidity on a 12 h light/dark cycle. Water and food were provided ad libitum. All animal experiments were approved by the Animal Ethics Committee of China Pharmaceutical University (No. CPU-PCPK-1622010751).

Experimental Design

Twenty-four beagle dogs were randomly divided into four groups, with six dogs in each group (half male and half female). I group, which received a single oral dose of 2.5 mg/kg HY-021068. About 1 ml blood samples were collected from the cephalic vein of the forelimb at pre-dose and at 0.0833, 0.25, 0.5, 0.75, 1, 1.5, 2, 3, 4, 6, 8, 10, 12, 14 h after the drug administration. The collected blood samples were divided in two aliquots. One aliquot was used to determine the concentration of HY-021068. The other was used for the platelet aggregation test. II group, which received 5 mg/kg HY-021068

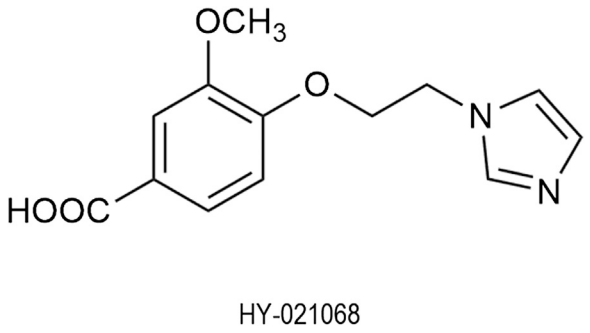

FIGURE 1 | Chemical structure of HY-021068.

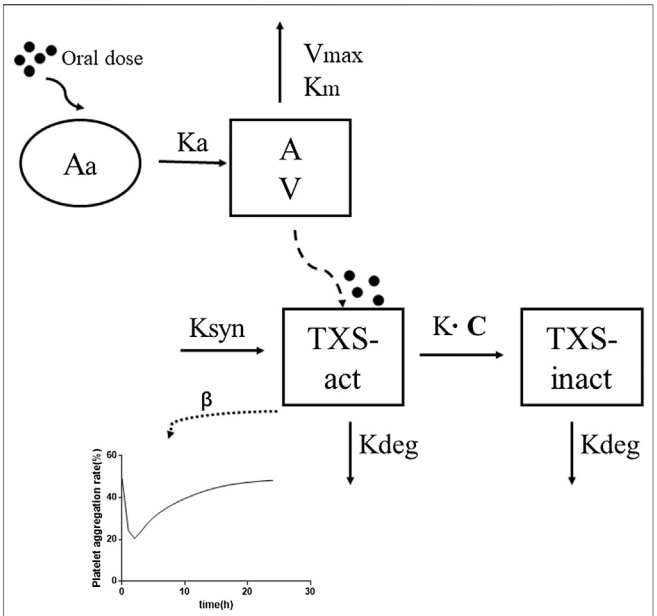

FIGURE 2 | The schematic diagram of pharmacokinetic/pharmacodynamic model of HY-021068.

once daily for consecutive 7 days. After the first and last drug administration, blood samples were collected as the same time points as before. III group (blank control), which received the same volume of vehicle (0.5% sodium carboxymethycellulose). Blood samples were collected as the same time points as before. Shuldiner Blood samples were collected at pre-dose and at 0.25, 0.5, 0.75, 1, 1.5, 2, 3, 4, 6, 8, 10, 12 h after aspirin administration for the platelet aggregation test.

Platelet Aggregation Test

One aliquot of the blood sample collected from six beagle dogs in each group at each timepoint was used for platelet aggregation test. The anti-platelet activity of HY-021068 was evaluated by platelet aggregation test according to previous studies (Shuldiner et al., 2009; Andrioli et al., 2015; Olivier et al., 2016). Platelet-rich plasma (PRP) was isolated by centrifugation of blood samples at 160 g for 10 min. The supernatant was PRP and the remaining specimen was further centrifuged at 2000 g for 10 min to obtain platelet-poor plasma (PPP). The platelet counting and platelet aggregation were both measured by LBY-NJ4 platelet aggregation analyzer (Precil, Beijing, China). The platelet concentration was adjusted to 20×10^4/μl for PRP before aggregation analysis. 100% transmission values were calibrated using PPP samples. The measurements were performed by adding 10 μl AA (1 mM) to 200 μl PRP in a transparent silica tank maintained at 37°C with agitation at 1,000 rpm. Platelet aggregation was monitored for 5 min. The maximum PAR was the maximum percent change in optical density with PRP after adding aggregation agonist. The results of platelet aggregation were expressed as the maximum PAR.

Model Development

The PK profiles of HY-021068 was first analyzed by non-compartmental analysis using Phoenix WinNonlin software. The dose-normalized area under the curve (AUC) values were compared by Student's t test. The PK/PD analysis was performed using Phoenix NLME (version 7.0, Certara, Co., Princeton, NJ, United States). All parameters were estimated using NLME's first-order conditional estimated extended least squares (FOCE-ELS) method. The PK/PD parameters of HY-021068 in beagle dogs were estimated by 2.5 and 5 mg/kg dosing on the 1st day, and then used to simulate the PAR of HY-021068 on the 7th day after 5 mg/kg dosing daily. The schematic diagram of PK/PD model was shown in **Figure 2**. The details of PK/PD model were as follows.

Pharmacokinetic Model

HY-021068 concentration-time profiles were described by compartmental models in beagle dogs. One-, two-, three-compartment model with first-order absorption and saturable Michaelis-Menten elimination were tested to fit the pharmacokinetic data. The equations for final selected model are shown below:

$$\frac{dA_a}{dt} = -K_a \times A_a$$

$$\frac{dA_1}{dt} = -K_a \times A_a - \frac{V_{max} \times C}{K_m + C}$$

$$C = A_1/V$$

Where A_a and A_1 are amounts of HY-021068 in the absorption and central compartments, respectively. V_{max} and K_m are the Michaelis-Menten constants for elimination process.

Pharmacodynamic Model

A sequential PK-PD modeling approach (Zhang et al., 2003) was applied to describe the time course of concentration of HY-021068 and PAR. Irreversible inhibitory effect model was used based on its pharmacology mechanism. We assume 1) HY-021068 reduced TXA_2 entirely by inactivating TXS. 2) PAR was directly proportional to the amount of active TXS.

$$\frac{dE_{act}}{dt} = K_{syn} - K_{deg} \times E_{act} - K \times C \times E_{act}$$

$$PAR = \beta \times \frac{E_{act}}{E_0} \times 100\%$$

$$E_0 = \frac{K_{syn}}{K_{deg}}$$

Where β is a coefficient corresponding to HY-021068 efficacy, E_{act} is the amount of active TXS *in vivo*, K_{syn} is the zero-order synthesis rate and K_{deg} is a first-order elimination rate constant of TXS. HY-021068 inactivates platelet TXS irreversibly with the second-order rate constant, K. E_0 is the amount of active TXS in blood before HY-021068 administration.

Random Effect Model

The intra-individual variability for PK data between observed and predicted values was best described by proportional model.

$$\mathrm{CObs} = \mathrm{C} \times (1 + \mathrm{Ceps})$$

The intra-individual variability for PD data between observed and predicted values was best described by a mixed error model as follows.

$$\mathrm{PARObs} = \mathrm{PAR} + \mathrm{PAReps} \times \sqrt{1 + (\mathrm{multStdev/sigma}())^2}$$

The inter-individual variablity model used log-additive model.

$$\mathrm{P}_i \times \mathrm{tvP} \times \exp(\eta_i)$$

Where CObs and PARObs are the observed values for PK and PD data, and Ceps and PAReps are the residual error assumed to be normally distributed with mean 0 and variance of σ^2. Multiplicative sigma is a fixed effect called multStdev. "sigma()" is a built-in function which means the estimate of SD of PAReps. $\mathrm{P_i}$ is the parameter for the *i*th individual. TvP is the typical value of the parameter in the population, and ηi is the interindividual variability of the parameter with mean 0 and variance of ω^2.

Model Evaluation and Validation

General goodness-of-fit was evaluated by diagnostic plots, such as observed HY-021068 plasma concentration or PAR vs. predicted concentration or PAR, conditional weighted residuals (CWRES) vs. predicted values or time.

Final population PK/PD models were evaluated using a simulation that involves 1,000 data sets from the final model parameters, 90% confidence intervals were computed and presented for visual inspection along with the original dataset. The predictive ability of our model was further assessed in the remaining dataset gained from 5 mg/kg oral dosing for consecutive 7 days.

LC-MS/MS Analysis of HY-021068

The LC–MS/MS system consisted of a Shimadzu Nexera HPLC system and a triple-quadrupole tandem mass spectrometer of Shimadzu MS-8030 system (Kyoto, Japan). An aliquot of 5 μL extracted sample was performed at 40°C using a Shim-pack VP-ODS analytical column (2.0 × 150 mm, 5 μm, Shimadzu, Japan) for separation. The mobile phase consisted of Milli-Q water containing 0.1% formic acid (mobile phase A) and methanol (mobile phase B) at a flow rate of 0.2 ml/min. The gradient elution was: 0–0.2 min, 12% B; 0.2–0.4 min, 12–60% B; 0.4–4.5 min, 60% B; 4.5–4.7 min, 60–12% B; 4.7–8.5 min,12% B (v/v). The last 3.8 min was held to re-equilibrate. The overall run time to determine the concentration of HY-021068 was 8.5 min.

The mass spectrometer used electrospray ionization in the positive ion mode, and the detection of the ions was obtained in the multiple reaction monitoring (MRM) mode. It monitored the transitions of protonated precursor ion at m/z 263.10→68.10 for HY-021068 and m/z 388.15→290.20 for internal standard (IS, terazosin). Mass spectrometric conditions for analysis were optimized as follows: 4.5 kV interface voltage, 1.72 kV detector voltage, 300°C desolation temperature, 400°C heat block temperature, 3 L/min nebulizing gas flow (nitrogen), 15 L/min drying gas flow (nitrogen), and 230 kPa collision induced dissociation (CID) gas pressure (argon). Compounds parameters, Q1 Pre Bias, collision energy (CE) and Q3 Pre Bias, were −23, −38 and −14 V for HY-021068 and −13, −30 and −18 V for IS, respectively.

Stock solutions of both HY-021068 and IS were prepared by dissolving required amounts of reference standard in methanol at a 1.0 mg/ml concentration. The stock solution was serially diluted to working solution of desired concentrations with methanol. The IS working solution was performed by diluting the IS stock solution (1 mg/ml) to final concentration of 1,000 ng/ml with methanol. Calibration standards were prepared by adding the appropriate amounts of the standard solutions into blank plasma giving concentrations of 7.8, 15.6, 31.25, 62.5, 125, 250, 500 and 1,000 ng/ml for HY-021068. For method validation, three concentration levels (15.6, 125 and 800 ng/ml) were prepared for the quality control (QC) samples as the low, medium and high concentration.

An aliquot of 50 μl plasma and 10 μl of IS (1,000 ng/ml) were added into a 1.5 ml centrifuge tube. The mixture was extracted by 1 ml of ethyl acetate, with vertexing for 10 min. After centrifugation at 11,350 g for 10 min, the supernatant (800 μl) was quantitatively transferred into a clean 1.5 ml centrifuge tube and then evaporated to dryness in a vacuum evaporator (Thermo, Waltham, Massachusetts, United States). The residue was reconstituted in 500 μL mobile phase followed by ultracentrifugation at 26000 g for 10 min. An aliquot of 5 μL supernatant was injected into the LC-MS/MS system for analysis.

Bioanalytical Method Validation

According to FDA guidance (FDA, 2018)for bioanalytical method validation, a full validation was performed for the concentration measurement of HY-021068 in beagle dogs.

Selectivity

Selectivity was investigated by the comparison of blank plasma from six individual beagle dogs to the corresponding spiked plasma samples to exclude interference of endogenous substances and metabolites. No obvious interferences from endogenous plasma substances were observed at the retention time of the analytes or IS.

Linearity and Lower Limits of Quantification

Three calibration curves of HY-021068 were performed with eight concentrations (7.8, 15.6, 31.25, 62.5, 125, 250, 500 and 1,000 ng/ml). The linearity of each calibration curve was determined by plotting the peak area ratio (y) of analytes to IS vs. the corresponding concentration (x) of analytes with weighted ($1/x^2$) least square linear regression. The LLOQ of HY-021068 was defined as the lowest concentration plasma level on the calibration curves (7.8 ng/ml), at which the analyte should be

TABLE 1 | The intra- and inter-day precision and accuracy of analytes (3 days, five replicates per-day).

Spiked conc. (ng/ml)	Inter-day (n = 15)			Intra-day (n = 5)		
	Measured conc. (ng/ml)	RSD (%)	Accuracy (%)	Measured conc. (ng/ml)	RSD (%)	Accuracy (%)
7.8	7.7 ± 0.5	6.52	98.68	7.54 ± 0.51	6.79	96.68
15.6	15.94 ± 0.89	5.56	102.04	16.33 ± 0.84	5.17	104.48
125	127.28 ± 5.86	4.6	101.82	132.85 ± 5.17	3.89	106.28
800	759.81 ± 33.91	4.46	94.98	787.41 ± 18.98	2.41	98.43

TABLE 2 | The long-term (15 days) stability of analytes.

Spiked conc. (ng/ml)	Stability (n = 5)		
	Measured conc. (ng/ml)	RSD (%)	Accuracy (%)
15.6	14.31 ± 1.85	12.9	91.73
800	837.59 ± 109.99	13.13	104.7

quantified with acceptable accuracy (80–120%) and precision (≤20%).

Calibration curve showed good linearity at 7.8–1,000 ng/ml for HY-021068. The mean (±SD) regression equation from three replicate calibration curves was:

$$Y = (0.0094 \pm 0.0003) \times X + (0.027 \pm 0.0047) \left(R^2 \geq 09969\right)$$

where Y was the ratio of peak area of HY-021068 to IS, and X was the HY-021068 concentration. The LLOQ of HY-021068 was 7.8 ng/ml. Data for lower limits of quantifications (LLOQ) are shown in **Table 1**.

Precision and Accuracy

The intra-day precision and accuracy of the method were assessed by analyzing the QC samples five times on a single day, and the inter-day precision and accuracy were estimated by determining the QC samples over three consecutive days. Relative standard deviation (RSD) and relative error (RE) were used to express the precision and accuracy, respectively. The intra- and inter-day precision should not exceed 15% for the QC samples and accuracy should be within ±15% for the QC samples. The data for accuracy and precision are shown in **Table 1**. These results demonstrated that the method was reliable and reproducible.

Matrix Effect

The matrix effect was evaluated by comparing the analyte peak areas resolved in the blank extracted plasma samples with the same pure reference standard solutions prepared in the reconstitution solution.

The matrix effects of the analytes derived from QC samples were 98.44 and 107.46% for low and high concentration. The results indicated that no apparent matrix effect was observed.

Stability

The long-term stability test of analytes in beagle dog plasma was assessed by analyzing the QC samples at low and high concentration levels (n = 5) stored at −80°C for 15 days.

Results of long-term stability are shown in **Table 2**. The results showed good stability under the storage condition.

Dilution Integrity Test

Concentrations of the HY-021068 obtained from beagle dog plasma may be higher than the calibration range used for the validation analysis. In such cases, dilution integrity experiment should be investigated to analyze higher analyte concentrations above upper limit of quantification (ULOQ). Dilution of samples should not interfere with the accuracy and precision. The test was carried out at eight times the ULOQ concentration. Five replicates each of 1/10 concentration were prepared and their concentrations were calculated by applying the dilution factor 10 against the freshly prepared calibration curve.

The dilution integrity test was determined by measuring the accuracy and precision for samples which underwent ten times dilution with blank beagle dog plasma. The accuracy was 100.36%, representing that a ten times dilution with blank beagle dog plasma was stable.

RESULT

Pharmacokinetics

Noncompartmental analysis of the PK profiles indicated nonlinear PK in the beagle dogs. Dose normalized AUC values after a single oral dose of 2.5 and 5 mg/kg HY-021068 were 0.030 ± 0.008 min × kg/ml and 0.046 ± 0.011 min × kg/ml respectively (p = 0.017), so saturable elimination was assumed. Inclusion of more compartment did not improve the model fit. The pharmacokinetic of HY-021068 was well described using a one-compartment model with saturate elimination. Model fitting and observed plasma concentration following oral dosing was shown in **Figure 3A** and the parameters estimates were presented in **Table 3**. The inter-individual variability (ω) with high shrinkage value (>0.4) was excluded from the PK model to avoid over-parameterization.

The mean V of the population was estimated to be 447.58 ml/kg, suggesting that the distribution of HY-021068

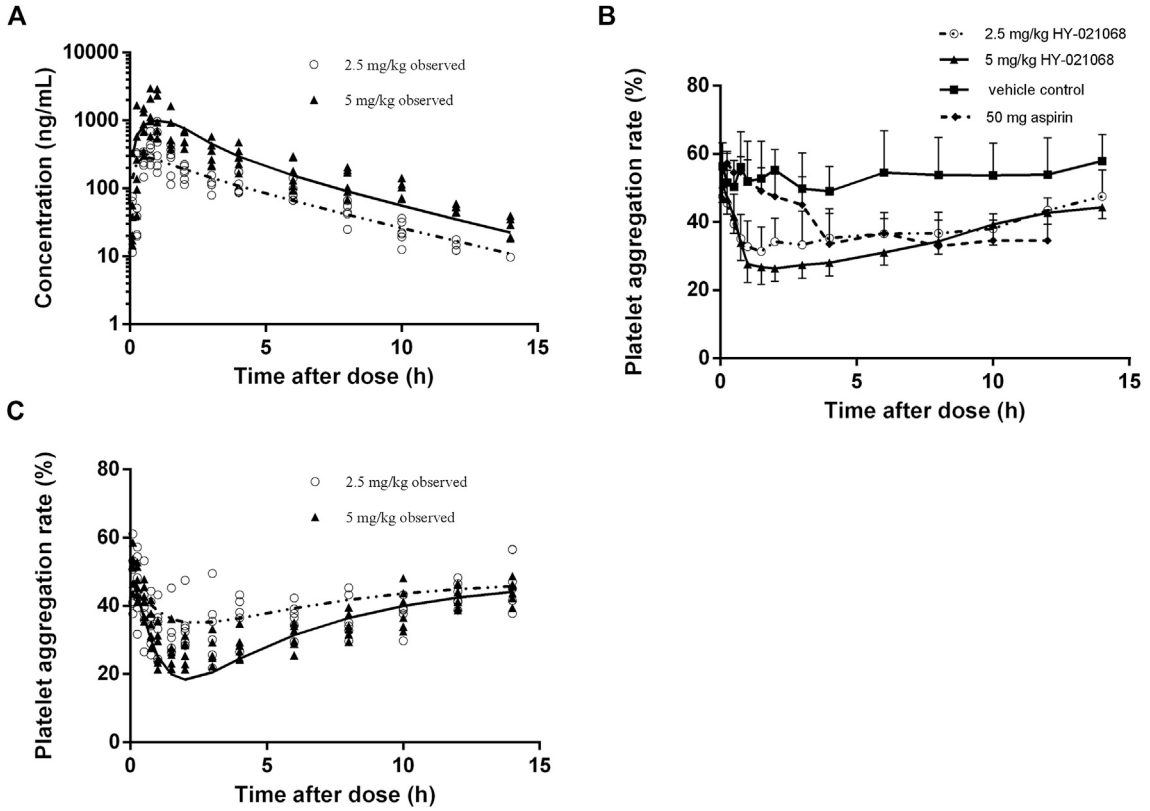

FIGURE 3 | Observed plasma HY-021068 concentration **(A)** and platelet aggregation rate (PAR) **(C)** after a single oral dose of 2.5 mg/kg (open circles, n = 6) and the first administration of multiple doses of 5 mg/kg HY-021068 (triangles, n = 6) to beagle dogs. Curves depict population fittings. (Solid line: 2.5 mg/kg; dashed line: 5 mg/kg). **(B)** Time course of PAR in beagle dogs after oral administration of 2.5 mg/kg HY-021068 (open circles, mean ± SD, n = 6), 5 mg/kg HY-021068 (triangles, mean ± SD, n = 6), 50 mg aspirin (diamond, mean ± SD, n = 6) or vehicle (square, mean ± SD, n = 6).

TABLE 3 | Population PK results of oral administration of HY-021068 to beagle dogs.

Parameter	TvP	CV%	ω
K_a (1/h)	0.21	7.52	0.015
V (ml/kg)	447.58	41.95	0.474
K_m (ng/ml)	237.60	23.85	0.041
V_{max} (ng/h/kg)	1,252,830	14.20	—
Res. Error	1.04	6.81	—

CV%, coefficient of variation; Res. Error, residual error.

TABLE 4 | Population PD results of oral administration of HY-021068 to beagle dogs.

Parameter	TvP	CV%	ω
β	0.475	3.11	—
K_{syn} (ng/h)	88.501	2.54	—
K_{deg} (1/h)	0.515	28.36	0.466
K (ml/ng/h)	0.002	24.96	0.775
MultStdev	0.122	7.27	—
Res. Error	0.003	4.49	—

CV%, coefficient of variation; Res. Error, residual error.

mainly in the body fluid of beagle dogs. The V_{max} and K_m were estimated to be 1,252,830 ng/h/kg and 237.60 ng/ml, which indicated high dose group was more easily to be affected by nonlinear elimination.

Pharmacodynamics

Both 2.5 and 5 mg/kg oral administration of HY-021068 significantly inhibited the aggregation of platelet. The PAR was about 55% at baseline (pre-dose), which reduced to 31.4 and 26.4% after oral administration of 2.5 and 5 mg/kg HY-021068.2.5 mg/kg HY-021068 can achieve similar minimum PAR with aspirin (HY-021068 vs aspirin: 31.4 ± 7.1% vs. 33.6 ± 10.3%) (**Figure 3B**). Model fitting and observed PAR after single oral 2.5 and 5 mg/kg HY-021068 administration were displayed in **Figure 3C** and parameter estimates were listed in **Table 4**. The inter-individual variability (ω) with high shrinkage value (>0.4) was excluded from the PD model to avoid over-parameterization.

Model Evaluation and Validation

The diagnostic plots of the PK-PD model were shown in **Figure 4**. The population-predicted and individual predicted concentration and PAR vs observed values indicated no obvious bias. The

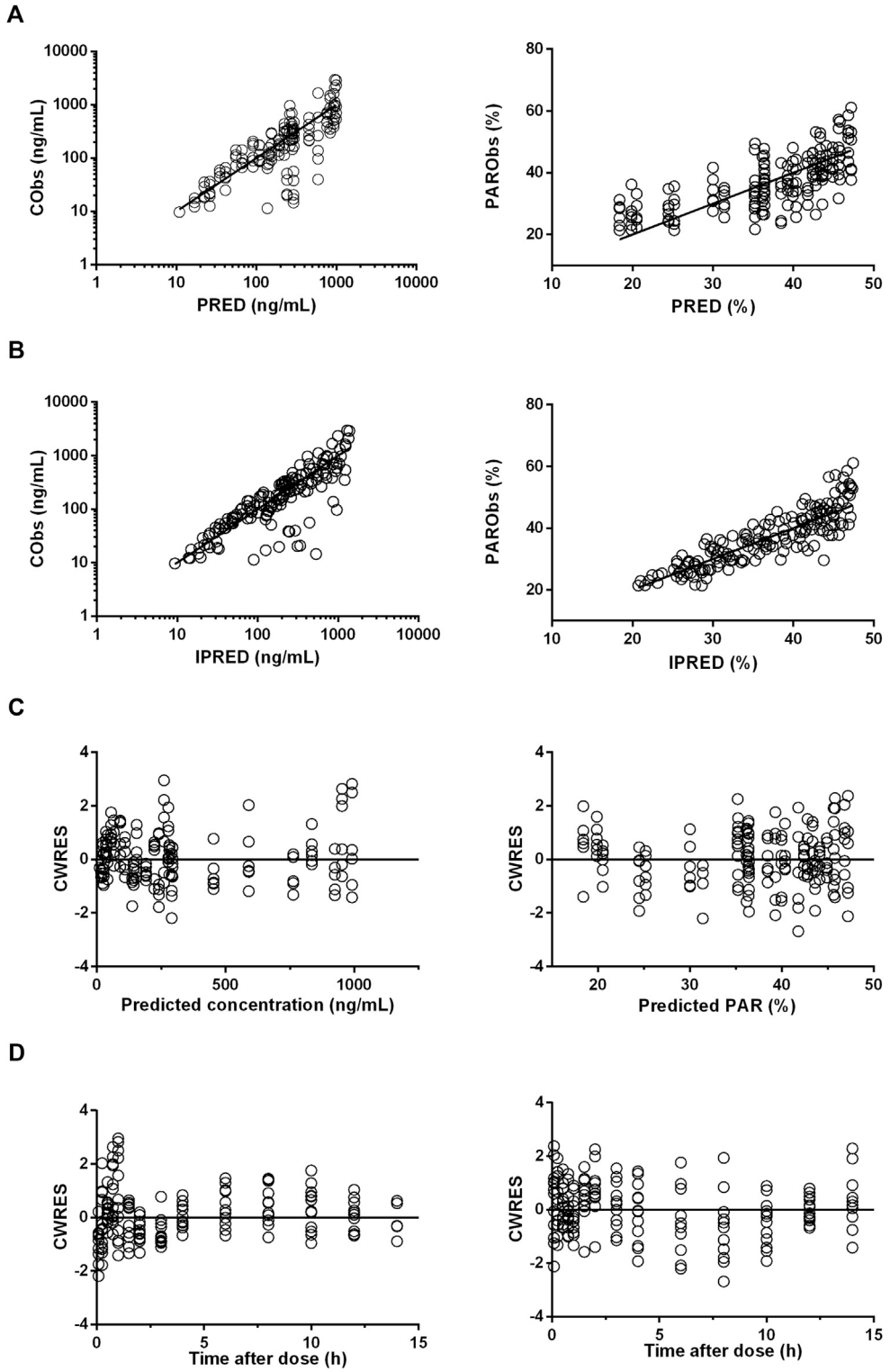

FIGURE 4 | Diagnostic plots for pharmacokinetic (PK) (left panels) and pharmacodynamic (PD) (right panels) profile estimations. **(A)**, The observed values (Obs) vs. population predicted values (PRED). **(B)**, The observed values vs. individual predicted values (IPRED). **(C)**, CWRES vs. population predictions. **(D)**, CWRES vs. time after dose.

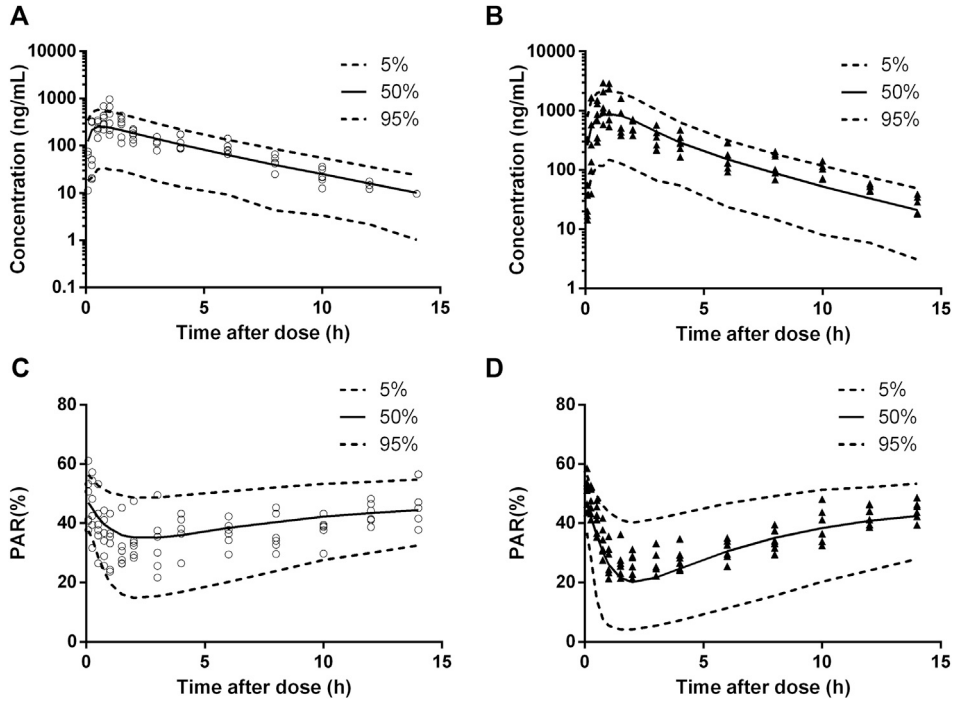

FIGURE 5 | Visual prediction check for pharmacokinetic (PK) and pharmacodynamic (PD) estimation after a single oral dose of 2.5 mg/kg (cicles, n = 6) and the first administration of multiple doses of 5 mg/kg (triangles, n = 6). **(A),** 2.5 mg/kg dosing for PK. **(B),** 5 mg/kg dosing for PK. **(C),** 2.5 mg/kg dosing for PD. **(D),** 5 mg/kg dosing for PD. Solid and dashed lines depict median and 90% CI of model predictions.

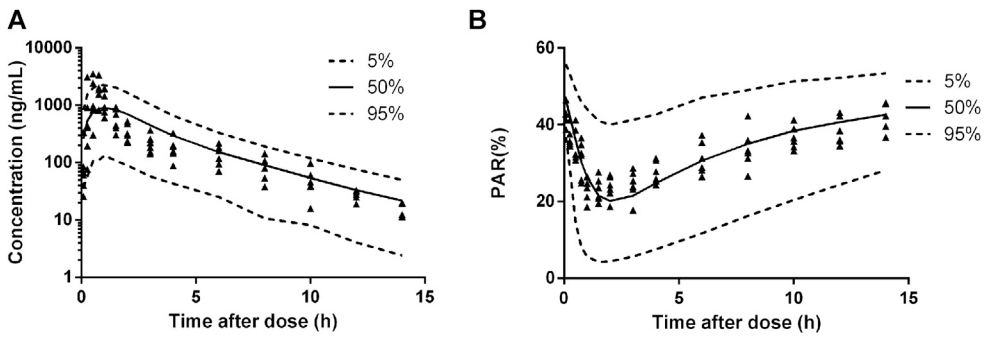

FIGURE 6 | Predicted plasma HY-021068 concentration-time profiles **(A)** and PAR **(B)** in beagle dogs on the 7th day following oral 5 mg/kg administration for consecutive 7 days (n = 6). Solid and dashed lines depict median and 90% CI of model predictions.

scatter plot of CWRES vs predicted values or time after dose (TAD) for PK and PD data showed most conditional weighted residual lay within the range of −2 to 2. The bias for a few concentrations and PAR may due to the variability of C_{max} and determination of efficacy index. Visual prediction check for 2.5 and 5 mg/kg showed almost all observed concentrations and PAR fell into the 5th and 95th percentiles of the simulated data (**Figure 5**). An internal-external validation model was applied (Steyerberg and Harrell, 2015). Simulated results showed that the predicted concentrations and PAR matched well with the observed values on the 7th day after 5 mg/kg dosing for consecutive 7 days (**Figure 6**). No cumulative effect was observed. All of these indicated our model is reasonable and powerful.

DISCUSSION

In this study, a semi-mechanistic PK/PD model based on the irreversible inhibitory of TXS was successfully constructed to model the time course of plasma concentrations of HY-021068 and the PAR.

Many models aimed to depict the time course of PAR have been established before (Awa et al., 2012; Yun et al., 2014). However, this is the first PK-PD model in which irreversible combination of drugs and TXS is considered. By comparing the objective function value under different PK models, the PK of HY-021068 was depicted best using a one-compartment model with first-order absorption and saturated elimination. The population typical values and relative standard errors of K_a, V, K_m and V_{max} for HY-021068 were 0.211 1/h (7.52%), 447.579 ml/kg (41.95%), 237.603 ng/ml (23.85%), 1,252,830 ng/h/kg (14.2%), respectively. This showed the main inter-individual variability of PK data may be due to the differences in apparent volume of distribution among beagle dogs.

Many reports have also demonstrated that platelet activity can be reduced by inhibiting the formation of TXA_2 (Banerjee et al., 2014; Fang et al., 2014). AA was widely used as platelet agonists (Pyo et al., 2007; Andrioli et al., 2015; Olivier et al., 2016) in the platelet aggregation test. HY-021068 targeted the TXS on the AA pathway and inhibited the platelet aggregation by reducing the transformation of AA to TXA_2 (Yang et al., 2015). No active metabolites of HY-021068 were found in previous studies, so anti-platelet activity was only influenced by the parent drug. The indirect effect model and irreversible model were tried to fit the relationship between plasma concentrations and PAR. Although both models showed similar goodness-of-fit during the model fitting process, the irreversible model showed better predictive ability when extrapolated to the multiple dose administration. This also hinted that the underlying binding pattern of HY-021068 and TXS was probably irreversible, which still remains unclear. The population typical values and relative standard errors of β, K_{syn}, K_{deg} and K were 0.475 (3.11%), 88.501 ng/h (2.54%), 0.515 1/h (28.36%) and 0.002 ml/ng/h (24.96%), respectively. The inter-individual variability of PD data may be linked to the differences in the degradation rate of TXS as well as the affinity between HY-021068 and TXS among beagle dogs.

A limitation of the present study was that the synthesis and degradation rate of TXS in beagle dogs have not been reported before, so we obtained the parameters according to the estimate of the model. If the related physiological parameters are reported in the future, the K_{syn} and K_{deg} can be fixed before the run of the PD model. It may be more related to the physical conditions with a minor modification of the present model. Additionally, the structure of the model may be further utilized in clinical experiments in the future.

In conclusion, this study established a mechanism-based PK/PD model for characterizing the pharmacokinetics of HY-021068 and its effect in beagle dogs. The integrated PK/PD model enabled the quantitative description of the relationship between the HY-021068 plasma concentration and its inhibitory effect on platelet aggregation based on the drug pharmacological mechanisms. The final model can be subsequently used to predict the concentration and corresponding effect under different dosages. It provides reference to other drugs that share a similar mechanism with HY-021068. It also offers a fundamental PK/PD model that could be used in humans.

DATA AVAILABILITY STATEMENT

The raw data supporting the conclusions of this article will be made available by the authors, without undue reservation.

ETHICS STATEMENT

The animal study was reviewed and approved by Animal Ethics Committee of China Pharmaceutical University.

AUTHOR CONTRIBUTIONS

PL, JH, JZ, GY, LL participated in research design. DG, PHL, ZC, PL conducted experiments. PL, JH, DG performed data analysis. PL and LL wrote the manuscript.

FUNDING

This work was supported by the National Natural Science Foundation of China (No. 81673505 and 81872930) and the "Double First-Class" University project (No. CPU2018GY22).

REFERENCES

Alkagiet, S., Papagiannis, A., and Tziomalos, K. (2018). Associations between nonalcoholic fatty liver disease and ischemic stroke. *World. J. Hepatol.* 10, 474–478. doi:10.4254/wjh.v10.i7.474

Andrioli, G., Minuz, P., Solero, P., Pincelli, S., and Bellavite, P. (2015). Defective platelet response to arachidonic acid and thromboxane A_2 in subjects with PIA_2 polymorphism of β3 subunit (glycoprotein IIIa). *Br. J. Haematol.* 110, 911–918. doi:10.1046/j.1365-2141.2000.02300.x

Awa, K., Satoh, H., Hori, S., and Sawada, Y. (2012). Prediction of time-dependent interaction of aspirin with ibuprofen using a pharmacokinetic/pharmacodynamic model. *J. Clin. Pharm. Therapeut.* 37, 469–474. doi:10.1111/j.1365-2710.2011.01313.x

Banerjee, D., Mazumder, S., and Sinha, A. K. (2014). The role of inhibition of nitric oxide synthesis in the aggregation of platelets due to the stimulated production of thromboxane A2. *Blood Coagul. Fibrinol.* 25, 585–591. doi:10.1097/MBC.0000000000000111

Cho, H. J., Choi, S. A., Kim, C. G., Jung, T. S., and Park, H. J. (2011). Spinach saponin-enriched fraction inhibits platelet aggregation in cAMP- and cGMP-dependent manner by decreasing TXA_2 production and blood coagulation. *Biomol. Ther.* 19, 218–223. doi:10.4062/biomolther.2011.19.2.218

Fang, W., Wei, J., Han, D., Chen, X., He, G. W., Wu, Q., et al. (2014). MC-002 exhibits positive effects against platelets aggregation and endothelial dysfunction through thromboxane A2 inhibition. *Thromb. Res.* 133, 610–615. doi:10.1016/j.thromres.2014.01.029

FDA (2018). FDA guidance for industry: bioanalytical method validation. Available at: https://www.fda.gov/regulatory-information/search-fda-guidance-documents/bioanalytical-method-validation-guidance-industry (Accessed July, 15 2020).

Hochlolzer, W., Trenk, D., Frundi, D., Blanke, P., Fischer, B., and Andris, K. (2005). Time dependence of platelet inhibition after 600-mg loading dose of clopidogrel in a large, unselected cohort of candidates for percutaneous coronary

intervention. *Circulation* 111, 2560–2564. doi:doi:10.1161/01.CIR. 0000160869. 75810.98

Jiang, X. L., Samant, S., Lewis, J. P., Horenstein, R. B., Shuldiner, A. R., Yerges-Armstrong, L. M., et al. (2016). Development of a physiology-directed population pharmacokinetic and pharmacodynamic model for characterizing the impact of genetic and demographic factors on clopidogrel response in healthy adults. *Eur. J. Pharmaceut. Sci.* 82, 64–78. doi:10.1016/j.ejps. 2015.10.024

Lee, J., Hwang, Y., Kang, W., Seong, S. J., Lim, M. S., Lee, H. W., et al. (2012). Population pharmacokinetic/pharmacodynamic modeling of clopidogrel in Korean healthy volunteers and stroke patients. *J. Clin. Pharmacol.* 52, 985–995. doi:10.1177/0091270011409228

Li, J. Y., Ren, Y. R., Yuan, Y., Ji, S. M., Zhou, S. P., Wang, L. J., et al. (2016). Preclinical PK/PD model for combined administration of erlotinib and sunitinib in the treatment of A549 human NSCLC xenograft mice. *Acta Pharmacol. Sin.* 37, 903–940. doi:10.1038/aps.2016.55

Liu, D., Lon, H. K., Dubois, D. C., Almon, R. R., and Jusko, W. J. (2011). Population pharmacokinetic-pharmacodynamic-disease progression model for effects of anakinra in Lewis rats with collagen-induced arthritis. *J. Pharmacokinet. Pharmacodyn.* 38, 769–786. doi:10.1007/s10928-011-9219-z

Mayr, F. B., and Jilma, B. (2006). Current developments in anti-platelet therapy. *Wien. Med. Wochenschr.* 156, 472–480. doi:10.1007/s10354-006-0330-5

Mckenzie, M. E., Gurbel, P. A., and Levine, D. J. (1999). Clinical utility of available methods for determining platelet function. *Cardiology* 92, 240–247. doi:10. 1159/000006981

Murdoch, D., and Plosker, G. L. (2006). Triflusal: a review of its use in cerebral infarction and myocardial infarction, and as thromboprophylaxis in atrial fibrillation. *Drugs* 66, 671–692. doi:10.1109/IGIC.2012.6329858

Olivier, C. B., Weik, P., Meyer, M., Weber, S., Diehl, P., Bode, C., et al. (2016). Dabigatran and rivaroxaban do not affect AA- and ADP-induced platelet aggregation in patients receiving concomitant platelet inhibitors. *J. Thromb. Thrombo* 42, 161–166. doi:10.1007/s11239-016-1350-7

Pyo, M. K., Kim, J. M., Jin, J. L., Chang, K. C., Lee, D. H., and Yun-Choi, H. S. (2007). Effects of higenamine and its 1-naphthyl analogs, YS-49 and YS-51, on platelet TXA_2 synthesis and aggregation. *Thromb. Res.* 120, 81–86. doi:10.1016/ j.thromres.2006.07.006

Ruzov, M., Rimon, G., Pikovsky, O., and Stepensky, D. (2015). Celecoxib interferes to a limited extent with aspirin-mediated inhibition of platelets aggregation. *Br. J. Clin. Pharmacol.* 81, 316–326. doi:10.1111/bcp.12801

Shin, J. H., Kwon, H. W., Rhee, M. H., and Park, H. J. (2018). Inhibitory effects of thromboxane A2 generation by ginsenoside Ro due to attenuation of cytosolic phospholipase A2 phosphorylation and arachidonic acid release. *Jo. Ginseng Res.* 43, 236–241. doi:10.1016/j.jgr.2017.12.007

Shuldiner, A. R., O'Connell, J. R., Bliden, K. P., Gandhi, A., Ryan, K., Horenstein, R. B., et al. (2009). Association of Cytochrome P450 2C19 genotype with the antiplatelet effect and clinical efficacy of clopidogrel therapy. *JAMA* 302, 849–857. doi:10.1001/jama.2009.1232

Sila, C., and Schoenberg, M. R. (2011). *Cerebrovascular disease and stroke. The little black book of neuropsychology*. New York, NY: Springer US.

Steyerberg, E. W., and Harrell, F. E. (2015). Prediction models need appropriate internal, internal-external, and external validation. *J. Clin. Epidemiol.* 69, 245–247. doi:10.1016/j.jclinepi.2015.04.005

Temperilli, F., Rina, A., Massimi, I., Montemari, A. L., Guarino, M. L., Zicari, A., et al. (2015). Arachidonic acid-stimulated platelet tests: identification of patients less sensitive to aspirin treatment. *Platelets* 26 (8), 1–5. doi:10.3109/ 09537104.2014.1003291

Vittorio, B., Falanga, A., Tomasiak, M., Cerletti, C., and Gaetano, G. D. (1984). SQ 22536, an adenylate-cyclase inhibitor, prevents the antiplatelet effect of dazoxiben, a thromboxane-synthetase inhibitor. *Thromb. Haemost.* 51, 125–128. doi:10.1055/s-0038-1661037

Woo, S. K., Kang, W. K., and Kwon, K. I. (2002). Pharmacokinetic and pharmacodynamic modeling of the antiplatelet and cardiovascular effects of cilostazol in healthy humans. *Clin. Pharmacol. Ther.* 71, 246–252. doi:10.1067/ mcp.2002.122474

Yang, L. J., Chen, X., Wang, S. Q., Fei, Y. M., Wang, D., Li, Y. M., et al. (2015). N_2 extenuates experimental ischemic stroke through platelet aggregation inhibition. *Thromb. Res.* 136, 1310–1317. doi:10.1016/j.thromres.2015. 10.039

Yun, H. Y., Kang, W., Lee, B. Y., Park, S., and Kwon, K. I. (2014). Semi-mechanistic modelling and simulation of inhibition of platelet aggregation by antiplatelet agents. *Basic. Clin. Pharmacol. Toxicol.* 115, 352–359. doi:10.1111/bcpt.12222

Zhang, L., Beal, S. L., and Sheiner, L. B. (2003). Simultaneous vs. sequential analysis for population PK/PD data I: best-case performance. *J. Pharmacokinet. Pharmacodyn.* 30, 387–404. doi:10.1023/b:jopa.0000012998.04442.1f

Zhou, Y., Huang, J., He, W., Fan, W. X., Fang, W. R., He, G. W., et al. (2014). N_2 ameliorates neural injury during experimental ischemic stroke via the regulation of thromboxane A2 production. *Pharmacol. Biochem. Behav.* 124, 458–465. doi:10.1016/j.pbb.2014.06.009

Conflict of Interest: The authors declare that the research was conducted in the absence of any commercial or financial relationships that could be construed as a potential conflict of interest.

frontiers in Pharmacology

ORIGINAL RESEARCH
published: 15 December 2020
doi: 10.3389/fphar.2020.604404

Subacute Toxicity Study of Nicotinamide Mononucleotide via Oral Administration

Yingnan You[1,2], *Yang Gao*[1,2], *Han Wang*[1,2], *Jingshu Li*[1,2], *Xiang Zhang*[3], *Zhengjiang Zhu*[1] *and Nan Liu*[1]*

[1]Interdisciplinary Research Center on Biology and Chemistry, Shanghai Institute of Organic Chemistry, Chinese Academy of Sciences, Shanghai, China, [2]University of Chinese Academy of Sciences, Beijing, China, [3]GeneChic Genomics, Shanghai, China

Nicotinamide mononucleotide (NMN), a key precursory metabolite of NAD^+, has been shown to elevate the cellular level of NAD^+ and ameliorate various age-related diseases. Despite these progresses, systemic evaluation pertaining to the subacute toxicity of NMN remains to be determined. Here, we examine the subacute toxicity of NMN in mice and beagle dogs. Mice were gavaged with a saturated concentration of NMN solution at the maximum intragastric dose once or twice per day for 7 days. Dogs were gavaged twice per day for 14 days. In mice, NMN administrated once per day for 7 days is well tolerated with minimal deleterious effects. Upon higher dosage, we observe slightly increased level of alamine aminotransferase, while other biomarkers remain unchanged. Consistently, administration of NMN in beagle dogs only results in mild increases in creatinine and uric acid. Together, our study highlights the safety of NMN, providing a possible safe dose range for oral administration of NMN.

Keywords: nicotinamide mononucleotide, subacute toxicity, mice, beagle dogs, oral administration

OPEN ACCESS

Edited by:
Constantin Mircioiu, Carol Davila University of Medicine and Pharmacy, Romania

Reviewed by:
Stanislav Yanev, Bulgarian Academy of Sciences (BAS), Bulgaria
Jinyao Li, Xinjiang University, China

***Correspondence:**
Nan Liu
liunan@sioc.ac.cn

Specialty section:
This article was submitted to Drug Metabolism and Transport, a section of the journal Frontiers in Pharmacology

Received: *09 September 2020*
Accepted: *22 October 2020*
Published: *15 December 2020*

Citation:
You Y, Gao Y, Wang H, Li J, Zhang X, Zhu Z and Liu N (2020) Subacute Toxicity Study of Nicotinamide Mononucleotide via Oral Administration. Front. Pharmacol. 11:604404. doi: 10.3389/fphar.2020.604404

INTRODUCTION

Aging is characterized by the progressive decline in cellular and organismal functions that lead to reduction of fitness and increased risks to diseases and death (Lopez-Otin et al., 2013). Decline in metabolic homeostasis represent a prominent hallmark of aging (Lopez-Otin et al., 2016). NAD^+ is the dominant metabolite for cells, which is essentially involved in a wide-range of biological processes (Braidy et al., 2019). In rodents and humans, studies have revealed that the NAD^+ level declines with age in critical organs, such as heart (Braidy et al., 2011), pancreas (Yoshino et al., 2011), adipose tissue (Yoshino et al., 2011), skeletal muscle (Yoshino et al., 2011), liver (Yoshino et al., 2011), skin (Massudi et al., 2012), and brain (Zhu et al., 2015). Importantly, it has been demonstrated that increasing cellular of NAD^+ extends lifespan in yeast (Anderson et al., 2002), worms (Mouchiroud et al., 2013), flies (Balan et al., 2008) and mice (Zhang et al., 2016). Thus, enhancing NAD^+ biosynthesis by pharmaceutical approach is expected to provide preventive effects on various pathophysiological changes associated with disease as well as during the natural process of aging.

Nicotinamide mononucleotide (NMN), a key precursor metabolite for NAD^+ biogenesis, could be such a candidate (Partridge et al., 2020). Notably, administration of NMN has been reported to have remarkable therapeutic effects on age-related diseases. For examples, NMN maintains the neural stem/progenitor cell population (Stein and Imai, 2014), restores skeletal muscle mitochondrial function (Gomes et al., 2013), arterial function (de Picciotto et al., 2016), and ameliorates cognitive function (Kiss et al., 2019) in aged and diseased mouse models.

Mounting evidence associates the exogenously administered NMN with improved adult fitness, For instance, it is reported that long-term administration of NMN could mitigate age-associated physiological decline in mice (Mills et al., 2016) and short-term administration of NMN could induce similar reversal of the glucose intolerance induced by obesity (Uddin et al., 2016). But the proper dosage of NMN is only beginning to be investigated. Mouse models have routinely used the NMN dosage of 500 mg/kg/d, which have thus far been safe (Yoshino et al., 2018). Moreover, a preliminarily report has shown that the single oral administration of 100, 250, and 500 mg NMN per day appear to be safe in healthy human subjects (Irie et al., 2020). Despite these progresses, systemic evaluation regarding the subacute toxicity of NMN remain to be determined. In the present research, we examine the subacute toxicity of NMN in mice and beagle dogs. Mice were gavaged with saturated concentration of NMN solution at the maximum intragastric dose once or twice per day for 7 days. Dogs were gavaged twice per day with 10 ml saturated concentration of NMN solution for 14 days. We subsequently assess the hepatotoxicity and nephrotoxicity of animals following NMN treatment. Despite high-intake of NMN employed throughout this study, our data indicates that oral administration of NMN has minor adverse effects on animals.

MATERIALS AND METHODS

Ethics Statement

All animal procedures have been reviewed and approved by the Institutional Animal Care and Use Committee at Chinese Academy of Sciences and are in accordance with the Guide for the Care and Use of Laboratory Animals of Chinese Academy of Sciences. All efforts were made to minimize the suffering of the animals.

Animal Experimentation

The subacute toxicity was tested in healthy male C57BL6J mice aged 8 weeks with weight between 20 and 30 g. NMN was supplied from Shokou Life Tech (Shokou, Japan) and dissolved in sterile water. Mice were randomly divided into four groups: mice gavaged with water once daily; mice gavaged with NMN once daily; mice gavaged with water twice daily; and mice gavaged with NMN twice daily. three to five mice were in each group. Blood was collected via cardiac puncture. After collection of the whole blood, allow the blood to clot by leaving it undisturbed at room temperature. Remove the clot by centrifuging at 3000 g for 15 min at 4 °C. The resulting supernatant is designated serum. Liver and kidney were collected after NMN administration.

10 beagle dogs aged 4 years with weight between 9 and 11 kg were randomly divided into two groups: dogs were gavaged twice per day each with 10 ml water and dogs were gavaged twice per day each with 10 ml NMN; serum was collected before and after NMN administration.

General Observation

Cage-side examinations for apparent signs (behavior, mental status, gland secretion, respiration status, feces characters, genitals, and death) of toxicity or injury were conducted once a day after daily drug exposure.

Histopathological Evaluations

Kidney and liver were harvested and immersed in fixative (4% paraformaldehyde). Tissues were dehydrated by ethanol solution in serial concentrations, cleared with xylene and embedded with paraffin. Paraffin blocks were sectioned with microtome into 5 μm thickness and each tissue section was stained with hematoxylin and eosin followed by microscopic examination by light microscope (Nikon Ds-Ri2).

PolyA-Selected mRNA-Seq

RNA isolation was followed in accordance with manufacturer's instruction (Takara Bio, Japan). RNA was re-suspended in DEPC-treated RNase free water (Invitrogen, United States). TURBO DNA free kit was used to remove residual DNA contamination according to manufacturer's instruction (Invitrogen, United States). A concentration of 1 μg of total RNA was used to generate sequencing library using Vazyme VAHTS mRNA-seq v3 library Prep Kit for Illumina. The library quality was checked by Bioanalyzer 2,100 (Agilent, United States). The quantification was performed by qRT-PCR with a reference to a standard library. The libraries were pooled together in equimolar amounts to a final 2 nM concentration. The normalized libraries were denatured with 0.1 M NaOH (Sigma, United States). Pooled denature libraries were sequenced on the Illumina NextSeq 550 or Illumina Hiseq Xten. Sequencing reads were mapped to the reference genome mm19 with STAR by default parameter. The read counts for each gene were calculated by HTSEQ_COUNT (version 0.11.0.) with parameters "-m intersection-strict -s no." The count files were used as input to R package DESeq2 (version 1.24.0.) for normalization.

Serum Biochemistry Evaluation

Serum was analyzed for the function of liver, function of kidney, insulin and blood lipids using automatic hematology analyzer (Beckman AU5811). Biochemistry and hematological analyses were performed in ADICON clinical laboratories (Shanghai, China).

NAM Measurements of Serum

400 μL MeOH and 400 μL ACN were added to 100 μL serum. Incubated for 1 h at −20 °C, centrifuged for 15 min at 13,000 rpm and 4 °C. Took the supernatant and evaporated to dryness at 4 °C. Reconstituted with 100 μL ACN/H2O (volume/volume, 1:1), vortexed for 30 s, sonicated for 10 min (4 °C water bath). Centrifuged for 15 min at 13,000 rpm and 4 °C. Supernatants were analyzed by LC-MS. The LC–MS analysis was performed using an UHPLC system (1,290 series, Agilent Technologies) coupled to a triple quadrupole mass spectrometer (Agilent 6,495 QqQ, Agilent Technologies). Chromatographic separation was performed on the Merck ZIC-pHILIC column (100 × 2.1 mm, 5 μm). The column was maintained at room temperature, and the flow rate was 0.2 ml/min. Mobile phase A was 100% H2O, 25 mM CH3COONH4, and 25 mM NH4OH, and mobile phase B was 100% acetonitrile. The column was eluted with a linear gradient system (B %): 0 min, 80%; 1 min, 80%; 3 min, 65%; 7 min, 50%; 7.1, 20%; 9.5 min, 20%; 9.6 min, 80%; 13 min, 80%. Optimized MRM

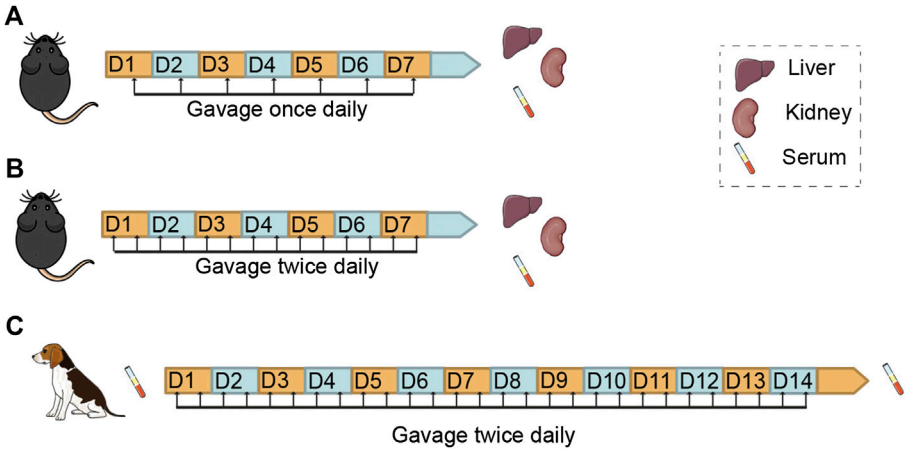

FIGURE 1 | Study Design for the Examination of Subacute Toxicity of Nicotinamide Mononucleotide (NMN) in Mice and Dogs Schemes showing the route, frequency and duration of NMN administration and sampling in mice. **(A,B)** and beagle dogs **(C)**.

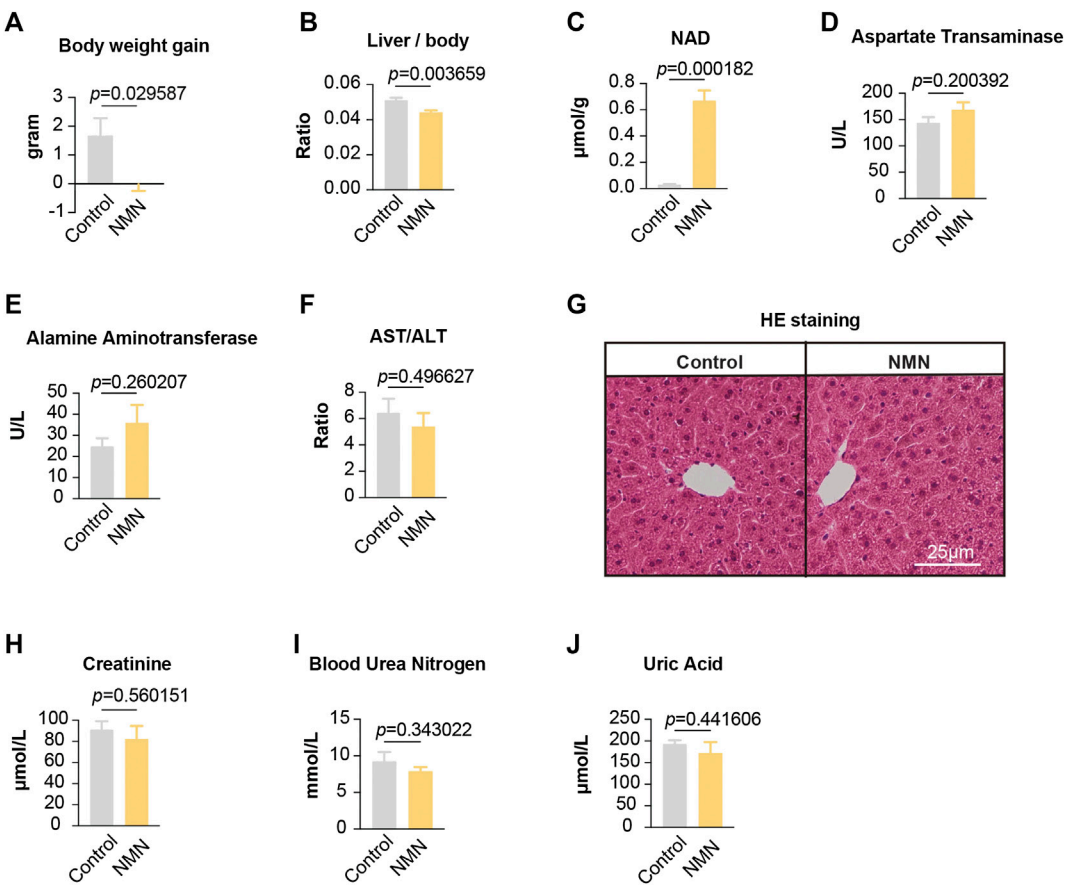

FIGURE 2 | Data for mice treated with NMN once per day **(A)**The body weight was decreased after NMN administration. **(B)** The ratio between liver weight and body weight was decreased after NMN administration **(C)** Liver NAD^+ levels were increased after NMN administration. **(D–F)** Liver function was analyzed after NMN administration. **(G)** Photomicrograph of liver sections from NMN-administered mice exhibited normal hepatocytes (H&E stain). **(H–J)** Kidney function were analyzed after NMN administration.

transition 123.1/53.1 in positive mode was utilized for quantifying NAM.

NAD^+ Measurements of Liver

Assays were assembled according to the instruction of manufacturers (Beyotime, China).

Statistical Analysis

Data were calculated and analyzed with Graph Pad Prism version 8.1.1 (Prizm, United States). All values were presented as mean ± standard error and calculated using an unpaired Student t-test.

RESULTS

Oral Administration of NMN Substantially Increases Tissue NAD^+ Levels With Minimal Adverse Effects

To evaluate the subacute toxicity of NMN, we treated 8-week-old male mice with a saturated concentration of NMN solution (67 mg/ml) at the maximum intragastric dose (20 ml/kg). After 24 h of NMN supplementation, all animals remained alive and exhibited no difference in fur and eye color. Compared to control animals, NMN-treated mice had similar locomotion activity with no occurrence of piloerection and diarrhea. Following the same NMN feeding scheme, we gavaged the mice once per day (1,340 mg/kg/d) for a week (**Figure 1A**). After 7 days of NMN administration, animals were viable with no obvious behavioral and morphological deficits. The body weight from NMN-treated mice was decreased compared to control animals (**Figure 2A**). Similarly, the ratio between liver and body weight was also decreased upon NMN treatment (**Figure 2B**).

To confirm whether our feeding scheme had an impact on the level of NAD^+ in tissues, we measured liver NAD^+. Our data showed that NAD^+ in liver was dramatically increased (**Figure 2C**), suggesting that oral administration of NMN efficiently boosts NAD^+ in tissue. To determine the effects of NMN on liver, we assessed liver function and anatomy (**Figures 2D–G**). Measurements of Aspartate Transaminase (AST), Alamine Aminotransferase (ALT), and AST/ALT found no significant difference (**Figures 2D–F**). Photomicrograph of liver sections from NMN-administered mice exhibited normal hepatocytes (**Figure 2G**). Furthermore, we examined the kidney

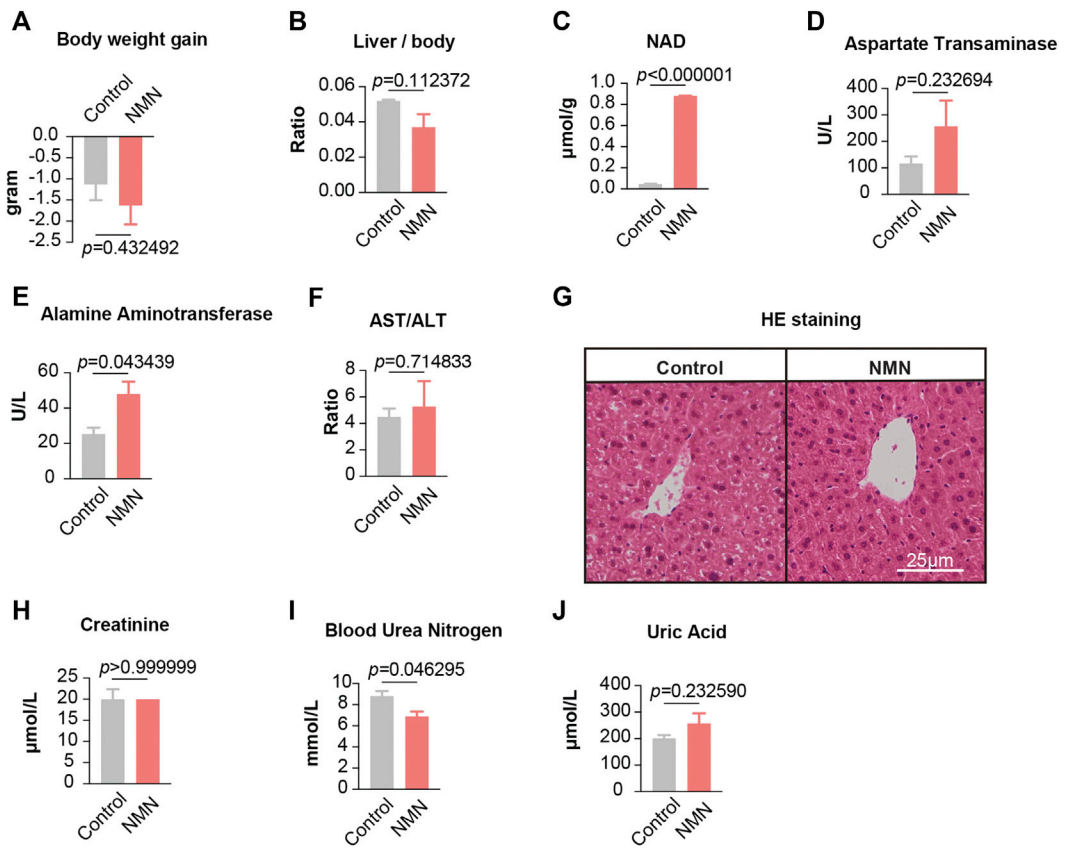

FIGURE 3 | Data for mice treated with NMN twice per day **(A)** The body weights were measured before and after higher NMN administration. **(B)** The ratio between liver weight and body weight was measured after higher NMN administration. **(C)** Liver NAD^+ levels were increased after higher NMN administration. **(D–F)** Liver function were analyzed after higher NMN administration. **(E)** Alamine aminotransferase was evaluated in higher NMN-administered mice. **(G)** Photomicrograph of liver sections from higher NMN-administered mice exhibited normal hepatocytes (H&E stain). **(H–J)** Kidney function were analyzed after higher NMN administration. **(I)** Blood urea nitrogen was decreased in 1340 mg/kg/d NMN-administered mice.

function by assessing creatinine, blood urea nitrogen, and uric acid. These analyses showed comparable levels between control and NMN-treated animals (**Figures 2H–J**). Taken together, our data demonstrate that oral gavage of NMN substantially elevates NAD^+ in tissue with no significant side effects on liver and kidney.

Gavage of Higher NMN Mildly Elevates Alamine Aminotransferase Levels

Since gavage once per day demonstrates minimal adverse effects, we further increased the frequency of gavage to two times per day (2,680 mg/kg/d) (**Figure 1B**). After 7 days, all animals survived but had a comparable weight loss in both control and NMN-treated mice (**Figure 3A**). Though the extent of decrease did not reach statistical significance, the ratio between liver and body weight was decreased in NMN-treated mice (**Figure 3B**). Consistently, NAD^+ levels in liver were substantially increased (**Figure 3C**). Unlike gavage once per day, alamine aminotransferase levels were elevated upon the use of higher dosage of NMN (**Figure 3E**). Histopathological examinations, however, found no defect in liver anatomy (**Figure 3G**). Similarly, metabolites that reflect kidney function were examined (**Figures 3H–J**). Although blood urea nitrogen concentration was slightly decreased in the NMN-treated mice (**Figure 3I**), there was no difference in the serum concentration of creatinine and uric acid between control and NMN-treated animals, suggesting minimal adverse effects on kidney function. Taken together, despite the fact that alamine aminotransferase is mildly increased, overall physiological functions of liver and kidney remain intact when higher dosage of NMN is employed.

Transcriptomic Analysis in NMN Administrated Mice Liver

Using liver tissue, we performed transcriptomic analysis by polyA-selected RNA sequencing (RNA-seq). In mice gavaged once per day, only a subset of 74 genes were significantly altered in liver ($p < 0.05$), with 45 genes up-regulated and 29 genes down-regulated (**Figure 4A**). Gene ontology (GO) analysis showed lipid metabolic process being the biological processes significantly enriched (**Figure 4A**). Given this result, we measured profile

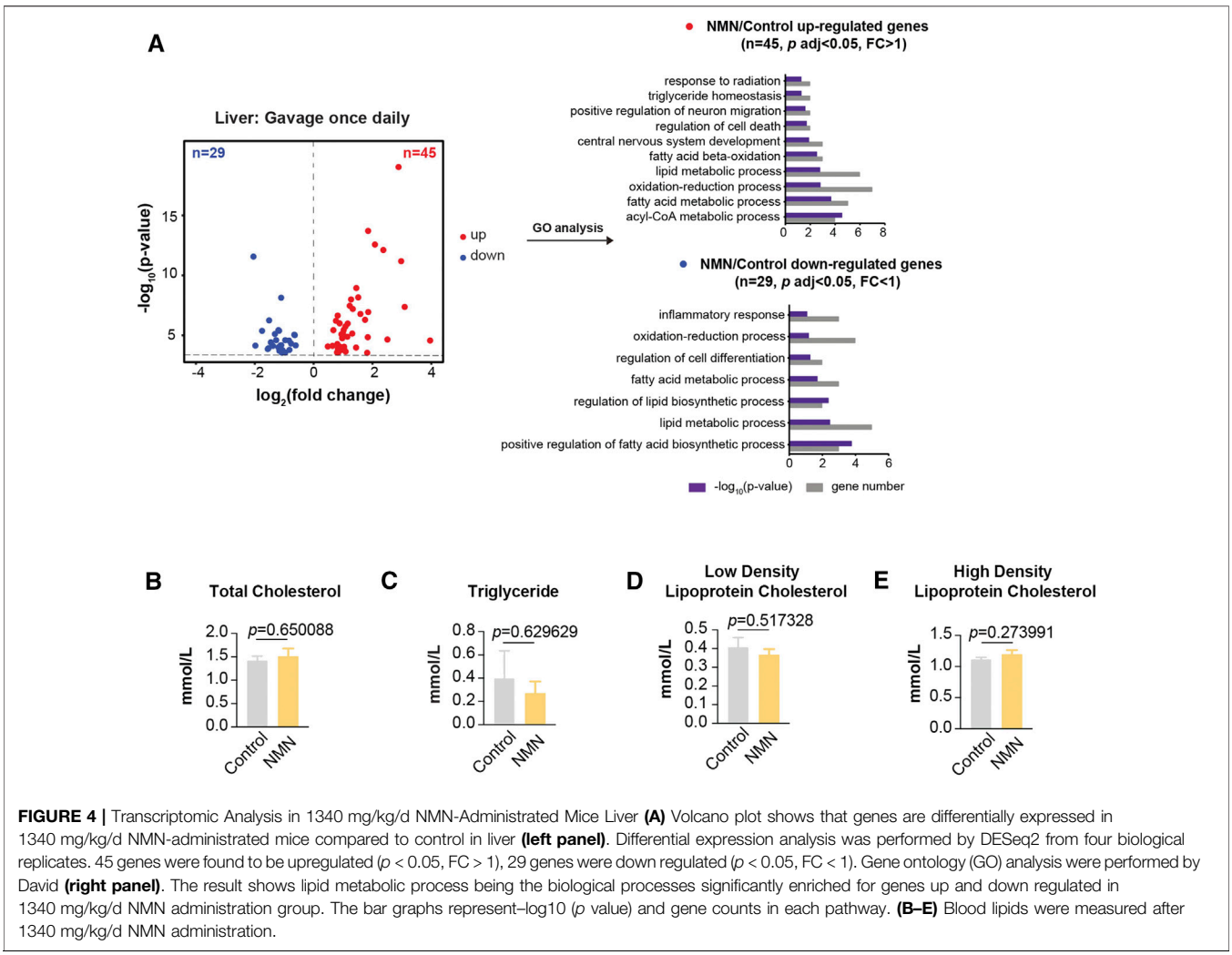

FIGURE 4 | Transcriptomic Analysis in 1340 mg/kg/d NMN-Administrated Mice Liver **(A)** Volcano plot shows that genes are differentially expressed in 1340 mg/kg/d NMN-administrated mice compared to control in liver **(left panel)**. Differential expression analysis was performed by DESeq2 from four biological replicates. 45 genes were found to be upregulated ($p < 0.05$, FC > 1), 29 genes were down regulated ($p < 0.05$, FC < 1). Gene ontology (GO) analysis were performed by David **(right panel)**. The result shows lipid metabolic process being the biological processes significantly enriched for genes up and down regulated in 1340 mg/kg/d NMN administration group. The bar graphs represent–log10 (p value) and gene counts in each pathway. **(B–E)** Blood lipids were measured after 1340 mg/kg/d NMN administration.

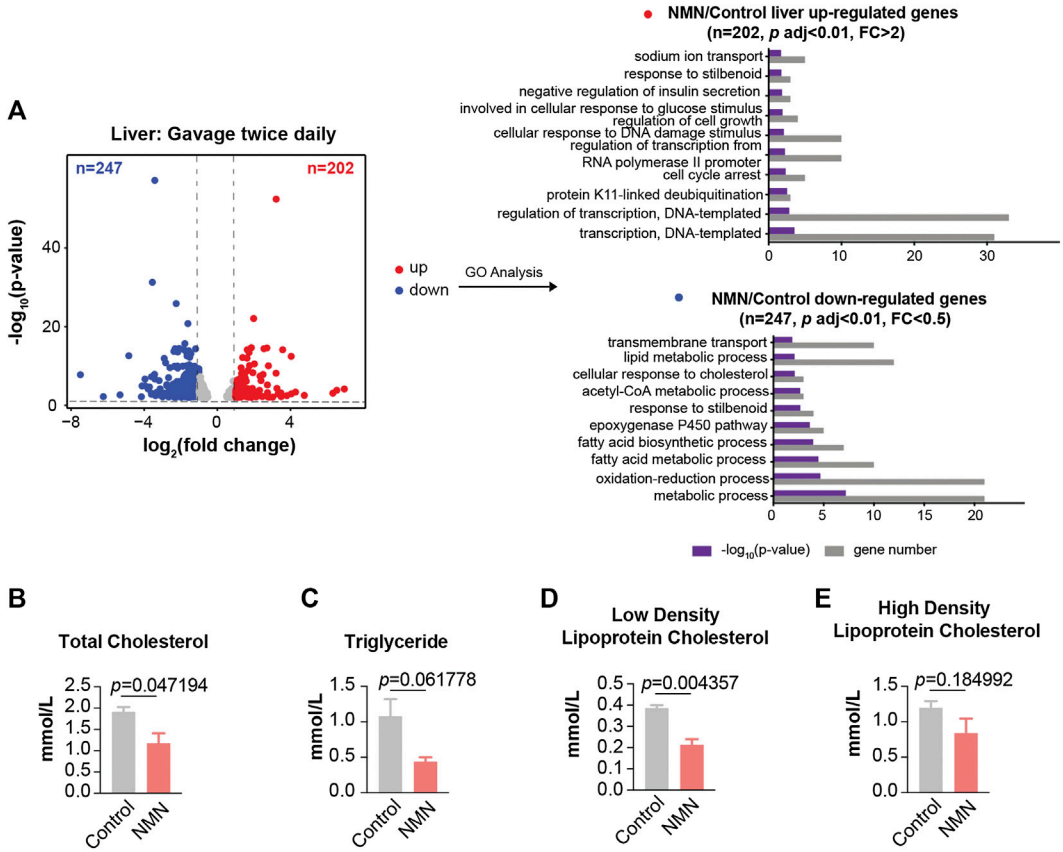

FIGURE 5 | Transcriptomic Analysis in 2680 mg/kg/d NMN-Administrated Mice Liver **(A)** Volcano plot shows that genes are differentially expressed in 2680 mg/kg/d NMN-administrated mice compared to control in liver **(left panel)**. Differential expression analysis was performed by DESeq2 from three biological replicates. 202 genes were found to be upregulated ($p < 0.01$, FC > 2), 247 genes were down regulated ($p < 0.01$, FC < 0.5). Gene ontology (GO) analysis were performed by David **(right panel)**. The result shows lipid metabolic process being the biological processes significantly enriched for genes down regulated in 2680 mg/kg/d NMN administration group. The bar graphs represent–log10 (p value) and gene counts in each pathway. **(B–E)** Blood lipids were measured after 2680 mg/kg/d NMN administration. **(B)** Total Cholesterol was decreased in 2680 mg/kg/d NMN-administered mice. **(D)** Low density lipoprotein cholesterol was decreased in 2680 mg/kg/d NMN-administered mice.

of select lipids. As noted, blood lipids were comparable between control and NMN-treated animals (**Figures 4B–E**).

In mice that received higher NMN dosage, a broad change in the transcriptome was observed, in which 449 genes were significantly altered in liver ($p < 0.01$; fold change > 2 or fold change < 0.5) (**Figure 5A**). GO analysis also indicated lipid metabolic process being prominently highlighted. Measurements of blood lipids, including total cholesterol, triglyceride, and low density lipoprotein cholesterol, were significantly decreased in NMN-treated animals (**Figures 5B–E**). This data suggests that the effect of NMN on blood lipid is dose-dependent.

Transcriptomic Analysis in NMN Administrated Mice Kidney

We further extended RNA-seq analysis to kidney. In mice gavaged once daily, GO analysis showed that up-regulated genes were enriched in circadian rhythm and sodium ion transport, while down-regulated genes were enriched in ion transport (**Figure 6A**). In mice gavaged twice daily, up-regulated genes were enriched in oxidation-reduction process (**Figure 6B**). Interestingly, "response to insulin" was enriched for genes up-regulated (**Figure 6B**). Since it has been reported that NMN-administered mice show improved insulin sensitivity (Yoshino et al., 2011), we conducted insulin test in serum, which revealed a decreased concentration of insulin (**Figure 6C**). Down-regulated genes, on the other hand, were enriched in the metabolic process (**Figure 6B**).

The Effect of Oral 1,340 mg/d NMN-Administration on Liver Function, Kidney Function and Blood Lipids in Beagle Dogs

To gain insight of the toxicity of NMN in large mammal, we design oral gavage test using beagle dogs. 10 beagle dogs were randomly divided into two groups (**Table 1**). Dogs were gavaged twice per day with 10 ml saturated concentration of NMN solution for 14 days (1340 mg/d) (**Figure 1C**). During the experiment, animals were found to be in good condition, with

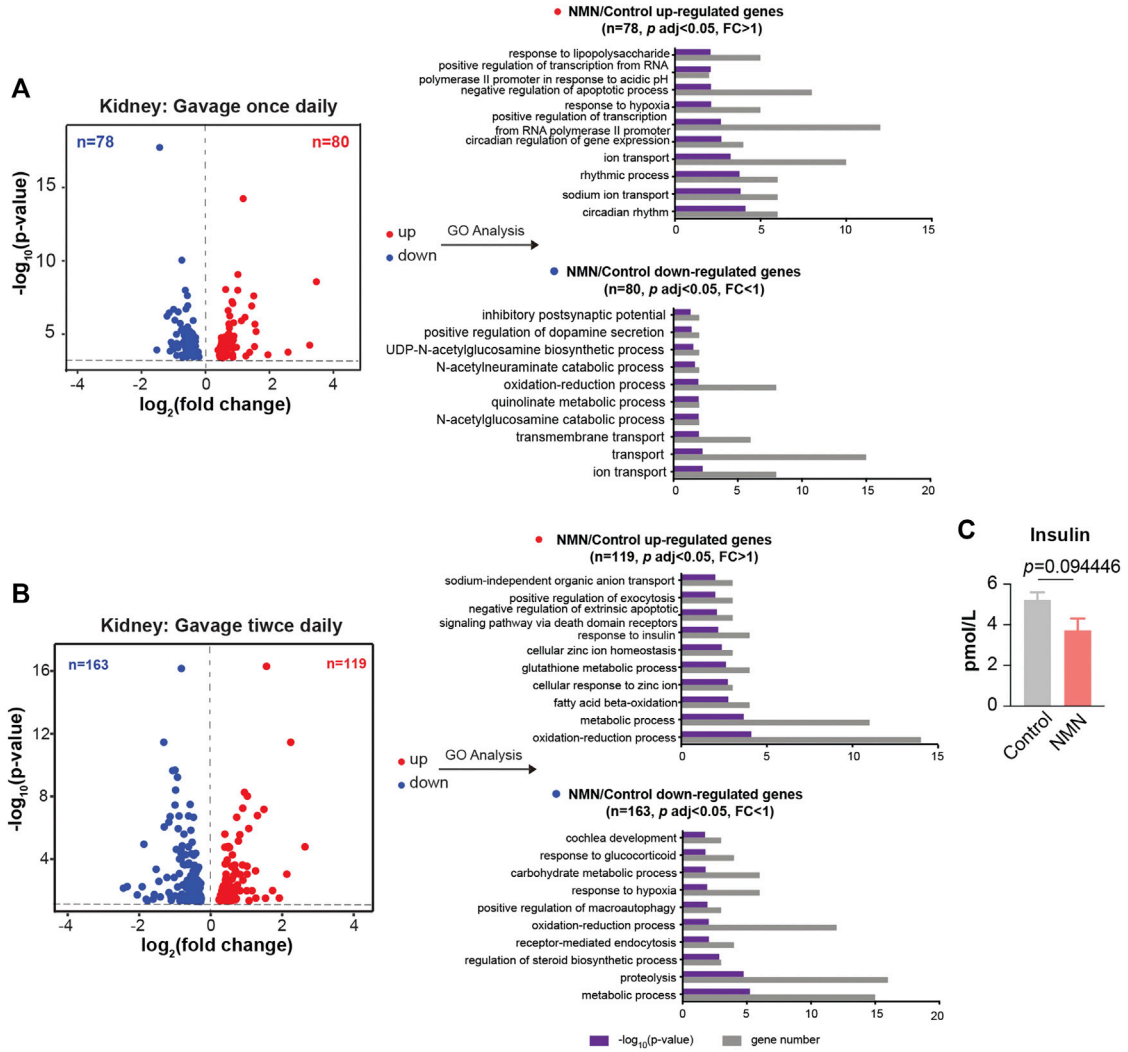

FIGURE 6 | Transcriptomic Analysis in NMN Administrated Mice Kidney. **(A)** Volcano plot shows that genes are differentially expressed in 1340 mg/kg/d NMN-administrated mice compared to control in kidney **(left panel)**. Differential expression analysis was performed by DESeq2 from four biological replicates. 80 genes were found to be upregulated ($p < 0.05$, FC > 1), 79 genes were down regulated ($p < 0.05$, FC > 1). Gene ontology (GO) analysis were performed by David **(right panel)**. **(B)**. Volcano plot shows that genes are differentially expressed in 2680 mg/kg/d NMN-administrated mice compared to control in kidney **(left panel)**. Differential expression analysis was performed by DESeq2 from three biological replicates. 119 genes were found to be upregulated ($p < 0.05$, FC > 1), 163 genes were down regulated ($p < 0.05$, FC < 1). Gene ontology (GO) analysis were performed by David **(right panel)**. Gene ontology (GO) analysis (performed by David) shows response to insulin being the biological processes significantly enriched for genes down regulated in 2680 mg/kg/d NMN administration group. **(C)** The insulin level in serum was measured after NMN administration.

TABLE 1 | The age, weight and groups of beagle dogs.

No	Group	Age (y)	Weight (kg)
1	Control	4	10.0
2	Control	4	10.0
3	Control	4	9.0
4	Control	4	10.3
5	Control	4	9.9
6	NMN-treated	4	10.7
7	NMN-treated	4	10.1
8	NMN-treated	4	11.0
9	NMN-treated	4	9.0
10	NMN-treated	4	10.0

normal autonomic activities and clean coats. After two weeks of NMN administration, the body weight of NMN-treated dogs was increased than that of the control dogs (**Figure 7A**). Since NAD^+ has exceedingly low level in plasma and urine (Trammell et al., 2016), we measured NAM in serum which has been shown be converted from exogenous NMN (Liu et al., 2018). Notably, NAM levels were dramatically increased in NMN-treated dogs (**Figure 7B**). To evaluate the hepatotoxicity and nephrotoxicity, blood metabolites were analyzed (**Figures 7C–H**). In NMN-treated, creatinine and uric acid were increased, indicating kidney response. Blood lipids were measured (**Figures 7I–L**), which showed comparable levels between control and NMN-treated dogs.

DISCUSSION

Emerging studies have heightened the fact that the cellular level of NAD^+ decreases with age, predisposing individuals to physiological decline as well as late-onset diseases (Rajman et al., 2018). Thus, enhancing NAD^+ availability by supplementing precursory metabolites, such as NMN and NR, promises to ameliorate a broad spectrum of age-associated deficits (Partridge et al., 2020). However, prior to the application in humans, systemic evaluation of the NMN toxicity especially in model organisms and large mammals remains to be determined. In the present study, we assess the subacute toxicity of NMN in mice and dogs.

Previous studies in mice apply 100–500 mg/kg/d of NMN, equivalent surface area dose for a human adult being approximately 0.5–2.5 g, depending on the weight of individuals. To examine subacute toxicity, we substantially increase NMN dosage to 1,340 mg/kg/d and 2680 mg/kg/d in mouse models. To our knowledge, such high intake of NMN for animal test has not yet been used. As noted, administrating 1,340 mg/kg/d NMN for 7 days is well tolerated with no deleterious effects. However, as the dose doubled, we observe slightly increased level of alamine aminotransferase among all the biomarkers examined. On the other hand, administrating 1340 mg/d NMN in beagle dogs only results in mild increases in creatinine and uric acid, while other biomarkers remain unchanged. Taken together,

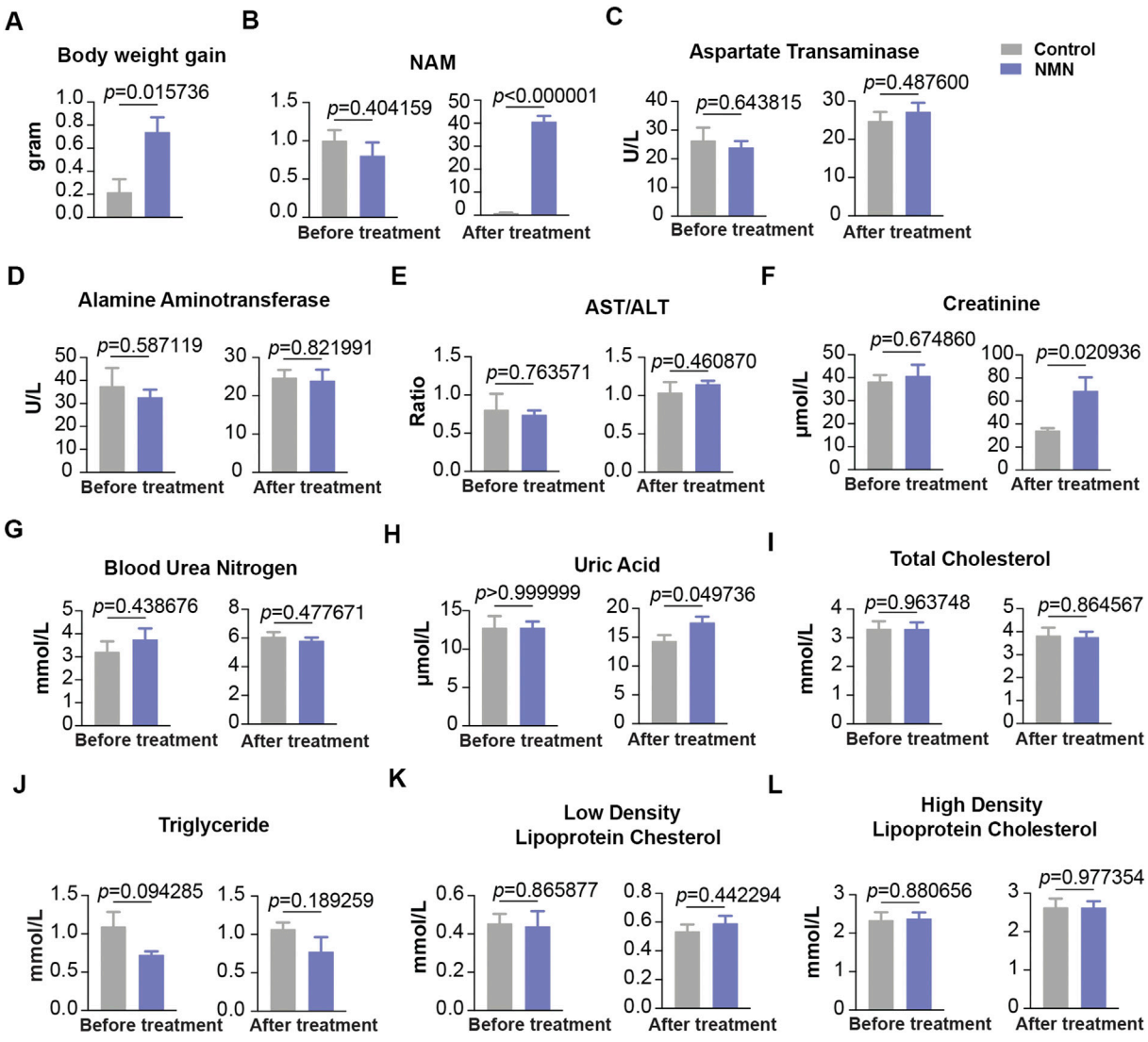

FIGURE 7 | The effect of oral 1340 mg/d NMN-administration on liver function, kidney function and blood lipids in beagle dogs **(A)** Body weights were measured before and after NMN administration. **(B)** Serum NAM levels were increased after NMN administration. **(C–E)** Liver function was analyzed after NMN administration. **(F–H)** Kidney function was analyzed after NMN administration. **(F)** Creatinine was evaluated in 1340 mg/kg/d NMN-administered dogs. **(H)** Uric acid was evaluated in 1340 mg/kg/d NMN-administered dogs. **(I–L)** Blood lipids were measured before and after NMN administration.

our data indicates that high-dose and short-term oral administration of NMN has mild or minimal deleterious effects.

Interestingly, our analysis reveals that NMN administration has beneficial effects to lower lipid and insulin levels. Although it has been shown that long-term supplementation of NMN improves glucose intolerance and lipid profiles in a mouse model of age-induced type-2 diabetes (Yoshino et al., 2011), our data suggests that high-dose NMN within a week is sufficient to reduce blood lipids and improve insulin sensitivity. NMN therefore has the potential to be implemented as safe therapeutic agent against age-associated physiological decline and disease. Our findings from this short-term administration study provide a possible safe dose range for oral administration of NMN, hoping to translate the results to humans.

DATA AVAILABILITY STATEMENT

The datasets presented in this study can be found in online repositories. The names of the repository/repositories and accession number(s) can be found below: https://www.ncbi.nlm.nih.gov/geo/GSE157594.

ETHICS STATEMENT

The animal study was reviewed and approved by Institutional Animal Care and Use Committee at Chinese Academy of Sciences.

AUTHOR CONTRIBUTIONS

YY and NL contributed to concept and design of the study. YG and ZZ contributed to the detection of NAM. YY, JL, and HW collected the mouse samples. NL, YY, and XZ collected the dog samples. YY performed the statistical analysis. NL and YY wrote the manuscript.

FUNDING

This work was supported in part by grants from the National Key Research and Development Program of China (2016YFA0501900) and the China National Natural Science Foundation (91849109) (to NL).

REFERENCES

Anderson, R. M., Bitterman, K. J., Wood, J. G., Medvedik, O., Cohen, H., Lin, S. S., et al. (2002). Manipulation of a nuclear NAD^+ salvage pathway delays aging without altering steady-state NAD^+ levels. *J. Biol. Chem.* 277, 18881–18890. doi:10.1074/jbc.M111773200

Balan, V., Miller, G. S., Kaplun, L., Balan, K., Chong, Z. Z., Li, F., et al. (2008). Life span extension and neuronal cell protection by Drosophila nicotinamidase. *J. Biol. Chem.* 283, 27810–27819. doi:10.1074/jbc.M804681200

Braidy, N., Guillemin, G. J., Mansour, H., Chan-Ling, T., Poljak, A., and Grant, R. (2011). Age related changes in NAD^+ metabolism oxidative stress and Sirt1 activity in wistar rats. *PLoS One* 6, e19194. doi:10.1371/journal.pone.0019194

Braidy, N., Berg, J., Clement, J., Khorshidi, F., Poljak, A., Jayasena, T., et al. (2019). Role of nicotinamide adenine dinucleotide and related precursors as therapeutic targets for age-related degenerative diseases: rationale, biochemistry, pharmacokinetics, and outcomes. *Antioxidants Redox Signal.* 30, 251–294. doi:10.1089/ars.2017.7269

de Picciotto, N. E., Gano, L. B., Johnson, L. C., Martens, C. R., Sindler, A. L., Mills, K. F., et al. (2016). Nicotinamide mononucleotide supplementation reverses vascular dysfunction and oxidative stress with aging in mice. *Aging Cell* 15, 522–530. doi:10.1111/acel.12461

Gomes, A. P., Price, N. L., Ling, A. J., Moslehi, J. J., Montgomery, M. K., Rajman, L., et al. (2013). Declining NAD(+) induces a pseudohypoxic state disrupting nuclear-mitochondrial communication during aging. *Cell* 155, 1624–1638. doi:10.1016/j.cell.2013.11.037

Irie, J., Inagaki, E., Fujita, M., Nakaya, H., Mitsuishi, M., Yamaguchi, S., et al. (2020). Effect of oral administration of nicotinamide mononucleotide on clinical parameters and nicotinamide metabolite levels in healthy Japanese men. *Endocr. J.* 67, 153–160. doi:10.1507/endocrj.EJ19-0313

Kiss, T., Balasubramanian, P., Valcarcel-Ares, M. N., Tarantini, S., Yabluchanskiy, A., Csipo, T., et al. (2019). Nicotinamide mononucleotide (NMN) treatment attenuates oxidative stress and rescues angiogenic capacity in aged cerebromicrovascular endothelial cells: a potential mechanism for the prevention of vascular cognitive impairment. *Geroscience* 41, 619–630. doi:10.1007/s11357-019-00074-2

Liu, L., Su, X., Quinn, W. J., III, Hui, S., Krukenberg, K., Frederick, D. W., et al. (2018). Quantitative analysis of NAD synthesis-breakdown fluxes. *Cell Metabol.* 27, 1067–1080. doi:10.1016/j.cmet.2018.03.018

Lopez-Otin, C., Blasco, M. A., Partridge, L., Serrano, M., and Kroemer, G. (2013). The hallmarks of aging. *Cell* 153, 1194–1217. doi:10.1016/j.cell.2013.05.039

Lopez-Otin, C., Galluzzi, L., Freije, J. M. P., Madeo, F., and Kroemer, G. (2016). Metabolic control of longevity. *Cell* 166, 802–821. doi:10.1016/j.cell.2016.07.031

Massudi, H., Grant, R., Braidy, N., Guest, J., Farnsworth, B., and Guillemin, G. J. (2012). Age-associated changes in oxidative stress and NAD^+ metabolism in human tissue. *PLoS One* 7, e42357. doi:10.1371/journal.pone.0042357

Mills, K. F., Yoshida, S., Stein, L. R., Grozio, A., Kubota, S., Sasaki, Y., et al. (2016). Long-term administration of nicotinamide mononucleotide mitigates age-associated physiological decline in mice. *Cell Metabol.* 24, 795–806. doi:10.1016/j.cmet.2016.09.013

Mouchiroud, L., Houtkooper, R. H., Moullan, N., Katsyuba, E., Ryu, D., Cantó, C., et al. (2013). The NAD(+)/Sirtuin pathway modulates longevity through activation of mitochondrial UPR and FOXO signaling. *Cell* 154, 430–441. doi:10.1016/j.cell.2013.06.016

Partridge, L., Fuentealba, M., and Kennedy, B. K. (2020). The quest to slow ageing through drug discovery. *Nat. Rev. Drug Discov.* 19, 513–532. doi:10.1038/s41573-020-0067-7

Rajman, L., Chwalek, K., and Sinclair, D. A. (2018). Therapeutic potential of NAD-boosting molecules: the in vivo evidence. *Cell Metabol.* 27, 529–547. doi:10.1016/j.cmet.2018.02.011

Stein, L. R., and Imai, S. (2014). Specific ablation of Nampt in adult neural stem cells recapitulates their functional defects during aging. *EMBO J.* 33, 1321–1340. doi:10.1002/embj.201386917

Trammell, S. A., Schmidt, M. S., Weidemann, B. J., Redpath, P., Jaksch, F., Dellinger, R. W., et al. (2016). Nicotinamide riboside is uniquely and orally bioavailable in mice and humans. *Nat. Commun.* 7, 12948. doi:10.1038/ncomms12948

Uddin, G. M., Youngson, N. A., Sinclair, D. A., and Morris, M. J. (2016). Head to head comparison of short-term treatment with the NAD(+) precursor nicotinamide mononucleotide (NMN) and 6 weeks of exercise in obese female mice. *Front. Pharmacol.* 7, 258. doi:10.3389/fphar.2016.00258

Yoshino, J., Mills, K. F., Yoon, M. J., and Imai, S. (2011). Nicotinamide mononucleotide, a key NAD(+) intermediate, treats the pathophysiology of diet- and age-induced diabetes in mice. *Cell Metabol.* 14, 528–536. doi:10.1016/j.cmet.2011.08.014

Yoshino, J., Baur, J. A., and Imai, S. I. (2018). NAD(+) intermediates: the biology and therapeutic potential of NMN and NR. *Cell Metabol.* 27, 513–528. doi:10.1016/j.cmet.2017.11.002

Zhang, H., Ryu, D., Wu, Y., Gariani, K., Wang, X., Luan, P., et al. (2016). NAD^+ repletion improves mitochondrial and stem cell function and enhances life span in mice. *Science* 352, 1436–1443. doi:10.1126/science.aaf2693

Zhu, X. H., Lu, M., Lee, B. Y., Ugurbil, K., and Chen, W. (2015). *In vivo* NAD assay reveals the intracellular NAD contents and redox state in healthy human brain and their age dependences. *Proc. Natl. Acad. Sci. U.S.A.* 112, 2876–2881. doi:10.1073/pnas.1417921112

Conflict of Interest: The authors declare that the research was conducted in the absence of any commercial or financial relationships that could be construed as a potential conflict of interest.

frontiers in Pharmacology

ORIGINAL RESEARCH
published: 11 January 2021
doi: 10.3389/fphar.2020.614756

Characterization of Formononetin Sulfonation in SULT1A3 Overexpressing HKE293 Cells: Involvement of Multidrug Resistance-Associated Protein 4 in Excretion of Sulfate

*Fanye Liu[1], Shuhua Pei[1], Wenqi Li[1], Xiao Wang[1], Chao Liang[1], Ruohan Yang[1], Zhansheng Zhang[1], Xin Yao[1], Dong Fang[1], Songqiang Xie[2] and Hua Sun[1]**

[1]Institute for Innovative Drug Design and Evaluation, School of Pharmacy, Henan University, Kaifeng, China, [2]Institute of Chemical Biology, School of Pharmacy, Henan University, Kaifeng, China

OPEN ACCESS

Edited by:
Constantin Mircioiu,
Carol Davila University of Medicine and Pharmacy, Romania

Reviewed by:
Zifei Qin,
First Affiliated Hospital of Zhengzhou University, China
Cristina Ghiciuc,
Grigore T. Popa University of Medicine and Pharmacy, Romania
Ana I. Alvarez,
Universidad de León, Spain

***Correspondence:**
Hua Sun
sunhua_rain@hotmail.com

Specialty section:
This article was submitted to Drug Metabolism and Transport, a section of the journal Frontiers in Pharmacology

Received: 07 October 2020
Accepted: 16 November 2020
Published: 11 January 2021

Citation:
Liu F, Pei S, Li W, Wang X, Liang C, Yang R, Zhang Z, Yao X, Fang D, Xie S and Sun H (2021) Characterization of Formononetin Sulfonation in SULT1A3 Overexpressing HKE293 Cells: Involvement of Multidrug Resistance-Associated Protein 4 in Excretion of Sulfate. Front. Pharmacol. 11:614756. doi: 10.3389/fphar.2020.614756

Formononetin is one of the main active compounds of traditional Chinese herbal medicine *Astragalus membranaceus*. However, disposition of formononetin via sulfonation pathway remains undefined. Here, expression-activity correlation was performed to identify the contributing of SULT1A3 to formononetin metabolism. Then the sulfonation of formononetin and excretion of its sulfate were investigated in SULT1A3 overexpressing human embryonic kidney 293 cells (or HKE-SULT1A3 cells) with significant expression of breast cancer resistance protein (BCRP) and multidrug resistance-associated protein 4 (MRP4). As a result, formononetin sulfonation was significantly correlated with SULT1A3 protein levels ($r = 0.728$; $p < 0.05$) in a bank of individual human intestine S9 fractions ($n = 9$). HEK-SULT1A3 cells catalyzed formononetin formation of a monosulfate metabolite. Sulfate formation of formononetin in HEK-SULT1A3 cell lysate followed the Michaelis-Menten kinetics (V_{max} = 13.94 pmol/min/mg and K_m = 6.17 μM). Reduced activity of MRP4 by MK-571 caused significant decrease in the excretion rate (79.1%–94.6%) and efflux clearance (85.3%–98.0%) of formononetin sulfate, whereas the BCRP specific inhibitor Ko143 had no effect. Furthermore, silencing of MRP4 led to obvious decrease in sulfate excretion rates (>32.8%) and efflux clearance (>50.6%). It was worth noting that the fraction of dose metabolized (f_{met}), an indicator of the extent of drug sulfonation, was also decreased (maximal 26.7%) with the knockdown of MRP4. In conclusion, SULT1A3 was of great significance in determining sulfonation of formononetin. HEK-SULT1A3 cells catalyzed formononetin formation of a monosulfate. MRP4 mainly contributed to cellular excretion of formononetin sulfate and further mediated the intracellular sulfonation of formononetin.

Keywords: formononetin, sulfonation, efflux transporter, MRP4, HEK293 cells

Abbreviations: HEK, human embryonic kidney; F-O-S, formononetin sulfate; Km, Michaelis-Menten constant; MRP, multidrug resistance-associated protein; PAPS, 3′-phosphoadenosine-5′-phosphosulfate; shRNA, short-hairpin RNA; SULT, Sulfotransferase; Vmax, maximal velocity.

INTRODUCTION

Traditional Chinese Medicine (TCM) has a history of more than 2000 years in diagnosis and treatment of diseases. In recent years, more and more research has been devoted to the study of TCM, including their pharmacological activities, effective forms, and mechanisms of action. *Astragalus membranaceus* (Huangqi), one of the most well-known TCM in China and other oriental countries, is widely used as an important component in many Chinese medicine formulas. In more than 2000 years of clinical practice and pharmacological research, *Astragalus membranaceus* has shown multiple effects, such as protection of cardiovascular system (Liu D. et al., 2018), liver-protective functions (Mohibbullah et al., 2019), antioxidant (Shanzad et al., 2016), antidiabetes (Li et al., 2019a), immunomodulatory (Li et al., 2020), and antitumor (Liu et al., 2019; Cheon and Ko, 2020) activities. It is worth noting that the phase 1 dose-escalation study of a new herbal medicine SH003, containing Huangqi (*Astragalus membranaceus*), has been finished in patients with solid cancers. Due to extensive research, triterpene saponins, flavonoids, polysaccharides, and phenolic acids were identified as the main active components (Li et al., 2019b; Wang et al., 2019).

Formononetin is one of the most investigated ingredients in *Astragalus membranaceus* (Huangqi) (Zheng et al., 2019). Formononetin has been under intense investigation for the past decade and numerous biological activities have been reported. Strong evidence has shown that formononetin can be used as an anticancer agent against diverse cancers through promoting apoptosis, working against proliferation, and inhibiting metastasis of cancer cells *in vitro* and *in vivo* (Ong et al., 2019). Also, formononetin's antioxidant and neuroprotective effects suggest its potential for Alzheimer's disease treatment (Sun et al., 2012; Xiao et al., 2019). Further, formononetin can effectively inhibit atherosclerosis, thus showing protective effect on cardiovascular system (Ma et al., 2020).

Till now, extensive research has focused on pharmacology activities of formononetin. Several studies have investigated the pharmacokinetic of formononetin in human, rats, or mice after oral administration of individual compound, Chinese patent medicine, herbal extracts of *Astragalus membranaceus*, or Chinese herbal formulas (Guan et al., 2014; Guo et al., 2015; Liu et al., 2015; Luo et al., 2018; Rao et al., 2019). However, the metabolic pathway of formononetin *in vivo or in vitro* is not reported. Formononetin is a member of the class of 7-hydroxy isoflavones according to its chemical structure. It was known that flavonoids could be rapidly metabolized to form their phase II metabolites (such as glucuronides and sulfates), especially in intestine, thus limiting their oral absorption, resulting in exceedingly low exposure (Chen et al., 2014; Chalet et al., 2018; Ravisankar et al., 2019). Further, inhibition of phase II metabolism could effectively increase bioavailability of flavonoids (Zhang et al., 2016; Ravisankar et al., 2019). Therefore, to clarify the disposition of formononetin *in vivo* is very necessary, especially phase II metabolism.

It has been certified that the plasma concentration of formononetin glucuronide in rats, generated by UDP-glucuronosyltransferase (UGTs) after oral administration, was much higher than the parent compound (Shi et al., 2015). However, the sulfonation of formononetin was rarely reported. Sulfonation is another important phase II metabolism mediated by sulfotransferase (SULTs), in addition to glucuronidation. Moreover, several researches have revealed that ATP-binding cassette (ABC) transporters, such as breast cancer resistance protein (BCRP) and multidrug resistance-associated proteins (MRPs), mediated the transmembrane transport of glucuronides and sulfates of flavonoids (Sun et al., 2015; Liu et al., 2018; Qi et al., 2019). Inhibition of the effect of efflux transporters on metabolites excretion could significantly decrease the cellular glucuronidation or sulfonation (Zhang et al., 2015; Liu et al., 2018). However, the effects of efflux transporters on formononetin sulfate excretion or sulfonation have not been determined.

Here, we have investigated sulfonation disposition of formononetin using HEK-SULT1A3 cells model in this study. SULT1A3 was appropriately selected because it is exclusively sulfated at 7-hydroxy (7-OH) position of flavonoids (Meng et al., 2012). Also, SULT1A3 was one of the most expressed SULT family isoforms in human intestine which indicated that it may play an important role in flavonoids disposition *in vivo* (Riches et al., 2009). Furthermore, the contributions of efflux transporters (i.e., BCRP and MRPs) to formononetin sulfate excretion were determined by using combined approaches of chemical inhibition (Ko143 for BCRP and MK-571 for MRPs) and biological inhibition (shRNA-mediated gene silencing).

MATERIALS AND METHODS

Chemicals and Reagents

Recombinant human SULT1A3 enzymes (rSULT1A3) were purchased form Sekisui XenoTech LCC (Kansas, USA). Formononetin (purity >98%) was purchased from Baoji Herbest Bio-Tech Co., Ltd. (Baoji, China). Acetonitrile, methanol, and water, which were of LC-MS grade, were bought from Merk KGaA (Darmstadt, Germany).

Sulfonation Assay

Enzyme kinetic of formononetin incubated with recombinant human SULT1A3 enzyme (rSULT1A3) was evaluated. The reaction was activated after the coenzyme PAPS (which provides sulfonate group to the substrates) was added. The incubation reaction was conducted in 200 μL potassium phosphate buffer (50 mM, pH 7.4) at 37°C, containing SULT1A3 enzyme (0.1 mg/ml), formononetin (0.16–40 μM), and PAPS (a final concentration of 0.10 mM). After incubation for 120 min, the reaction was terminated by adding 100 μL ice-cold acetonitrile. Then the samples were vortexed and centrifuged at 15,000 g for 15 min. The supernatant was analyzed by HPLC for sulfate quantification. All incubations were performed in triplicate. Preliminary experiments were performed to ensure that the rates of sulfation were determined under linear conditions with respect to incubation time and protein concentration.

Kinetic Evaluation

The sulfonation rates of formononetin at different concentrations were determined according to the sulfonation assay protocol. The kinetic model Michaelis-Menten (**Eq. 1**) was fitted to the data of sulfonation rates vs. formononetin concentrations. Model selection was based on visual inspection of the Eadie-Hofstee plot. Linearization of the Eadie-Hofstee plots indicated that the data were best described by Michaelis-Menten model. Model fitting and kinetic parameters evaluation were performed using GraphPad Prism software (5.3 version).

$$V = \frac{V_{max} \cdot [S]}{K_m + [S]} \quad (1)$$

where V_{max} is the maximal velocity and K_m is the Michaelis constant. The intrinsic clearance (CL_{int}) was calculated by V_{max}/K_m.

Structure Identification of Formononetin Sulfate by UPLC-QTOF/MS

The structure of formononetin sulfate was identified using UPLC-QTOF/MS method. Briefly, samples were separated using the Waters ACQUITY UPLC system and BEH column (2.1 × 50 mm, 1.7 μm; Waters, Milford, MA). Gradient elution was performed using formic acid (0.1%) in water (mobile phase A) and acetonitrile (mobile phase B) at a flow rate of 0.45 ml/min. Elution condition was 10% B at 0–1.0 min, 10%–90% B at 1.0–3.0 min, 90% B at 3.0–3.5 min, and 90%–10% B at 3.5–4.0 min. After chromatographic separation, samples were analyzed through Xevo G2 QTOF/MS (Waters) in the negative mode. The precursor and fragment ion information was collected using the electrospray ionization source (ESI) in MSMS mode. The collision energy was 15 eV. Data were analyzed using MassLynx version 4.1.

Quantification of Formononetin Sulfate by HPLC Analyses

Quantification of formononetin sulfate was performed using Agilent 1,260 Infinity II HPLC system with a ZORBAX SB-C18 column (4.6 × 250 mm, 5 μm; Agilent). The temperature of the column was set at 40 °C. The samples were analyzed using a gradient of ammonium acetate (2.5 mM) in water (mobile phase A) vs. acetonitrile (mobile phase B) at a flow rate of 1.0 ml/min. The gradient elution condition was 15% B at 0–2.0 min, 15–95% B at 2.0–12 min, 95% B at 12–15 min, and 95–15% B at 15–18 min. The waiting time was 7.0 min at 15% B in order to ensure the column pressure is back to a stable state before the next injection. The injection volume was 25 μL and the detection wavelength of formononetin sulfate was 250 nm. The standard curve was conducted using formononetin sulfate purified by our laboratory.

Correlation Analysis

Expression-activity correlation was performed to identify the role of SULT1A3 enzyme in formononetin sulfonation. The protein expression of SULT1A3 in individual human intestine S9 fractions (n = 9) was evaluated using western blotting assay. The sulfonation activities of nine individual human intestine S9 fractions toward formononetin were determined according to the sulfonation assay protocol. Correlation (Pearson) analyses were performed between protein expression levels of SULT1A3 enzyme and formononetin sulfonation in nine individual human intestine S9 fractions by GraphPad Prism software (5.3 version).

Functional Identification of SULT1A3 Overexpressing HKE293 Cells

HEK293 cells were stably transfected with the cDNA of Human SULT1A3 enzyme through the lentiviral transduction approach (Sun et al., 2015), which were named as HEK-SULT1A3 cells. The transduction efficiency was evaluated by measuring the SULT1A3 protein levels in both control and transfected cells. The enzyme function of HEK-SULT1A3 cells was further determined using sulfonation assay. In brief, HEK-SULT1A3 cell lysate was collected. Then, in order to identify the function of HEK-SULT1A3 cells in sulfate generation, formononetin was incubated with the HEK-SULT1A3 cell lysate and enzyme kinetic was determined as described above.

Sulfate Excretion Experiments

The sulfate excretion experiments were conducted using HEK-SULT1A3 cells model. In brief, HEK-SULT1A3 cells were washed with Hank's Balanced Salt Solution (HBSS) buffer (37°C, pH = 7.2) for three times. Then the cells were incubated with 2 ml HBSS buffer containing different concentrations of formononetin (final concentrations of 2.5 μM or 10 μM) at 37°C. 200 μL of incubation medium was sampled from each well at various times (0.5, 1.0, 1.5, and 2.0 h). Meanwhile, 200 μL of dosing solution was added immediately. The extracted samples were mixed with 100 μL ice-cold acetonitrile and vortexed for 1 min. The supernatant after centrifugation (15,000 g; 15 min) was injected into HPLC for analysis. After the last samples were taken, cells were collected into 400 μL ice-cold MeOH:H_2O (1:1, v/v) and processed to measure the intracellular amount of formononetin sulfate. The excretion rate (ER) of intracellular sulfate was calculated exactly as described in our publications (Liu et al., 2018). The apparent efflux clearance ($CL_{ef,app}$) was derived as the excretion rate divided by the intracellular concentration of sulfate (Ci). Ci was determined by dividing intracellular amount of sulfate at 2 h by intracellular volume. The intracellular volume of HEK293 cells was measured using sulfanilamide as described (Zhou et al., 2015).

Effect of Chemical Inhibitor on Sulfate Excretion

For this study, Ko143 (the specific inhibitor of BCRP) or MK-571 (the span inhibitor of MRPs) was used to inhibit the efflux transport function of BCRP or MRP4, and then the excretion rate and apparent efflux clearance ($CL_{ef,app}$) of formononetin sulfate in HEK-SULT1A3 cells were evaluated as described above.

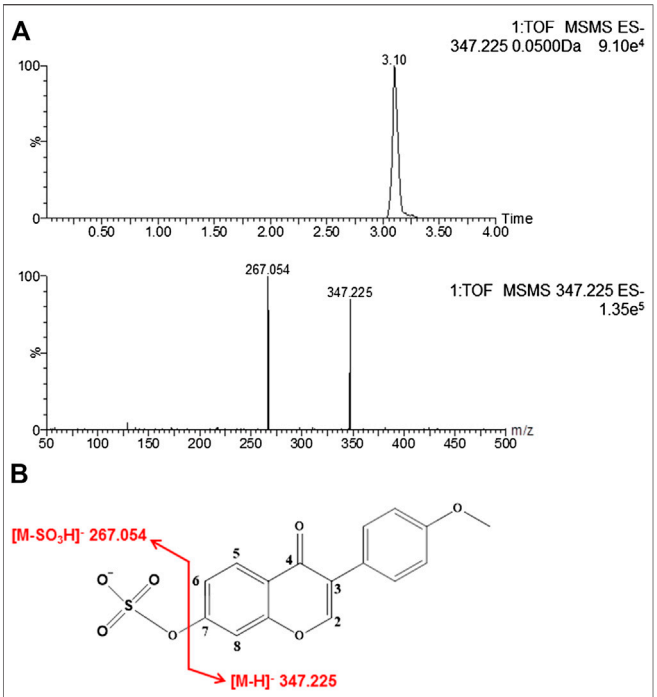

FIGURE 1 | The chromatogram of formononetin sulfate under MS/MS scanning **(A)** and the fragmentation pathways of formononetin sulfate **(B)**.

Transient Transfection of Short-Hairpin RNA Targeting BCRP or MRP4

The shRNA targeting MRP4 (NM_005845) was subcloned to the pLKO.1-Puro vector. Then the recombinant plasmid or blank vector (scramble) was transfected into HEK-SULT1A3 cells using Lipofectamine 2000 reagent (Invitrogen, Waltham, MA). Cells were used for sulfate excretion experiments 48 h after transfection. Further, the fraction of dose metabolized (f_{met}), an indicator of the extent of drug sulfonation, was calculated according to **Eq. 2**.

$$f_{met} = \frac{\text{excreted sulfate} + \text{intracellular sulfate}}{\text{total dosed aglycone}} \quad (2)$$

Western Blotting Analysis

The cells were collected and lysed in RIPA Lysis Buffer (Beyotime, Shanghai) in advance. After quantified using BCA protein assay kit (Thermo Scientific, Waltham, Massachusetts), the cells samples or individual human intestine S9 fractions were analyzed by sodium dodecyl sulfate polyacrylamide gel electrophoresis (10% acrylamide gels) and transferred to polyvinylidene fluoride membranes (0.22 μM, Millipore, Bedford, MA). After blocking for 1 h, the membranes were incubated with primary antibodies (1: 1,000 dilution) at 4°C overnight, followed by anti-rabbit or anti-mouse horseradish peroxidase conjugated secondary antibody. Target protein bands were visualized with enhanced chemiluminescence and imaged by autoradiography. And then the protein bands were scanned in grayscale and subjected to semiquantitative analysis using Quantity One software.

Statistical Analysis

Data were presented as mean ± standard deviation (SD). Statistically significant differences between two group data were analyzed by two-tailed Student's t-test. The level of significance was set at $p < 0.05$.

RESULTS

Structure Identification of Formononetin Sulfate

The retention time of formononetin sulfate was 3.10 min (**Figure 1A**). Formononetin sulfate formed a deprotonated molecule $[M-H]^-$ at m/z 347.225 in the negative ion scan mode. The major fragment ion of the sulfate was observed at m/z 267.054, which corresponded exactly to the parent compound (formononetin). The $[M-H]^-$ mass of formononetin sulfate showed an exact mass difference of a sulfonate group compared to the parent compound, indicating that this metabolite was a monosulfate of formononetin (**Figure 1A,B**).

Generation of Formononetin Sulfate in rSULT1A3 and HEK-SULT1A3 Cell Lysate

3′-Phosphoadenosine-5′-phosphosulfate (PAPS) was necessary for sulfonation reaction catalyzed by sulfotransferases. When incubating formononetin with rSULT1A3 enzyme, one formononetin sulfate (F-O-S) was generated in the presence of PAPS (**Figure 2A**). By contrast, no sulfate formed in the absence of PAPS under the same incubation condition (**Figure 2A**). Under the effect of sulfotransferases, a sulfonate group was transformed form PAPS to the 7-hydroxy of formononetin. As a result, the water solubility of metabolite was enhanced compared to parent compound formononetin. Accordingly, the metabolite was eluted much earlier (7.25 min) compared with formononetin (10.79 min) (**Figure 2A**). In addition, the metabolite showed high similarity of UV absorption spectrum (λ_{max} = 252 nm) with that of parent compound (**Figure 2B**).

When formononetin (2.5 μM or 10 μM) was incubated with HEK-SULT1A3 cells, F-O-S was generated and excreted into the extracellular media. The amount of metabolite increased with the incubation time (**Figure 3A**). Further, the extracellular amounts of F-O-S were significantly increased ($p < 0.001$) as the dose increased from 2.5 to 10 μM (**Figure 3B**). Increased sulfate excretion was associated with an elevated level of formononetin within the cells (**Figure 3C**). The above results indicated that HEK-SULT1A3 cells were a suitable model to investigate the disposition of drugs and excretion of their sulfate metabolites.

Activity-Expression Correlation

The SULT1A3 levels in a bank of individual human intestine S9 fractions (n = 9) were quantified using the immunoblotting technique (**Figure4A**). The sulfonation activities of these nine individual human intestine S9 fractions toward formononetin (5 μM) were measured. It was found that formononetin sulfonation velocity was significantly correlated with the

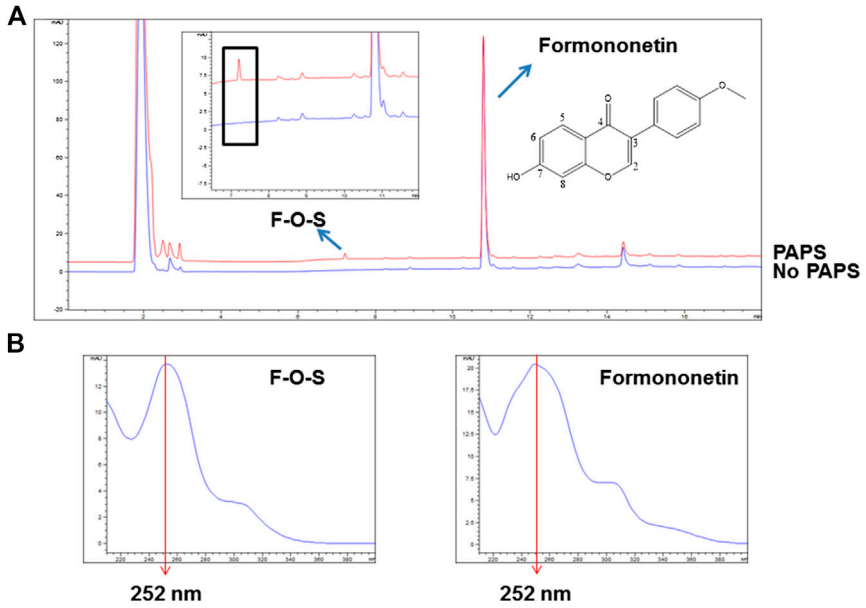

FIGURE 2 | (A) Chemical structure of formononetin and representative HPLC chromatograms for quantitative analyses of formononetin and its sulfate (F-O-S). **(B)** UV absorption spectra of formononetin and F-O-S.

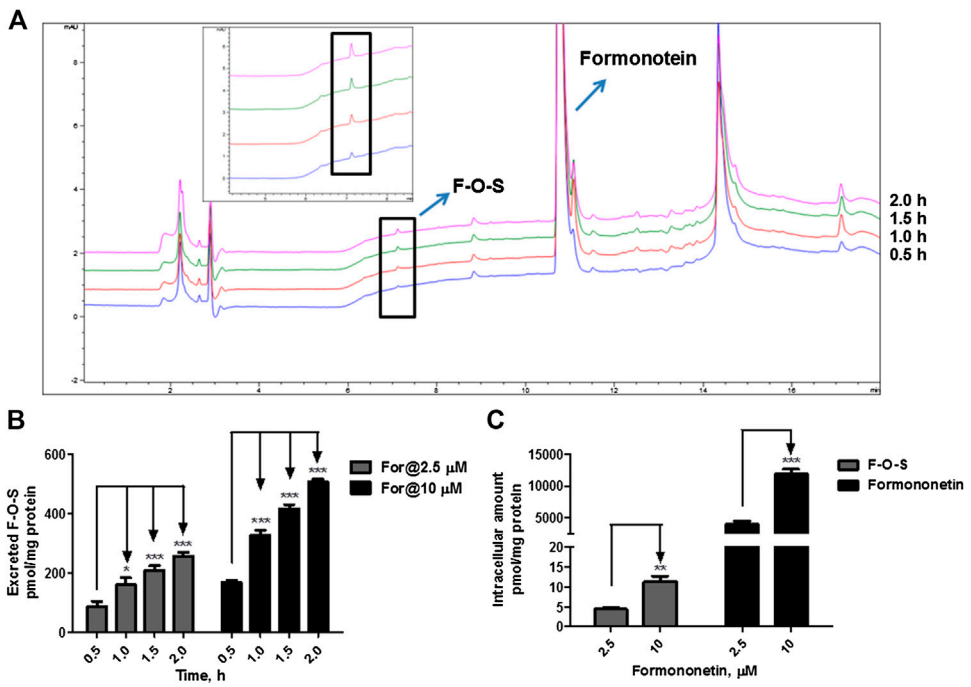

FIGURE 3 | Disposition of formononetin in HEK-SULT1A3 cells at different loading doses. **(A)** Representative HPLC chromatograms showing that formononetin sulfate (F-O-S) was generated after incubation with HEK-SULT1A3 cells at different time points and excreted into extracellular medium. **(B)** Excretion rates of formononetin sulfate (F-O-S) at dose of 2.5 μM and 10 μM, respectively. **(C)** Intracellular amounts of formononetin and F-O-S at 2 h after incubation under different loading doses. *$p < 0.05$, **$p < 0.01$, ***$p < 0.001$ compared with control. Each data point was shown as mean ± SD (n = 3).

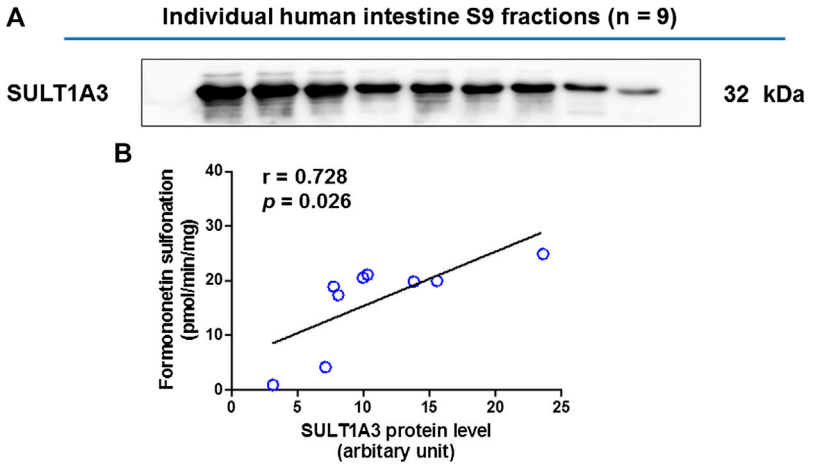

FIGURE 4 | (A) Protein expression of SULT1A3 in a bank of individual human intestine S9 fractions (n = 9). **(B)** Correlation analysis between formononetin sulfonation and SULT1A3 protein levels in individual human intestine S9 fractions (n = 9).

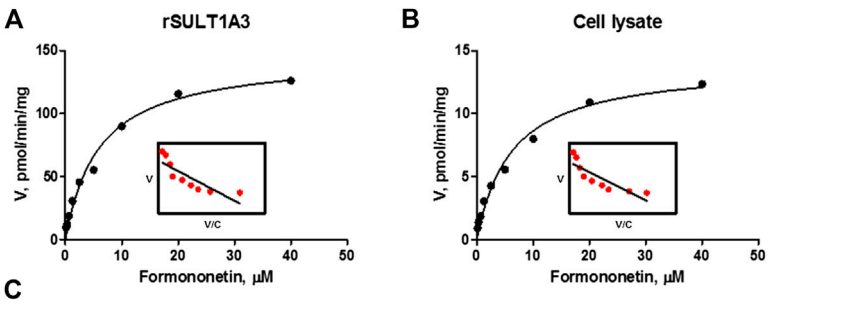

C

Enzyme	V_{max} *pmol/min/mg*	K_m *μM*	CL_{int} *μl/min/mg*	Fitted model
rSULT1A3	145.30 ± 7.91***	6.01 ± 0.97	24.18 ± 4.13***	MM
Cell lysate	13.94 ± 0.83	6.17 ± 1.09	2.26 ± 0.42	MM

FIGURE 5 | (A) Enzyme kinetic profile and Eadie-Hofstee plot (insert) of formononetin sulfonation in rSULT1A3. **(B)** Enzyme kinetic profile and Eadie-Hofstee plot (insert) of formononetin sulfonation in HEK-SULT1A3 cell lysate. **(C)** Kinetic parameters derived for formononetin sulfonation in rSULT1A3 enzyme and HEK-SULT1A3 cells lysate. Each data point was shown as mean ± SD (n = 3). ***$p < 0.001$ compared with cell lysate. Each data point was shown as mean ± SD (n = 3).

protein levels of SULT1A3 (r = 0.728; $p < 0.05$) (**Figure 4B**). These results indicated that SULT1A3 was of great significance in determining sulfonation of formononetin.

Enzyme Kinetics of Formononetin in rSULT1A3 and HEK-SULT1A3 Cell Lysate

As shown in **Figure 5A**, B, formation of F-O-S in rSULT1A3 and HEK-SULT1A3 cell lysate both followed the classical Michaelis-Menten kinetics. The value of V_{max} was 145.30 ± 7.91 pmol/min/mg and 13.94 ± 0.83 pmol/min/mg for formononetin in rSULT1A3 and cell lysate, respectively. The value of K_m was 6.01 ± 0.97 μM and 6.17 ± 1.09 μM in rSULT1A3 and cell lysate, respectively. Because the protein purity of SULT1A3 enzyme was different, the V_{max} of formononetin sulfonation was much lower ($p < 0.001$) in cell lysate than that in rSULT1A3 enzyme (**Figure 5C**). However, the K_m value in cell lysate and rSULT1A3 was similar (**Figure 5C**), which indicated that HEK-SULT1A3 cells have displayed the activity of SULT1A3 enzyme to catalyze sulfonation reaction.

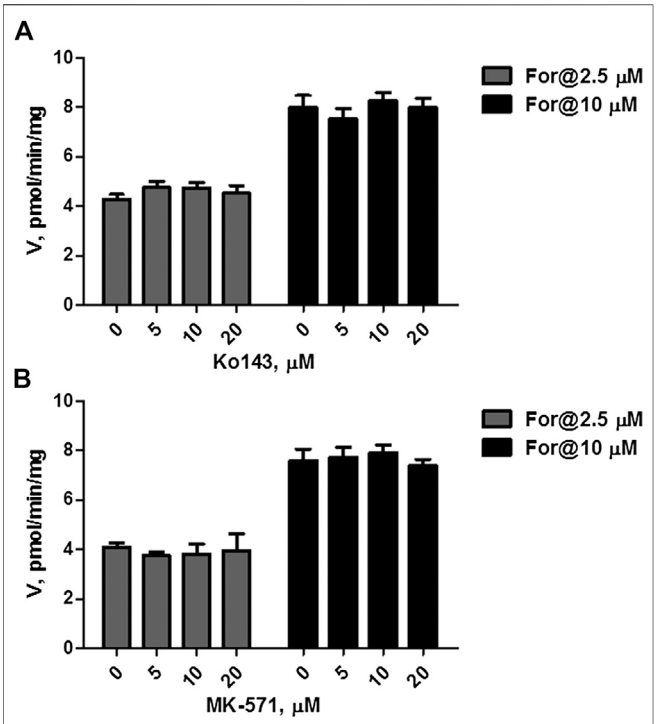

FIGURE 6 | Effects of chemical inhibitors on formononetin (2.5 and 10 μM) sulfonation in HEK-SULT1A3 cell lysate. **(A)** Effects of Ko143 on formononetin sulfonation. **(B)** Effects of MK-571 on formononetin sulfonation. Each data point was shown as mean ± SD (n = 3).

Effect of Chemical Inhibitor on Formononetin Sulfonation

The effects of Ko143 (a selective BCRP inhibitor) and MK-571 (a pan MRPs inhibitor) on formononetin (2.5 and 10 μM) sulfonation were evaluated using HEK-SULT1A3 cell lysate. Ko143, at the concentration of 5–20 μM, did not show any effects on formononetin sulfonation (**Figure 6A**, $p > 0.05$). Likewise, MK-571 at all tested concentrations (5–20 μM) did not alter the generation of F-O-S (**Figure 6B**, $p > 0.05$). These results indicated that sulfonation of formononetin mediated by cell lysate was not modulated by Ko143 and MK-571.

Effect of Chemical Inhibitor on Sulfate Excretion

Cellular expression of MRPs family transporters in wild type HKE293 and HEK-SULT1A3 cells has been detected using reverse transcription-polymerase chain reaction and western blotting method in our previous publications (Sun et al., 2015). The results indicated that BCRP and MRP4 were the dominant efflux transporters in HEK293 cells. And compared to wild type HEK293 cells, the expression level of BCRP and MRP4 was not changed in the engineered HEK-SULT1A3 cells. Furthermore, the role of BCRP and MRP4 involvement into formononetin sulfate excretion was determined using HEK-SULT1A3 cells. At a low loading concentration of formononetin (2.5 μM), Ko143 (5–20 μM) showed no or negligible effects on excretion rate and intracellular accumulation amount of F-O-S (**Figure 7A,B**, $p > 0.05$). Similarly, the sulfate excretion and intracellular accumulation were also not modulated by Ko143 (5–20 μM) when a high loading concentration (10 μM) of formononetin was used (**Figure 7C,D**, $p > 0.05$). These results suggested that BCRP was not involved in the excretion of formononetin sulfate in HEK-SULT1A3 cells.

However, coincubation of MK-571 (5–20 μM) and formononetin (dosing of 2.5 μM) resulted in substantial reduction (79.1%–94.6%, $p < 0.001$) in excretion of F-O-S (**Figure 8A**, B). On the contrary, MK-571 at higher concentrations (5–20 μM) caused an obvious elevation (145.6%–197.8%, $p < 0.01$ and $p < 0.001$) in intracellular amount of F-O-S (**Figure 8C**). It was not surprising that a remarkable decrease of $CL_{ef,app}$ (85.3%–98.0%, $p < 0.001$) was observed in the presence of MK-571 at all tested concentrations (**Figure 8D**).

Similar effects of MK-571 on sulfate disposition were observed when a higher loading dose of formononetin (10 μM) was used. MK-571 (at the concentration of 5–20 μM) markedly decreased (79.8%–95.7%, $p < 0.001$) the excretion rates (**Figure 8E,F**) while it increased (160.6%–188.8%, $p < 0.001$) the intracellular level of F-O-S (**Figure 8G**). Further, $CL_{ef,app}$ values of F-O-S were obviously reduced (87.3%–97.7%, $p < 0.001$, **Figure 8H**) under effect of MK-571. Taken together, the effect of MK-571 on formononetin sulfonation indicated that one or more MRPs family transporters played an important role in the excretion of formononetin sulfate.

Effect of MRP4 Knockdown on Formononetin Sulfonation in HEK-SULT1A3 Cells

MRP4 was the only expressed MRPs family transporter in HEK-SULT1A3 cells, and the effect of MRP4 on formononetin sulfonation transport was determined through gene silencing. The protein expression of MRP4 in HEK-SULT1A3 cells was significantly knocked down through transient transfection of selected shRNA (**Figure 9A**). Semiquantitative analysis of MRP4 was performed depending on band intensities, and β-actin was used as internal control. After transfection with shRNA, the protein expression of MRP4 was reduced by 44.7% ($p < 0.01$) (**Figure 9B**) in HKE-SULT1A3 cells. MRP4 knockdown led to obvious reductions (>32.8%, $p < 0.01$) in sulfate excretion rates (**Figure 9C**) but with significant elevations (>127.4%, $p < 0.05$) in intracellular amounts of F-O-S (**Figure 9D**) as expected. Accordingly, shMRP4 also caused obvious decrease (>50.6%, $p < 0.01$) in $CL_{ef,app}$ values of F-O-S (**Figure 9E**). These results indicated that MRP4 was involved in excretion of formononetin sulfate. Furthermore, the role of MRP4 in formononetin cellular sulfonation was evaluated according to the f_{met} values. Interestingly, MRP4 silencing caused substantial decreases in cellular sulfonation of formononetin (17.3%–26.7%, $p < 0.01$) (**Figure 9F**).

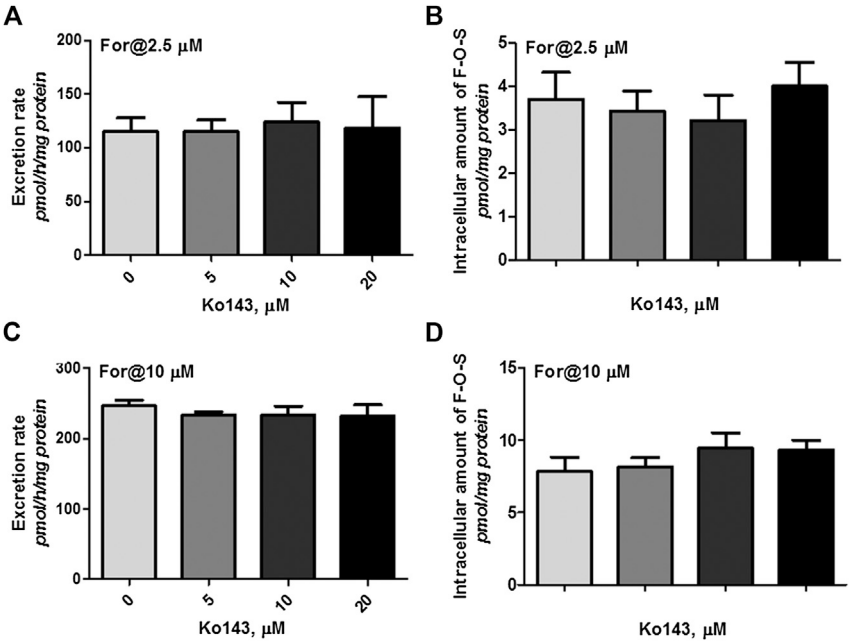

FIGURE 7 | Effects of Ko143 (5–20 μM) on formononetin (2.5 and 10 μM) disposition in HEK-SULT1A3 cells. Effects of Ko143 on the excretion rates **(A)** and intracellular amounts **(B)** of formononetin sulfate at a low loading concentration of formononetin (2.5 μM). Effects of Ko143 on the excretion rates **(C)** and intracellular amounts **(D)** of formononetin sulfate at a high loading concentration of formononetin (10 μM). Each data point was shown as mean ± SD (n = 3).

DISCUSSION

Sulfonation is an important phase II metabolism mediated by sulfotransferases (Kauffman, 2004; Dubaisi et al., 2019) and regulates the disposition of numerous endo- and xenobiotics (James and Ambadapadi, 2013; Garbacz et al., 2017). Moreover, we and other researchers have discovered that phenolic compounds, especially the flavonoids, are susceptible to glucuronidation and sulfonation (two important metabolic pathways) (Chen et al., 2014; Najmanova et al., 2019; El Daibani et al., 2020). Due to the attention, the glucuronide metabolite of formononetin has been identified and quantified in rat plasma after oral administration (Wang et al., 2014; Shi et al., 2015), which indicated that glucuronidation may be an important clearance mechanism for formononetin *in vivo*. However, no sulfonation of formononetin has been reported, which means that the contribution of sulfonation to formononetin disposition may be ignored. Hence, it is necessary to evaluate the characterization of formononetin sulfonation. Furthermore, elucidation of the transporters responsible for excretion of formononetin sulfate will help promote understanding of pharmacokinetic behaviors of formononetin and its sulfate metabolites.

Oral bioavailability is a major factor in determining the biological actions of formononetin *in vivo*. Hence, it is critical to clarify the important factors involved in its oral bioavailability. As sulfonation was an important pathway for drugs clearance, characterization of formononetin sulfonation assumes great importance in understanding of its disposition and bioavailability. In this study, we for the first time identified that SULT1A3 played important role in formononetin sulfonation, because formononetin sulfonation was significantly correlated with SULT1A3 protein levels in a bank of individual human intestine S9 factions (**Figure 4**). It is well known that SULT1A3 is barely detected in human liver, but it is highly expressed in jejunum and intestine (Gamage et al., 2006). Thus, it was highly possible that intestinal sulfonation had impact on the oral bioavailability.

Further, the sulfonation of formononetin and its sulfate excretion were determined using SULT1A3 overexpressing HEK293 cells (HEK-SULT1A3). As expected, HKE-SULT1A3 cells catalyzed formononetin formation of one sulfate like the expressed human SULT1A3 enzyme. Sulfonation of formononetin followed the classical Michaelis-Menten kinetics (**Figure 5**). It was not surprising because SULT1A3 mediated sulfonation of flavonoids (e.g., chrysin, apigenin, and hesperetin) often showed Michaelis-Menten kinetics (Li et al., 2015; Sun et al., 2015). The V_{max} value of rSULT1A3 was much higher than cell lysate (**Figure 5C**), because the SULT1A3 enzyme was more concentrated in rSULT1A3 than in cell lysate. In addition, the K_m values of formononetin sulfonation derived from two types of enzyme materials were similar ($p > 0.05$). The results indicated that the rSULT1A3 enzyme and HEK-SULT1A3 cell lysate showed a high similarity in the sulfonation profile, providing strong evidence that HEK-SULT1A3 cells possessed a high conjugation activity toward formononetin owing to stable transfection of SULT1A3.

Furthermore, MRP4 was primarily responsible for the excretion of formononetin sulfate. These results were confirmed by the following strong evidence. First, the pan inhibitor of MRP family transporters (MK-571) at 20 μM

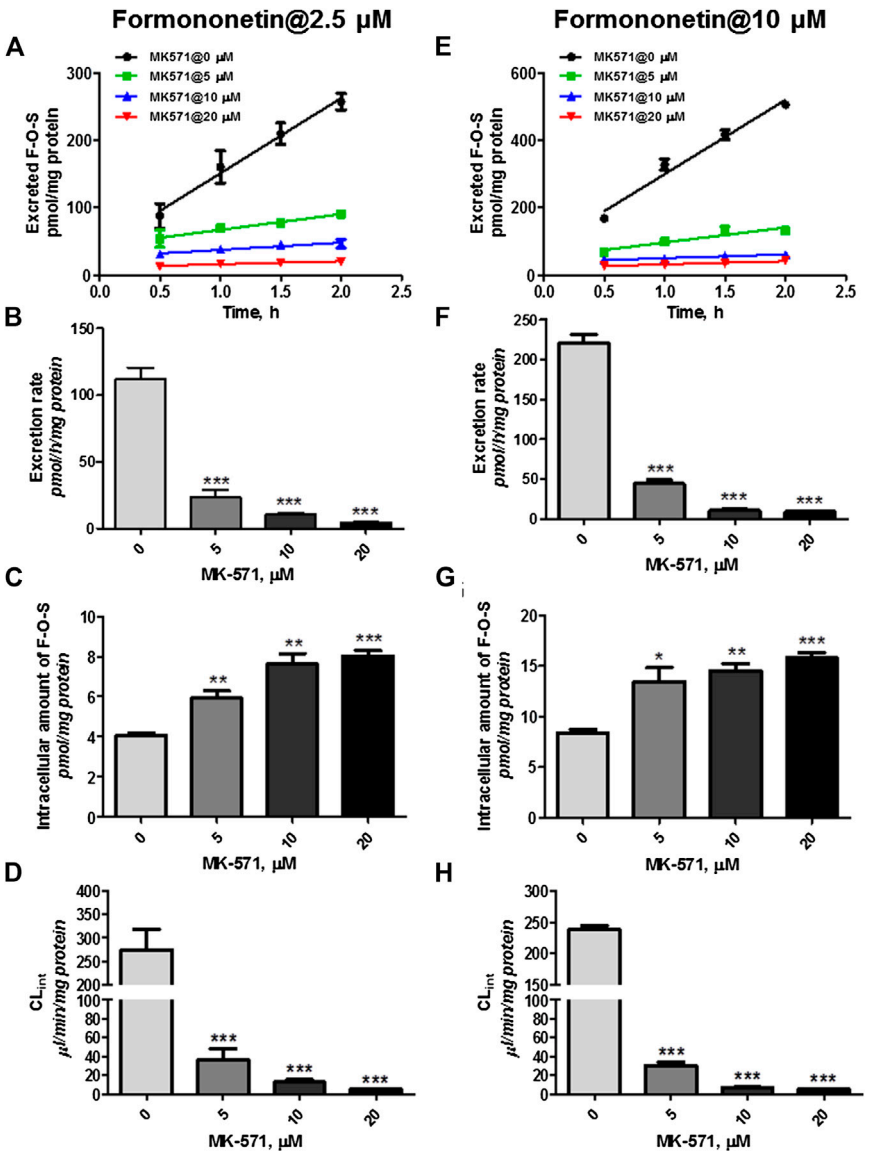

FIGURE 8 | Effects of MK-571 (5–20 μM) on formononetin (2.5 and 10 μM) disposition in HEK-SULT1A3 cells. Effects of MK-571 on the excretion profile **(A)**, intracellular amounts **(B),** and efflux clearances **(C)** of formononetin sulfate at a low loading concentration of formononetin (2.5 μM). Effects of MK-571 on the excretion profile **(D)**, intracellular amounts **(E),** and efflux clearances **(F)** of formononetin sulfate at a high loading concentration of formononetin (10 μM). *$p < 0.05$, **$p < 0.01$, ***$p < 0.001$ compared with control. Each data point was shown as mean ± SD (n = 3).

almost completely suppressed (>94%) excretion of formononetin sulfate (**Figure 8**). Second, MK-571 showed no effects on formononetin sulfonation (**Figure 6**), which made it clear that alterations in sulfate excretion caused by MK-571 were mainly attributable to suppression of the functions of MRPs. Third, selective knockdown of MRP4 was followed by observable reduction in sulfate excretion rates (**Figure 9**).

Because BCRP was one of the major efflux transporters expressed in HEK-SULT1A3 cells (Sun et al., 2015), the contribution of BCRP to sulfate excretion was also determined. All results proved that contribution of BCRP to the excretion of formononetin sulfate was none or negligible. That is because when Ko143 (a potent and selective inhibitor of BCRP) was used, the excretion rates and intracellular levels of formononetin sulfate were not altered compared to the control (**Figure 7**). This was not surprising, as similar results have been obtained in our previous studies (Sun et al., 2015; Li et al., 2015; Liu T. et al., 2018). In addition, sulfonation of formononetin was not affected by Ko143 (**Figure 6**), which further convinced us that BCRP was not responsible for the efflux of formononetin sulfate. In a recent study, chrysin and chrysin-7-sulfate have shown stronger inhibitory effects on BCRP (Mohos et al., 2020). Therefore, we speculate that formononetin and/or its sulfate may also be an inhibitor of BCRP, which will prove why

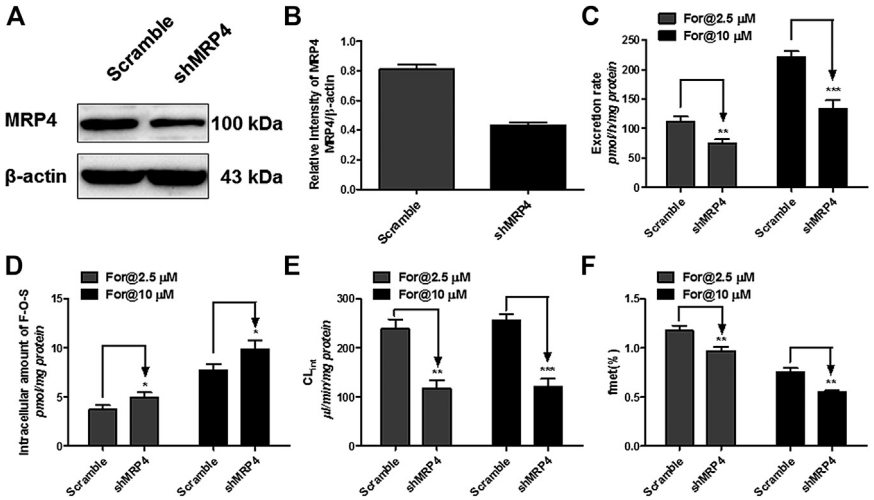

FIGURE 9 | Effect of MRP4 silencing on formononetin (2.5 and 10 μM) disposition in HEK-SULT1A3 cells. **(A)** Western blot of MRP4 after transient transfection by selected shRNA. **(B)** Effects of gene silencing on the protein level of MRP4. **(C)** Effects of gene silencing on the excretion rates of formononetin sulfate. **(D)** Effects of gene silencing on the intracellular amounts of sulfate. **(E)** Effects of gene silencing on the excretion rates of sulfate. **(F)** Effects of gene silencing on the cellular sulfonation (f_{met}) of formononetin. $^{*}p < 0.05$, $^{**}p < 0.01$, $^{***}p < 0.001$ compared with control. Each data point was shown as mean ± SD (n = 3).

BCRP does not participate in the cellular excretion of formononetin sulfate. However, further evidence should be provided to support or disprove this hypothesis.

Ko143 and MK-571 have been widely used as the chemical inhibitor of BCRP and MRP4 *in vitro* and *in vivo* (Bertollotto et al., 2018; Drennen et al., 2018; Kanda et al., 2018; Feng et al., 2019). Hence, we have selected and used Ko143 and MK-571 to inhibit the transport activities of BCRP and MRPs in our study. Due to complicacies of chemical inhibitors in evaluation of sulfate excretion, the effects of Ko143 and MK-571 on formononetin sulfonation were determined. It was shown that both Ko143 and MK-571 did not alter sulfonation rates of formononetin mediated by HKE-SULT1A3 cell lysate (**Figure 6**). This result provided strong evidence that the reduction in sulfate excretion was mainly due to activities inhibition of transporters.

Our finding that human cells expressing SULT1A3 were active in metabolizing formononetin lent a strong support to notion that sulfonation plays an important role in disposition of formononetin. The sulfate metabolite of formononetin was also efficiently generated upon incubation of Caco-2 cells (Chen et al., 2005). In addition, significant amount of formononetin sulfate was found in intestine using mouse intestinal perfusion model (Jeong et al., 2005). Therefore, the role of sulfonation in determining the pharmacokinetics of formononetin might have been underestimated. Based on previous studies, flavonoids and/or their conjugate metabolites (glucuronide or sulfate) have shown significant interactions with metabolism enzymes and transporters (Li and Paxton, 2013; Mohos et al., 2020), raising the potential for interactions with conventional drug therapies. Furthermore, formononetin was identified as an inhibitor of CYP enzymes (Arora et al., 2015). However, the biological activities of formononetin sulfate remain underexplored. Due to the considerable sulfonation metabolism of formononetin, further studies should be devoted to the potential pharmacological effect of its sulfate and the impact of sulfate on the pharmacokinetics, efficacy, and toxicity of drugs.

HEK-SULT1A3 cells have been proved to be an appropriate model for evaluation of the cellular disposition processes of formononetin and its sulfate. That is because 1) formononetin sulfate did not need to be prepared as it could be generated during the experiments; and 2) formononetin has been reported to enter cells mainly through passive diffusion (Singh and Wahajuddin, 2011). Therefore, the uptake rates and intracellular amounts of formononetin when incubated with HEK-SULT1A3 cells have not been affected by chemical inhibitors (Ko143 and MRP4) and protein knockdown of efflux transporters. Furthermore, the rapid uptake of formononetin into HEK-SULT1A3 cells indicated that the sulfonation of formononetin by SULT1A3 in HEK-SULT1A3 cells will not be restricted by the intracellular amounts of parent compound. The results convinced us that efflux transporter MRP4 played an important role in the disposition of sulfate metabolite and formononetin.

We have shown for the first time that MRP4 silencing led to obvious reductions in cellular sulfonation (f_{met}) of formononetin (**Figure 9**), which suggested that MRP4 potentially mediated the total sulfonation in cells. However, the values of f_{met} obtained at 10 μM were lower than that at 2.5 μM formononetin dose. That was not surprising, because f_{met} (%) was calculated by dividing the total amount of sulfate generated (including excreted and intracellular sulfate) by dosed formononetin. Although the amount of sulfate formed at 10 μM of formononetin was higher, when divided by the larger dosing, the calculated f_{met} (%) turned into lower than that at 2.5 μM of formononetin. It was noteworthy that the f_{met} (%) values showed a contradictory result with that in our previous publication (Liu et al., 2018). There was a possibility that the sulfonation rate of liquiritigenin was much higher than formononetin. Therefore, the amount ratio of liquiritigenin sulfate generated at 10 μM over at 2.5 μM in

HEK-SULT1A3 cells was much higher than that of formononetin sulfate, which led to contradictory result in spite of the similar experimental conditions.

Although formononetin has shown satisfactory intestinal uptake (Singh and Wahajuddin, 2011; Almeida et al., 2015), the bioavailability of unchanged formononetin was found to be poor, approximately 3% (Singh and Wahajuddin, 2011). It was noted that glucuronide and/or sulfate of formononetin in circulating plasma were much higher than parent compound (Singh and Wahajuddin, 2011; Shi et al., 2015), which indicated that the poor bioavailability may be due to the extensive conjugation reaction (i.e., glucuronidation and/or sulfonation) *in vivo*. Hence, inhibition of the corresponding metabolism or activities of enzymes will contribute to the improvement of bioavailability (Izgelov et al., 2018; Najmanova et al., 2019; Ravisankar et al., 2019). In the present study, we have confirmed that inhibition of MRP4 activity or decreasing MRP4 expression led to a reduced formononetin sulfonation. Due to the extensive distribution of MRP4 in various tissues/organs, MRP4 should be a key factor for the elimination and distribution of formononetin sulfate, even the bioavailability of formononetin.

CONCLUSION

Formononetin generated one sulfate metabolite after incubation with rSULT1A3 and HEK-SULT1A3 cell lysate, and the enzyme kinetics followed Michaelis-Menten model. HEK-SULT1A3 cells could mediate the formation and excretion of formononetin sulfate (F-O-S). Furthermore, MK-571 (the pan inhibitor of MRPs) at all test concentrations remarkably decreased the excretion rate and efflux clearance ($CL_{ef,app}$) of formononetin sulfate, whereas Ko143 (the selected inhibitor of BCRP) showed no effect on sulfate excretion. Knockdown of MRP4 also caused substantial reduction in sulfate excretion. It was worth noting that MRP4 gene slicing further led to significant reduction in cellular sulfonation of formononetin. Taken together, MRP4 could effectively mediate the excretion of formononetin sulfate into extracellular media and played a regulation role in cellular sulfonation.

DATA AVAILABILITY STATEMENT

The datasets presented in this study can be found in online repositories. The names of the repository/repositories and accession number(s) can be found in the article/ Supplementary Material.

AUTHORS CONTRIBUTIONS

HS and FL participated in research design. HS, FL, SP, WL, XW, CL, RY, ZZ, and XY conducted experiments. DF and SX contributed new reagents or analytic tools. HS, FL, SP, and WL performed data analysis. HS wrote or contributed to the writing of the manuscript.

FUNDING

This work was supported by the National Natural Science Foundation of China (81703801), Postdoctoral Research Foundation of China (2018M632764), Henan Province Young Talents Lifting Project (2019HYTP025), Postdoctoral Research grant in Henan Province (001801014), Innovative Research Team (in Science and Technology) in University of Henan Province (19IRTSTHN004), Key Project of Science and Technology Research Funded by the Educational Commission of Henan Province (18A350004), and Guangdong Provincial Key Laboratory of Drug Non-Clinical Evaluation and Research (2018B030323024).

REFERENCES

Almeida, I. M., Rodrigues, F., Sarmento, B., Alves, R. C., and Oliveira, M. B. P. P. (2015). Isoflavones in food supplements: chemical profile, label accordance and permeability study in Caco-2 cells. *Food Funct.* 6 (3), 938–946. doi:10.1039/c4fo01144a

Arora, S., Taneja, I., Challagundla, M., Raju, K. S., Singh, S. P., and Wahajuddin, M. (2015). *In vivo* prediction of CYP-mediated metabolic interaction potential of formononetin and biochanin A using *in vitro* human and rat CYP450 inhibition data. *Toxicol. Lett.* 239 (1), 1–8. doi:10.1016/j.toxlet.2015.08.202

Bertollotto, G. M., de Oliveira, M. G., Alexandre, E. C., Calmasin, F. B., Passos, G. R., Antunes, E., et al. (2018). Inhibition of multidrug resistance proteins by MK 571 enhances bladder, prostate, and urethra relaxation through cAMP or cGMP accumulation. *J. Pharmacol. Exp. Therapeut.* 367 (1), 138–146. doi:10.1124/jpet.118.250076

Chalet, C., Rubbens, J., Tack, J., Duchateau, G. S., and Augustijns, P. (2018). Intestinal disposition of quercetin and its phase-II metabolites after oral administration in healthy volunteers. *J. Pharm. Pharmacol.* 70 (8), 1002–1008. doi:10.1111/jphp.12929

Chen, J., Lin, H., and Hu, M. (2005). Absorption and metabolism of genistein and its five isoflavone analogs in the human intestinal Caco-2 model. *Canc. Chemother. Pharmacol.* 55 (2), 159–169. doi:10.1007/s00280-004-0842-x

Chen, Z., Zheng, S., Li, L., and Jiang, H. (2014). Metabolism of flavonoids in human: a comprehensive review. *Curr. Drug Metabol.* 15 (1), 48–61. doi:10.2174/1389200215011402181250 20

Cheon, C., and Ko, S. G. (2020). A phase I study to evaluate the safety of the herbal medicine SH003 in patients with solid cancer. *Integr. Canc. Ther.* 19, 1534735420911442. doi:10.1177/1534735420911442

Drennen, C., Gorse, E., and Stratford, R. E., Jr (2018). Cellular pharmacokinetic model-based analysis of genistein, glyceollin, and MK-571 effects on 5 (and 6)-carboxy-2',7'-dichloroflourescein disposition in caco-2 cells. *J. Pharmacol. Sci.* 107 (4), 1194–1203. doi:10.1016/j.xphs.2017.12.004

Dubaisi, S., Caruso, J. A., and Gaedigk, R. (2019). Developmental expression of the cytosolic sulfotransferases in human liver. *Drug Metab. Dispos.* 47 (6), 592–600. doi:10.1124/dmd.119.086363

El Daibani, A. A., Xi, Y., Luo, L., Hou, C., Liu, W., Yan, T., et al. (2020). Sulfation of hesperetin, naringenin and apigenin by the human cytosolic sulfotransferases: a comprehensive analysis. *Nat. Prod. Res.* 34 (6), 797–803. doi:10.1080/14786419.2018.1503264

Feng, S., Zheng, L., Tang, S., Gu, J., Jiang, X., Wang, L., et al. (2019). *In-vitro* and *in situ* assessment of the efflux of five antidepressants by breast cancer resistance protein. *J. Pharm. Pharmacol.* 71 (7), 1133–1141. doi:10.1111/jphp.13100

Gamage, N., Barnett, A., Hempel, N., Duggleby, R. G., Windmill, K. F., Martin, F. L., et al. (2006). Human sulfotransferases and their role in chemical metabolism. *Toxicol. Sci.* 90 (1), 5–22. doi:10.1093/toxsci/kfj061

Garbacz, W. G., Jiang, M., and Xie, W. (2017). Sex-dependent role of estrogen sulfotransferase and steroid sulfatase in metabolic homeostasis. *Adv. Exp. Med. Biol.* 1043, 455–469. doi:10.1007/978-3-319-70178-3_21

Guan, J., Wang, L., Jin, J., Yang, Y., Hu, F., Zhu, R., et al. (2014). Simultaneous determination of calycosin-7-O-β-D-glucoside, ononin, calycosin, formononetin, astragaloside IV, and astragaloside II in rat plasma after oral administration of Radix Astragali extraction for their pharmacokinetic studies by ultra-pressure liquid chromatography with tandem mass spectrometry. *Cell Biochem. Biophys.* 70 (1), 677–686. doi:10.1007/s12013-014-9972-x

Guo, P., Dong, L., Yan, W., Wei, J., Wang, C., and Zhang, Z. (2015). Simultaneous determination of linarin, naringenin and formononetin in rat plasma by LC-MS/MS and its application to a pharmacokinetic study after oral administration of Bushen Guchi Pill. *Biomed. Chromatogr.* 29 (2), 246–253. doi:10.1002/bmc.3267

Izgelov, D., Cherniakov, I., Aldouby Bier, G., Domb, J. A., and Hoffman, A. (2018). The effect of piperine pro-nano lipospheres on direct intestinal phase II metabolism: the raloxifene paradigm of enhanced oral bioavailability. *Mol. Pharm.* 15 (4), 1548–1555. doi:10.1021/acs.molpharmaceut.7b01090

James, M. O., and Ambadapadi, S. (2013). Interactions of cytosolic sulfotransferases with xenobiotics. *Drug Metab. Rev.* 45 (4), 401–414. doi:10.3109/03602532.2013.835613

Jeong, E. J., Jia, X., and Hu, M. (2005). Disposition of formononetin via enteric recycling: metabolism and excretion in mouse intestinal perfusion and Caco-2 cell models. *Mol. Pharm.* 2 (4), 319–328. doi:10.1021/mp0498852

Kanda, K., Takahashi, R., Yoshikado, T., and Sugiyama, Y. (2018). Total hepatocellular disposition profiling of rosuvastatin and pitavastatin in sandwich-cultured human hepatocytes. *Drug Metabol. Pharmacokinet.* 33 (3), 164–172. doi:10.1016/j.dmpk.2018.04.001

Kauffman, F. C. (2004). Sulfonation in pharmacology and toxicology. *Drug Metab. Rev.* 36 (3–4), 823–843. doi:10.1081/dmr-200033496

Li, Y., and Paxton, J. W. (2013). The effects of flavonoids on the ABC transporters: consequences for the pharmacokinetics of substrate drugs. *Expet Opin. Drug Metabol. Toxicol.* 9 (3), 267–285. doi:10.1517/17425255.2013.749858

Li, W., Sun, H., Zhang, X., Wang, H., and Wu, B. (2015). Efflux transport of chrysin and apigenin sulfates in HEK293 cells overexpressing SULT1A3: the role of multidrug resistance-associated protein 4 (MRP4/ABCC4). *Biochem. Pharmacol.* 98 (1), 203–214. doi:10.1016/j.bcp.2015.08.090

Li, J., Huang, Y., Zhao, S., Guo, Q., Zhou, Jie., Han, W., et al. (2019a). Based on network pharmacology to explore the molecular mechanisms of astragalus membranaceus for treating T2 diabetes mellitus. *Ann. Transl. Med.* 7 (22), 633. doi:10.21037/atm.2019.10.118

Li, Y., Guo, S., Zhu, Y., Yan, H., Qian, D. W., Wang, H.-Q., et al. (2019b). Comparative analysis of twenty-five compounds in different parts of Astragalus membranaceus var. mongholicus and Astragalus membranaceus by UPLC-MS/MS. *J Pharm Anal.* 9 (6), 392–399. doi:10.1016/j.jpha.2019.06.002

Li, S., Sun, Y., Huang, J., Wang, B., Gong, Y., Fang, Y., et al. (2020). Anti-tumor effects and mechanisms of Astragalus membranaceus (AM) and its specific immunopotentiation: status and prospect. *J. Ethnopharmacol.* 258, 112797. doi:10.1016/j.jep.2020.112797

Liu, M., Li, P., Zeng, X., Wu, H., Su, W., and He, J. (2015). Identification and pharmacokinetics of multiple potential bioactive constituents after oral administration of radix astragali on cyclophosphamide-induced immunosuppression in Balb/c mice. *Int. J. Mol. Sci.* 16 (3), 5047–5071. doi:10.3390/ijms16035047

Liu, D., Chen, L., Zhao, J., and Cui, K. (2018). Cardioprotection activity and mechanism of Astragalus polysaccharide *in vivo* and *in vitro*. *Int. J. Biol. Macromol.* 111, 947–952. doi:10.1016/j.ijbiomac.2018.01.048

Liu, T., Zhang, X., Zhang, Y., Hou, J., Fang, D., Sun, H., et al. (2018). Sulfation disposition of liquiritigenin in SULT1A3 overexpressing HEK293 cells: the role of breast cancer resistance protein (BCRP) and multidrug resistance-associated protein 4 (MRP4) in sulfate efflux of liquiritigenin. *Eur. J. Pharmaceut. Sci.* 124, 228–239. doi:10.1016/j.ejps.2018.08.041

Liu, C., Wang, K., Zhuang, J., Gao, C., Li, H., Liu, L., et al. (2019). The modulatory properties of Astragalus membranaceus treatment on triple-negative breast cancer: an integrated pharmacological method. *Front. Pharmacol.* 10, 1171. doi:10.3389/fphar.2019.01171

Luo, L. Y., Fan, M. X., Zhao, H. Y., Li, M. N., Wu, Y., and Gao, W. Y. (2018). Pharmacokinetics and bioavailability of the isoflavones formononetin and ononin and their *in Vitro* absorption in ussing chamber and caco-2 cell models. *J. Agric. Food Chem.* 66 (11), 2917–2924. doi:10.1021/acs.jafc.8b00035

Ma, C., Xia, R., Yang, S., Liu, L., Zhang, J., Feng, K., et al. (2020). Formononetin attenuates atherosclerosis via regulating interaction between KLF4 and SRA in apoE-/- mice. *Theranostics.* 10 (3), 1090–1106. doi:10.7150/thno.38115

Meng, S., Wu, B., Singh, R., Yin, T., Morrow, J. K., Zhang, S., et al. (2012). SULT1A3-mediated regiospecific 7-O-sulfation of flavonoids in Caco-2 cells can be explained by the relevant molecular docking studies. *Mol. Pharm.* 9 (4), 862–873. doi:10.1021/mp200400s

Mohibbullah, M., Bashir, K. M. I., Kim, S. K., Hong, Y.-K., Kim, A., Ku, S. K., et al. (2019). Protective effects of a mixed plant extracts derived from Astragalus membranaceus and Laminaria japonica on PTU-induced hypothyroidism and liver damages. *J. Food Biochem.* 43 (7), e12853. doi:10.1111/jfbc.12853

Mohos, V., Fliszár-Nyúl, E., Ungvári, O., Bakos, E., Kuffa, K., Bencsik, T., et al. (2020). Effects of chrysin and its major conjugated metabolites chrysin-7-sulfate and chrysin-7-glucuronide on cytochrome P450 enzymes and on OATP, P-gp, BCRP, and MRP2 transporters. *Drug Metab. Dispos.* 48 (10), 1064–1073. doi:10.1124/dmd.120.000085

Najmanova, I., Vopršalová, M., Saso, L., and Mladěnka, P. (2019). The pharmacokinetics of flavanones. *Crit. Rev. Food Sci. Nutr.*, 1–17. doi:10.1080/10408398.2019.1679085

Ong, S. K. L., Shanmugam, M. K., Fan, L., Fraser, S. E., Arfuso, F., Ahn, K. S., et al. (2019). Focus on formononetin: anticancer potential and molecular Targets. *Cancers* 11 (5), E611. doi:10.3390/cancers11050611

Qi, C., Fu, J., Zhao, H., Xing, H., Dong, D., and Wu, B. (2019). Identification of UGTs and BCRP as potential pharmacokinetic determinants of the natural flavonoid alpinetin. *Xenobiotica* 49 (3), 276–283. doi:10.1080/00498254.2018.1440657

Rao, T., Gong, Y. F., Peng, J. B., Wang, Y.-C., He, K., Zhou, H.-H., et al. (2019). Comparative pharmacokinetic study on three formulations of Astragali Radix by an LC–MS/MS method for determination of formononetin in human plasma. *Biomed. Chromatogr.* 33 (9), e4563. doi:10.1002/bmc.4563

Ravisankar, S., Agah, S., Kim, H., Talcott, S., Wu, C., and Awika, J. (2019). Combined cereal and pulse flavonoids show enhanced bioavailability by downregulating phase II metabolism and ABC membrane transporter function in Caco-2 model. *Food Chem.* 279, 88–97. doi:10.1016/j.foodchem.2018.12.006

Riches, Z., Stanley, E. L., Bloomer, J. C., Emma, L., and Coughtrie, M. W. H. (2009). Quantitative evaluation of the expression and activity of five major sulfotransferases (SULTs) in human tissues: the SULT "pie". *Drug Metab. Dispos.* 37 (11), 2255–2261. doi:10.1124/dmd.109.028399

Shanzad, M., Shabbir, A., Wojcikowski, K., Wohlmuth, H., and Gobe, G. C. (2016). The antioxidant effects of radix astragali (Astragalus membranaceus and related species) in protecting tissues from injury and disease. *Curr. Drug Targets.* 17 (12), 1331–1340. doi:10.2174/1389450116666150907104742

Shi, J., Zheng, L., Lin, Z., et al. (2015). Study of pharmacokinetic profiles and characteristics of active components and their metabolites in rat plasma following oral administration of the water extract of Astragali radix using UPLC-MS/MS. *J. Ethnopharmacol.* 169, 183–194. doi:10.1016/j.jep.2015.04.019

Singh, S. P., and Wahajuddin, T. D. (2011). PAMPA permeability, plasma protein binding, blood partition, pharmacokinetics and metabolism of formononetin, a methoxylated isoflavone. *Food Chem. Toxicol.* 49 (5), 1056–1062. doi:10.1016/j.fct.2011.01.012

Sun, M., Zhou, T., Zhou, L., Chen, Q., Yu, Y., Yang, H., et al. (2012). Formononetin protects neurons against hypoxia-induced cytotoxicity through upregulation of ADAM10 and sAβPPα. *J. Alzheimers Dis.* 28 (4), 795–808. doi:10.3233/JAD-2011-110506

Sun, H., Wang, X., Zhou, X., Lu, D., Ma, Z., and Wu, B. (2015). Multidrug resistance-associated protein 4 (MRP4/ABCC4) controls efflux transport of hesperetin sulfates in sulfotransferase 1A3-overexpressing human embryonic kidney 293 cells. *Drug Metab. Dispos.* 43 (10), 1430–1440. doi:10.1124/dmd.115.065953

Wang, P., Yin, Q. W., Zhang, A. H., Sun, H., Wang, X.-J., and Wu, X.-H. (2014). Preliminary identification of the absorbed bioactive components and metabolites in rat plasma after oral administration of Shaoyao-Gancao decoction by ultra-performance liquid chromatography with electrospray ionization tandem mass spectrometry. *Phcog. Mag.* 10 (40), 497–502. doi:10.4103/0973-1296.141774

Wang, C. J., He, F., Huang, Y. F., Ma, H.-L., Wang, Y.-P., Cheng, C.-S., et al. (2019). Discovery of chemical markers for identifying species, growth mode and production area of Astragali Radix by using ultra-high-performance liquid chromatography coupled to triple quadrupole mass spectrometry. *Phytomedicine* 67, 153155. doi:10.1016/j.phymed.2019.153155

Xiao, H., Qin, X., Wan, J., and Li, R. (2019). Pharmacological targets and the biological mechanisms of formononetin for Alzheimer's disease: a network analysis. *Med. Sci. Mon. Int. Med. J. Exp. Clin. Res.* 25, 4273–4277. doi:10.12659/MSM.916662

Zhang, X., Dong, D., Wang, H., Ma, Z., Wang, Y., and Wu, B. (2015). Stable knockdown of efflux transporters leads to reduced glucuronidation in UGT1A1-overexpressing HeLa cells: the evidence for glucuronidation-transport interplay. *Mol. Pharm.* 12 (4), 1268–1278. doi:10.1021/mp5008019

Zhang, T., Dong, D., Lu, D., Wang, S., and Wu, B. (2016). Cremophor EL-based nanoemulsion enhances transcellular permeation of emodin through glucuronidation reduction in UGT1A1-overexpressing MDCKII cells. *Int. J. Pharm.* 501 (1–2), 190–198. doi:10.1016/j.ijpharm.2016.01.067

Zheng, Y., Duan, W., Sun, J., Zhao, C., Cheng, Q., Li, C., et al. (2019). Structural identification and conversion analysis of malonyl isoflavonoid glycosides in astragali radix by HPLC coupled with ESI-Q TOF/MS. *Molecules* 24 (21), E3929. doi:10.3390/molecules24213929

Zhou, X., Wang, S., Sun, H., and Wu, B. (2015). Sulfonation of raloxifene in HEK293 cells overexpressing SULT1A3: involvement of breast cancer resistance protein (BCRP/ABCG2) and multidrug resistance-associated protein 4 (MRP4/ABCC4) in excretion of sulfate metabolites. *Drug Metabol. Pharmacokinet.* 30 (6), 425–433. doi:10.1016/j.dmpk.2015.09.001

Conflict of Interest: The authors declare that the research was conducted in the absence of any commercial or financial relationships that could be construed as a potential conflict of interest.

frontiers in Pharmacology

ORIGINAL RESEARCH
published: 20 January 2021
doi: 10.3389/fphar.2020.620451

Single Dose Study Assessing the Pharmacokinetic and Metabolic Profile of Alverine Citrate in Healthy Volunteers

Simona Rizea-Savu[1,2], *Simona Nicoleta Duna*[2,3]* *and Roxana Colette Sandulovici*[2]

[1]3S-Pharmacological Consultation & Research GmbH, Harpstedt, Germany, [2]Faculty of Pharmacy, Titu Maiorescu University, Bucharest, Romania, [3]3S-Pharmacological Consultation & Res. SRL, Bucharest, Romania

Alverine citrate is a spasmolytic commonly prescribed in conditions such as irritable bowel syndrome, painful diverticular disease of the colon, and primary dysmenorrhea. While clinical efficacy data on alverine alone or in combination with simethicone is freely available, surprisingly little information regarding the pharmacokinetics and metabolism of alverine can be found in literature. The first HPLC-MS/MS analytical protocol for determination of alverine parent, 4-hydroxy alverine, N-desethyl alverine and 4-hydroxy alverine glucuronide in human plasma was developed and validated. The two validated methods were used for analyzing plasma samples collected during an open label, non-comparative, single dose, one-period, one-treatment, pharmacokinetic and metabolic profile study of Spasmonal® Forte 120 mg hard capsule, conducted in 12 fasting healthy male and female volunteers of Caucasian descent. The study confirmed previous suspicions that parent alverine is subject to high pharmacokinetic variability and also revealed that the metabolic process most susceptible to outlying performance in Caucasians is hydroxylation to the active metabolite 4-hydroxy alverine. Another interesting observation made is that alverine parent accounts for only 3%, whereas total 4-hydroxy alverine (free and conjugated) accounts for 94% of alverine-related moieties in circulation (based on comparisons of total exposure).

Keywords: alverine citrate, 4-hydroxy alverine, 4-hydroxy alverine glucuronide, N-desethyl alverine, pharmacokinetics, *in-vivo* metabolism

OPEN ACCESS

Edited by:
Adrian Nicolescu,
Queen's University, Canada

Reviewed by:
Cristina Ghiciuc,
Grigore T. Popa University of Medicine and Pharmacy, Romania
Stanislav Yanev,
Bulgarian Academy of Sciences (BAS), Bulgaria
John M. Rimoldi,
University of Mississippi, United States

***Correspondence:**
Simona Nicoleta Duna
nicoleta.duna@3spharma.net

Specialty section:
This article was submitted to Drug Metabolism and Transport, a section of the journal Frontiers in Pharmacology

Received: *22 October 2020*
Accepted: *07 December 2020*
Published: *20 January 2021*

Citation:
Rizea-Savu S, Duna SN and Sandulovici RC (2021) Single Dose Study Assessing the Pharmacokinetic and Metabolic Profile of Alverine Citrate in Healthy Volunteers. Front. Pharmacol. 11:620451. doi: 10.3389/fphar.2020.620451

INTRODUCTION

Alverine citrate is a spasmolytic with specific action on the smooth muscle of the alimentary tract and uterus, which, at therapeutic doses, does not affect the heart, blood vessels or tracheal muscle (Boudghène et al., 2001; Annaházi et al., 2014). It belongs to a class of antispasmodic drugs which reduce the sensitivity of smooth muscle contractile proteins to calcium. By selectively binding with 5-HT1A receptors it acts as an antagonist that reduces the visceral pronociceptive effect of serotonin (5-HT) (Antoine et al., 2001). Due to these properties, alverine is used for the relief of smooth muscle spasm in conditions such as irritable bowel syndrome, painful diverticular disease of the colon and primary dysmenorrhea (Annaházi et al., 2014).

An independent meta-analysis and systematic review of clinical trials data relating to the effect of antispasmodic agents, alone or in combination, in the treatment of Irritable Bowel Syndrome showed

TABLE 1 | Optimal positive ion ESI mass spectrometric conditions for multiple reaction monitoring.

Method	Analyte	Ion transition	Dwell time (ms)	Declustering potential (V)	Collision energy (V)	Collision cell exit potential (V)
A	Alverine	282.194 >> 91.200	75	200	37	24
	D5-alverine (IS)	287.230 >> 91.200	75	200	53	24
	4-Hydroxy alverine	298.169 >> 106.900	75	200	37	16
	D5-4-hydroxy alverine (IS)	303.685 >> 106.600	75	200	39	12
	N-desethyl alverine	253.989 >> 90.600	75	200	35	10
B	4-Hydroxy alverine glucuronide	474.256 >> 298.000	150	100	39	32
	Buprenorphine-3-β-D-glucuronide (IS)	644.259 >> 467.900	150	100	53	40

superiority of the alverine/simethicone combination over other antispasmodic agents such as pinaverium bromide, mebeverine, trimebutine, hyoscine, fenoverine and dicyclomine, in terms of both patient global assessment on symptoms relief and pain relief (Martínez-Vázquez et al., 2012).

Clinical efficacy data on alverine alone or in combination with simethicone is freely available (Wittmann et al., 2010; Martínez-Vázquez et al., 2012; Ducrotte et al., 2014). The sparse information regarding the metabolism of alverine available in scientific literature is solely centered on the pharmacokinetics of the parent compound and the active metabolite 4-hydroxy alverine (Gomes et al., 2009; Ghosh et al., 2010; Seelam et al., 2015; Rathod et al., 2017) and is only derived from studies conducted on Indian population, where intra-subject variability of the main pharmacokinetic parameters of the parent compound seems quite low based on the required sample size for successful demonstration of bioequivalence between distinct oral dosage forms.

In terms of data reviewed by the European Medicines Agency and found to be representative for the general population, the summary of product characteristics of Spasmonal (SmPC Spasmonal Forte 120 mg, 2018) briefly describes that after oral administration of alverine, it is rapidly converted to its primary active metabolite (T_{max} between 1 and 1 ½ hours after dosing) and the latter is then converted to two secondary (unnamed) metabolites. Renal clearance is reported as high for all metabolites, indicating that they are eliminated by active renal secretion.

The present study aimed to contribute more concrete information with respect to the pharmacokinetic and metabolic profile of alverine citrate in Caucasian population, by simultaneous quantification of the parent compond, the active metabolite and the two secondary metabolites, following the administration of a single oral dose of the marketed reference product Spasmonal® Forte 120 mg hard capsule.

MATERIALS AND METHODS

Standards and Reagents

The reference standards of alverine citrate (99.2% purity), 4-hydroxy alverine hydrochloride (98.3% purity), 4-hydroxy alverine glucuronide (98.6% purity), N-desethyl alverine hydrochloride (99.9% purity) and the internal standards (IS) D5-alverine citrate (99.2% purity) and D5-4-hydroxy alverine hydrochloride (98.2% purity) were obtained from TLC Pharmaceutical Standards (Ontario, Canada). The internal standard buprenorphine-3-β-D-glucuronide (98.5% purity) was sourced from Cerilliant Analytical Reference Standards (Texas, USA). Methanol, acetonitrile and ammonium formate were of high-performance liquid chromatography (HPLC) grade, purchased from Merck (Darmstadt, Germany). Water was purified using Milli-Q water purification system from Millipore.

Equipment

A Shimadzu HPLC system, consisting of a CTC autosampler, LC-20AD binary pump, DGU-20A5 degassing unit, and CTO-20AC thermostatted column oven (Shimadzu, Kyoto, Japan), were used for the validation tests as well as real samples analysis. The mass spectrometer utilized for this work was a Sciex API 5500 triple-quadrupole mass spectrometer equipped with atmospheric pressure electrospray ionization interface (Turbo V) (AB Sciex, Foster City CA). Study data were collected using Analyst® (Version 1.7 Applied Biosystems). MPX Driver (using MPX SW version 2.0) software was used to control the LC parameters.

Liquid Chromatography and Mass Spectrometric Conditions

Two separate analytical methods were developed, validated, and used for real samples analysis: the first one (from here on referred to as Method A) allowed for the simultaneous quantification of alverine parent, 4-hydroxy alverine and N-desethyl alverine; the second one (from here on referred to as Method B) was used for quantification of 4-hydroxy alverine glucuronide. All chromatographic separations were carried out using Discovery C18 (12.5 cm × 2.1 mm; 5 μm) silica packing reversed phase analytical columns. For both methods the mobile phase consisted of 10 mM ammonium formate in water (pH 4.5) and acetonitrile. Samples of 40 μl were loaded onto the column, separated and eluted in gradient conditions. The total run time was 4.5 min for Method A and respectively 3.5 min for Method B. In both cases the autosampler temperature was held at 10°C and the mass spectrometer was run in positive ion ESI mode using multiple-reaction monitoring (MRM) to monitor the mass transitions. Research grade nitrogen was used as curtain gas and collision gas (CAD). The resolutions for both Q1 and Q3 were set at unit. A summary of the ion transitions, declustering potentials, collision

TABLE 2 | Concentrations of the QC samples and range of the calibration curves by analyte.

Method	Analyte	Calibration range		QC samples
		LLOQ	ULOQ	
A	Alverine	20 pg/ml	15,000 pg/ml	60–1,000 - 6,000–12,000 pg/ml
	4-Hydroxy alverine	20 pg/ml	15,000 pg/ml	60–1,000 - 6,000–12,000 pg/ml
	N-desethyl alverine	20 pg/ml	15,000 pg/ml	60–1,000 - 6,000–12,000 pg/ml
B	4-Hydroxy alverine glucuronide	1 ng/ml	750 ng/ml	3–50 - 300–600 ng/ml

energies, and collision cell exit potentials are presented for both methods in **Table 1**.

Calibration Curves and Quality Control Samples

Stock solutions of each analyte (alverine, 4-hydroxy alverine, N-desethyl alverine and 4-hydroxy alverine glucuronide) were prepared in DMSO at a concentration of 1.000 mg/ml. The stock solutions of internal standards for Method A (d5-alverine and d5-4-hydroxy alverine) were prepared at 1.000 mg/ml and for Method B (buprenorphine-3-β-D-glucuronide) at 500.000 ng/mL, in methanol. These solutions were stored at −20°C. A series of working solutions for preparation of the eight points calibration curves and the plasma QC samples were obtained by mixing and diluting the stock solutions with pooled human plasma deriving from blank blood samples collected on Li-heparin from healthy volunteers. The concentrations of the spiked QC samples and the range of the calibration curves by analyte are presented in **Table 2**.

Pharmacokinetic Study in Healthy Volunteers

The validated methods were used for analysis of real samples from an open label, non-comparative, single dose pharmacokinetic and metabolic profile study of Spasmonal® Forte 120 mg hard capsule (containing 120 mg alverine citrate), manufactured by MEDA Pharmaceuticals Ltd, UK under license of Mylan Products Limited, UK, sourced from the UK market.

The study included 12 fasting healthy male and female volunteers, Caucasian (Eastern Europeans of Moldavian nationality), adults (between 18 and 55 years of age) with a body mass index within 18.5–30.0 kg/m^2. All subjects gave their written informed consent before they underwent any study-related procedures and were free to withdraw from the trial at any time. The study medication administration consisted of one single 120 mg hard capsule of alverine citrate (trade name: Spasmonal® Forte) taken orally with 200 ml of still bottled water after at least 10 h of overnight fasting. For the analytical determination of alverine, hydroxy alverine (free and conjugated) and N-desethyl alverine plasma levels, venous blood samples of 5 ml were drawn in tubes containing Li-heparin as anticoagulant before study drug administration and at 0.25, 0.5, 0.75, 1.0, 1.5, 2.0, 2.5, 3.0, 4.0, 5.0, 6.0, 8.0, 10.0, 12.0, 14.0, 16.0, 24.0, 30.0, 36.0, 48.0 and 72.0 h post dose. The pharmacokinetic parameters calculated for each analyte were $AUC_{0\text{-}t}$, C_{max}, T_{max}, $AUC_{0\text{-}\infty}$, $t_{1/2}$ and MRT. The study was conducted in the Republic of Moldavia following unconditional approval from the National Ethics Committee and the National Medicine Agency. Clinical investigations were conducted according to the Declaration of Helsinki principles and Good Clinical Practice.

Handling of Study Samples

After collection, the blood samples were centrifuged under refrigeration (10 min at 1,500 (±5) g and a nominal temperature of 4°C). Plasma was separated, divided into duplicate aliquots and, within 60 min from collection, frozen for storage at −20°C nominal until shipped to the analytical laboratory. Plasma samples (first aliquot) were sent from the clinical site to the analytical facility in a thermo-insulated box containing an adequate amount of dry ice. During transport, an electronic logger was used for monitoring plasma samples temperature. Once received at the analytical laboratory, the samples were stored at −20°C or colder until submitted to analysis. Before analysis, plasma samples were thawed, mixed for 3 min and centrifuged for 3 min at 4,000 rpm and 20°C nominal. Aliquots of samples isolated for Analytical Method A were: spiked with internal standards (d5-alverine and d5-4-hydroxy alverine), diluted, vortexed and centrifuged; supernatants were evaporated to dryness under air stream, reconstructed with a water/acetonitrile solution (1/1, v/v), mixed and centrifuged; finally, the samples have been transferred in the autosampler to be injected. Aliquots of samples isolated for Analytical Method B were: spiked with internal standard (buprenorphine-3-β-D-glucuronide), diluted, vortexed and centrifuged; supernatants were diluted with water, mixed and centrifuged; finally, the samples have been transferred in the autosampler to be injected. Representative chromatograms for each analyte vs. the reference internal standard are presented as **Supplementary Material**.

The analytical work was performed according to GLP principles and FDA requirements (FDA, 2018 Bioanalytical Method Validation Guidance, 2018). The analytical methods were fully validated before starting the analysis of study plasma samples. The methods were verified for linearity, quantification limits, assay specificity, between-run and within-run precision and accuracy, analyte recovery, and stability in stock solution and biological matrix under processing conditions during the entire period of storage.

Pharmacokinetic and Statistical Analysis

Non-compartmental PK analysis was performed using SAS® statistical software, version 9.4 (SAS Institute Inc., Cary, North Carolina, USA). Maximum plasma concentration (C_{max}) and time to reach maximum plasma concentration (T_{max}) were obtained directly from the plasma values. The linear trapezoidal rule was used to calculate the area under the concentration-time curve from time zero to the last quantifiable concentration (AUC_{0-t}). The apparent elimination rate constant (K_{el}) was estimated by regression of the terminal ln-linear portion of the plasma concentration–time profile; apparent terminal half-life ($t_{½}$) was calculated as the quotient of ln (2) and K_{el}. Area under the curve to infinity ($AUC_{0-\infty}$) was estimated as the sum of AUC_{0-t} and the extrapolated area given by the quotient of the last quantifiable plasma concentration and K_{el}. ANOVA was performed on ln-transformed C_{max}, AUC_{0-t} and $AUC_{0-\infty}$ using the General Linear Models (GLM) procedure fitted in SAS® software using the method of least squares. Descriptive statistics were performed for all pharmacokinetic parameters.

RESULTS

Method Validation Results

Selectivity

Analyses were performed on 8 blank plasma samples from different healthy volunteers (including a lipemic and a hemolytic sample) without any addition and then with addition of internal standards or alverine or 4-hydroxy alverine or 4-hydroxy alverine glucuronide or N-desethyl alverine or possible co-medication; no peak, interfering with those of the analytes or the internal standards appeared in the blank samples. Same test was applied to all types of LLOQ samples. None of the blank plasma sources showed any obvious interference.

Calibration Curve: Fitting, Precision and Accuracy

The precision and the accuracy, at all concentrations, were satisfactory; the curve fittings were also optimal in the whole range with correlation coefficients (r) = 0.99790 for alverine (r) = 0.99740 for 4-hydroxy alverine (r) = 0.99740 for 4-hydroxy alverine glucuronide and (r) = 0.99750 for N-desethyl alverine.

Extraction Recovery

The extraction recoveries of QC samples, calculated on the peak areas of alverine (mean recovery across the three QC levels tested: 75%), 4-hydroxy alverine (mean recovery across the three QC levels tested: 84%), 4-hydroxy alverine glucuronide (mean recovery across the three QC levels tested: 87%) and N-desethyl alverine (mean recovery across the three QC levels tested: 76%) put in evidence that the extraction was effective at all tested concentrations with all compounds, being above 70.0% for all individual tests; therefore, adequate for an analytical method. The extraction recoveries of the internal standards were also effective, being above 70.0%, and adequate for a reliable analytical method.

Matrix Effect

The matrix effect was also evaluated. Matrix Factor (MF) extracted individual blank plasma samples (8 blank plasma samples from different healthy volunteers including a lipemic and a hemolytic sample for each concentration level) spiked with standard of extraction solutions in mobile phase at the concentrations of QC1 and QC4 (after extraction) were analyzed; the peak areas were compared to the same standard of extraction solution peak areas in mobile phase. The matrix factors obtained for alverine/d5-alverine, 4-hydroxy alverine/d5-4-hydroxy alverine, 4-hydroxy alverine glucuronide/buprenorphine glucuronide, and N-desethyl alverine/d5-alverine were slightly lower than one and suggest that no significant ionization suppression occurs in presence of matrix ions. The precision of the IS normalized matrix factors was always less than 15% and therefore adequate for reliable bio-analytical assay.

Carry-Over Effect

The carry-over effect was assessed by injecting blank samples after high concentrated samples (CAL 8) in six consecutive series. The analytes blank chromatographic response was supposed to be 5 times smaller than the one given by calibrator 1 samples. The internal standards blank chromatographic response was supposed to be 20 times smaller than the one given by the previous CAL8 sample. The results showed that no signal was detectable in blank samples injected after high concentrated samples (calibrator 8) and therefore can be concluded that no carry-over effect was present.

Spiked Plasma Samples Stability

The results obtained in all storage conditions show that alverine, 4-hydroxy alverine, 4-hydroxy alverine glucuronide and N-desethyl alverine are stable in plasma for the following durations: up to 6 h at room temperature (benchtop stability), up to 1 week at −5°C (autosampler stability), up to 3.5 weeks below −20°C (storage stability covering the timeframe from collection of the first sample to assay of the last sample) and up to 1 week below −70°C (transport stability fully covering the transit time from the clinic to the analytical laboratory).

Stability of Spiked Plasma Samples Extract

The results obtained show that alverine, 4-hydroxy alverine and N-desethyl alverine are stable in plasma extracts and dry extracts up to 96 h when kept at 10°C nominal and that 4-hydroxy alverine glucuronide is stable in plasma samples extract up to 48 h when kept at 10°C nominal (short-term refrigerated storage stability).

Dilution Test

Since there is always a chance that real samples have analytes levels exceeding the maximum concentrations of the calibration curves, a past-dilution method 1 + 19 with blank plasma was validated. The mean dilution accuracy was within the range of variation accepted for QC samples with all compounds.

Stock Solutions Stability

The stock solutions of the analytes and internal standards are stable up to 12 days when stored below −20°C and up to 6 h if kept at room temperature.

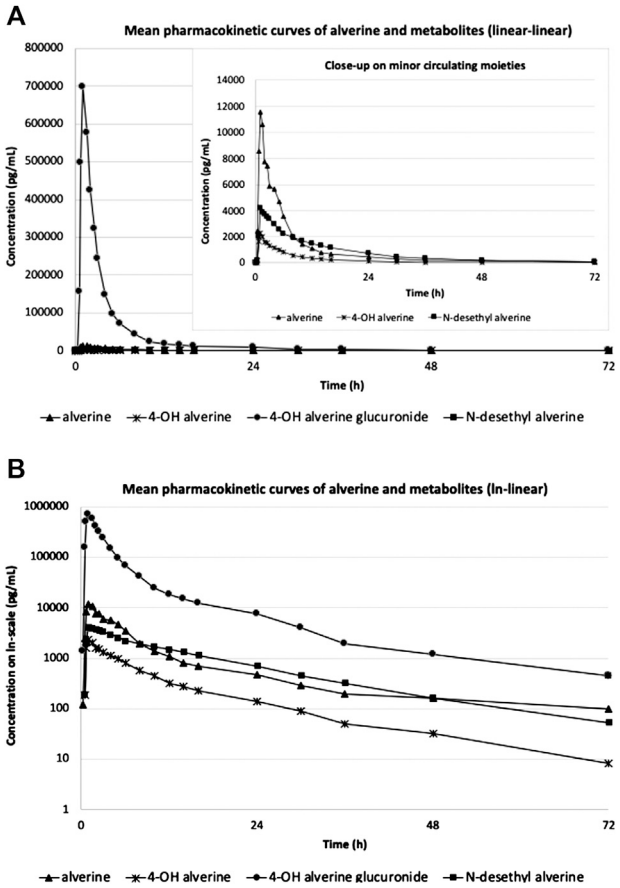

FIGURE 1 | Mean pharmacokinetic curves of alverine parent and metabolites (*N* = 12) in linear-linear display **(A)** and ln-linear display **(B)**.

System Suitability Test Solution Stability

The suitability test solutions of the analytes and internal standards were stable up to 12 days when stored below −20°C.

Blood Sampling Tubes Validation

The risk of unreliable quantitation results was excluded for all analytes after testing the Monovette tubes (Sarstedt, Germany) pre-filled with lithium heparin as anticoagulant.

Plasma Hemolyzation Impact on Accuracy of Analytes Determination

The accuracies have been calculated from the samples prepared at QC3 concentration level at three hemolyzation levels (low, middle and high) and at QC1 concentration level (middle hemolyzation level). It was concluded that the measurement accuracy was not affected in hemolytic samples.

Interconversion (Conversion And/Or Back-Conversion) Tests

The interconversion of alverine, 4-hydroxy alverine, 4-hydroxy alverine glucuronide or N-desethyl alverine was evaluated both in plasma samples before analyses and during the analytical phase. The mean results at all tested concentrations were in range (±15% (85–115%) vs. nominal). The measurements were adequate in all tested conditions thus excluding the relevance of analytes interconversion.

From the results previously reported it can be concluded that the developed analytical methods had adequate sensitivity, precision, accuracy, and specificity to quantitatively determine

TABLE 3 | Mean Pharmacokinetic Parameters after a single dose of Spasmonal® Forte 120 mg hard capsule, administered to fasting healthy volunteers (N = 12). Presented in bold are the mean values.

PK parameter	Alverine	4-OH alverine	4-OH alverine glucuronide	N-desethyl alverine
C_{max} (pg/ml)	**12,967**	**2,871**	**752,123**	**4,329**
Mean (CV %)	(219%)	(123%)	(35%)	(183%)
AUC_{0-t} (pg/ml*h)	**64,743**	**15,336**	**1,996,700**	**51,746**
Mean (CV %)	(209%)	(111%)	(45%)	(163%)
$AUC_{0-\infty}$ (pg/ml*h)	**70,557**	**16,130**	**2,021,278**	**90,612**
Mean (CV %)	(221%)	(108%)	(44%)	(133%)
T_{max} (h)	**0.75**	**1.00**	**1.00**	**1.00**
Median (range)	(0.50–1.50)	(0.50–2.50)	(0.75–1.50)	(0.50–2.50)
K_{el} (1/h)	**0.08**	**0.04**	**0.10**	**0.15**
Mean (CV %)	(75%)	(25%)	(85%)	(98%)
$t_{½}$ (h)	**16.52**	**15.37**	**8.42**	**8.37**
Mean (CV %)	(103%)	(38%)	(62%)	(70%)

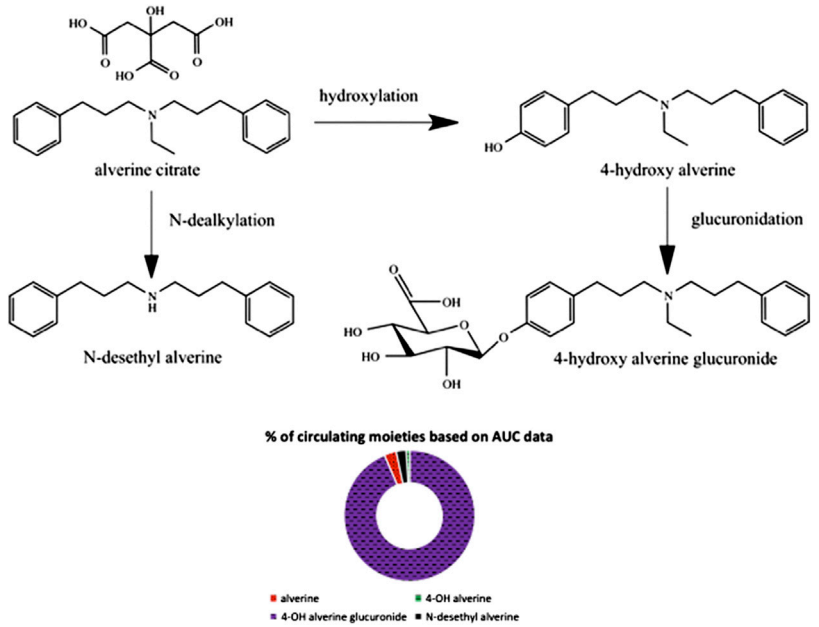

FIGURE 2 | Schematic representation of metabolic pathways and individual contribution of each moiety to the overall alverine-related exposure.

alverine, 4-hydroxy alverine, 4-hydroxy alverine glucuronide or N-desethyl alverine together or separately at the concentrations expected in alverine clinical studies samples.

Concentrations in validation samples were estimated on the regression curves obtained from the data of the calibration samples run in the same sequence.

Calculations were carried out on alverine (chromatographic trace m/z 282.194/91.200) peak areas normalized to the internal standard (d5-alverine) peak areas (chromatographic trace m/z 287.230/91.200) or 4- hydroxy alverine (chromatographic trace m/z 298.169/106.900) peak areas normalized to the internal standard (d5-4-hydroxy alverine) peak areas (chromatographic trace m/z 303.685/106.600) or 4- hydroxy alverine glucuronide (chromatographic trace m/z 474.256/298.000) peak areas normalized to the internal standard (buprenorphine-3-β-D-glucuronide) peak areas (chromatographic trace m/z 644.259/467.900) or N-desethyl alverine (chromatographic trace m/z 253.989/90.600) peak areas normalized to the internal standard (d5-alverine) peak areas (chromatographic trace m/z 287.230/91.200). The calculations of concentrations were performed using weighted (1/x2) linear regression models for alverine, 4-hydroxy alverine, and N-desethyl alverine and respectively (1/x) quadratic regression models for 4-hydroxy alverine glucuronide.

There were no interferences of endogenous compounds at the retention times of alverine, 4-hydroxy alverine, 4-hydroxy alverine glucuronide or N-desethyl alverine for double blank plasma, blank plasma, samples spiked at LLOQ concentration and subject samples at C_{max} and IS after oral administration.

Pharmacokinetic Results

The need of performing a metabolic characterization of alverine citrate was identified after a close analysis of observations made in a previous pivotal fully-replicate design study conducted on a sample size of 42 healthy volunteers. At that time, analysis of parent alverine alone revealed that a number of subjects exhibited consistent (same pattern observed across study periods) subject-specific outlying pharmacokinetic trends which led to a huge inter-individual variability (coefficient of variation within treatment group of approximately 300% for both C_{max} and AUC_{0-t}). Also, a very high within-subject variability of the primary PK parameters was noted within the replicate reference group (Reference intra-subject CV calculated by EMA Method A (EMA, 2011) for alverine C_{max} data for the purpose of applying scaled bioequivalence limits was 84%). In the absence of own metabolite data or revealing literature information to support the high variability observed, a more detailed pharmacokinetic profiling of alverine and its metabolites was pursued in the new exploratory study presented in this article.

A total of 12 healthy male and female volunteers were enrolled and completed the exploratory study. All subjects were Caucasian with the mean age of 33.42 years (range 18–55 years) and mean BMI of 25.13 kg/m^2 (range 20.8–29.6 kg/m^2).

The mean alverine, 4-hydroxy alverine, N-desethyl alverine and 4-hydroxy alverine glucuronide concentration-time curves are shown in **Figure 1** (linear-linear display in panel A and ln-linear display in panel B) while mean pharmacokinetic parameters are summarized in **Table 3**.

A schematic representation of the metabolic pathways which lead to formation of the quantified moieties and the individual contributions of the respective moieties to the overall alverine-related exposure (based on AUC_{0-t} data) are presented in **Figure 2**.

Very high coefficients of variation were noted for AUC_{0-t} data of alverine parent (209%) as well as metabolites 4-hydroxy alverine (111%) and N-desethyl alverine (163%). A statistical test for identification of outliers was subsequently applied to the

exploratory study data in order to identify the subjects contributing to the high variability observed and to check with which metabolic step the outlying behavior interfered. The test identified two (out of twelve) subjects with extreme outlying behavior (observations outside 3rd Quantile +3 x Interquartile Range) specific to the hydroxylation pathway (both subjects being identified as outliers in the parent alverine and 4-hydroxy alverine analysis, while no statistically significant differences from the mean of the general population were noted for 4-hydroxy alverine glucuronide or N-desethyl-alverine). The total exposure of circulating unchanged alverine was 122 and respectively 199 times higher for the two outlying subjects as compared to the regular metabolizers within the study population. For the two poor hydroxylators, abundant availability of unchanged product for minor metabolic pathways has also translated into higher than average concentrations of N-desethyl alverine (though not statistically significant based on the applied outliers test). The same pattern of behavior was noted also in a different metabolic profiling study conducted in house (data not authorized for publication yet) where the incidence of poor alverine hydroxylators in Caucasian subjects was 21% (three out of fourteen subjects).

The cause for the different metabolic behavior noted in outliers could not be linked to any external factors. All clinical laboratory parameters determined for the outlying subjects revealed unremarkable results and none of them experienced adverse events nor took any medication during the two weeks prior to dosing or throughout the clinical part of the study. All subjects were non-smokers so tobacco-mediated enzymatic inhibition/induction can also be excluded. No CYP-inhibiting/inducing foods or drinks were consumed during the 72 h before administration or throughout the clinical part of the study.

Being a weak base and highly lipophilic (logP = 5.46 (Alverine citrate Drug Bank Monograph, 2020)), although administered as citrate salt, one of the possible explanations for the observed pharmacokinetic behavior could be the tendency of aliverine to precipitate at intestinal pH. Biopharmacists consider this a frequently met phenomenon (Mircioiu et al., 2012; Preda et al., 2012) typically resulting in a high variability in absorption. All lipophilic drugs are extensively metabolized, the pharmacokinetics of both parent compound and metabolites being highly variable, and as a result, some subjects behave as outliers due to a combination of variability in intestinal solubility (Sandulovici et al., 2009; Mircioiu et al., 2010; Tandel et al., 2013; Sandulovici et al., 2020) and genetic polymorphism. The type of genetic polymorphism affecting the activities of drug-metabolizing enzymes in the case of alverine citrate remains yet unidentified (more specific information not available as the subjects were not screened for CYP- phenotype or -genotype), however the effect observed in outliers was a decrease in the magnitude of an otherwise significant first-pass effect.

Despite the high variability in hydroxylation, the subsequent glucuronidation step was observed to be a stable and abundant metabolic process. The coefficient of variation for 4-hydroxy alverine glucuronide over the entire study population was only 45%, there were no subjects with outlying AUC_{0-t} data, and the metabolite represented about 94% of alverine-derived moieties circulating (see **Figure 2**).

The metabolism of alverine, apart from being extensive, was also noted to be fast (0.75 h median T_{max} for unchanged alverine and 1.00 h median T_{max} for the metabolites 4-hydroxy alverine, 4-hydroxy alverine glucuronide and N-desethyl alverine).

Safety Results

One adverse event occurred during the present study (mild dizziness, lasting 12 min). The medication Spasmonal® Forte 120 mg hard capsule, administered as single dose in fasting state, was very well tolerated by the healthy volunteers participating in this study.

DISCUSSION

The first HPLC-MS/MS analytical protocol for determination of alverine parent, 4-hydroxy alverine, N-desethyl alverine (detected simultaneously with one analytical method) and 4-hydroxy alverine glucuronide (separately, with a different analytical method) in human plasma was developed and validated according to current regulatory requirements.

These validated methods were then applied for analyzing plasma samples collected during an open label, non-comparative, single dose, one-period, one-treatment, pharmacokinetic and metabolic profile study of Spasmonal® Forte 120 mg hard capsule, conducted in 12 fasting healthy male and female volunteers.

The study confirmed previous observations that pharmacokinetic variability of parent alverine far exceeds the expectations one would get upon review of literature data, albeit from studies conducted on Indian population (Gomes et al., 2009; Ghosh et al., 2010; Seelam et al., 2015; Rathod et al., 2017). The metabolic process most susceptible to outlying performance in Caucasian population was found to be hydroxylation to the active metabolite 4-hydroxy alverine. Exogenous factors excluded, it is believed that the poor hydroxylator status observed in about 17% of the study population could stem from either biopharmaceutical properties of the formulation, or, most likely, genetic polymorphism (as this would explain also the inconsistencies in degree of variability as compared to the studies conducted on Indian population).

Another interesting aspect revealed was that alverine parent accounts for only 3%, whereas total 4-hydroxy alverine (free and conjugated) accounts for about 94% of alverine-related moieties in circulation (based on comparisons of total exposure). This finding would strongly suggest that the research and development program for future generic alverine formulations would benefit from integrating pharmacokinetic metabolite data in both IVIVC (Savu et al., 2016; Mircioiu et al., 2019) and *in vivo* bioequivalence testing models.

Safety data collected during the study permitted to conclude that alverine citrate, administered in single 120 mg dose to healthy volunteers, was very well tolerated. This observation is line with the known good tolerability profile of the molecule, as ascertained in larger clinical studies (Wittmann et al., 2010; Martínez-Vázquez et al., 2012; Ducrotte et al., 2014).

Pharmacokinetic data collected during the study permitted to conclude that alverine undergoes extensive and fast metabolism.

DATA AVAILABILITY STATEMENT

The raw data supporting the conclusions of this article will be made available by the authors, without undue reservation.

ETHICS STATEMENT

The studies involving human participants were reviewed and approved by the Moldavian National Ethics Committee. The "healthy volunteers" provided their written informed consent to participate in this study.

AUTHOR CONTRIBUTIONS

SR-S and SD were involved in the clinical and analytical conduct of the study. All three authors contributed to the data analysis process and drafting of the manuscript.

SUPPLEMENTARY MATERIAL

The Supplementary Material for this article can be found online at: https://www.frontiersin.org/articles/10.3389/fphar.2020.620451/full#supplementary-material.

REFERENCES

Alverine citrate Drug Bank Monograph (2020). Alverine citrate Drug Bank monograph, *Drug Bank*. Available at: https://go.drugbank.com/salts/DBSALT000008.

Annaházi, A., Róka, R., Rosztóczy, A., and Wittmann, T. (2014). Role of antispasmodics in the treatment of irritable bowel syndrome. *World J. Gastroenterol.* 20 (20), 6031–6043. doi:10.3748/wjg.v20.i20.6031

Boudghène, F. P., Bazot, M., Robert, Y., Perrot, N., Rocourt, N., et al. (2001). Assessment of Fallopian tube patency by HyCoSy: comparison of a positive contrast agent with saline solution. *Ultrasound Obstet. Gynecol.* 18 (5), 525–530. doi:10.1046/j.0960-7692.2001.00513.x

Antoine, A. M., Jacob, L., Fioramonti, J., and Bueno, L. (2001). Rectal antinociceptive properties of alverine citrate are linked to antagonism at the 5-HT1A receptor subtype. *J. Pharm. Pharmacol.* 53 (10), 1419–1426. doi:10.1211/0022357011777783

Ducrotte, P., Grimaud, J. C., Dapoigny, M., Personnic, S., O'Mahony, V., et al. (2014). On-demand treatment with alverine citrate/simeticone compared with standard treatments for irritable bowel syndrome: results of a randomised pragmatic study. *Int. J. Clin. Pract.* 68 (2), 245–254. doi:10.1111/ijcp.12333

EMA (2011). EMA/618604/2008. Positions on specific questions addressed to the pharmacokinetics working party. Amsterdam, Netherlands: European Medicines Agency.

FDA (2018). *Bioanalytical method validation.* Montgomery, MD: FDA, CDER Guidance for Industry.

Ghosh, C., Jha, V., Ahir, R., Shah, S., Shinde, C. P., and Chakraborty, B. S. (2010). A rapid and most sensitive liquid chromatography/tandem mass spectrometry method for simultaneous determination of alverine and its major metabolite, para hydroxy alverine, in human plasma: application to a pharmacokinetic and bioequivalence study. *Drug Test. Anal.* 2 (6), 284–291. doi:10.1002/dta.130

Gomes, N. A., Laud, A., Pudage, A., Joshi, S. S., Vaidya, V. V., et al. (2009). Validated LC-MS/MS method for determination of Alverine and one of its hydroxy metabolites in human plasma along with its application to a bioequivalence study. *J Chromatogr B Analyt Technol Biomed Life Sci.* 877 (3), 197–206. doi:10.1016/j.jchromb.2008.12.013

Martínez-Vázquez, M. A., Vázquez-Elizondo, G., González-González, J. A., Gutiérrez-Udave, R., Maldonado-Garza, H. J., et al. (2012). Effect of antispasmodic agents, alone or in combination, in the treatment of Irritable Bowel Syndrome: systematic review and meta-analysis. *Rev. Gastroenterol. México.* 77 (2), 82–90. doi:10.1016/j.rgmx.2012.04.002

Mircioiu, C., Ionica, G., Danilceac, A., Miron, D., Mircioiu, I., and Radulescu, F. (2010). Pharmacokinetic and mathematical outliers for drugs with active metabolites. Note i. Model independent analyses for pentoxifylline. *FARMACIA.* 58 (3), 264–278.

Mircioiu, I., Anuta, V., Ibrahim, N., and Mircioiu, C. (2012). Dissolution of tamoxifen in biorelevant media. A two phase release model. *FARMACIA.* 60 (3), 315–324.

Mircioiu, C., Anuta, V., Mircioiu, I., Nicolescu, A., and Fotaki, N. (2019). Vitro-in vivo correlations based on in vitro dissolution of parent drug diltiazem and pharmacokinetics of its metabolite. *Pharmaceutics.* 11 (7), 344. doi:10.3390/pharmaceutics11070344

Preda, I. A., Mircioiu, I., Mircioiu, C., Corlan, G., Pahomi, G., Prasacu, I., et al. (2012). Research concerning the development of A biorelevant dissolution test for formulations containing norfloxacin. I. Modelling of *in Vitro* release kinetics. *FARMACIA.* 60 (5), 675–687.

Rathod, D. M., Patel, K. R., Mistri, H. N., Jangid, A. G., Shrivastav, P. S., and Sanyal, M. (2017). An improved LC-MS/MS method for the quantification of alverine and para hydroxy alverine in human plasma for a bioequivalence study. *J Pharm Anal.* 7 (2), 95–102. doi:10.1016/j.jpha.2016.11.003

Sandulovici, R., Prasacu, I., Mircioiu, C., Voicu, V., Medvedovici, A., and Anuta, V. (2009). Mathematical and phenomenological criteria in selection of pharmacokinetic model for M1 metabolite of pentoxyphylline. *FARMACIA.* 57 (2), 235–247.

Sandulovici, R., Mircioiu, I., Aboul-Enein, H. Y., Manolache, M., Mircioiu, C., Voicu, V., et al. (2020). Sources of outlier data in the bioanalytical and clinical part of a piroxicam bioequivalence study. *Int. J. Clin. Pharm. Ther.* 58 (11), 652–663. doi:10.5414/CP203794

Savu, S. N., Silvestro, L., Mircioiu, C., and Anuta, V. (2016). Development of *in-vitro in-vivo* correlation models for clopidogrel tablets to describe administration under fasting and fed conditions. *FARMACIA.* 64 (2), 302–312.

Seelam, R. R., Irisappan, S. C., Seelam, R. R., and Seelam, S. S. R. (2015). Bioequivalence comparison between two different Formulations of alverine citrate 120mg capsules: an open label, balanced, randomized-sequence, single-dose, two period crossover study in healthy male volunteers. *J Compr Phar.* 2 (3), 105–114. doi:10.13140/RG.2.1.1456.3602

SmPC Spasmonal Forte 120 mg (2018). *Spasmonal Forte 120 mg, Hard capsules.* Hertfordshire, UK: Mylan.

Tandel, D., Nicoleta, R., Miron, D. S., Radulescu, F. S., Anuta, V., Mircioiu, I., et al. (2013). Comparative pharmacokinetics of rifampicin and 25-desacetyl rifampicin in healthy volunteers after single oral dose administration. *FARMACIA.* 61 (2), 398–410.

Wittmann, T., Paradowski, L., Ducrotté, P., Bueno, L., and Andro Delestrain, M. C. (2010). Clinical trial: the efficacy of alverine citrate/simeticone combination on abdominal pain/discomfort in irritable bowel syndrome - a randomized, double-blind, placebo-controlled study. *Aliment. Pharmacol. Ther.* 31 (6), 615–624. doi:10.1111/j.1365-2036.2009.04216.x

Conflict of Interest: SR-S is employed by the company 3S-Pharmacological Consultation & Research GmbH and author SD is employed by the company 3SPharmacological Consultation & Res. SRL.

The remaining author declares that the research was conducted in the absence of any commercial or financial relationships that could be construed as a potential conflict of interest.

The reviewer CG declared a past collaboration with one of the authors RS to the handling editor.

frontiers in Pharmacology

ORIGINAL RESEARCH
published: 15 February 2021
doi: 10.3389/fphar.2020.621667

Estimation of the *In Vivo* Release of Amiodarone From the Pharmacokinetics of Its Active Metabolite and Correlation With Its *In Vitro* Release

Maytham Razaq Shleghm[1†], *Constantin Mircioiu*[1*], *Victor A. Voicu*[1], *Ion Mircioiu*[2†] *and Valentina Anuta*[1]

[1]*Carol Davila University of Medicine and Pharmacy, Bucharest, Romania,* [2]*Titu Maiorescu University, Bucharest, Romania*

OPEN ACCESS

Edited by:
Sara Eyal,
Hebrew University of Jerusalem, Israel

Reviewed by:
Andrei Adrian Tica,
University of Medicine and Pharmacy of Craiova, Romania
Andrei Medvedovici,
University of Bucharest, Romania

***Correspondence:**
Constantin Mircioiu
constantin.mircioiu@yahoo.com

[†]*These authors have contributed equally to this work.*

Specialty section:
This article was submitted to Drug Metabolism and Transport, a section of the journal Frontiers in Pharmacology

Received: *26 October 2020*
Accepted: *16 December 2020*
Published: *15 February 2021*

Citation:
Shleghm MR, Mircioiu C, Voicu VA, Mircioiu I and Anuta V (2021) Estimation of the In Vivo *Release of Amiodarone From the Pharmacokinetics of Its Active Metabolite and Correlation With Its* In Vitro *Release. Front. Pharmacol. 11:621667. doi: 10.3389/fphar.2020.621667*

Due to its very low water solubility and complex pharmacokinetics, a reliable point-to-point correlation of its *in vitro* release with its pharmacokinetics has not been achieved so far with amiodarone. The correlation of the *in vitro* dissolution of a drug with the pharmacokinetics of one of its metabolites was recently proposed by the authors of the article as an additional or alternative analysis to the usual *in vitro* correlations *in vivo*, mainly in the case of fast-absorbing drugs that have metabolites with a significant therapeutic effect. The model proposed by the authors considers that amiodarone has a slow dissolution, rapid absorption, and rapid metabolism, and before returning to the blood from other compartments, its pharmacokinetics is determined mainly by the kinetics of release in the intestine from the pharmaceutical formulation. Under these conditions, the rate of apparition of desethylamiodarone in the blood is a metric of the release of amiodarone in the intestinal fluid. Furthermore, it has been shown that such an estimated *in vivo* dissolution is similar, after time scaling, to the dissolution measured experimentally *in vitro*. Dissolution data of amiodarone and the pharmacokinetic data of its active metabolite desethylamiodarone were obtained in a bioequivalence study of 24 healthy volunteers. The elimination constant of the metabolite from plasma was estimated as the slope of the linear regression of logarithmically transformed data on the tail of plasma levels. Because the elimination of desethylamiodarone was shown to follow a monoexponential model, a Nelson–Wagner-type mass equilibrium model could be applied to calculate the time course of the "plasma metabolite fraction." After Levi-type time scaling for imposing the *in vitro–in vivo* correlation, the problem became that of the correlation between *in vitro* dissolution time and *in vivo* dissolution time, which was proven to follow a square root model. To validate the model, evaluations were performed for the reference drug and test drug separately. In both cases, the scaled time for *in vivo* dissolution, t^*, depended approximately linearly on the square root of the *in vitro* dissolution time t, with the two regression lines being practically parallel.

Keywords: amiodarone, desethylamiodarone, pharmacokinetics, in vivo release, in vitro in vivo correlation

INTRODUCTION

Amiodarone (AMD) has been shown to have variable oral bioavailability (20–80%). After absorption, AMD undergoes extensive metabolism, is distributed in the blood, lipids, and in deep compartments, and undergoes enterohepatic circulation (Holt et al., 1983). Metabolism includes a first and second N-dealkylation, an O-dealkylation as well as a first and second hydroxylation. Glucuronidation was also highlighted. The major and active metabolite is desethylamiodarone (DAMD) (Berger and Harris, 1986; Deng et al., 2015).

Concentrations in the myocardium have been shown to be 35 times higher than in the plasma (Djiane et al., 1984). The pharmacokinetic model is usually considered to be multicompartmental, including the central compartment, the lipid compartment, and a deep compartment (Freedman and Somberg, 1991).

In vitro–in vivo correlations (IVIVCs) are correlations between *in vitro* dissolution data and *in vivo* release kinetics, estimated by the deconvolution of pharmacokinetic IVIVCs were constantly recommended by regulatory authorities in the last decades when developing extended-release formulations (US Food and Drug Administration, 1997a; US Food and Drug Administration, 1997b; European Medicines Agency, 2014a; European Medicines Agency, 2014b). The correlation can be good and even linear (Humbert et al., 1994; Eddington et al., 1998; Emami 2006) or nonlinear [Lake et al., 1999; Varshosaz et al., 2000; Rao et al., 2001; Al-Behaisi et al., 2002], or even obscure (Eddington et al., 1998; Mircioiu et al., 2005; Meyer et al., 1998; Mircioiu et al., 2018). Complex models were proposed in cases of nonlinearity (Polli et al., 1996; Dunne et al., 1997; Dunne et al., 1999), but the number of parameters of models is higher, and the fitting algorithms are more unstable (Sandulovici et al., 2009; Tvrdonova et al., 2009).

A major complication occurs when *in vitro* dissolution is forced to be rapid and complete by the addition of surfactants in the dissolution medium, in which case the need arises to scale the time before correlation (Levy et al., 1967).

A first correlation between amiodarone *in vitro* dissolution and its *in vivo* dissolution estimated by the deconvolution of plasma levels was performed by Emami; however, as a consequence of very complex pharmacokinetics, results were reliable only for types B and C correlations.

The present article attempts to apply a recent method (Mircioiu et al., 2019a) of correlation between the dissolution of the parent drug and the pharmacokinetics of one of its metabolites, to the correlation between the *in vitro* dissolution of amiodarone and the rate of plasma desethyl active metabolite of amiodarone, based on data from a bioequivalence study.

MATERIALS AND METHODS

In Vitro Dissolution

The release of amiodarone from six tablets was evaluated using a USP 2 dissolution apparatus (DT 800 Erweka GmbH) at 100 rpm. The dissolution medium was sodium lauryl sulfate 10 g/L in ultrapure water (1,000 ml). Samples of 5 ± 0.1 ml were collected at 5, 15, 30, 45, and 60 min and subsequently replaced with an equal volume of medium. AMD concentrations were determined at 242 nm on a V-530 UV-VIS spectrophotometer (JASCO Ltd., Tokyo, Japan).

Clinical Trial

In vivo data were obtained in a bioequivalence study by comparing a tested formulation (T) with reference (R) Cordarone 200 mg, Sanofi Synthelabo. The study was approved by the Romanian National Medicines Agency and Ethics Committee of the Army Center for Medical Research.

Venous blood samples (5 ml) were collected into heparinized tubes through a catheter inserted in the antecubital vein before (time 0) and at 1, 1.5, 2, 3, 3.5, 4, 4.5, 5, 5.5, 6, 6.5, 7, 7.5, 8, 9, 10, 12, 24, 48, 72, 96, and 120 h. Blood samples were centrifuged at 5°C for 6 min at ~3,000 rpm. Plasma was immediately frozen and stored at −30°C until analysis.

Bioanalytical Method

Sample Treatment

Plasma samples (1,000 µL) were transferred to 10 ml disposable polypropylene tubes, to which 50 µL internal standard (IS) solution (20 µg/ml fenofibrate in methanol), 500 µL pH 4.5 phosphate buffer, and 4 ml methyl tert-butyl ether were added. The tubes were vortex mixed for 10 min and then centrifuged for 10 min at 4,000 rpm. Of the organic layer, 3 ml were retaken and evaporated to dryness at 40°C under a gentle nitrogen steam. The sample was reconstituted into 200 µL of mobile phase. Of each sample, 100 µL were injected into the chromatographic column.

Chromatographic Analysis

The chromatographic analyses were performed on a Waters liquid chromatographic system (Milford, MA 01757, United States) consisting of a 600E quaternary gradient system, an AF model in line degasser, 486 UV-VIS tunable absorbance detector, and a 717 plus auto sampler. Empower Pro software (Waters, Milford, MA 01757, United States) was used to control the system and acquire and process data. The UV detector was set at 242 nm. A 15 cm × 4.6 mm i.d Microsorb-MV C18 column (Varian, Crawley, United Kingdom) and a guard column packed with C18 were used for separation. The mobile phase consisted of a phosphate buffer solution containing 7 mM Na_2HPO_4 and 11 mM KH_2PO_4, adjusted to pH 4.5 (Solvent A) and a 1:1 (v:v) acetonitrile methanol mixture (Solvent B), and delivered in a 20:80 (v:v) ratio. The mobile phase was prepared daily, filtered, and degassed before use. The flow rate was 1.0 ml/min, and all work was carried out at 40°C.

The method was validated in accordance with the bioanalytical method validation guidelines of the FDA, including linearity, limits of quantification, selectivity, accuracy, precision, recovery, dilution effects, and stability. The specificity was evaluated related to interferences from the endogenous matrix components of drug-free plasma samples of six different origins. The calibration curves of AMD and DAMD were constructed in the range in the range 20–1,000 ng/ml for both AMD and DAMD, by plotting the ratios between their peak areas and IS peak areas vs. concentration (ng/ml), using data obtained from triplicate analysis of the calibration standard solution. The lower limit of quantification (LLOQ) was

set as the lowest concentration on the calibration curve. Within-run and between-run precision and accuracy were estimated by analyzing five replicates of the LLOQ and quality control (QC) samples in a single analytical run and on five consecutive days, respectively. The absolute recovery of AMD and DAMD was determined using five replicates of the three concentration level QC samples and was determined to be 74% for AMD and 97% for DAMD. Benchtop, extract, stock solution, freeze-and-thaw, long-term, and post-preparative stability studies were also performed to evaluate the stability of both analytes.

Statistical Analysis

Pharmacokinetics parameters area under curve ($AUC_{0-\infty}$) and maximum concentration (C_{max}) were considered as random variables with the following structure (Chow et al., 1997):

$$Y_{ijk} = \mu + S_{ik} + P_j + F_{(j,k)} + C_{(j-1,k)} + e_{ijk},$$

where μ = the overall mean, i = index for subject, i = 1, n_k, j = index for period, k = index for sequence, $F_{(j,k)}$ = the direct fix effect of the formulation in the kth sequence which is administered at the jth period, $C_{(j-1,k}$ = the fixed first-order carryover effect of the formulation in the kth sequence which is administered at the (j-1)th period, where $C_{(0,k)} = 0$ and $\Sigma C_{(j-1,k)} = 0$, and e_{ijk} = the within-subject random error in observing Y_{ijk}.

All parameters were evaluated by analyses of variance to determine statistically significant ($\alpha = 0.05$) differences between the drug formulations using the program Kinetica, version 4.2. InnaPhase Corporation.

To demonstrate bioequivalence, the 90% confidence intervals for AMD (DAMD) test/reference ratios of $AUC_{0-\tau}$ and $AUC_{0-\infty}$ were shown to lie within the 80–125% interval.

Modeling

Modeling of *In Vitro* Release Kinetics Data

In vitro dissolution data were modeled using a square root law and a power law model, used in linear forms, as previously described (Mircioiu et al., 2013).

The law of square root can result from a phenomenological model that involves the diffusion of the drug into the solvent that penetrates the matrix of the pharmaceutical formulation (Higuchi model) or from a model that considers release from the pharmaceutical formulation as an infinite reservoir across the interfaces with the solvent in a long diffusion path (Mircioiu et al., 2019b):

$$r(t) = k\sqrt{t},$$

where *r(t)* is the ratio of cumulated released substance at the moment t. It should be noted that *r(t)* is sometimes written in the form $r(t) = M(t)/M_\infty$, where M_∞ is the amount released at infinity; however, in all cases, this is not the total amount of diffusing component. In case of nanosystems, for example, the release most frequently involves only a part of the active substance, which we can consider as the "available fraction for release," with another part of it remaining sequestered. Whatever the case, in practice, in most cases, the experimentally determined quantity tends to reach a saturation value. If this value remains constant for a sufficient period of time, it is reliable to consider it as M_∞.

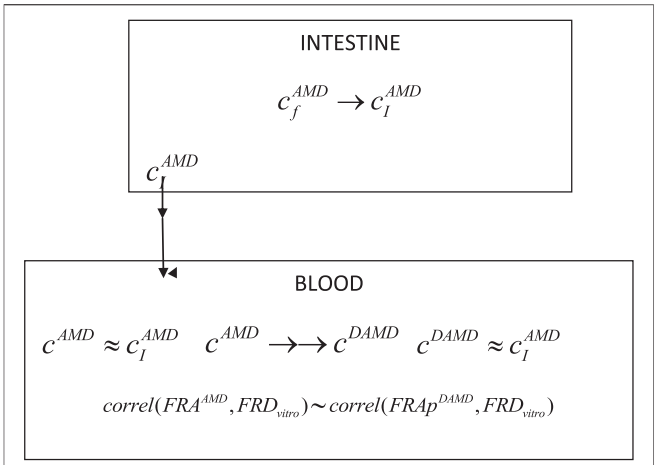

SCHEME 1 | Schematic representation of the main processes involved in the pharmacokinetics of AMD and its DAMD metabolite.

Power law is an empirical law which combines two release kinetics as a result of the diffusion and the erosion of a matrix, is linearized in the form

$$\ln(r) = \ln k + n \ln(t),$$

and is known in case of release from pharmaceutical formulations, under the name Peppas law (Peppas 1985).

Modeling of AMD and DAMD Pharmacokinetics

Analysis of time evolution of plasma levels of AMD and DAMD and estimation of the pharmacokinetic parameters was performed by both non-compartmental and compartmental methods, based on the data obtained in the 0–120 h time interval.

There were estimated partial and cumulated areas under curves. It was tested if, after logarithmic transformation, a good regression line on the tail of the curve was obtained, in order to define an elimination constant. Mono- and bicompartmental modeling was tested for AMD and DAMD pharmacokinetics.

Pharmacokinetic Model for Dissolution, Absorption, and Metabolism of AMD and Formation and Elimination of DAMD

Amiodarone, a lipophilic drug (logP = 7.24), undergoes substantial metabolism, being classified as BDDCS (biopharmaceutics drug disposition classification system) Class 2 compounds (Wu and Benet, 2005).

The hypothesis of this article, presented previously by the authors (Mircioiu et al., 2019a), was that if the absorption and metabolism can be assumed to be rapid, then the apparition of metabolite in plasma $FRAp^{dAMD}$ (*t*) could be considered an estimation of the absorption of the parent drug from the intestine $FRA(t_i)$. Based on this hypothesis, a correlation between *in vitro* dissolution and the *in vivo* pharmacokinetics of metabolites would be expected, which was indeed found in the case of diltiazem.

Because the pharmacokinetics was measured after a single dose, the return from the "deep compartment," where accumulation occurs over time, was neglected. Furthermore,

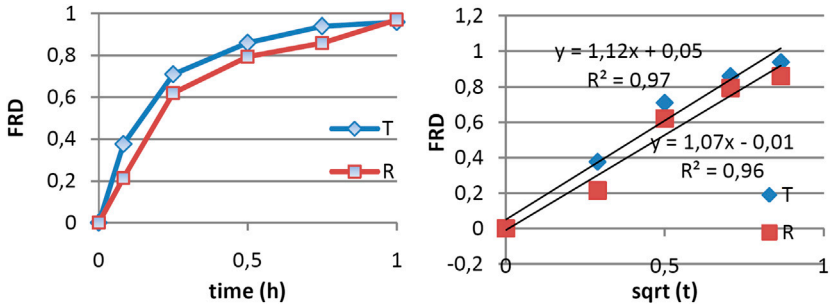

FIGURE 1 | *In vitro* release data of AMD and modeling using the square law.

because metabolites occur at the same time as plasma AMD, metabolism is considered a rapid process.

Consequently, the slowest, rate-determining step for the chain of kinetics leading to the apparition of metabolite in plasma remains the release kinetics of the parent drug in the gastrointestinal tract.

Again, because AMD is lipophilic, the rate of transfer from the blood to the lipid compartment is higher than that of reverse transport; the return of AMD to the blood may be neglected, and the transfer from blood to lipids will become a component of the elimination of the parent drug.

Consequently, in a simplified one-compartment model for DAMD, it was considered only two processes, corresponding to the appearance of the metabolite in the blood and its total elimination (**Scheme 1**).

Where c_f^{AMD} is the concentration in the tablet formulation, c^{AMD} and c^{dAMD} are, respectively, the concentrations of the parent drug and metabolite in blood compartment.

$\rightarrow$ represents a slow process and $\rightarrow\rightarrow$ a rapid process, FRA^{AMD} is the absorption fraction of AMD, $FRAp^{dAMD}$ is the fraction of apparition of DAMD in blood, *FRD* is the dissolution fraction, and *correl* denotes correlation.

Calculation of fraction of apparition of DAMD in plasma

A modified, Wagner–Nelson-type equation (Mircioiu et al., 2019a) was applied for the calculation of the "fraction of apparition" in plasma of the metabolite (*FRAp*):

$$FRAp^{dAMD}(t_i) = \frac{c^{dAMD}(t_i) + \int_0^{t_i} k_e^{dAMD} c^{dAMD} dt}{\int_0^{\infty} k_e^{dAMD} c^{dAMD} dt},$$

where $FRAp^{DAMD}$ is the fraction of the apparition of the metabolized drug at time t_i, $c^{dAMD}(t_i)$ is the plasma concentration of the metabolite at time t_i, and k_e^{dAMD} denotes the apparent elimination rate constant.

The elimination rate constant was estimated as the slope of linear regression of the last points of the logarithmic transformed data. Integrals were approximated by areas under plasma levels of DAMD.

The model could actually be much more general. In the case of compounds subject to extended metabolism (BDDCS classes 1 and 2 compounds), because the rate of absorption and metabolism are usually high, the rate of occurrence of metabolites in the plasma is determined by the rate and extent of the parent drug release from the pharmaceutical formulation.

RESULTS AND DISSCUSSION

In Vitro Dissolution of Amiodarone

Since amiodarone is lipophilic (logP 7.24) [Amiodarone DrugBanK], its dissolution in water is very low, meaning that it is necessary to add surface-active agents in dissolution medium. The FDA recommends sodium lauryl sulfate (SLS) 1% or Tween 80 1% (accessdata.fda). In these conditions, the dissolution of AMD was rapid, being complete within 1 h in all cases. The mean amiodarone dissolution profiles are presented in **Figure 1A**.

Modeling of the *In Vitro* Release

Dissolution is forced by the addition of a high concentration of surfactant in the release medium, which is a good test for quality control, but dissolution in the presence of great concentrations of surface-active agents is not biorelevant (Preda et al., 2012; Mircioiu et al., 2013).

The modeling of release kinetics was performed using both the square root and power law model. It appeared that both models work well enough. Correlation coefficient was higher in the case of the power law, but the number of points approximated by the square root law was greater. Fitting with the square root law for tested and reference drug are presented in **Figure 1**.

Pharmacokinetics of AMD and DAMD

Individual pharmacokinetics curves for AMD and mean curves for AMD and DAMD, for the reference (R) and tested (T) formulations are presented in **Figure 2**.

There is a great variability of concentrations between subjects from 12 h, but it is, at the same time, to note that the tails of curves are approximately parallel, suggesting a common pattern for elimination in all subjects. AMD has unpredictable absorption and therefore bioavailability (Martin Algara et al., 1994).

In the first phase, a rapid decrease in plasma levels appeared, with lipids and deep compartments becoming depots for both AMD and DAMD. Later, both of them return to the central compartment, and a long and variable terminal elimination half-life appears (Holt et al., 1983).

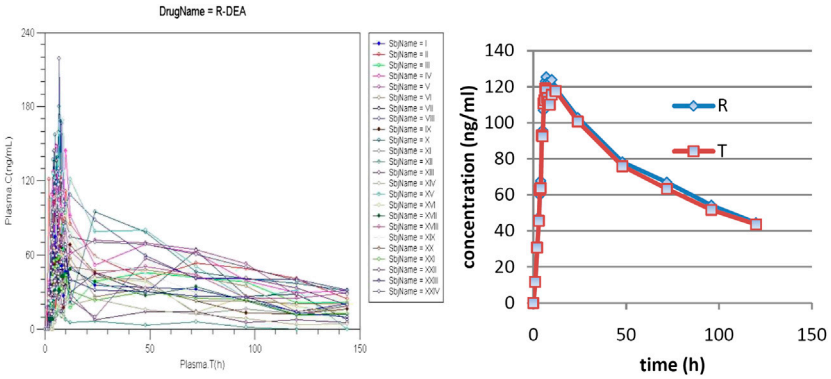

FIGURE 2 | Plasma levels of DAMD.

TABLE 1 | Pharmacokinetic parameters of DAMD, non-compartmental analysis.

Pharmacokinetic parameter	Amiodarone (tested)	Cordarone	90% confidence interval
C_{max} (ng/ml)	103.6 ± 44.8	105.5 ± 48.3	88–111
T_{max} (h)	8.2 ± 8.8	6.1 ± 2.8	
$AUC_{0-120\ h}$	4507.9 ± 2043.1	4880.8 ± 2159.6	
$AUC_{0-\infty}$	6142.8 ± 2836	6783.2 ± 3154	84–104

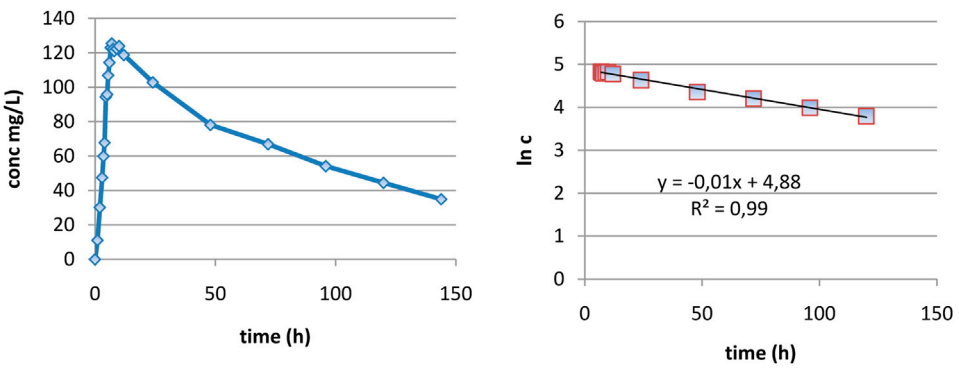

FIGURE 3 | Evaluation of the elimination part of plasma level curves: **(A)** linear representation and **(B)** logarithmic representation.

A naked eye analysis suggests that the formulations are bioequivalent. Mean pharmacokinetic parameters and 90% confidence intervals for mean ratios μ^T_{AUC}/μ^R_{AUC} and $\mu^T_{C_{max}}/\mu^R_{C_{max}}$ presented in **Table 1** confirmed the bioequivalence.

Calculation of the *In Vivo* Dissolution/ Absorption Fraction as a Function of Time by Deconvolution of DAMD Plasma Levels

As the formulations proved to be bioequivalent in spite of their high variability, starting from AUC and Cmax, a first analysis was performed on the entire set of data in the study (joint, reference and tested, 48 curves).

To apply the mass balance of the Wagner–Nelson type in the calculation of the fraction of drug absorbed and, in our case, the fraction of AMD dissolved *in vivo*, the elimination constants for AMD and DAMD were estimated.

Half-time was not well defined in the case of AMD, with the result depending on the interval selected on the tail of the plasma level curves. Three, very different values were obtained: 7 h in the 7–12 h interval, 23 h in the 12–48 h interval, and 77 h in the 48–120 h interval. In the label of the AMD reference drug, a half-time of 53 days is reported. This evolution is a result of the distribution in lipids and enterohepatic circulation, as well as returning AMD back to the central compartment from the accumulations in lipid and deep compartments.

Comparative *in vitro* and *in vivo* evaluations of three tablet formulations of amiodarone in healthy subjects were previously reported by Emami (2010). He considered the last sampling time

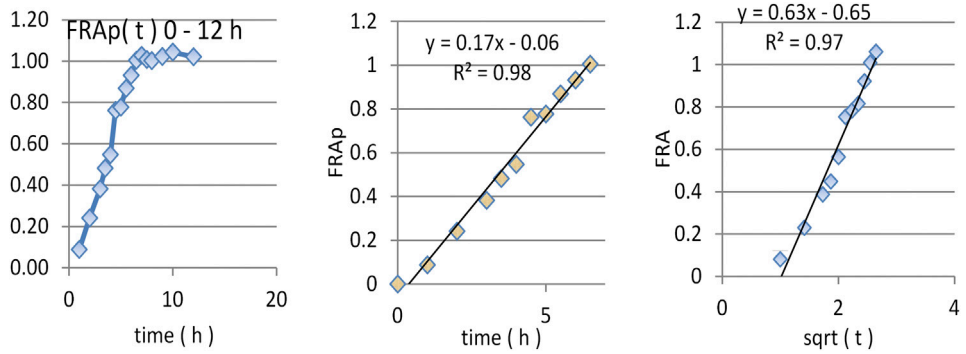

FIGURE 4 | Dependence of FRAp(t) on time **(A,B)** and square root of time **(C)**.

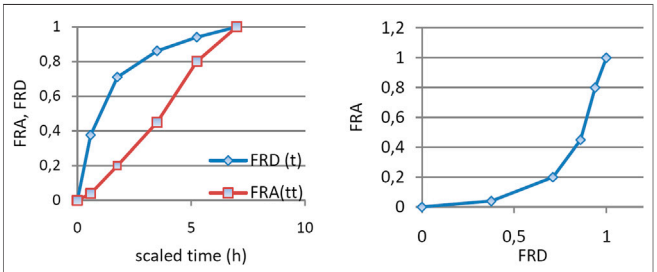

FIGURE 5 | (A) FRA and FRD as functions of time scaled using a constant factor and **(B)** dependence of FRA of FRD.

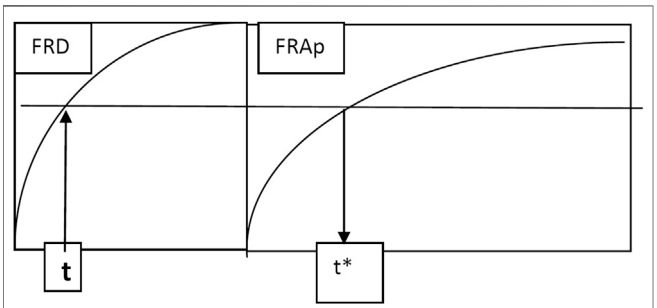

FIGURE 6 | Graphical presentation of the time scaling t–t* algorithm.

for *in vitro* dissolution, 120 min, and the *in vivo* time points of up to 18 h. He applied a time scale, following the FDA recommendation: "Time scaling may be used as long as the time scaling factor is the same for all formulations." His conclusion was that "a point-to-point acceptable and reliable correlation was not achieved" and "dissolution data could be used only for routine and in-process quality control of amiodarone tablet formulations."

In the case of DAMD, as can be seen in **Figure 3A**, curves are very smooth and elimination appears to be well described as monoexponential. In the interval 7–120 h, the logarithm of concentration was excellent linearly correlated with the time (**Figure 3B**), proving really a monoexponential behavior, and it was possible to calculate the half-time of DAMD, with a value of 70 h being obtained.

By introducing this value in the proposed deconvolution formula and making the calculation, as can be seen in **Figure 4A**, a standard "absorption fraction" was obtained: a continuous smooth function increase followed by a saturation portion, at the limit value 1. This is a good result since, in the case of AMD, the curve had several maxima and even maxima greater than 1.

As the pharmacokinetic model supposes that the apparition of DAMD in plasma equals the release of AMD *in vivo*, an FRAp dependence on time similar to the model of dissolution kinetics *in vitro* could be expected. A naked eye examination suggests a linear model. A good fit of FRA as a function of the square root of time was also was obtained.

The linear correlation is just slightly better, but the small lag time appeared in the square root of time scale; this was a good result since absorption and metabolism are not instantaneous.

In Vitro–In Vivo Dissolution Time Scaling

Following the low solubility of AMD and the small volume of GI liquids, dissolution had reason to be slow and limited. Release is also influenced by the secretion of bile salts and lecithine (Pahomi et al., 2012). Release in 1 h obtained in conditions of compendium test is a forced release. It is expected that *in vivo* release is much slower.

n circumstances of the model, the apparition of metabolite in plasma is correlated with *in vivo* dissolution of the parent drug. In order to correlate the *in vitro* dissolution fraction with the *in vivo* appearance of metabolite, time scaling was performed. Time in the interval 0–60 min, corresponding to *in vitro* dissolution, was transformed in time t* in the interval 0–7 h.

An exponential dependence of the FRA on FRD (**Figure 5**) is difficult to interpret. Usually, a linear dependence is desired.

It has been used in the literature as a factor for time transformation in the ratio T50% *in vivo* dissolution/T50% *in vivo* dissolution (Yuen et al., 1983). In our case, this would

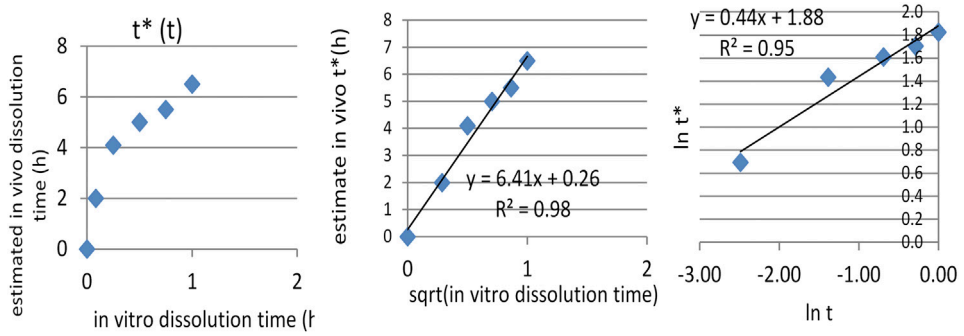

FIGURE 7 | Dependence of t* on t **(A)**, of square root of t **(B)**.

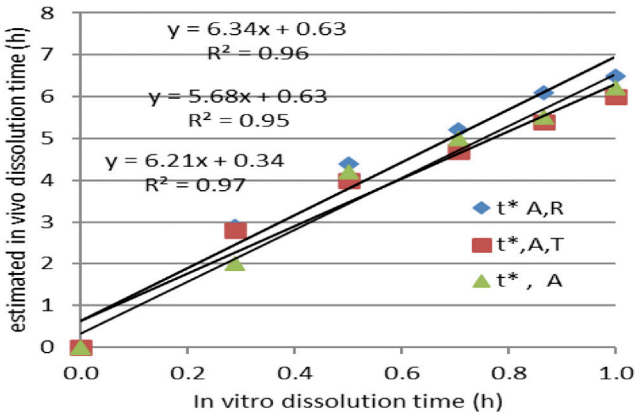

FIGURE 8 | Modeling the dependency $t^*(t)$ as a square root–type law for the reference drug, tested drug, and joint data.

give a factor of approximately 10, which is too much since FRA attains the value 1 at 7 h. Such an approach is imposed when the value 1 is reached asymptotically, not sudden, as in our case. However, following the complexity of the release *in vivo* and absorption, such an approach remains a rough approximation, which leaves out a lot of information deduced from dissolution and blood level profiles. This is also a common feature of other proposed methods, based on statistical moment analysis (Tanigawara et al., 1982).

The application of a constant factor, the same for different formulations, is an ideal method. Unfortunately, it is expected that in different segments of the GI tract, the influence on the dissolution rate is different and the application of a single factor leads to a too rough approximation (Cardot and Davit, 2012; Marvola et al., 2004; Hemmingsen et al., 2011).

The alternative method used in this article was to look for a transformation of time (**Figure 6**) which leads to a linear dependence between FRA(t*) and FRD(t*).

Transformation of time was performed, as can be seen in **Figure 3**. Time t was transformed in time t*, for which FRA(t*) = FRD(t). In fact, this is a method to obtain a Levy plot.

After Levi-type time scaling for imposing the *in vitro–in vivo* correlation, the problem became that of the correlation between *in vitro* dissolution time *t*, and *in vivo* dissolution time *t**, which was proven to follow a square root model.

IA function $t^*(t)$ was obtained, as can be seen in **Figure 7A**. The dependence t* on the square root of *t* (**Figure 7C**) seemed to be reliable. This function has a much more mechanistic resonance. Although usually applied for describing the release kinetics data, it proved to also be applicable in the case of AMD tablets in both our experiments (**Figure 8**). This represents a more general phenomenon: release from infinite reservoirs, similar to thermostats in heat transfer theory (Mircioiu et al., 2019b).

CONCLUSION

In the case of lipophilic drugs, due to slow dissolution, rapid absorption, and rapid metabolism, the pharmacokinetics of both the parent drug and metabolites before the return of the drug from other compartments in the blood is mainly determined by the kinetics of release in the intestine from the pharmaceutical formulation.

For long-life lipophilic drugs, as shown for DMA, it is possible to estimate the absorption fraction of the parent drug from the simpler pharmacokinetics of the metabolite, in which case it is possible to calculate an elimination constant.

The similarity between *in vitro* dissolution and the *in vivo* estimated dissolution models as well as the similar dependence of scaled time on *in vitro* time in the case of bioequivalent formulations can be considered a validation of the metabolite approach of the *in vitro–in vivo* correlation model.

DATA AVAILABILITY STATEMENT

The raw data supporting the conclusions of this article will be made available by the authors, without undue reservation.

ETHICS STATEMENT

The studies involving human participants were reviewed and approved by Institutional Ethics Committee. The patients/participants provided their written informed consent to participate in this study.

AUTHOR CONTRIBUTIONS

MS collected materials and wrote the paper, CM coordinated the mathematical modeling and statistical analysis, VV coordinated the clinical trial and analyzed the pharmacological aspects, and IM and VA developed the methods and performed the experiments.

REFERENCES

Al-Behaisi, S., Antal, I., Morovján, G., Szúnyog, J., Drabant, S., Marton, S., et al. (2002). *In vitro* simulation of food effect on dissolution of deramciclane film-coated tablets and correlation with *in vivo* data in healthy volunteers. *Eur. J. Pharmaceut. Sci.* 15, 157–162. doi:10.1016/s0928-0987(01)00195-6

Berger, Y., and Harris, L. (1986). *Amiodarone, pharmacology-pharmacokinetics-toxicology-clinical effects*. Paris: Medsi, 59.

Cardot, J. M., and Davit, B. M. (2012). *In vitro in vivo* correlations: tricks and traps. *AAPS J.* 14, 491–499. doi:10.1208/s12248-012-9359-0

Chow, S. C., Liu, J. P., and Bolton, S. (1997). *Design and analysis of bioavailability and bioequivalence studies, cap. III, cap. IV*. Pharmaceutical Statistics, M. Dekker.

Deng, P., You, T., Chen, X., Yuan, T., Huang, H., and Zhong, D. (2015). Identification of amiodarone metabolites in human bile by ultraperformance liquid chromatography/quadrupole time-of-flight mass spectrometry. *Drug Metab. Dispos.* 39 (6), 1058–1069. doi:10.1124/dmd.110.037671

Djiane, P., Marchiset, D., Bory, M., Bailie, Y., Serradimigni, A., and Cano, J. P. (1984). Myocardial and plasma drug levels of amiodarone and its des-ethyl metabolite. *Eur. Heart J.* 5 (Suppl. 1), 112.

Dunne, A., O'Hara, T., and Devane, J. (1999). A new approach to modelling the relationship between *in vitro* and *in vivo* drug dissolution/absorption. *Stat. Med.* 18, 1865–1877. doi:10.1002/(SICI)1097-0258(19990730)18:14<1865::AID-SIM223>3.0.CO;2-P

Dunne, A., O'Hara, T., DeVane, J., and Dunne, A. (1997). Level A *in vivo-in vitro* correlation: nonlinear models and statistical methodology. *J. Pharm. Sci.* 86, 1245–1249. doi:10.1021/js970155d

Eddington, N. D., Marroum, P., Uppoor, R., Hussain, A., and Augsburger, L. (1998). Development and internal validation of an *in vitro-in vivo* correlation for a hydrophilic metoprolol tartrate extended release tablet formulation. *Pharm. Res.* 15, 466–473. doi:10.1023/a:1011988601696

Emami, J. (2010). Comparative *in vitro* and *in vivo* evaluation of three tablet formulations of amiodarone in healthy subjects. *Daru* 18 (3), 193–199.

Emami, J. (2006). *In vitro-in vivo* correlation: from theory to applications. *J. Pharm. Pharmaceut. Sci.* 9, 169–189.

European Medicines Agency (2014a). Guideline on the pharmacokinetic and clinical evaluation of modified release dosage forms (EMA/CPMP/EWP/280/96 Corr1). Available at: https://www.ema.europa.eu/en/documents/scientific-guideline/guideline-pharmacokinetic-clinical-evaluation-modified-release-dosage-forms_en.pdf (Accessed October 05, 2020).

European Medicines Agency (2014b). Guideline on quality of oral modified release products (EMA/CHMP/QWP/428693/2013). Available at: https://www.ema.europa.eu/en/documents/scientific-guideline/guideline-quality-oral-modified-release-products_en.pdf (Accessed October 02, 2020).

Freedman, M. D., and Somberg, J. C. (1991). Pharmacology and pharmacokinetics of amiodarone. *J. Clin. Pharmacol.* 31 (11), 1061–1069. doi:10.1002/j.1552-4604.1991.tb03673.x

Hemmingsen, P., Haahr, A. M., Gunnergaard, C., and Cardot, J. M. (2011). Development of a new type of prolonged release hydrocodone formulation based on Egalet® ADPREM technology using *in vivo in vitro* correlation. *Pharmaceutics* 3, 73–87. doi:10.3390/pharmaceutics3010073

Holt, D. W., Tucker, G. T., Jackson, P. R., and Storey, G. C. (1983). Amiodarone pharmacokinetics. *Am. Heart J.* 106 (4), 840–847. doi:10.1016/0002-8703(83)90006-6

Humbert, H., Bosshardt, H., Cabiac, M. D., and Cabiac, M. (1994). *In vitro in vivo* correlation of a modified-release oral form of ketotifen: *in vitro* dissolution rate specification. *J. Pharm. Sci.* 83, 131–136. IVIVCs are supported by regulatory authorities since the late 1990s and sponsors are encouraged 475 to attempt. doi:10.1002/jps.2600830205

Lake, O., Olling, M., and Barends, D. (1999). *In vitro in vivo* correlations of dissolution data of carbamazepine immediate release tablets with pharmacokinetic data obtained in healthy volunteers. *Eur. J. Pharm. Biopharm.* 48, 13–19. doi:10.1016/s0939-6411(99)00016-8

Levy, G., Leonards, J. R., and Procknal, J. A. (1967). Interpretation of *in vitro* dissolution data relative to the gastrointestinal absorption characteristics of drugs in tablets. *J. Pharm. Sci.* 56 (10), 1365–1367. doi:10.1002/jps.2600561039

Martin Algarra, R. V., Pascual Costa, R. M., and Casabo, V. G. (1994). Effect of surfactants on amiodarone intestinal absorption. I. Sodium laurylsulfate. *Pharm. Res.* 11, 1042–1047. doi:10.1023/a:1018947723406

Marvola, J., Kanerva, H., Slot, L., Lipponen, M., Kekki, T., Hietanen, H., et al. (2004). Neutron activation-based gamma scintigraphy in pharmacoscintigraphic evaluation of an Egalet® constant-release drug delivery system. *Int. J. Pharm.* 281, 3–10. doi:10.1016/j.ijpharm.2004.05.022

Meyer, M. C., Straughn, A. B., Mhatre, R. M., Shah, V. P., Williams, R. L., and Lesko, L. J. (1998). Lack of *in vivo in vitro* correlations for 50 mg and 250 mg primidone tablets. *Pharm. Res.* 15, 1085–1089. doi:10.1023/a:1011942530288

Mircioiu, C., Anuta, V., Mircioiu, I., Nicolescu, A., and Fotaki, N. (2019a). *In vitro in vivo* correlations based on in vitro dissolution of parent drug diltiazem and pharmacokinetics of its metabolite. *Pharmaceutics* 11, 344. doi:10.3390/pharmaceutics11070344

Mircioiu, C., Mircioiu, I., Voicu, V., and Miron, D. (2005). Dissolution-bioequivalence non-correlations. *Basic Clin. Pharmacol. Toxicol.* 96, 262–264. doi:10.1111/j.1742-7843.2005.pto960324.x.

Mircioiu, C., Voicu, V., Anuta, V., Tudose, A., Celia, C., Paolino, D., et al. (2019b). Mathematical modeling of release kinetics from supramolecular drug delivery systems pharmaceutics. *Pharmaceutics* 11, 140. doi:10.3390/pharmaceutics11030140

Mircioiu, I., Anuta, V., Purcaru, S. O., and Flavian, R. (2013). *In vitro* dissolution of poorly soluble drugs in the presence of surface active agents – *in vivo* pharmacokinetics correlations. II. Nimesulide. *Farmacia* 61 (1), 88–102.

Mircioiu, I., Anuta, V., and Stanciu, G. (2018). Non-linear and linearized IVIV correlations for tablets containing a large molecule polar compound. *J. Sci. Arts Issue* 1, 203–210.

Pahomi, G., Corlan, G., Anuta, V., Sandulovici, R., and Mircioiu, I. (2012). Study of the influence of bile salts and lecithin on distribution of ketoconazole between plasma and methylene chloride. *Farmacia* 60 (6), 809–821.

Peppas, N. A. (1985). Analysis of Fickian and non-Fickian drug release from polymers. *Pharm. Acta Helv.* 60, 110–111.

Polli, J. E., Crison, J. R., and Amidon, G. L. (1996). Novel approach to the analysis of *in vitro-in vivo* relationships. *J. Pharm. Sci.* 85, 753–760. doi:10.1021/js9503587

Preda, I. A., Mircioiu, I., Mircioiu, C., Corlan, G., Pahomi, G., Prasacu, I., et al. (2012). Research concerning the development of A biorelevant dissolution test for formulations containing norfloxacin. I. Modelling of *in vitro* release kinetics. *Farmacia* 60 (5), 675–687.

Rao, B. S., Seshasayana, A., Saradhi, S. P., Kumar, N. R., Narayan, C. P., and Murthy, K. R. (2001). Correlation of '*in vitro*' release and '*in vivo*' absorption characteristics of rifampicin from ethylcellulose coated nonpareil beads. *Int. J. Pharm.* 230, 1–9. doi:10.1016/s0378-5173(01)00835-3

Sandulovici, R., Prasacu, I., Mircioiu, C., Voicu, V. A., Medvedovici, A., and Anuta, V. (2009). Mathematical and phenomenological criteria in selection of pharmacokinetic model for m1 metabolite of pentoxyphylline. *Farmacia* 57, 235–246.

Tanigawara, Y., Yamaoka, K., Nakagawa, T., Nagakawa, M., and Uno, T. (1982). Correlation between *in vivo* mean dissolution time and *in vitro* mean dissolution time of amoxicillin products. *J. Pharmacodiobyn.* 5 (5), 370–372. doi:10.1248/bpb1978.5.370

Tvrdonova, M., Dedik, L., Mircioiu, C., Miklovicova, D., and Ďurišová, M. (2009). Physiologically motivated time-delay model to account for mechanisms underlying enterohepatic circulation of piroxicam in human beings. *Basic Clin. Pharmacol. Toxicol.* 104, 35–42. doi:10.1111/j.1742-7843.2008.00304.x

US Food and Drug Administration (1997a). Guidance for Industry. Extended Release Oral Dosage Forms: Development, Evaluation, and Application of In Vitro/In Vivo Correlations. Available at: https://www.fda.gov/media/70939/download (Accessed October 09, 2020).

US Food and Drug Administration (1997b). Guidance for Industry. SUPAC-MR: Modified Release Solid Oral Dosage Forms. Available at: https://www.fda.gov/media/70956/download (Accessed October 05, 2020).

Varshosaz, J., Ghafghazi, T., Raisi, A., and Falamarzian, M. (2000). Biopharmaceutical characterization of oral theophylline and aminophylline tablets. Quantitative correlation between dissolution and bioavailability studies. *Eur. J. Pharm. Biopharm.* 50, 301–306. doi:10.1016/s0939-6411(00)00074-6

Wu, C. Y., and Benet, L. Z. (2005). Predicting Drug disposition via application of BCS: transport/absorption/elimination interplay and development of a biopharmaceutics. drug disposition classification system. *Pharm. Res.* 22, 11–23. doi:10.1007/s11095-004-9004-4

Yuen, K. H., Desmukh, A., and Newton, J. M. (1983). *In vitro*/*in vivo* correlation of experimental sustained-ReleasenThophylline formulations. *Pharm. Res.* 10 (4), 588–592. doi:10.1023/a:1018910421840

Conflict of Interest: The authors declare that the research was conducted in the absence of any commercial or financial relationships that could be construed as a potential conflict of interest.

frontiers in Pharmacology

ORIGINAL RESEARCH
published: 04 March 2021
doi: 10.3389/fphar.2021.640705

Study on Acute Toxicity of Amiodarone New Complexes With Cyclodextrin

Cristina Mihaela Ghiciuc[1†], Maytham Razaq Shleghm[2†], Cornelia Vasile[3], Gladiola Tantaru[4], Andreea Creteanu[5*] and Lacramioara Ochiuz[5]*

[1]Department of Pharmacology, Faculty of Medicine, "Grigore T. Popa" University of Medicine and Pharmacy, Iasi, Romania, [2]Department of Applied Mathematics and Biostatistics, Faculty of Pharmacy, "Carol Davila" University of Medicine and Pharmacy, Bucharest, Romania, [3]Physical Chemistry of Polymers Department, Petru Poni Institute of Macromolecular Chemistry, Iasi, Romania, [4]Department of Analytical Chemistry, Faculty of Pharmacy, "Grigore T. Popa" University of Medicine and Pharmacy, Iasi, Romania, [5]Department of Pharmaceutical Technology, Faculty of Pharmacy, "Grigore T. Popa" University of Medicine and Pharmacy, Iasi, Romania

Amiodarone's low solubility and high permeability is the limiting step for its bioavailability, therefore new formulations are needed to improve the solubility of amiodarone either to increase its oral bioavailability or to reduce its toxic effects. Complexation of amiodarone with cyclodextrin results in an improved dissolution rate, solubility, and allows for a more controlled drug release. We characterized the acute toxicity of a new amiodarone 2-hydroxypropyl-β-cyclodextrin complex (AMD/HP-β-CD) in a powdered form and as a matrix based on Kollidon® and chitosan, administered intraperitoneally in laboratory animals. There were developed two formulations of matrix: one containing only pure AMD as a control sample (Fc) and one containing the inclusion complex with the optimal solubility (F). AMD was equitoxic with HP-β-CD after intraperitoneal administration (289.4 mg/kg for AMD and 298.3 mg/kg for AMD/HP-β-CD), with corresponding histopathological changes. The matrix based formulations presented higher LD50 values for acute toxicity, of 347.5 mg/kg for Fc and 455.6 mg/kg for F10, leading to the idea of a safer administration because KOL and CHT matrix modified the solubility and controlled the AMD release. The LD50 value is 1.5 times higher for AMD/HP-β-CD included in a KOL and CHT based matrix compared to the pure AMD, administered intraperitoneally.

Keywords: amiodarone, cyclodextrin complex, acute toxicity, laboratory animals, new complexes

OPEN ACCESS

Edited by:
Sabina Passamonti, University of Trieste, Italy

Reviewed by:
Adrian Nicolescu, Queen's University, Canada
Sarasija Suresh, Institute for Drug Delivery and Biomedical Research, India
Erem Bilensoy, Hacettepe University, Turkey

****Correspondence:***
Cristina Mihaela Ghiciuc
cristina.ghiciuc@umfiasi.ro
Andreea Creteanu
acreteanu@gmail.com

†These authors have contributed equally to this work and share first authorship

Specialty section:
This article was submitted to Drug Metabolism and Transport, a section of the journal Frontiers in Pharmacology

Received: *11 December 2020*
Accepted: *17 February 2021*
Published: *04 March 2021*

Citation:
Ghiciuc CM, Shleghm MR, Vasile C, Tantaru G, Creteanu A and Ochiuz L (2021) Study on Acute Toxicity of Amiodarone New Complexes With Cyclodextrin. Front. Pharmacol. 12:640705. doi: 10.3389/fphar.2021.640705

INTRODUCTION

Many generic formulations of Amiodarone hydrochloride (AMD) are available for the clinical practice, but there is a high inter-individual variability for AMD (Atanasova and Terziivanov, 2001). There is a need to develop and implement new delivery systems, which combines safety and efficacy, to improve the solubility of amiodarone either to increase its oral bioavailability or to reduce its toxic effects, or intended to shorten the onset of AMD action. AMD is a Class II drug (according to the Biopharmaceutical Classification System) because it has low solubility and high membrane permeability, therefore dissolution in gastrointestinal fluids is the limiting step for its oral bioavailability (Amidon et al., 1995; Benet, 2005). The solubility of a drug influence the choice of formulation for oral or parenteral administration, dissolution, and absorption from the digestive tube, therefore, development of new formulations with high solubility for low solubility compounds is a challenge.

The hydroxypropyl-β-cyclodextrin (HP-β-CD) is a cyclodextrin with very good solubility and lowest toxicity, used to increase the solubility of various poorly soluble drugs (Gould and Scott, 2005; Jacob and Nair, 2018; Muankaew and Loftsson, 2018). Cyclodextrins (CD) are a family of cyclic oligosaccharides with a hydrophobic cavity containing the active compound which is internalized forming an inclusion complex with the drug. Complexation of a drug with cyclodextrins has numerous advantages such as an improved dissolution rate, improved bioavailability, safety, and stability and allows for a more controlled drug release (Szejtli, 2005; Tiwari et al., 2010). Thus, enhanced solubility and dissolution rate was obtained *in vitro* in the case of amiodarone complexation with β-cyclodextrin (Riekes et al., 2010). A recent *in vitro* study (Rubim et al., 2017) evaluated the influence of the CD type (β-cyclodextrin, methyl-β-cyclodextrin, and 2-hydroxypropyl-β-cyclodextrin) on the complexation with AMD and on dissolution rate and found enhanced solubility and dissolution rates for inclusion complexes (Rubim et al., 2017). Only a few studies reported *in vitro* characterization of inclusion complexes of HP-β-CD with amiodarone (Rubim et al., 2017; Creteanu et al., 2019), but there is no data available about the acute toxicity of these systems.

Complexation of AMD with HP-β-CD (AMD/HP-β-CD) increases its solubility and bioavailability without any modification of its structure (Păduraru et al., 2013; Creteanu et al., 2016a; Creţeanu et al., 2016b; Creteanu et al., 2017), therefore also the acute toxicity should increase. In one of our previous papers (Creteanu et al., 2019), the physicochemical properties have been evaluated for the inclusion complex formation with AMD and for two new formulations with a matrix based on Kollidon® (KOL) and chitosan (CHT), and it was established a considerably increase of the dissolution rate of AMD from the inclusion complexes, compared to dissolution of the pure AMD. The aim of this study was to evaluate the acute toxicity of AMD from new complexes with cyclodextrin AMD/HP-β-CD as powdered form and as a matrix based KOL and CHT, administered intraperitoneally in laboratory animals. There were developed two matrix based inclusion complex formulations: one containing only pure AMD as a control sample (Fc) and one containing the inclusion complex with the optimal solubility (F10).

MATERIALS AND METHODS

Materials

Amiodarone (AMD) (Mw = 645.32 Da) of 99.85% purity has been obtained from Zhejiang Sanmen Hengkang Pharmaceutical Co. Ltd., China. HP-β-CD of 99.70% purity has been obtained from Roquette, France. Polyoxyethylene (Hodge and Sterner, 1949) sorbitan monooleate (polysorbate 80, Tween 80) has been obtained from Sigma-Aldrich, Inc. Kollidon® SR (KOL), a mixture constituted from 80% poly(vinyl acetate) and 20% polyvinylpyrrolidone (povidone), and chitosan (CHT) were purchased from BASF, Germany.

AMD/HP-β-CD contains AMD:cyclodextrin in a ratio 1:1. The substances were administered in constant volume (0.1 ml/10 g b.w.) as freshly prepared suspension with distilled water and 1% Tween-80. The solutions for acute toxicity study were prepared using the same weight of powder of AMD, respectively of AMD/HP-β-CD, Fc and F10 powders.

Experimental Animals

The protocol of the experimental study was approved by the Institutional Ethics Committee of "Grigore T. Popa" University of Medicine and Pharmacy of Iasi, Romania (No. 23983/2014). Healthy nulliparous and non-pregnant female Balb/C mice (weighting 20–25 g) were purchased from Cantacuzino Institute (Bucharest, Romania). The animal study was done in accordance with the international guidelines (National Research Council US Committee for the Update of the Guide for the Care and Use of Laboratory Animals, 2011). The animals were housed in plastic cages with stainless steel mesh lids in a ventilated room with standard environmental conditions: 12 h light-dark cycle, room temperature 24 ± 2°C and 50–70% relative humidity. They were provided *ad libitum* with standard rodent pellet food and tap water, for 5 days before testing.

Acute Toxicity Testing

To obtain the 50% lethal dose (LD50) of the AMD, respectively AMD/HP-β-CD, the experiments were designed in accordance with the "Up and Down Procedure" (UDP) provided by the Organization for Economic Cooperation and Development (OECD) Guideline 425 (OECD, 2008) and described by Dixon (Dixon, 1965). Limit test was performed at 2,000 mg/kg p.o. as single dose administered according to body weight. Main test was performed with doses adjusted by a constant multiplicative factor (namely 1.6) for this experiment: 175, 275, 440, 690 and 1,090 mg/kg b.w. The animals were fasted for 12 h prior to dosing and the single dose for each successive animal was adjusted up or down depending on the previous outcome, after 24 h one by one. Animals were closely observed during the first 30 min, then hourly for the next 6 h, at 24 h and daily for the next 14 days to record mortality and all the relevant clinical symptoms of acute toxicity (evaluation of skin and fur, grooming, posture and gait, salivation, tremor, convulsion, hyperactivity, apathy, respiratory depression, and coma). The LD50 is calculated using the maximum likelihood method with a sigma of 0.5 (OECD, 2008).

Histopathological Study

The vital organs (liver, kidney, lungs and heart) isolated from the dead mice were preserved in 10% formalin, then embedded in paraffin wax. Paraffin sections (5 mm) were stained with hematoxylin and eosin (HE) to be studied under a light microscope for morphological alterations.

RESULTS

Acute Toxicity of AMD, of AMD/HP-β-CD, of AMD Control Matrix (Fc), and of AMD/HP-β-CD Fatrix (F)

Vital Signs

During the entire study period, no unusual clinical signs were observed in the mice that received 175 mg/kg b.w of AMD,

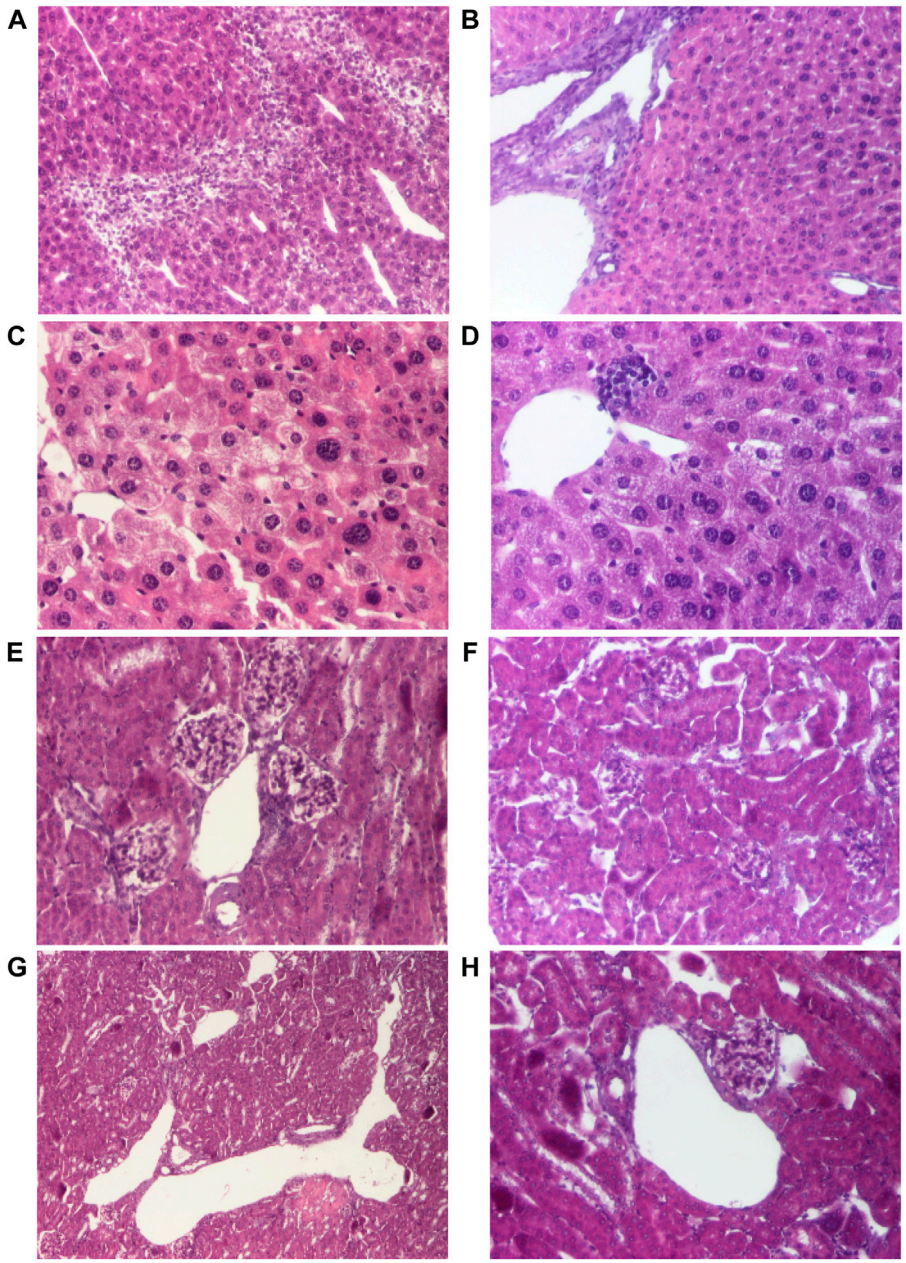

FIGURE 1 | Histological changes of the main organs in the dead mice after doses of 690 mg/kg of AMD **(A, C, E, G)** compared to 440 mg/kg of AMD **(B, D, F, H)**. Representative pictures from HE staining sections of the liver with hepatitis aspect (hematoxylin-eosin HE stain, ×100) **(A)**, liver–portal space (hematoxylin-eosin HE stain, ×100) **(B)**, degeneration of hepatocytes (hematoxylin-eosin HE stain, ×200) **(D)**, hepatocytes (hematoxylin-eosin HE stain, ×200) **(D)**, renal cortex and arteriole (hematoxylin-eosin HE stain, ×200) **(E)**, renal cortex (hematoxylin-eosin HE stain, ×100) **(F)**, renal cortex and dilated renal veins (hematoxylin-eosin HE stain, ×40) **(G)**, renal cortex and dilated renal veins (hematoxylin-eosin HE stain, ×100) **(H)**.

respectively AMD/HP-β-CD, Fc, and F. **Supplementary Table S1** summarizes some behavioral responses of mice from the first 30 min and hourly during the first 6 h after administration of a single dose of administered substances. A decrease in sensitivity and activity, tremor and convulsions were observed at 690 mg/kg b.w., during the first hour, followed by death in the case of AMD, respectively AMD/HP-β-CD. A few animals (3 out of 4) showed slight symptoms after the dose of 275 mg/kg for AMD/HP-β-CD and died 6 h after the administration of the substance. For matrix based inclusion complexes, a decrease in sensitivity and activity, tremor and convulsions were observed at 1,090 mg/kg b.w., during the first hour, followed by death for Fc and F10.

LD50 values of AMD, respectively AMD/HP-β-CD, using up and down procedure were determined to be 289.4 mg/kg for AMD and 298.3 mg/kg for AMD/HP-β-CD. For the matrix based

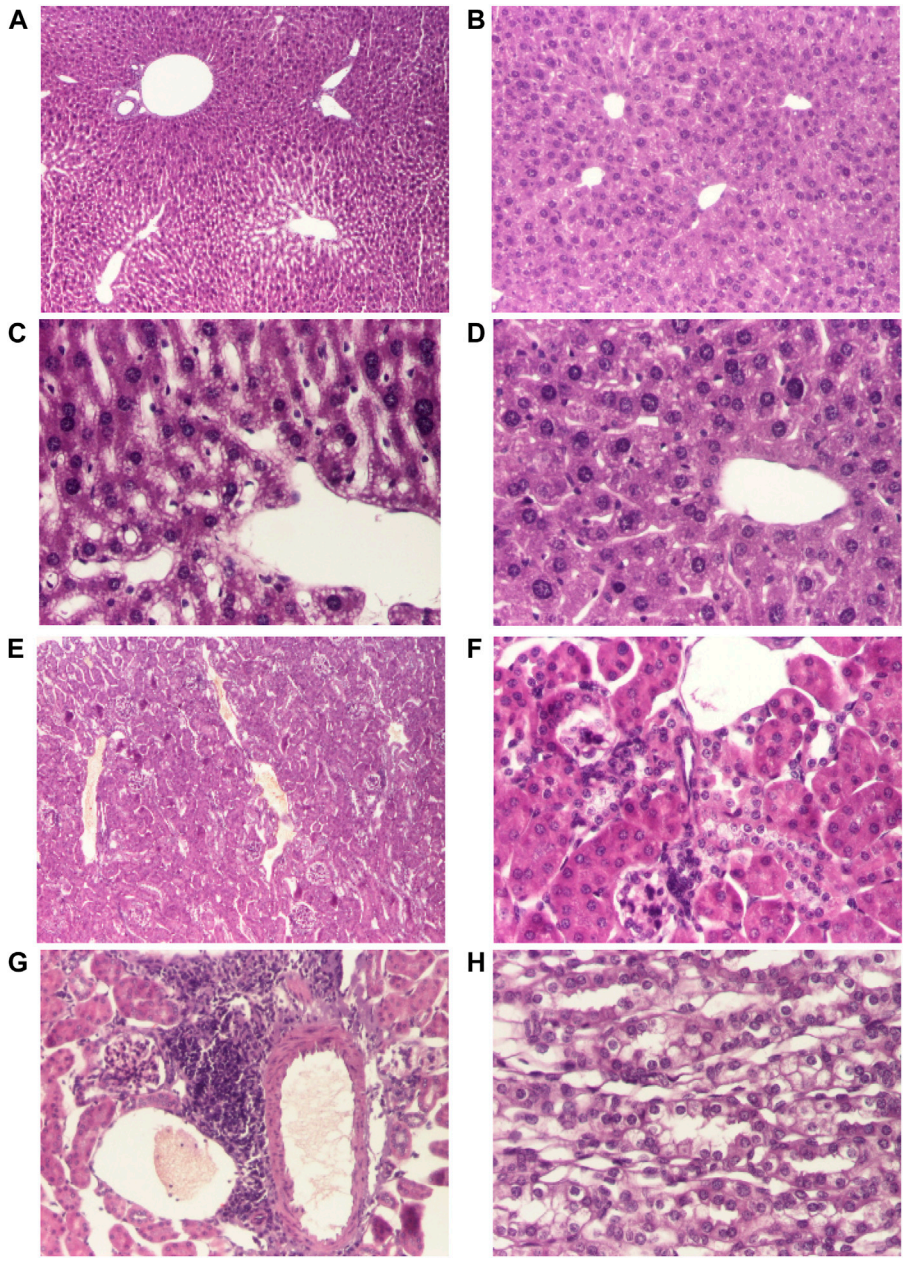

FIGURE 2 | Histological changes of the main organs in the dead mice after doses of 690 mg/kg of AMD/HP-β-CD **(A, C, E, G)** compared to 440 mg/kg of AMD/HP-β-CD **(B, D, F, H)**. Representative pictures from HE staining sections of the liver (hematoxylin-eosin HE stain, ×40) **(A, B)**, hepatocytes (hematoxylin-eosin HE stain, ×200) **(C, D)**, renal cortex (hematoxylin-eosin HE stain, ×40) **(E)**, renal cortex (hematoxylin-eosin HE stain, ×100) **(F)**, interstitial nephritis (hematoxylin-eosin HE stain, ×100) **(G)**, renal medulla (hematoxylin-eosin HE stain, ×200) **(H)**.

formulations, LD50 values were 347.5 mg/kg for Fc and 455.6 mg/kg for F10.

Histopathological Evaluation

Necropsy was carried out in all animals immediately after death. Internal organs (liver, kidney, lungs and heart) were examined for macroscopic alterations induced by AMD, respectively AMD/HP-β-CD, and collected to perform histopathological analysis (**Figures 1**, **2**). No macroscopic changes were observed.

Histopathological examination of liver and kidney fragments in animals which received toxic doses of 690 mg/kg of AMD revealed suggestive aspects of drug-induced hepatotoxicity (**Figures 1A,C**), compared to doses of 440 mg/kg of AMD

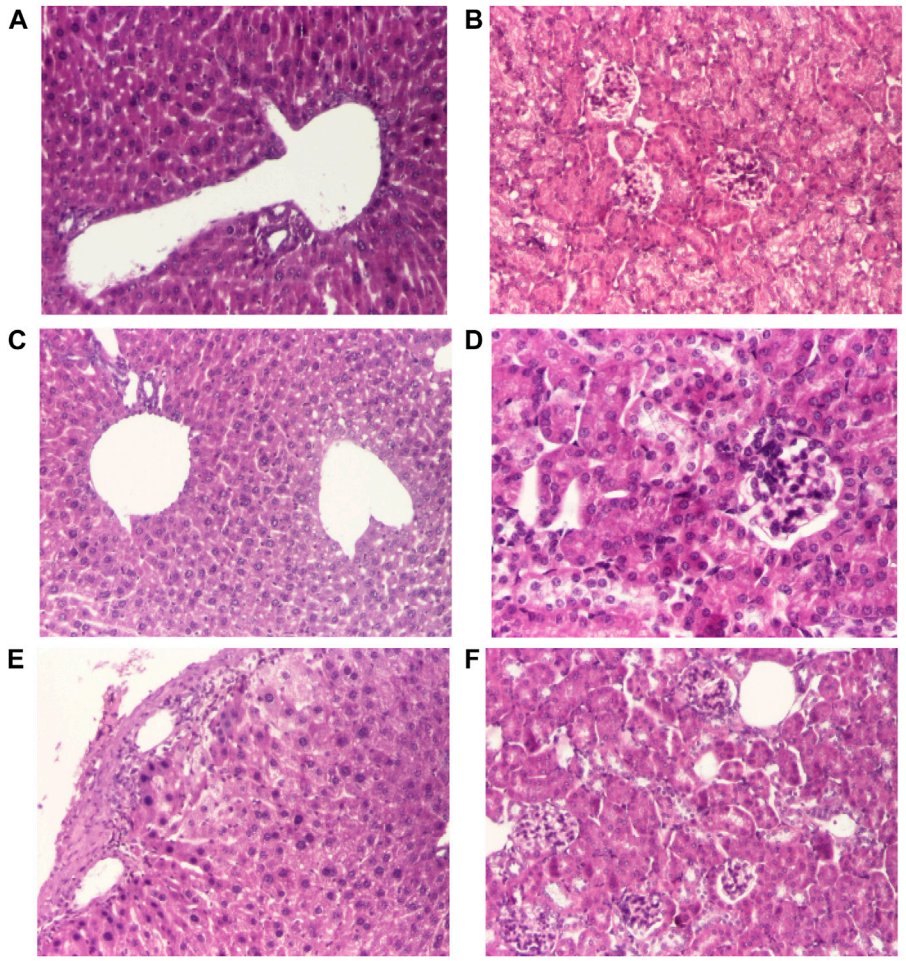

FIGURE 3 | Histological changes of the main organs in the dead mice after doses of 690 mg/kg of Fc **(A, B)** and F10 **(C, D)** and after doses of 1,090 mg/kg of F10 **(E, F)**. Representative pictures from HE staining sections of the liver (hematoxylin-eosin HE stain, ×100) **(A, C, E)**, renal (hematoxylin-eosin HE stain, ×100) **(C, D, F)**.

(**Figures 1B,D**). In the kidney, there are typical changes induced by 690 mg/kg of AMD (**Figures 1E,G**) compared to doses of 440 mg/kg of AMD (**Figures 1F,H**).

Histopathological examination of liver fragments in animals which received toxic doses of 690 mg/kg of AMD/HP-β-CD revealed suggestive aspects of drug-induced hepatotoxicity (**Figures 2A,C**), compared to doses of 440 mg/kg of AMD/HP-β-CD (**Figures 2B,D**). Histopathological examination at the renal level revealed a few changes characteristic of nephrotoxicity induced by 690 mg/kg of AMD/HP-β-CD (**Figures 2E,G**) and by 440 mg/kg of AMD/HP-β-CD (**Figures 2F,H**.).

Histopathological examination of liver and kidney fragments in animals which received toxic doses of 690 mg/kg of Fc (**Figures 3A,B**) and F10 (**Figures 3C,D**) revealed a few changes characteristic of hepatic and nephrotoxicity. They were analyzed only for the doses of 1,090 mg/kg for F10 which revealed signs of hepatic and nephrotoxicity (**Figures 3E,F**).

DISCUSSION

Our study found that AMD/HP-β-CD has similar acute toxicity with pure AMD after oral administration in mice: 289.4 mg/kg for AMD and 298.3 mg/kg for AMD/HP-β-CD. Similar doses of these compounds produced equivalent degree of acute toxicity only for AMD, respectively AMD/HP-β-CD. For the matrix based formulations, LD50 values were 347.5 mg/kg for Fc and 455.6 mg/kg for F10. The KOL and CHT matrix induced high differences in the solubility and controlled AMD release: The LD50 is 1.5 times higher when AMD is complexed with HP-β-CD and included in F10 matrix than for pure AMD. These formulations are considered moderately toxic (dose between 50–500 mg/kg), according to Hodge and Sterner scale for the evaluation of toxicity with the help of LD50 (Hodge and Sterner, 1949), with F10 being closer to the limit of slightly toxic. Amiodarone is difficult to administer because of its narrow toxic-therapeutic range (Tamargo et al., 2015). In our study, intraperitoneal administration of AMD had comparable results to

other acute toxicity studies with Amiodarone: LD50 of 294.0 mg/kg body weight in female mice after intravenous administration (Barle et al., 2013). The matrix based formulation increased the solubility and modified the release of the substance from the formulation.

Hydroxypropyl-β-Cyclodextrin (HP-β-CD) is highly biocompatible and pharmacologically inactive, therefore it was considered a safe material to improve the solubility and the bioavailability of AMD (Patel and Hirlekar, 2019). A cyclodextrin-complex formulation containing a well-known long used drug is considered a "super generic", superior in its performance when compared to other products which contain the same known active substance (Szejtli, 2005). In the case of oral administration, pharmacokinetic studies showed that drug/cyclodextrin complexes have shorter Tmax, higher Cmax and larger AUC values as a result of the increased bioavailability (Szejtli, 2005). Pharmacodynamic studies showed that most drug/cyclodextrin complexes from the market belong to these super generic drugs having a higher and quicker therapeutic effect (Szejtli, 2005). A recent pharmacokinetic study conducted in rats after intravenous bolus administration showed that the inclusion of HP-β-CD in the solution of the administered substance improved blood compatibility (Mantik et al., 2019). Polysorbate 80 (Tween 80), a nonionic surfactant, is considered non-toxic, being used as an additive, as emulsifier, as dispersant, or as stabilizer in various type of foods, pharmaceutical preparations, or cosmetics (National Toxicology Program, 1992; EFSA FEEDAP Panel, 2016).

On the other hand, Amiodarone has a narrow therapeutic ratio and it is considered a critical dose drug, therefore, increasing the solubility and the controlled AMD release to reduce the active drug dose in the new super generic cyclodextrin formulation was considered an obvious idea. In our experiment, LD50, based on up and down procedure, was 289.4 mg/kg for AMD, similar to LD50 values from literature (Barle et al., 2013) and 298.3 mg/kg for the new inclusion cyclodextrine complex HP-β-CD, meaning that AMD and its complex, HP-β-CD, had equivalent degree of toxicity. Single dose administration of 440 mg/kg and of 690 mg/kg of the classical AMD or of our new formulation HP-β-CD produced equivalent toxic effects in mice: both caused complex symptoms such as changes in breathing, agitation, increased heart rhythm, convulsions, tremors, cyanosis, falls, defecation, urination, and piloerection. In mice, both AMD and HP-β-CD, and matrix formulations determined hepatic and renal toxicity lesions, similar to those reported in the literature after high doses of AMD. These effects were not seen in matrix formulations Fc and F10. In humans, AMD-induced acute toxicity syndrome is unusual, manifested with acute liver and renal failure (Paudel et al., 2016). Central nervous system manifestations were described in the literature when toxic doses of AMD were administered. In the literature, cases of pulmonary damage, e.g., acute pulmonary edema, have been reported following administration of toxic doses of AMD in humans (Kaya et al., 2017).

CONCLUSION

Our single dose acute toxicity study showed that the same amount of AMD was equitoxic with HP-β-CD, after intraperitoneal administration, the lethal doses (DL50) of these pharmaceutical forms included them into the category 3 of toxicity (moderately toxic substances). For the matrix based formulations, LD50 values were higher pointing to the idea of a safer administration because KOL and CHT matrix induced high differences in the solubility and controlled AMD release. The LD50 value is 1.5 times higher for AMD/HP-β-CD included in a KOL and CHT based matrix compared to the pure AMD, administered using the same route.

DATA AVAILABILITY STATEMENT

The original contributions presented in the study are included in the article/**Supplementary Material**, further inquiries can be directed to the corresponding authors.

ETHICS STATEMENT

The animal study was reviewed and approved by the Ethics Committee of "Grigore T. Popa" University of Medicine and Pharmacy of Iasi, Romania (No. 23983/2014). Written informed consent was obtained from the owners for the participation of their animals in this study.

AUTHOR CONTRIBUTIONS

Conceptualization: CG, MS, and LO. Writing—original draft preparation: CG, MS, AC, and GT. Writing—review and editing: CG, MS, CV, AC, and LO. Visualization: CG, MS, and GT. Supervision: CV and LO. Funding acquisition: GT. All authors contributed to the article and approved the submitted version.

FUNDING

The work was partially supported by personal funds. The formulations leading to these results have received funding from Grigore T. Popa - Iasi through the project 29025/2016.

SUPPLEMENTARY MATERIAL

The Supplementary Material for this article can be found online at: https://www.frontiersin.org/articles/10.3389/fphar.2021.640705/full#supplementary-material.

REFERENCES

Amidon, G. L., Lennernäs, H., Shah, V. P., and Crison, J. R. (1995). A theoretical basis for a biopharmaceutic drug classification: the correlation of *in vitro* drug product dissolution and *in vivo* bioavailability. *Pharm. Res.* 12 (3), 413–420. doi:10.1023/a:1016212804288

Atanasova, I., and Terziivanov, D. (2001). Evaluation of average bioequivalence of two oral formulations of amiodarone hydrochloride after single administration to healthy volunteers. *Clin. Drug Investig.* 21, 423–428. doi:10.2165/00044011-200121060-00005

Barle, E. L., Černe, M., Peternel, L., and Homar, M. (2013). Reduced intravenous toxicity of amiodarone nanosuspension in mice and rats. *Drug Chem. Toxicol.* 36 (3), 263–269. doi:10.3109/01480545.2012.710628

Benet, L. Z. (2005). There are no useful CYP3A probes that quantitatively predict the *in vivo* kinetics of other CYP3A substrates and no expectation that one will be found. *Mol. Interv.* 5 (2), 79–83. doi:10.1124/mi.5.2.5

Creteanu, A., Ochiuz, L., Vasile, C., Paduraru, O. M., Popescu, M.-C., Vieru, M., et al. (2016a). Thermal stability assesment OF amiodarone hydrochloride IN polymeric matrix tablets. *Farmacia* 64 (6), 940–945.

Creţeanu, A., Ochiuz, L., Vieriu, M., Panainte, A. D., and Ţântaru, G. (2016b). *In Vitro* dissolution studies of amiodarone hydrochloride from hydroxypropyl-β-cyclodextrin/amiodarone inclusion complex formulated into modified-release tablets. *Rev. Med. Chir. Soc. Med. Nat. Iasi* 120 (3), 715–719.

Creteanu, A., Ochiuz, L., Vasile, C., Vieru, M., and Ţântaru, G. (2017). Studies on the influence of amiodarone complexation with cyclodextrin derivatives ON the *In Vitro* release from matrix tablets. *Farmacia* 65(4), 545–549.

Creteanu, A., Pamfil, D., Vasile, C., Tantaru, G., Ghiciuc, C. M., Ochiuz, L., et al. (2019). Study on the role of the inclusion complexes with 2-Hydroxypropyl-β-cyclodextrin for oral administration of amiodarone. *Int. J. Polym. Sci.* 2019, 1–23. doi:10.1155/2019/1695189

Dixon, W. J. (1965). The up-and-down method for small samples. *J. Am. Stat. Assoc.* 60 (312), 967–978. doi:10.1080/01621459.1965.10480843

EFSA FEEDAP Panel (2016). EFSA Panel on Additives and Products or Substances used, in Animal Feed). Safety and efficacy of polyoxyethylene (20) sorbitan monooleate as a feed additive for all animal species. *EFSA J.* 14 (3), 4443–4461. doi:10.2903/j.efsa.2016.4443

Gould, S., and Scott, R. C. (2005). 2-Hydroxypropyl-β-cyclodextrin (HP-β-CD): a toxicology review. *Food Chem. Toxicol.* 43 (10), 1451–1459. doi:10.1016/j.fct.2005.03.007

Hodge, H. C., and Sterner, J. H. (1949). Tabulation of toxicity classes. *Am. Ind. Hyg. Assoc. Q.* 10 (4), 93–96. doi:10.1080/00968204909344159

Jacob, S., and Nair, A. B. (2018). Cyclodextrin complexes: perspective from drug delivery and formulation. *Drug Dev. Res.* 79 (5), 201–217. doi:10.1002/ddr.21452

Kaya, S. B., Deger, S., Hacievliyagil, S. S., and Aytemur, Z. A. (2017). Acute amiodarone toxicity causing respiratory failure. *Rev. Assoc. Med. Bras.* 63 (3), 210–212. doi:10.1590/1806-9282.63.03.210

Mantik, P., Xie, M., Wong, H., La, H., Steigerwalt, R. W., Devanaboyina, U., et al. (2019). Cyclodextrin reduces intravenous toxicity of a model compound. *J. Pharm. Sci.* 108 (6), 1934–1943. doi:10.1016/j.xphs.2019.01.004

Muankaew, C., and Loftsson, T. (2018). Cyclodextrin-based formulations: a non-invasive platform for targeted drug delivery. *Basic Clin. Pharmacol. Toxicol.* 122 (1), 46–55. doi:10.1111/bcpt.12917

National Research Council US Committee for the Update of the Guide for the Care and Use of Laboratory Animals (2011). Guide for the care and use of laboratory animals. 8th Edn. Washington, DC: National Academies Press (US). . Available at: http://www.ncbi.nlm.nih.gov/books/NBK54050/ (Accessed February 3, 2021).

National Toxicology Program (1992). NTP toxicology and carcinogenesis studies of polysorbate 80 (CAS No. 9005-65-6) in F344/N rats and B6C3F1 mice (feed studies). *Natl. Toxicol. Program Tech. Rep. Ser.* 415, 1–225.

OECD (2008). Test No. 425: acute oral toxicity: up-and-down procedure. Available at: https://www.oecd-ilibrary.org/content/publication/9789264071049-en. (Accessed February, 2021)

Patel, M., and Hirlekar, R. (2019). Multicomponent cyclodextrin system for improvement of solubility and dissolution rate of poorly water soluble drug. *Asian J. Pharm. Sci.* 14 (1), 104–115. doi:10.1016/j.ajps.2018.02.007

Paudel, R., Dogra, P., Suman, S., Acharya, S., and Matta, J. (2016). Acute liver and renal failure: a rare adverse effect exclusive to intravenous form of amiodarone. *Case Rep. Crit. Care* 2016, 5232804. doi:10.1155/2016/5232804

Păduraru, O. M., Bosînceanu, A., Ţântaru, G., and Vasile, C. (2013). Effect of hydroxypropyl-β-cyclodextrin on the solubility of an antiarrhythmic agent. *Ind. Eng. Chem. Res.* 52 (5), 2174–2181. doi:10.1021/ie303440w

Riekes, M. K., Tagliari, M. P., Granada, A., Kuminek, G., Silva, M. A. S., and Stulzer, H. K. (2010). Enhanced solubility and dissolution rate of amiodarone by complexation with β-cyclodextrin through different methods. *Mater. Sci. Eng. C* 30 (7), 1008–1013. doi:10.1016/j.msec.2010.05.001

Rubim, A. M., Rubenick, J. B., Maurer, M., Laporta, L. V., Rolim, C. M. B., Rubim, A. M., et al. (2017). Inclusion complex of amiodarone hydrochloride with cyclodextrins: preparation, characterization and dissolution rate evaluation. *Braz. J. Pharm. Sci.* 53 (2). doi:10.1590/s2175-97902017000216083

Szejtli, J. (2005). Cyclodextrin complexed generic drugs are generally not bio-equivalent with the reference products: therefore the increase in number of marketed drug/cyclodextrin formulations is so slow. *J. Incl. Phenom. Macrocycl. Chem.* 52 (1), 1–11. doi:10.1007/s10847-004-7161-z

Tamargo, J., Le Heuzey, J.-Y., and Mabo, P. (2015). Narrow therapeutic index drugs: a clinical pharmacological consideration to flecainide. *Eur. J. Clin. Pharmacol.* 71 (5), 549–567. doi:10.1007/s00228-015-1832-0

Tiwari, G., Tiwari, R., and Rai, A. (2010). Cyclodextrins in delivery systems: Applications. *J. Pharm. Bioall. Sci.* 2 (2), 72–79. doi:10.4103/0975-7406.67003

Conflict of Interest: The authors declare that the research was conducted in the absence of any commercial or financial relationships that could be construed as a potential conflict of interest.

frontiers in Pharmacology

CLINICAL TRIAL
published: 10 March 2021
doi: 10.3389/fphar.2021.626307

The Bioequivalence of Emulsified Isoflurane With a New Formulation of Emulsion: A Single-Center, Single-Dose, Double-Blinded, Randomized, Two-Period Crossover Study

*Hui Yang[1†], Qinqin Yin[1†], Luying Huang[1,2], Min Zhang[3], Xinxin Zhang[3], Qirong Sun[1], Xuewei Liu[1], Qi Wang[1], Xi Yang[1], Lingcan Tan[1], Mao Ye[1] and Jin Liu[1]**

[1]Department of Anesthesiology, West China Hospital, Sichuan University, Chengdu, China, [2]Department of Clinical Research Management, West China Hospital, Sichuan University, Chengdu, China, [3]Clinical Research Center, Yichang Humanwell Pharmaceutical CO., LTD, Yichang, China

OPEN ACCESS

Edited by:
Victor A Voicu,
Carol Davila University of Medicine and Pharmacy, Romania

Reviewed by:
Stanislav Yanev,
Bulgarian Academy of Sciences, Bulgaria
Constantin Mircioiu,
Carol Davila University of Medicine and Pharmacy, Romania

***Correspondence:**
Jin Liu
scujinliu@gmail.com

†These authors have contributed equally to this work

Specialty section:
This article was submitted to Drug Metabolism and Transport, a section of the journal Frontiers in Pharmacology

Received: 05 November 2020
Accepted: 26 January 2021
Published: 10 March 2021

Citation:
Yang H, Yin Q, Huang L, Zhang M, Zhang X, Sun Q, Liu X, Wang Q, Yang X, Tan L, Ye M and Liu J (2021) The Bioequivalence of Emulsified Isoflurane With a New Formulation of Emulsion: A Single-Center, Single-Dose, Double-Blinded, Randomized, Two-Period Crossover Study. Front. Pharmacol. 12:626307. doi: 10.3389/fphar.2021.626307

Background: Emulsified isoflurane is a novel intravenous general anesthetic obtained by encapsulating isoflurane molecules into emulsion. The formulation of emulsion has been improved according to the latest regulations of the China Food and Drug Administration. This study was designed to compare the bioequivalence of the new and previous formulation emulsion of isoflurane.

Methods: In a single-center, single-dose, double-blinded, randomized, two-period crossover study, healthy volunteers received intravenous injection of 30 mg/kg of isoflurane with either previous formulation of emulsion isoflurane (PFEI) or new formulation of emulsion isoflurane (NFEI). Arterial and venous blood samples were obtained for geometric mean test/reference ratios of C_{max}, $AUC_{0\text{-}t}$, and $AUC_{0\text{-}\infty}$, as well as their 90% confidence interval (CI90) as the primary outcome. The secondary outcomes were safety measurements such as vital signs, 12-lead electrocardiography, adverse effects, and laboratory tests; and anesthesia efficacy was assessed by Modified Observer's Assessment of Alertness/Sedation (MOAA/S) score, bispectral index (BIS), and loss/recovery of eyelash reflex.

Results: 24 subjects were eligible, of which 21 completed the whole experiment (NFEI n = 21, PFEI n = 23). Arterial geometric mean test/reference ratios of C_{max}, $AUC_{0\text{-}t}$, and $AUC_{0\text{-}\infty}$ were 104.50% (CI90 92.81%–117.65%), 108.23% (94.51%–123.96%), and 106.53% (93.94%~120.80%), respectively. The most commonly seen adverse effects for NFEI and PFEI were injection pain (38.1% vs. 34.8%), hypotension (19.0% vs. 13.0%), apnea (14.3% vs. 17.4%), and upper airway obstruction (14.3% vs. 13.0%). No severe adverse effect was observed. The effectiveness of general anesthesia was similar between the two formulations.

Conclusion: The CI90 of C_{max}, AUC_{0-t}, $AUC_{0-\infty}$, NFEI, and PFEI were within the range of 80%–125%, suggesting bioequivalence between NFEI and PFEI. The safety and anesthesia effectiveness were also similar.

Keywords: emulsified isoflurane, C_{max}, AUC_{0-t}, $AUC_{0-\infty}$, bioequivalence

INTRODUCTION

Isoflurane is one of the most widely used volatile anesthetics. The application of isoflurane, however, requires special devices and causes environmental issues. Emulsified isoflurane (EI) is isoflurane emulsified in Intralipid®.

EI has several advantages over inhaled isoflurane. First, EI is an intravenous anesthetic that can be easily injected into veins (Fan et al., 2014; Diao et al., 2016) instead of requiring unique device, saving medical resources and reducing air pollution in the operating room. Second, EI does not need the lung uptake to take effects; it also avoids the dilution of the drug resulting from the respiratory circuit and functional alveolar residue capacity; therefore, induction is faster (Yang et al., 2008). Third, EI is eliminated mostly *via* expiration; anesthesia level can be easily controlled by injection speed and ventilation adjustment in the stage of anesthesia maintenance and emergence (Huang et al., 2010; Zhou, et al., 2011b; Huang et al., 2016; Wang et al., 2016; Yang et al., 2020; Zhao et al., 2020). Fourth, EI is more potent than isoflurane. EI has greater C_{max} and AUC (Yang et al., 2013). At some doses, the exposure of EI was greater than that of isoflurane (Huang et al., 2016; Wang et al., 2016; Yang et al., 2020; Zhao et al., 2020). In general, EI combines the advantages of both volatile and intravenous anesthetics (Huang et al., 2014), making it valuable in the clinical application (Zhou and Liu 2012). Several clinical studies have proved that EI is capable of rapid-onset, short-lasting general anesthesia in humans (Huang et al., 2014) and animals (Zhou et al., 2006; Yang et al., 2013; Fan et al., 2014; Diao et al., 2016).

To convert isoflurane into EI, the key step is to encapsulate isoflurane molecules into the emulsion. In the early stage of EI trials, isoflurane was simply stirred in 30% emulsion with shearing and homogenization process, which resulted in 350 nm particles. These particles are composed of isoflurane–soybean oil core and lecithin shell; during vibration and heat sterilization process, the particles are polymerized and eventually break down. Some broken particles lose the lecithin shell, merge into granules >5 μm, block pulmonary capillaries (diameter 7–9 μm), and result in cough immediately after drug application in some subjects (Zhou et al.,2011a; Xu et al., 2013; Zhang et al., 2014).

According to the latest regulations from the China Food and Drug Administration, and in order to address the large granules issue described above, a new formulation of the emulsion was developed. The concentration of lecithin was increased, and the soybean oil reduced. This change in emulsion formulation will reduce the size of particles and increase the stability of EI. As a result, large granules <0.05% were obtained. The new formulation of emulsified isoflurane (NFEI) should have the same bioequivalence as the previous formulation of emulsified isoflurane (PFEI) since the isoflurane–soybean oil core remains. Moreover, deduced from chemo-physical properties, NPEI may have the same efficacy in general anesthesia, or smoother induction, for example, less incidence of cough.

Healthy volunteers were enrolled to testify the bioequivalence, anesthesia efficacy, and safety of NFEI and PFEI (Xu et al., 2013). It is a hypothesis that NFEI has the same bioequivalence, anesthesia efficacy, and safety as those of PFEI.

METHODS

Study Design and Approvals

This is a single-center, single-dose, double-blinded, randomized, two-period crossover study (ChiCTR1900025947), approved by the Chinese Food and Drug Administration of China (CYHB1803134) and West China Ethics Committee. Each healthy volunteer provided written informed content.

Subjects Eligibility

Individuals were eligible if they are 18–45 years old, with body mass ≥45 kg for female and ≥ 50 kg for male and BMI of 19–26 kg/m^2. Exclusion criteria included abnormal medical history/physical examination/vital signs/electrocardiogram (ECG)/laboratory test results, which were considered as clinically important; abuse of substances (except alcohol) that would affect the process of drug absorption, distribution, metabolism, or excretion; being positive for HIV, type B/C hepatic virus, or syphilis; allergy history or allergic to milk, pollen, or any drug gradient used in this study; alcohol addiction, or current alcohol consumption exceeding 21 (for male) or 14 (for female) units per week; for females, positive pregnant test or being in lactation period; tobacco consumption >5 cigarettes per day in the past 3 months before study entry; abnormal cognitive function test results; difficult airways (e.g., thyroid-mental distance ≤ 4 cm or Mallampati scores ≥3); previously participated in other clinical trials within three months; had donated blood within three months; and use of nicotine 48 h before study entry till the end of study.

Study Protocol

Subjects were enrolled and randomized to receive intravenous 30 mg/kg of either NFEI or PFEI (1:1) *via* infusion pumps within 2 min (the infusion speed varied between subjects due to weight difference). After a washout of three days, these subjects had an intravenous injection of the other drug. Subjects received two-week fat-limited and no-alcohol/caffeine diet. All the volunteers fasted for 10 h before the study started. Before the test drug injection, all subjects inhaled oxygen (10 L/min) *via* face masks, with standard anesthesia monitored (T8, Mindray Medical

International Ltd., Shenzhen, China) including 12-lead electrocardiogram (ECG), noninvasive blood pressure, pulse oximetry, respiratory rate, body surface temperature, bispectral index (BIS), and end-tidal carbon dioxide until subjects fully recovered. Vital signs were recorded continuously by the automatic monitor and manually at predefined time points: before drug application (as baseline), every minute for the first 15 min after dose, and every 5 min from 15 to 60 min after dose, respectively. One arm had venous and arterial catheterization before the experiment, to facilitate intravenous drug injection and arterial blood collection. Continuous noninvasive blood pressure monitoring and venous blood sample collection were performed in the other arm. Arterial blood and venous blood (4 ml, heparin treated) were simultaneously collected 10 min before drug injection and 1, 2, 2.5, 3, 4, 5, 7, 10, 20, 40, 60, and 70 min after intravenous drug administration. Baselines were recorded for vital signs (before and after oxygenation), consciousness state (Modified Observer's Assessment of Alertness/Sedation, MOAA/S), and BIS readings before drug injection. This study was conducted in the Good Clinical Practice Center of West China Hospital of Sichuan University.

Geometric Mean Reference Ratios of Pharmacokinetic Parameters

The primary outcomes for this study were geometric mean test/reference ratios of C_{max}, $AUC_{0\text{-}t}$, and $AUC_{0\text{-}\infty}$, as well as their 90% confidence interval (CI90). The geometric mean test/reference ratios were used to determine the bioequivalence of PFEI and NFEI (Bienvenu et al., 2017; Morton et al., 2018; Davanco et al., 2019). Other pharmacokinetic parameters were also investigated, including peak concentration (C_{max}); area under the plasma concentration–time curve ($AUC_{0\text{-}t}$); area under the concentration–time curve from time zero to infinity ($AUC_{0\text{-}\infty}$); time to plasma concentration peak (t_{max}); elimination rate constant (λ_z); half-life in the terminal elimination phase ($t_{1/2z}$); the percentage of the area under the curve that has been derived after extrapolation ($AUC_{\%Extrap}$), calculated as $[(AUC_{0\text{-}\infty}\text{-}AUC_{0\text{-}t})/AUC_{0\text{-}\infty}]\times100\%$); mean residence time (MRT); plasma apparent clearance (CL_z); and the apparent volume of distribution at the terminal elimination phase (V_z).

Testing of Plasma Concentration of Isoflurane

Blood samples were rapidly distributed into three headspace autosampler vials and stored in 2–8°C. The plasma concentration of isoflurane was tested by the two-stage headspace equilibrium gas chromatography method. Briefly, the blood sample at each test point was split into three parts: one for testing plasma concentration of isoflurane, one for incurred sample reanalysis (ISR), and one saved as backup. Plasma concentration of isoflurane was tested with headspace gas chromatography as previously reported (Yang et al., 2013). Isoflurane standard was used as an external standard. The determination range of isoflurane was 2.31 μg/ml to 500.00 μg/ml. The biological matrix was the whole blood sample. Agilent gas chromatograph 6890 N (instrument number: 20062567) with Agilent g1888 automatic sampler was used to detect the concentration of isoflurane. The chromatographic column was DB-WAX (30 m*530 μm*1 μm). The detector is a hydrogen flame ionization detector (FID). The detector temperature was 300°C, and the injection port temperature was 160°C. The carrier gas was nitrogen at 1.5 ml/min, and the split ratio was 1:1. The heating program is as follows: the initial temperature is 60°C and maintained for 2 min; then it is raised to 200°C at the rate of 10°C/min, maintained for 2 min, and then operated for 2 min. The injection volume was 1 ml. The method has been validated to verify the residue, system adaptability, selectivity, precision and accuracy, standard curve, and lower limit of quantification and stability of isoflurane under different conditions. The in-process analysis was performed on the subject samples to confirm the precision and accuracy of the bioanalysis method.

Pharmacodynamical Observations

The Modified Observer's Assessment of Alertness/Sedation (MOAA/S, where 0 = unresponsive and 5 = fully awake) was recorded every 1 min until the subjects were fully awake. The fully awake state was defined as consecutive MOAA/S = 5 for at least three times. The eyelash reflex was tested every 30 s from the beginning of drug injection until the eyelash reflex fully recovered. Central nervous system status (state of consciousness, cognitive function, and mental state) was evaluated after being fully awake. The sedative/anesthesia effects after intravenous EI were evaluated using MOAA/S scores, loss of eyelash reflex, and BIS (Huang et al., 2014). The following items were used to quantitatively assess the efficacy of EI: the minimal MOAA/S score ($MOAA/S_{min}$); area under the delta BIS-time curves ($BISAUC_{0\text{-}t}$), in which delta BIS was defined as the change in BIS from baselines to post-dose values; the minimal BIS value (BIS_{min}); time to BIS_{min} ($t\text{-}BIS_{min}$); time to loss of eyelash reflex; and time to recovery of eyelash reflex.

Safety Measurements

Subjects were measured by continuous vital signs monitoring (ECG, blood pressure, respiratory rate, heart rate, pulse oxygen saturation, body temperature, and end-tidal carbon dioxide), physical examination, laboratory tests, central nerve system function evaluation (mental status, cognitive function, and consciousness state), injection pain, and adverse effects (focus on coughs based on previous clinical trials). Discomfort reported by subjects or observed by researchers was documented, reviewed, and classified based on the Medical Dictionary for Regulatory Activities (MedDRA, v5.0). Adverse effects were graded as mild, moderate, severe, or life-threatening accordingly.

The trial ceased if the following criteria were met: over half of subjects developed adverse effects that were graded >2, over 1/4 subjects developed grade 3–4 adverse effects, clues indicating that the test drug was intolerable, inappropriate protocols that would fail to evaluate the test drug, or sponsor requiring cessation of the trial.

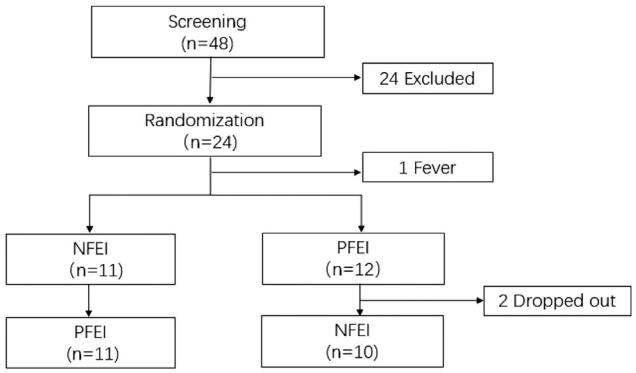

FIGURE 1 | The consort flow diagram for the patient progress through this trial. 48 subjects were enrolled; 24 met the exclusion criteria. The remaining 24 subjects received randomization; one subject had fever before receiving any drug. 11 subjects received new formulation of emulsified isoflurane (NFEI); the other 12 subjects received previous formulation of emulsified isoflurane (PFEI). During the 72-h washout period, the NFEI group had two subjects dropped out, and the remaining 21 subjects completed the whole trial.

TABLE 1 | Demographic data.

Demographic information	Value
Age (years)	26.3 ± 4.5
Body weight (kg)	60.3 ± 7.5
BMI (kg/m^2)	22.4 ± 1.6
Gender, n (%)	
Male	13 (56.5)
Female	10 (43.5)
Modified Mallampati, n (%)	
Grade 1	23 (100.0)

Randomization and Statistical Analysis

Statistical analysis was performed with software SAS (version 9.4). Pharmacological parameter analysis was conducted in WinNonlin (version 8.1). Sample size was calculated based on coefficient of variation = 20% (previous trials results), alpha = 0.05, power = 0.8, equivalent margin = 0.8–1.25, and the geometric mean test/reference ratio of NFEI/PFEI within 0.9–1.05. The minimal sample size was 19. C_{max}, AUC_{0-t}, and $AUC_{0-\infty}$ were used to calculate the geometric mean test/reference ratios and CI90 in linear mixed models. Bioequivalence between the new and old formulation of isoflurane was considered when the CI90 of C_{max}, AUC_{0-t}, and $AUC_{0-\infty}$ geometric mean ratio locates within 80%–125%. The other pharmacokinetic parameters of isoflurane were estimated by a non-compartmental model based on the plasma concentration data.

Comparison of pharmacodynamics parameters (t-MOAA/S_{min}, $BISAUC_{0-t}$, t-BIS_{min}, time to loss of eyelash reflex, and time to eyelash reflex recovery) was conducted using a nonparametric test (Wilcoxon, two-tailed). The incidences of adverse effects were analyzed with the *chi-square* test. The difference was considered significant when $p < 0.05$. Data were presented as mean ± standard variation (SD) where possible.

TABLE 2 | Pharmacokinetic parameters calculated from arterial blood samples after the intravenous new formulation of emulsified isoflurane (NFEI) or previous formulation of emulsified isoflurane (PFEI) in healthy volunteers.

Parameters	NFEI	PFEI
C_{max} (μg/ml)	109.01 ± 29.52	103.39 ± 29.51
AUC_{0-t} (min.μg/ml)	391.77 ± 111.35	362.02 ± 123.79
$AUC_{0-\infty}$ (min.μg/ml)	419.14 ± 111.73	391.35 ± 123.96
T_{max} (min)	2.30 ± 0.25	2.37 ± 0.37
$t_{1/2z}$ (min)	5.97 ± 2.02	6.00 ± 2.70
V_z (ml/kg)	665.78 ± 288.03	705.11 ± 322.19
CL_z (ml/min/kg)	77.33 ± 23.23	86.20 ± 34.19
λ_z (min^{-1})	0.14 ± 0.08	0.14 ± 0.06
MRT_{0-t} (min)	3.64 ± 1.02	3.31 ± 1.13
$MRT_{0-\infty}$ (min)	5.31 ± 1.60	5.11 ± 1.89
$AUC_{\%Extrap}$ (%)	7.00 ± 2.42	8.33 ± 4.16

RESULTS

Subjects Demography

The study was performed from October 10th, 2019 to December 6th, 2019. During screening, 24 subjects were excluded. During the crossover, two subjects quitted, and one subject had fever before drug injection. In total, 24 healthy volunteers were enrolled, 23 of them received drug injection, and 21 subjects completed the whole study (**Figure 1**). There is no statistical difference of demographic characteristics among the subjects (**Table 1**).

Pharmacokinetic Properties

There was no clinically important or statistically significant difference of pharmacokinetic parameters between NFEI and PFEI, calculated from arterial or venous blood samples. However, arterial C_{max}, AUC_{0-t}, and $AUC_{0-\infty}$ are higher than the venous ones (**Table 2**; **Figure 2**). The intraindividual coefficients of variation for arterial C_{max}, AUC_{0-t}, and $AUC_{0-\infty}$ were 21.7%, 24.8%, and 23.0%, respectively, lower than those for venous values (64.7%, 41.7%, and 31.2%, respectively).

The CI90 of arterial C_{max}, AUC_{0-t}, and $AUC_{0-\infty}$ were 92.81%–117.65%, 94.51%–123.96%, and 93.94%–120.80%, respectively, all within the range of 80%–125% (**Table 4**). The venous ones were 82.43%–171.46%, 90.13%–148.06%, and 94.14%–138.22%, respectively, exceeding the 80%–125% range (**Table 5**).

Pharmacodynamical Properties

There was no statistically significant difference among the t-BIS_{min}, t-MOAA/S_{min}, and the time of loss/recovery of eyelash reflex between NFEI and PFEI (**Table 6**; **Figure 3**). The time-course of MOAA/S and BIS value between NFEI and PFEI were also similar (**Figure 3**).

Safety Evaluation

There were no serious adverse events, nor suspected unexpected serious adverse reaction observed. Mild vital sign fluctuation was documented in 18 subjects, including tachycardia, hypotension, hypertension, apnea, fever, and peaked T wave (**Table 7**). Other

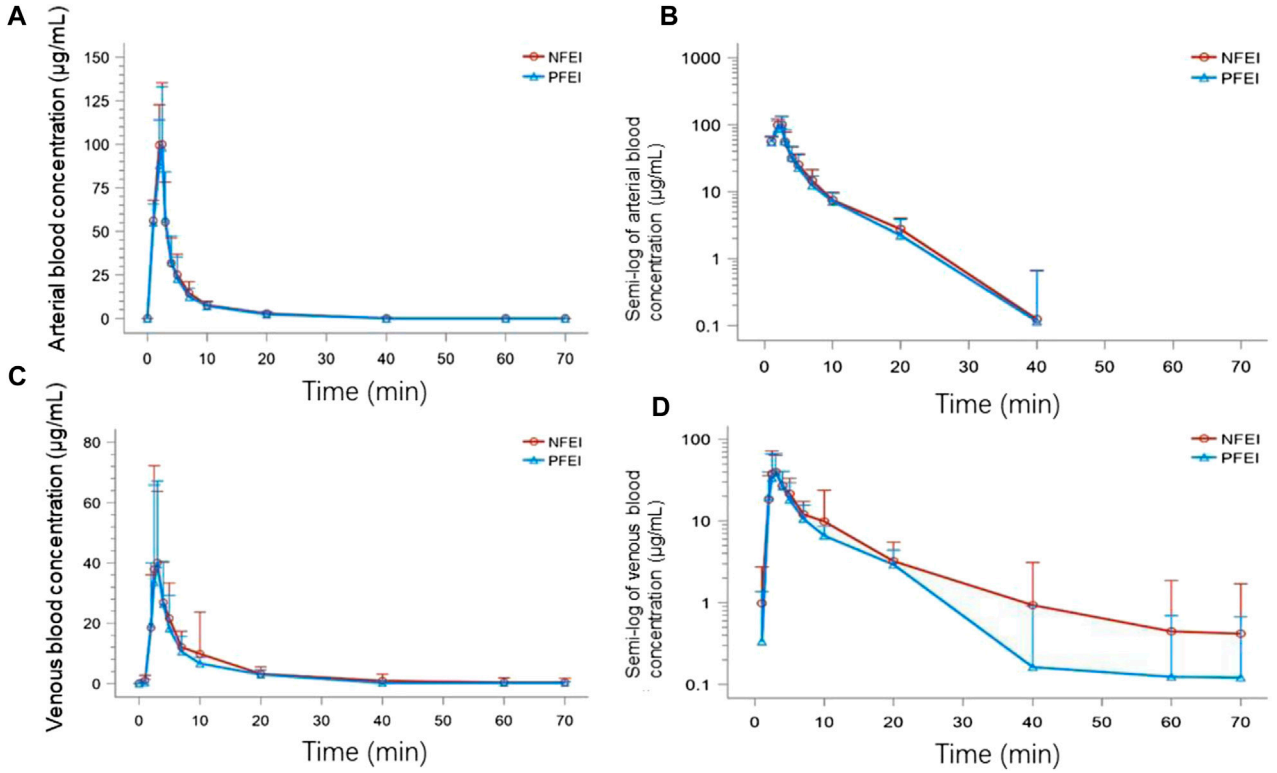

FIGURE 2 | The time–concentration curves of subjects receiving venous injection of 30 mg/kg of new formulation of emulsified isoflurane (NFEI) or previous formulation of emulsified isoflurane (PFEI). The actual arterial **(A)** and venous **(C)** blood isoflurane concentration over time, and the semi-log of arterial **(B)** and venous **(D)** blood drug concentration over time.

TABLE 3 | Pharmacokinetic parameters calculated from venous blood samples after the intravenous new formulation of emulsified isoflurane (NFEI) or previous formulation of emulsified isoflurane (PFEI) in healthy volunteers.

Parameter	NFEI	PFEI
C_{max} (μg/ml)	52.83 ± 26.53	48.47 ± 30.83
AUC_{0-t} (min*μg/ml)	226.01 ± 106.63	201.47 ± 105.53
$AUC_{0-\infty}$(min*μg/ml)	279.22 ± 117.11	246.67 ± 110.02
T_{max} (min)	3.19 ± 0.72	3.17 ± 0.76
$t_{1/2z}$ (min)	11.41 ± 8.06	9.61 ± 5.63
V_z (ml/kg)	1756.50 ± 884.66	1934.93 ± 1152.92
CL_z (ml/min/kg)	125.74 ± 50.14	146.67 ± 70.03
λ_z (min^{-1})	0.09 ± 0.04	0.09 ± 0.06
MRT_{0-t} (min)	7.06 ± 4.15	6.44 ± 3.44
$MRT_{0-\infty}$(min)	13.79 ± 9.17	12.48 ± 8.08
$AUC_{\%Extrap}$ (%)	20.18 ± 12.15	20.68 ± 12.50

TABLE 4 | Geometric mean test/reference ratios of arterial C_{max}, AUC_{0-t}, and $AUC_{0-\infty}$ and their 90% confidence interval (CI90) from arterial blood samples.

Parameters	Geometric mean		Reference ratio (%)	CI90 (%)
	NFEI	PFEI		
C_{max}	103.73	99.27	104.50	92.81~117.65
AUC_{0-t} (min·μg/ml)	369.18	341.09	108.23	94.51~123.96
$AUC_{0-\infty}$ (min·μg/ml)	396.70	372.39	106.53	93.94~120.80

TABLE 5 | Geometric mean test/reference ratios of venous C_{max}, AUC_{0-t}, and $AUC_{0-\infty}$ and their 90% confidence interval (CI90) from venous blood samples.

Parameters	Geometric mean		Reference ratio (%)	CI_{90} (%)
	NFEI	PFEI		
C_{max}	45.57	38.34	118.88	82.43~171.46
AUC_{0-t} (min·μg/ml)	207.27	179.43	115.52	90.13~148.06
$AUC_{0-\infty}$ (min·μg/ml)	262.32	229.96	114.07	94.14~138.22

TABLE 6 | The t-BIS_{min}, t-$MOAA/S_{min}$, and eyelash reflection loss/recovery time for PEFI and NEFI.

Parameter	NFEI (N = 21)	PFEI (N = 23)	Statistics	*p* value
t-BIS_{min}	6.38 ± 11.19	5.78 ± 6.71	−10.500	0.254
t-$MOAA/S_{min}$	2.05 ± 0.42	2.07 ± 0.38	−0.500	1.000
Time of eyelash reflex loss	1.79 ± 0.38	1.79 ± 0.30	−2.500	1.000
Time of eyelash reflex recovery	5.87 ± 1.60	5.82 ± 1.33	−3.500	0.839

adverse events were observed: injection pain, swelling of injection site, creatinine elevation, APTT prolongation, PT prolongation, conjugated bilirubin elevation, leukocytes in urine, urine sediment, bacteriuria, triglycerides elevation, upper airway

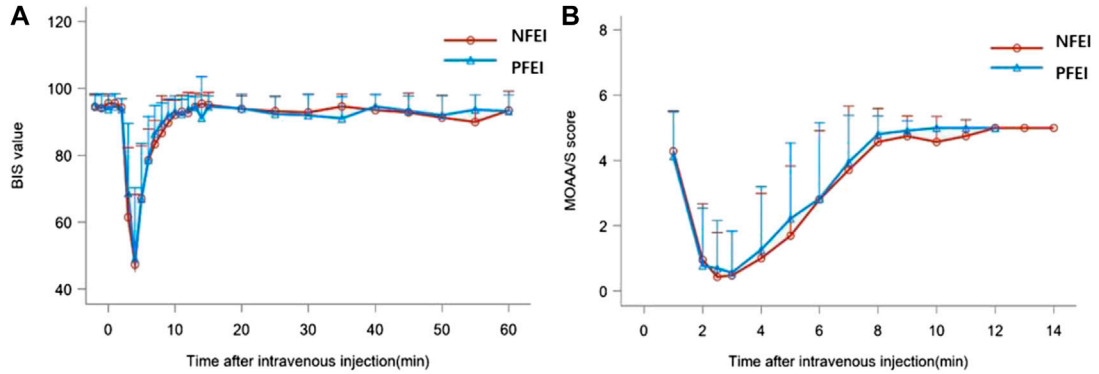

FIGURE 3 | BIS value **(A)** and MOAA/s score **(B)** after intravenous injection of 30 mg/kg of the new formulation of emulsified isoflurane (NFEI) or the previous formulation of emulsified isoflurane (PFEI).

TABLE 7 | Change in vital signs after intravenous 30 mg/kg NFEI or PFEI in healthy volunteers.

	NFEI		PFEI	
	n (%)	Case	n (%)	Case
Tachycardia	0	0	1 (4.3)	1
Hypotension	4 (19.0)	4	3 (13.0)	3
Hypertension	1 (4.8)	1	0	0
Apnea	3 (14.3)	3	4 (17.4)	4
Fever	0	0	1 (4.3)	1
Peaked T wave	0	0	1 (4.3)	1

TABLE 8 | Other adverse events after intravenous injection of 30 mg/kg NFEI or PFEI in healthy volunteers.

Adverse events	NFEI (N = 21)		PFEI (N = 23)	
	n (%)	Case	n (%)	Case
Injection pain	8 (38.1)	8	8 (34.8)	8
Swelling of injection site	1 (4.8)	1	1 (4.3)	1
Creatinine elevation	2 (9.5)	2	1 (4.3)	1
APTT prolongation	2 (9.5)	2	0 (0)	0
PT prolongation	2 (9.5)	2	0 (0)	0
Conjugated bilirubin elevation	1 (4.8)	1	0 (0)	0
Leukocytes in urine	0 (0)	0	1 (4.3)	1
Urine sediment	0 (0)	0	1 (4.3)	1
Bacteriuria	0 (0)	0	1 (4.3)	1
Triglycerides elevation	1 (4.8)	1	0 (0)	0
Upper airway obstruction	3 (14.3)	3	3 (13.0)	3
Dizziness	1 (4.8)	1	0 (0)	0
Upper airway infection	1 (4.8)	1	1 (4.3)	1
Coughing	0 (0)	0	1 (4.3)	1
Vomiting	0 (0)	0	1 (4.3)	1
Total	14 (66.7)	33	15 (65.2)	30

obstruction, dizziness, upper airway infection, cough, and vomiting (**Table 8**). The incidence for the above adverse events was similar between the two formulations ($p < 0.05$). Some of the adverse events require emergent treatment, such as upper airway obstruction, hypotension, and apnea, but all subjects relieved shortly spontaneously or after treatment. Total incidence of treatment emergent adverse events (TEAEs) for NFEI was 66.7% (14 out of 21 cases), compared with 65.2% (15 out of 23 cases) for PFEI (**Table 9**), with no statistical differences. The severity of all TEAEs was below grade 2. All TEAEs have spontaneously recovered or relieved.

TABLE 9 | Treatment-emergent adverse events incidence analysis (SS).

	NFEI, n (%)	PFEI, n (%)	Total, n (%)	p value
Adverse events	14 (66.7)	15 (65.2)	18 (78.3)	0.919
Adverse reaction	14 (66.7)	15 (65.2)	18 (78.3)	0.919

DISCUSSION

The CI90 of arterial C_{max}, AUC_{0-t}, and $AUC_{0-\infty}$ were within the range of 80%–125%. The pharmacodynamical parameters, such as time of loss/recovery of eyelash reflex, time-course of MOAA/S, and BIS value, were similar between NFEI and PFEI. The type and the incidence of adverse events were also similar, with no statistically significant difference.

The pharmacokinetic parameters for NFEI and PFEI were similar. The primary outcomes, CI90 of geometric means for three important parameters, C_{max}, AUC_{0-t}, and $AUC_{0-\infty}$, were between 80% and 125%. This result confirmed our hypothesis that the change of formulation for emulsion does not affect the basic chemo-physical, pharmacokinetic properties of isoflurane, especially drug exposure characteristics.

However, the arterial C_{max}, AUC_{0-t}, and $AUC_{0-\infty}$ were different from the venous values. We chose arterial C_{max}, AUC_{0-t}, and $AUC_{0-\infty}$ for bioequivalence analysis because the venous values from venous blood samples have greater intraindividual coefficient of variation. The reasons for the variation in venous parameters might be as follows: 1) venous blood was drawn from the same arms that had noninvasive blood pressure continuously monitored. The inflation and deflation of the cuff might affect the venous blood returning, therefore leading to the variation of blood concentration. 2) Drawing blood

samples from arteries was easier than that from veins; thus venous sample was obtained a little bit slower than arterial ones. Considering that isoflurane was rapidly eliminated in the pulmonary circulation, the slight lag time between might lead to variation in plasma concentration.

The pharmacodynamical properties for NFEI and PFEI were generally similar. Both drugs produced the loss of eyelash reflex within 2 min. The MOAA/S reached the minimal value shortly after the loss of eyelash reflex, approximately 2 min after drug injection. BIS decreased to the minimal value about 6 min after drug application. The development of unconsciousness, unresponsiveness, and depression of electroencephalogram conforms with clinical practice and previous study (Huang et al., 2014). The recovery of eyelash reflex, and the return of MOAA/S and BIS value were rapid and complete; within 10 min, all subjects were fully awake. In addition, the degree of decrease in MOAA/S and BIS values was synchronic between NFEI and PFEI. NFEI mostly inherited the effectiveness of PFEI, in terms of onset, duration, and magnitude.

The safety profile of NFEI did not differ from that of PFEI. No serious adverse effect was observed, indicating that NFEI is equally safe compared with PFEI at this dose. The most common adverse events for both NFEI and PFEI were injection pain, hypotension, apnea, and upper airway obstruction. Injection pain is common in general anesthetics with emulsion as solvent, such as propofol and etomidate. Dose-related hypotension, apnea, and upper airway obstruction are also common for anesthetics. Fortunately, injection pain is transient and spontaneously recovered. Hypotension could be easily treated with fluid infusion or vasoconstrictors; apnea and upper airway obstruction can be easily relieved by the "chin-lift" maneuver in combination with mask ventilation in general anesthesia induction period. There was no cough for NFEI, while one subject experienced cough using PFEI. Although this difference was of no statistical significance confining to the relatively small sample size, NFEI containing smaller particles might have advantage in reducing the risk of cough during general anesthesia induction. Overall, the incidence of adverse events from NFEI was similar to that of those from PFEI.

The incidences of injection pain and cough were less than those in the previous study (Hu et al., 2013; Liu et al., 2013; Wang et al., 2013; Xu et al., 2013; Yang et al., 2013; Huang et al., 2014). One possible explanation was that in a previous study, EI was given in bolus injection within seconds, while in this study, EI was given *via* an infusion pump within 2 min. Another explanation could be that NFEI has a smaller particle size, thus less likely to block pulmonary capillaries.

As the results demonstrated, NFEI has similar pharmacokinetics, pharmacodynamics, and safety properties to PFEI in healthy volunteers at a dose of 30 mg/kg.

CONCLUSION

The CI90 of C_{max}, AUC_{0-t}, and $AUC_{0-\infty}$ were 92.81%~117.65%, 94.51%~123.96%, and 93.94%~120.80%, respectively, within the range of 80%–125%, suggesting bioequivalence between the new and previous formulation of emulsified isoflurane.

DATA AVAILABILITY STATEMENT

The original contributions presented in the study are included in the article/Supplementary Material; further inquiries can be directed to the corresponding author.

ETHICS STATEMENT

The studies involving human participants were reviewed and approved by the Chinese Food and Drug Administration of China and West China Ethics Committee. The patients/participants provided their written informed consent to participate in this study.

AUTHOR CONTRIBUTIONS

Study concept and design: JL; acquisition of participants: HY, QY, LH, QS, XL, QW, LT, XY, MY, and JL; data analysis: HY, QY, and JL; interpretation of data: HY, QY, and JL; and preparation of the manuscript: HY and QY. Clinical monitor assistance: MZ and XZ.

FUNDING

This work was financially supported by Yichang Humanwell Pharmaceutical Co., Ltd.

ACKNOWLEDGMENTS

The authors thank all patients, staff, and investigators involved in this study. Yichang Humanwell Pharmaceutical Co., Ltd., sponsored the clinical trial.

REFERENCES

Bienvenu, B., Aouba, A., Gottenberg, J. E., and Verstuyft, C. (2017). Single-center, single-dose, open-label, randomized, two-period crossover study on the bioavailability of methotrexate administered using a novel prefilled, needle-free delivery system. *Curr. Med. Res. Opin.* 33 (4), 605–611. doi:10.1080/03007995.2016.1263611

Davanço, M. G., Meulman, J., Guzmán, M. R. P., Palomino, D. M. H., Tuiran, C. M. G., Duarte, F. G., et al. (2019). A randomized, single-dose, two-sequence, two-period, crossover study to assess the bioequivalence between two formulations of clonazepam tablet in healthy subjects. *Drug Dev. Ind. Pharm.* 45 (12), 1982–1987. doi:10.1080/03639045.2019.1689994

Diao, H. X., Jiang, S., Gao, P. Y., Liu, H. Y., Li, J. N., and Fan, H. G. (2016). Comparison of the effects of propofol and emulsified isoflurane alone or

combined with dexmedetomidine on induction of anesthesia in dogs. *Vet. Anaesth. Analg.* 43 (2), 145–152. doi:10.1111/vaa.12287

Fan, H. G., Jiang, S., Lin, D. Q., Lu, D. Z., Li, L., Ji, W., et al. (2014). Comparison of anaesthetic and analgesic effects of emulsified isoflurane used alone or combined with lidocaine and fentanyl in dogs. *N. Z. Vet. J.* 62 (3), 123–129. doi:10.1080/00480169.2013.859976

Hu, Z. Y., Abbott, G. W., Fang, Y. D., Huang, Y. S., and Liu, J. (2013). Emulsified isoflurane postconditioning produces cardioprotection against myocardial ischemia-reperfusion injury in rats. *J. Physiol. Sci.* 63 (4), 251–261. doi:10.1007/s12576-013-0261-z

Huang, H., Li, R., Liu, J., Zhang, W., Liao, T., and Yi, X. (2014). A phase I, dose-escalation trial evaluating the safety and efficacy of emulsified isoflurane in healthy human volunteers. *Anesthesiology* 120 (3), 614–625. doi:10.1097/ALN.0000000000000044

Huang, H., Zhang, W., Liu, S., Yanfang, C., Li, T., and Liu, J. (2010). Cardioprotection afforded by St Thomas solution is enhanced by emulsified isoflurane in an isolated heart ischemia reperfusion injury model in rats. *J. Cardiothorac. Vasc. Anesth.* 24 (1), 99–103. doi:10.1053/j.jvca.2009.10.016

Huang, H., Zhou, C., Liu, J., Song, H., and Qiu, Y. (2016). Adding emulsified isoflurane to cardioplegia solution produces cardiac protection in a dog cardiopulmonary bypass model. *Sci. Rep.* 6, 23572. doi:10.1038/srep23572

Liu, X., Guo, Q. L., Zhang, Z., Long, L., and Yang, Y. (2013). Effect of emulsified isoflurane on apoptosis of anoxia-reoxygenation neonatal rat cardiomyocytes. *Asian Pac. J. Trop. Med.* 6 (12), 977–981. doi:10.1016/S1995-7645(13)60175-3

Morton, K., Knight, K., Kalman, D., and Hewlings, S. (2018). A prospective randomized, double-blind, two-period crossover pharmacokinetic trial comparing green coffee bean extract-A botanically sourced caffeine-with a synthetic USP control. *Clin. Pharmacol. Drug Dev.* 7 (8), 871–879. doi:10.1002/cpdd.451

Wang, Y., Li, H., Huang, H., Liu, S., Mao, X., Wang, S., et al. (2016). Cardioprotection from emulsified isoflurane postconditioning is lost in rats with streptozotocin-induced diabetes due to the impairment of Brg1/Nrf2/STAT3 signalling. *Clin. Sci.* 130 (10), 801–812. doi:10.1042/CS20150617

Wang, Z., Lv, H., Song, S., Shen, X., Yang, L., and Yu, W. (2013). Emulsified isoflurane preconditioning protects isolated rat Kupffer cells against hypoxia/reoxygenation-induced injury. *Int. J. Med. Sci.* 10 (3), 286–291. doi:10.7150/ijms.5343

Xu, W. M., Zhang, J. Y., and Liu, J. (2013). [Effects of emulsified isoflurane preconditioning on LPS-induced acute lung injury in rats]. *Sichuan Da Xue Xue Bao Yi Xue Ban* 44 (4), 554–557.

Yang, J., Gong, C. Y., Chai, Y. F., Luo, N., Luo, N. F., and Liu, J. (2008). [Model establishment for emulsified isoflurane delivered selectively to the goat spinal cord and preliminary research on the immobility mechanism of isoflurane]. *Sichuan Da Xue Xue Bao Yi Xue Ban* 39 (2), 259–262.

Yang, X. L., Zhang, W. S., Liu, J., Yang, Z. B., and Jiang, X. H. (2013). Pharmacokinetics of intravenous emulsified isoflurane in beagle dogs. *Br. J. Anaesth.* 110 (1), 128–136. doi:10.1093/bja/aes311

Yang, Z. Y., Zhou, L., Meng, Q., Shi, H., and Li, Y. H. (2020). An appropriate level of autophagy reduces emulsified isoflurane-induced apoptosis in fetal neural stem cells. *Neural Regen. Res.* 15 (12), 2278–2285. doi:10.4103/1673-5374.285004

Zhang, F., Zhu, Z. Q., Liu, D. X., Zhang, C., Gong, Q. H., and Zhu, Y. H. (2014). Emulsified isoflurane anesthesia decreases brain-derived neurotrophic factor expression and induces cognitive dysfunction in adult rats. *Exp. Ther. Med.* 8 (2), 471–477. doi:10.3892/etm.2014.1769

Zhao, X., Chang, G., Cheng, Y., and Zhou, Z. (2020). GABAA receptor/STEP61 signaling pathway may Be involved in emulsified isoflurane anesthesia in rats. *Int. J. Mol. Sci.* 21 (11). doi:10.3390/ijms21114078

Zhou, C., and Liu, J. (2012). A novel intravenous general anesthetic--emulsified isoflurane: from bench to bedside. *Front. Med.* 6 (4), 381–387. doi:10.1007/s11684-012-0229-z

Zhou, C., Gan, J., Liu, J., Luo, W. J., Zhang, W. S., and Chai, Y. F. (2011a). The interaction between emulsified isoflurane and lidocaine is synergism in intravenous regional anesthesia in rats. *Anesth. Analg.* 113 (2), 245–250. doi:10.1213/ANE.0b013e31821e9797

Zhou, C., Wu, W., Liu, J., Liao, D. Q., Kang, Y., and Chen, X. D. (2011b). Inhibition of voltage-gated sodium channels by emulsified isoflurane may contribute to its subarachnoid anesthetic effect in beagle dogs. *Reg. Anesth. Pain Med.* 36 (6), 553–559. doi:10.1097/AAP.0b013e3182324d18

Zhou, J. X., Luo, N. F., Liang, X. M., and Liu, J. (2006). The efficacy and safety of intravenous emulsified isoflurane in rats. *Anesth. Analg* 102 (1), 129–134. doi:10.1213/01.ane.0000189612.24147.07

Conflict of Interest: MZ and XZ are employees of Yichang Humanwell Pharmaceutical Co., Ltd.

The remaining authors declare that the research was conducted in the absence of any commercial or financial relationships that could be construed as a potential conflict of interest.

frontiers in Pharmacology

ORIGINAL RESEARCH
published: 23 April 2021
doi: 10.3389/fphar.2021.582309

Toxicology and Pharmacokinetics Study of Intradiscal Injection of Simvastatin in Rabbits

Xiaodong Huang[1,2,3†], Wei He[4†], Weiheng Wang[3†], Quanchun Fan[5], Xiaojian Ye[3], Zenghui Wu[1] and Chia-Ying Lin[2*]*

[1]Department of Orthopedics, The Third Affiliated Hospital of Guangzhou Medical University, Guangdong, China, [2]Department of Orthopaedic Surgery, College of Medicine, University of Cincinnati, Cincinnati, OH, United States, [3]Department of Orthopaedics, Shanghai Changzheng Hospital, Shanghai, China, [4]Department of Spine Surgery, Beijing Jishuitan Hospital, 4th Medical College of Peking University, Beijing, China, [5]Department of Orthopaedics, Fuzhou Second Hospital Affiliated to Xiamen University, Fujian, China

To test the pharmacokinetics and toxicology of whole organs and tissues after intradiscal injection of simvastatin in rabbits. To provide the information needed to support human clinical trials. Twelve male and twelve female rabbits were randomly divided into four groups: control group (0 mg/ml), low dose group (0.1 mg/ml), medium dose group (1 mg/ml) and high dose group (10 mg/ml). Simvastatin at different concentrations of 10 μl was injected into L3/4, L4/5 and L5/6 intervertebral discs in each group. Poly (ethylene glycol) -poly (lactic-co-glycolic acid) -poly (ethylene glycol) (PEG-PLGA-PEG) polymer as the drug carrier. The pharmacokinetics of blood samples were measured by LC-MS/MS. Cerebrospinal fluid was obtained and the drug concentration was measured. Blood routine, blood biochemistry and urine of all animals were analyzed and evaluated. The heart, kidney, liver and spleen of each animal were observed and weighed. The intervertebral disc tissues were stained with hematoxylin and hematoxylin (H&E), and then qualitatively analyzed by optical microscopy. 28 days after intradiscal injection of simvastatin, 28 days after simvastatin intradiscal injection, there was no significant difference between the weight, food residue, blood routine, blood biochemistry, urine routine results and the weight of each organ in the four groups ($p > 0.05$). The serum concentration of simvastatin is lower than the lowest measurable concentration. The histological score of the intervertebral disc in the high-dose group was significantly higher than that in the other three groups at 28 days ($p < 0.05$). Three doses of simvastatin were injected into male and female animals respectively, showing no toxic effects. Microscopic histological evaluation of the intervertebral disc showed that the high dose group (10 mg/ml) had damage to the intervertebral disc tissue.

Keywords: intervertebral disc, simvastatin, pharmacokinetics, intradiscal injection, toxicity

OPEN ACCESS

Edited by:
Momir Mikov,
University of Novi Sad, Serbia

Reviewed by:
Stanislav Yanev,
Bulgarian Academy of Sciences (BAS), Bulgaria
Constantin Mircioiu,
Carol Davila University of Medicine and Pharmacy, Romania

****Correspondence:***
Zenghui Wu
13602892899@163.com
Chia-Ying Lin
linc9@ucmail.uc.edu

†These authors have contributed equally to this work

Specialty section:
This article was submitted to Drug Metabolism and Transport, a section of the journal Frontiers in Pharmacology

Received: *11 July 2020*
Accepted: *18 February 2021*
Published: *23 April 2021*

Citation:
Huang X, He W, Wang W, Fan Q, Ye X, Wu Z and Lin C-Y (2021) Toxicology and Pharmacokinetics Study of Intradiscal Injection of Simvastatin in Rabbits. Front. Pharmacol. 12:582309. doi: 10.3389/fphar.2021.582309

INTRODUCTION

Lower back pain (LBP) is a worldwide epidemic disease (Murray et al., 2013). About 80% of people have experienced LBP at some or a long time in their lives (Andersson, 1999). If the course of disease exceeds three months, it is called chronic low back pain. In the United States, LBP is one of the most frequently used opioids other than tumors (Andersson, 1981; Ringwalt et al., 2014). According to statistics, the annual cost of back pain in the United States is about 200 billion US dollars (Dieleman

et al., 2016) LBP not only greatly reduces people's quality of life, but also takes up a large part of medical resources. The main cause of LBP is the abnormal growth of nerve fibers into intervertebral discs, ligaments, articular processes, and other joints, causing pain below the costal margin and above the wrinkles below the hip. The main cause of LBP is from pain caused by degenerative disc (Adams, 2004), which accounts for more than 40% of LBP. Non-specific LBP caused by disc disease is called discogenic low back pain (DLBP).

The intervertebral disc is composed of an outer annulus fiberous, an inner gel-like center-nucleus pulposus, and cartilage end plates at both ends (Urban and Roberts, 2003), which are spinal cord remnants (McCann et al., 2012). It is the largest avascular tissue in the body. The nutrition of the intervertebral disc is mainly provided by the diffusion of the cartilage endplate. The annulus fiberous is composed of several layers of fibers, and the annulus fiberous is mainly composed of type I and type II collagen. Type I collagen is mainly concentrated in the outer layer of the annulus fiberous to provide greater strength. Type II collagen is mainly distributed in the inner layer of the annulus fiberous, maintaining the position and shape of the nucleus pulposus, and eventually migrating to the nucleus pulposus. The nucleus pulposus is a milky white translucent gelatinous body, rich in moisture and elasticity. It is the core of the intervertebral disc and acts as a shock absorber, absorbing the stress impact from the upper and lower end plates. The intervertebral disc contains an elastic nucleus pulposus, which helps to distribute the pressure uniformly in the intervertebral disc and avoid stress concentration, which may cause damage to the upper and lower end plates and the vertebral body and cause disc degeneration. The rigid end plate can withstand axial compressive forces and serves as the main channel for the nutritional supply of the disc.

With age, irreversible degeneration of the intervertebral disc occurs, the strength of the annulus fibrous decreases, the number of cells in the nucleus pulposus decreases, the elasticity decreases, and the cartilage endplate fragility increases. The clinical features of intervertebral disc degeneration include decreased intervertebral space height and decreased intervertebral disc water content. The factors of intervertebral disc degeneration are complex and multifactorial (Adams and Roughley, 2006). Mechanical stress, trauma, malnutrition, intravertebral disc inflammation, and aging are the main causes of disc degeneration (Adams and Roughley, 2006; Risbud and Shapiro, 2014). The risk factors of intervertebral disc degeneration have been extensively and thoroughly studied. When the disc is degenerated, the first matrix changes occur in the center of the nucleus pulposus, including the fragmentation of proteoglycan, followed by a decrease in proteoglycan and water content and a decrease in cell number (Buckwalter, 1995). Studies have shown that the role of proteoglycans in cartilage end plates is to regulate fluid balance in the disc (Roberts et al., 1996). When the disc is degenerated, the decrease of proteoglycan in the cartilage endplate will cause the decrease of proteoglycan in the nucleus pulposus. In addition, a reduction in lumbar blood flow reduces the ability of endplate cartilage to transport nutrients. Atherosclerosis and arterial calcification can cause lumbar artery blood flow to decrease, increase the possibility of disc degeneration, and eventually cause intervertebral DLBP (Kauppila et al., 1997). Intervertebral disc degeneration is closely related to intervertebral DLBP (Adams, 2004).

Recent studies have shown that bone morphogenetic proteins (BMP-2, -5, -6, -8, -9, and -14) play a crucial role in disc degeneration and cartilage endplate formation (Reddi, 1994; DiLeone et al., 1997; Sekiya et al., 2001; Rickert, 2008; Snelling et al., 2010). Studies have shown that statin cholesterol-lowering drugs that people take every day can stimulate bone formation by up-regulating the BMP-2 pathway (Mundy et al., 1999) simvastatin is an inhibitor of HMG-CoA reductase and a traditional inexpensive lipid-lowering drug. Simvastatin has been widely used as a drug for lowering blood lipids and preventing cardiovascular diseases, and its safety and cost in long-term clinical use have been widely recognized and accepted. Recent studies have shown that simvastatin can regulate bone and cartilage metabolism by up-regulating BMP-2A expression (Zhang and Lin, 2008). The effects and mechanisms of statins on lipid reduction have been widely studied and recognized, but their effects on bone and cartilage and their correlation have not been fully studied. Previous studies have shown that simvastatin can promote the proliferation of nucleus pulposus cells and the secretion of extracellular matrix *in vitro*. *In vivo* experiments of rat tail discs have also confirmed the effectiveness of simvastatin disc injection for disc degeneration, but its dose effect and toxicological effects have not been fully verified. At present, oral simvastatin has been recognized as very safe and reliable. The clinical application of simvastatin for the treatment of bone-related diseases requires a higher clinical dose than lipid-lowering, which will increase the statin-related side effects (Oryan et al., 2015), plus intervertebral discs. It is a relatively closed organ with relatively slow nutrient exchange. Therefore, the safety and pharmacokinetics of simvastatin through local injection of high concentration in the intervertebral disc are still unknown, which is related to the clinical application prospect of simvastatin.

Therefore, this study intends to conduct animal experiments on the pharmacokinetics and toxicological studies of simvastatin injected into the intervertebral disc for 28 days, in order to provide theoretical and experimental foundation for the clinical application of simvastatin.

METHODS AND MATERIALS

Experimental Animals

Fifteen male and 12 female 6-month-old New Zealand rabbits (3–3.5 kg) were purchased from Qingdao Kangda Biotechnology Co., Ltd. Each cage (815 mm × 500 mm × 340 mm) holds one rabbit. These rabbits are housed in a specific room. The air filtration rate is 10–20 air changes per hour; the temperature is 20°–26°C. The humidity is 40–70%, and the fluorescent light is dark for 12 h (08:00–20:00) and then 12 h every day. These rabbits were housed in an environment where they could eat and drink freely, and adapted to the environment for at least

TABLE 1 | Grouping and dosing schedule.

Group number	Group information	Drug concentration (mg/ml)	Injection volume (μL)	Number		Injection method	Autopsy (d)
				Male	Female		
G1	Control group	0	10	3	3	Intradisc injection, once	28
G2	Low dose group	0.1	10	3	3		28
G3	Middle dose group	1	10	3	3		28
G4	High dose group	10	10	3	3		28

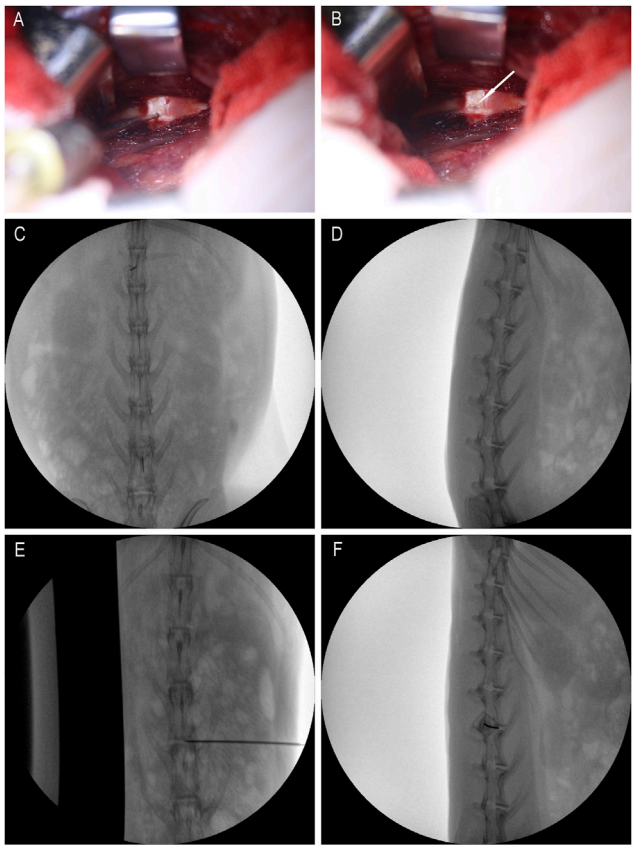

FIGURE 1 | Intraoperative rabbit picture. **(A)** is the picture when the micro-syringe is injected; **(B)** is the picture when the micro-syringe is withdrawn; the white arrows are pinholes; **(C,D)** are positioning films before exposure; **(E,F)** are X-ray films during puncture.

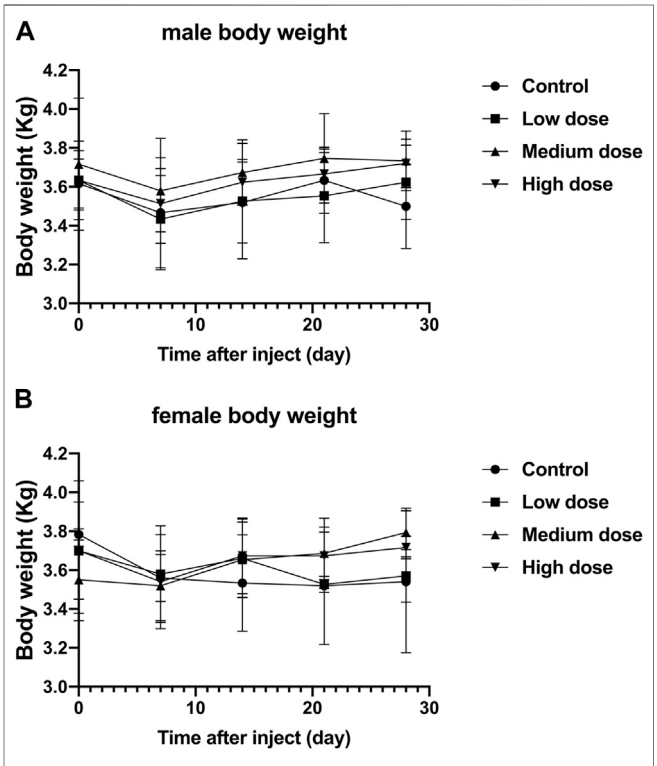

FIGURE 2 | Effect of intra-vertebral disc injection of drugs on animal weight. **(A)** refers to the change in body weight of male rabbits in four groups over time. **(B)** refers to the change of body weight of female rabbits in four groups over time. All data are expressed as mean ± standard deviation (SD) (n = 3).

2 weeks before surgery. All animal operations in this experiment were approved by the Animal Ethics Committee of Naval Military Medical University.

Animal Grouping

Based on body weight, a total of 12 male rabbits and 12 female rabbits were assigned to the treatment group by randomization in the BioBook system (IDBS). According to **Table 1**, 12 male rabbits and 12 female rabbits were used. Animals were evenly divided into four groups: the vehicle control group was injected with hydrogel + simvastatin (0 mg/ml, Control group), and the low-dose group was injected with hydrogel + simvastatin (0.1 mg/ml, Low dose group), The middle-dose group is injected hydrogel + simvastatin (1 mg/ml, Medium dose group), the high-dose group is injected hydrogel + simvastatin (10 mg/ml, High dose group, n = 6).

Surgical Methods and Simvastatin Treatment

The animal used in this experiment is a 6-month-old New Zealand male rabbit. At this time, the animal has matured (skeletal muscle, intervertebral disc, etc.), and it will not cause model failure or affect the experimental results due to development. All injectable drugs are administered intramuscularly (i.m.) during the perioperative period. Atropine (0.2 mg/kg) was administered preoperatively to reduce the production of bronchial secretions during surgery. After about

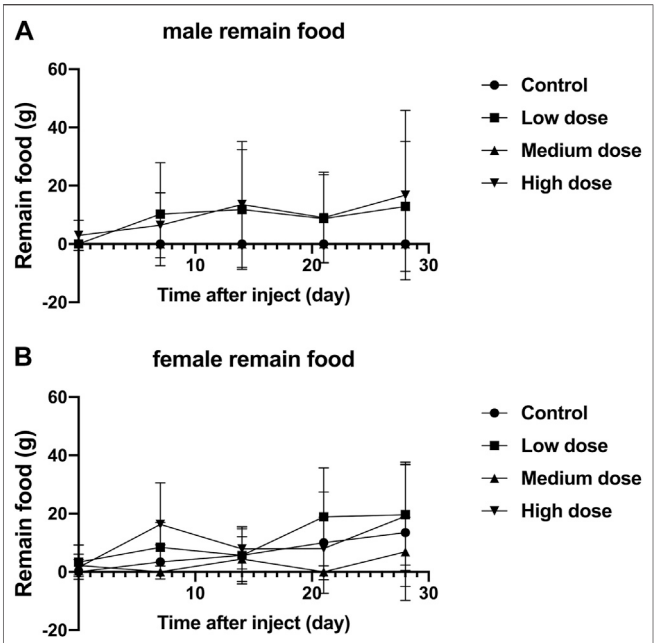

FIGURE 3 | Effect of intra-vertebral disc injection of drugs on animal food residues. **(A)** refers to the change of food residues of male rabbits over time. **(B)** refers to the change of the food residue amount of female rabbits in four groups over time.

5–10 min, all animals were first anesthetized with Shutai (10–15 mg/kg, i.m.). During surgery, 1.5–3.0% isoflurane is used to maintain anesthesia, and the oxygen flow used is 0.8–1.5 L.

After anesthesia, the rabbit was placed in the left lateral position, and the preoperative site was skinned. Sterilize the area to be punctured with iodophor and spread a towel. With the aid of a C-arm machine and a positioning needle, the position of the disc to be punctured is clarified. Make an incision of about 3 cm in length at 3/4 cm from the spinous process at L3/4, L4/5 and L5/6, and expose the L3/4, L4/5 and L5/6 intervertebral disc. Use a mini syringe to connect to a 23G needle to puncture the disc (**Figure 1A**). According to previous research, 23G needles do not cause disc degeneration. The puncture is performed under the guidance of X-rays (**Figures 1E,F**). The direction of the puncture needle is parallel to the upper and lower end plates. The depth of the puncture needle entering the disc is 5 mm with hemostats. The volume injected in each disc is 10 μL, and the injection time is 1 min. After the injection, maintaining the needle in the intervertebral disc for 1 min, slowly withdraw the puncture needle to prevent fluid leakage (Silveira et al., 2014). The administration schedule is shown in **Table 1** Either PEG-PLGA-PEG gel loaded with 2 μL of simvastatin (LKT Laboratories, St. Paul, MN, United States) or gel alone was slowly injected into the discs.

Animal Health Observation

The rabbit's weight and food residue were recorded once a week.

Pharmacokinetics and Toxicology

Blood samples were collected at the time points in **Table 2** for pharmacokinetic and toxicity studies. Prior to rabbit surgery, a catheter was placed through a ear marginal vein. Approximately 300 μL of a blood sample was collected through a venous catheter. Blood samples were collected in tubes coated with lithium heparin and containing 100 μM semicarbazide. The samples were stored on ice and plasma was obtained by centrifugation (approximately 100 μL). All blood samples are centrifuged within 30 min of blood collection and plasma samples are obtained. The method of centrifugation is: centrifugation at a temperature of 4°C for 5 min at a speed of 3,000 g. Plasma samples were collected after centrifugation and transferred to labeled polypropylene tubes for PK analysis. Plasma samples were stored frozen at −80°C until further analysis.

Low-dose and high-dose groups: Blood samples were collected from the low-dose and high-dose groups of three male animals in each group and processed into plasma at seven time points (see **Table 2**).

Medium dose group: Blood samples were collected from three male animals and processed into plasma at 11 time points (see **Table 2**).

Pharmacokinetic Analysis

Plasma samples were analyzed by liquid phase mass spectrometry (**Supplementary Table 1**). Determine pharmacokinetic parameters based on study-directed average concentration-time data in test drugs. The parameters (drug peak concentration, peak time and end elimination rate, etc.) were calculated using a non-isolated module from WinNonlin® Professional 6.3. Any BLQ (10 ng/ml) concentration was excluded from the calculation of the PK parameters **Supplementary Table S1**.

Collection and Detection of Cerebrospinal Fluid

Three male rabbits were also exposed to the L3/4, L4/5, and L5/6 discs via a retroperitoneal approach. These discs were injected with 10 μL of high concentration simvastatin (10 mg/ml). At the same time, a subdural catheter was placed on the back of the rabbit to obtain 100 μL of cerebrospinal fluid before, 3, 5, 8, 24 h, 3, 7, 14 and 28 days after the operation. Cerebrospinal fluid-liquid phase mass spectrometry (**Supplementary Table 2**) was used to analyze cerebrospinal fluid samples.

Clinical Blood and Urine Tests

On day 0 and day 28, blood and urine samples were collected from all rabbits, and blood routine, blood biochemical, and urine routines of all animals were analyzed and evaluated **Supplementary Table S2**.

Tissue and Organ Evaluation and Weighing

28 days after the intravertebral disc was injected with drugs, rabbits were sacrificed by injecting an excessive amount of anesthetics, and autopsies were performed on all animals. Observe the general morphology of the adrenal gland, brain, heart, kidney, liver, ovary, pituitary, prostate, spleen, thyroid, parathyroid gland, thymus, testis and uterus of each animal and weigh them.

Histological Assessment

Twenty-eight days after the disc was injected with the drug, rabbits were sacrificed by injection of an overdose of anesthetic,

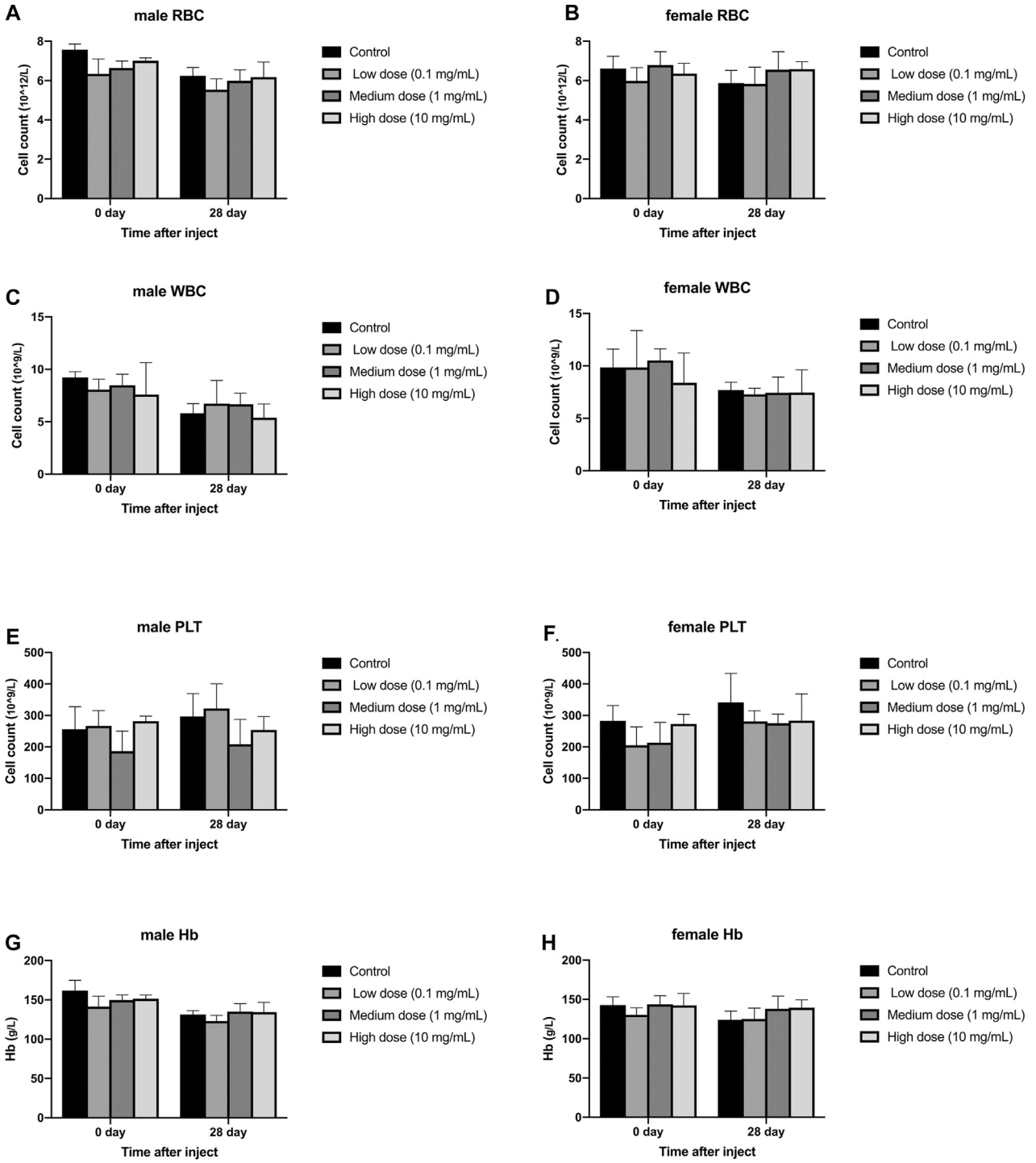

FIGURE 4 | Effect of drug injection into the disc on blood routine of animals. **(A)** refers to the change of red blood cells of male rabbits over time. **(B)** refers to the change of red blood cells of female rabbits over time. **(C)** refers to the change of white blood cells of male rabbits over time. **(D)** refers to the change of the white blood cells of the female rabbits of the four groups over time. **(E)** refers to the change in platelets of male rabbits over time. **(F)** refers to the change in platelets of female rabbits over time. **(G)** refers to the change in hemoglobin of the four groups of male rabbits over time. H refers to the change of hemoglobin of the four groups of female rabbits over time. All data are expressed as mean ± SD (n = 3).

and all disc tissues between L3-L6 were collected. These tissues were fixed in a 10% formaldehyde solution for at least 48 h. They were then decalcified for 5–7 d in 22.5% formic acid and 10% sodium citrate. Decalcification is regularly verified using radiography. They were then paraffin-embedded and sagittal (10 μm thick) using a microtome. Sections were stained with

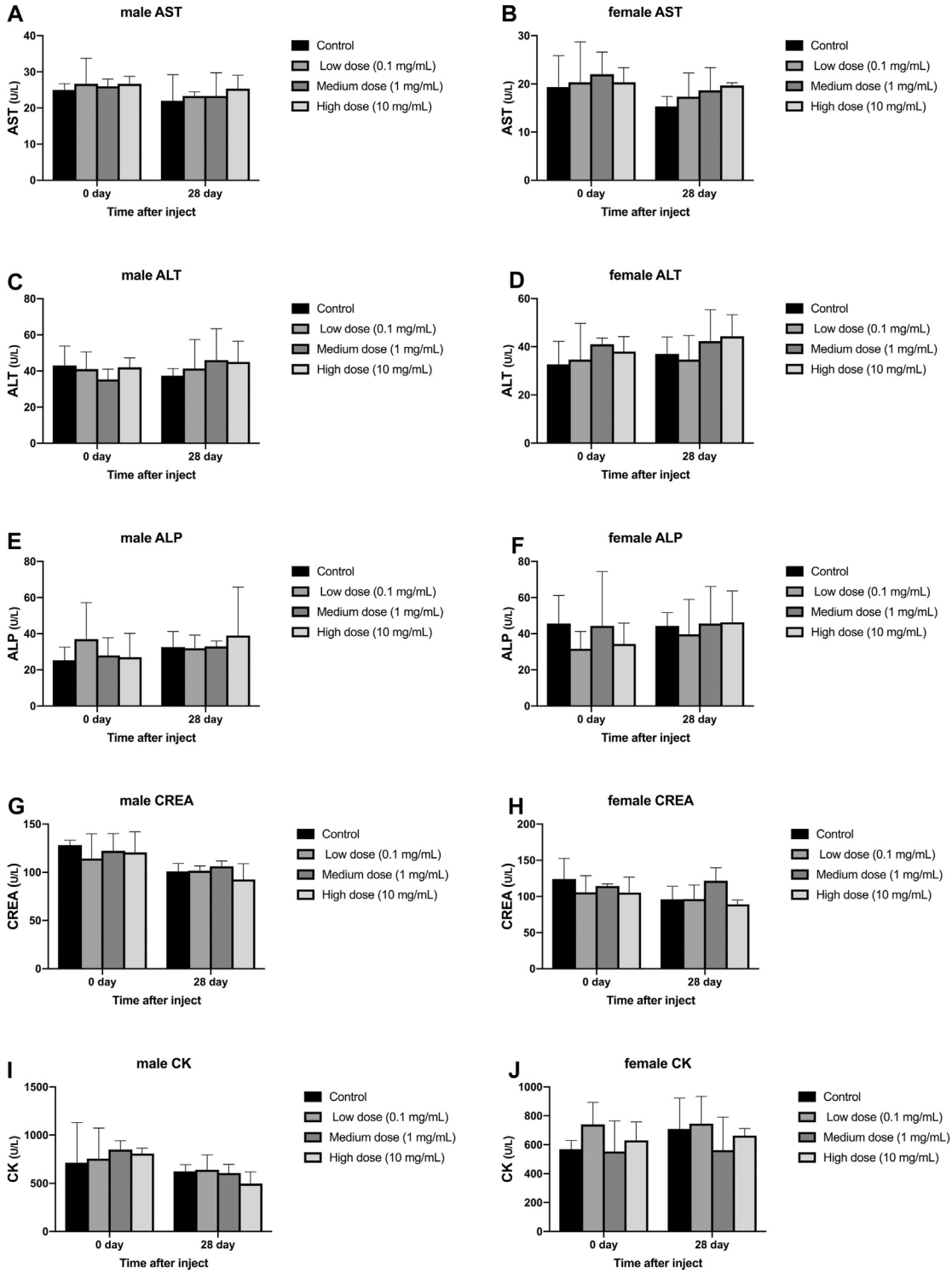

FIGURE 5 | Effect of drug injection into the intervertebral disc on blood biochemistry of animals. **(A)** refers to the change over time of aspartate aminotransferase in four groups of male rabbits. **(B)** refers to the change of aspartate aminotransferase of female rabbits in four groups over time. **(C)** refers to the change of the alanine aminotransferase of the four groups of male rabbits over time. **(D)** refers to the change of alanine aminotransferase of female rabbits in four groups over time. **(E)** refers to the change of serum alkaline phosphatase over time in the four groups of male rabbits. **(F)** refers to the change of serum alkaline phosphatase over time in the four groups of female rabbits. **(G)** refers to the change of urea of the four groups of male rabbits over time. **(H)** refers to the change of urea of the four groups of female rabbits over time. **(I)** refers to the change of creatine kinase over time in the four groups of female rabbits. **(J)** refers to the change of creatine kinase of female rabbits in four groups over time. All data are expressed as mean ± SD (n = 3).

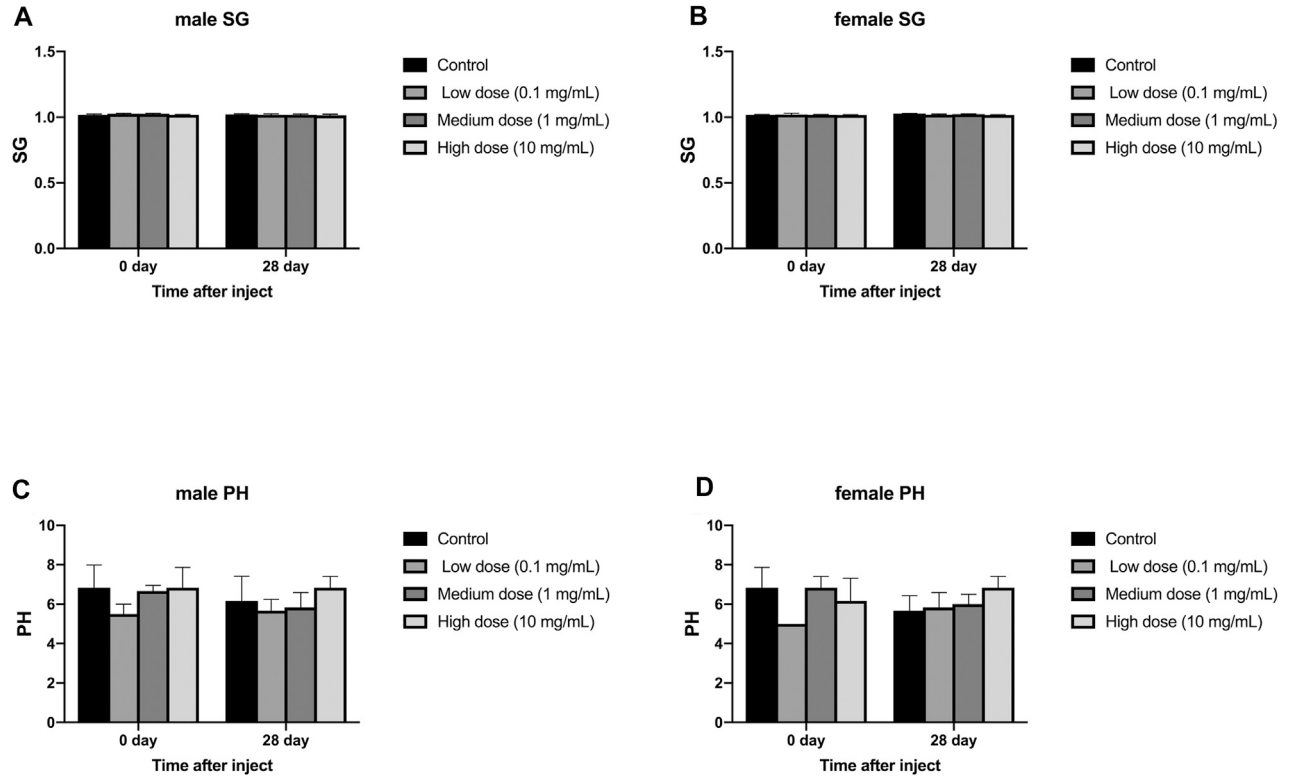

FIGURE 6 | Effect of intra-disc injection of drugs on animal urine routine. **(A)** refers to the change in urine specific gravity of the four groups of male rabbits over time. **(B)** refers to the change in urine specific gravity of the four groups of female rabbits over time. **(C)** refers to the change over time of urine pH of the four groups of male rabbits. **(D)** refers to the change of urine pH value of female rabbits in four groups over time. All data are expressed as mean ± SD (n = 3).

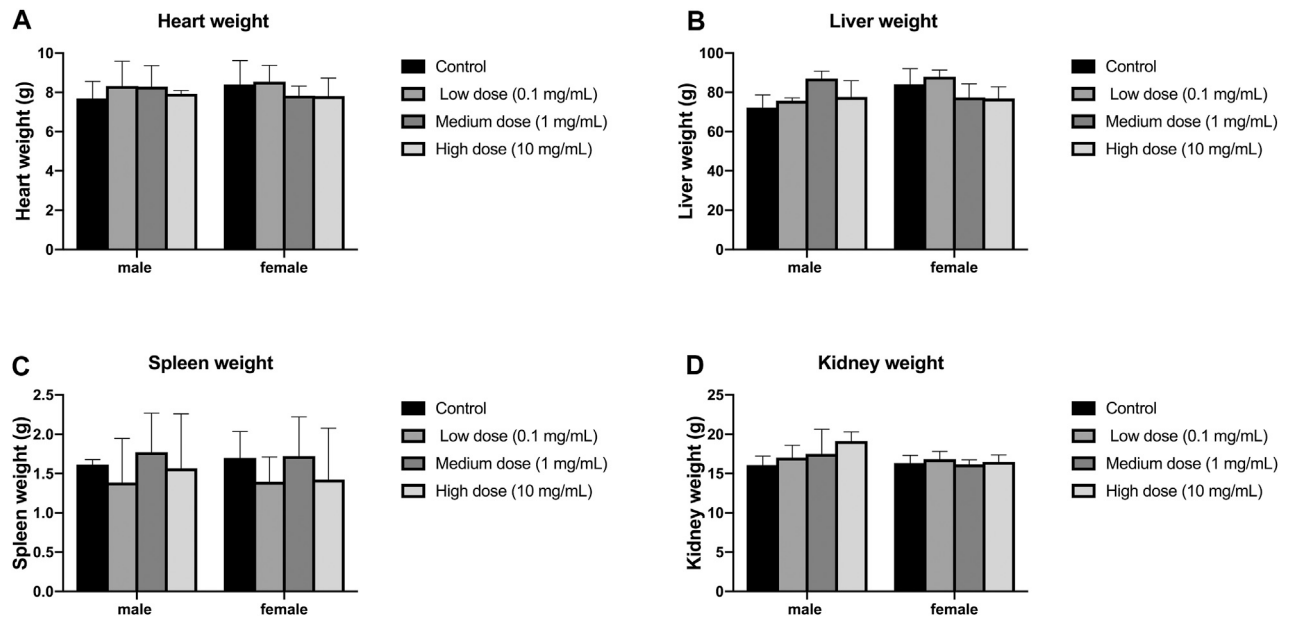

FIGURE 7 | Effect of intra-vertebral disc injection on animal organ weight. **(A)** refers to the heart weight of four groups of rabbits of different genders. **(B)** refers to the liver weight of four groups of rabbits of different sexes. **(C)** refers to the spleen weight of rabbits of four different sexes. **(D)** refers to the kidney weight of four groups of rabbits of different genders. All data are expressed as mean ± SD (n = 3).

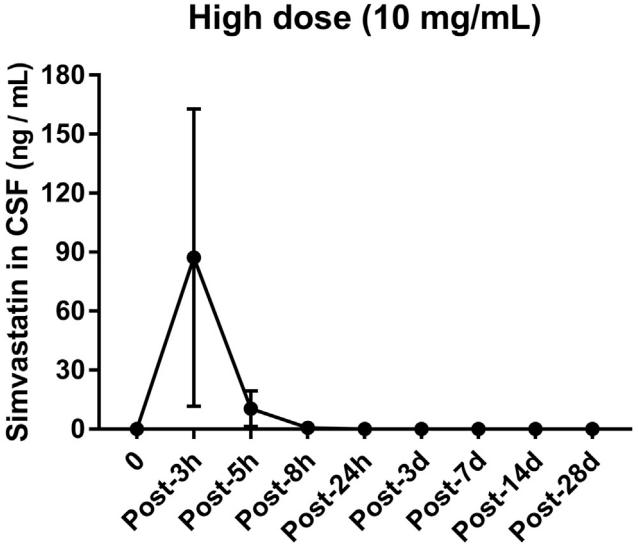

FIGURE 8 | Changes in the concentration of simvastatin in the cerebrospinal fluid of patients after intra-disc injection of drugs over time. All data are expressed as mean ± SD (n = 3).

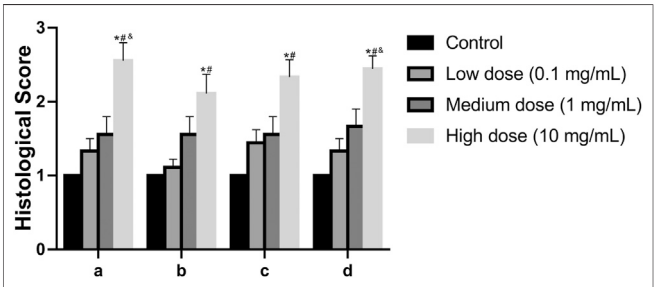

FIGURE 9 | Effect of the drug on the disc after injection into the disc. **(A)**: Annulus fibrosus, **(B)**: Border between the annulus fibrosus and nucleus pulposus, **(C)**: Cellularity of the nucleus pulposus, **(D)**: Matrix of the nucleus pulposus. All data are expressed as mean ± SD, $^{*}p < 0.05$ vs. vehicle control group; $^{\#}p < 0.05$ vs. low-dose group; $^{\&}p < 0.05$ vs. medium-dose group; (n = 3).

hematoxylin and eosin (H&E) and then qualitatively analyzed using an Olympus light microscope at magnifications ranging from 40 to 200 times. Observe the histological HE staining results and score according to the evaluation method in **Table 3**.

Statistical Analysis

Data analysis was performed using PASW Statistics 21.0 (SPSS Inc.) software and graphing was performed using GraphPad Prism 8 software. All experimental data are expressed as mean ± standard deviation. Comparisons between groups were performed using one-way variance for statistical analysis. If there are differences and a normal distribution is satisfied, Bonferroni's multiple comparison test is performed. If the normal distribution is not satisfied, use the Kruskal-Wallis H test. $p < 0.05$ means that the difference is significant.

RESULTS

Effect of Intravertebral Disc Drugs on Animal Weight

Regardless of male or female rabbits, all rabbits lost a little weight during the first 7 days after surgery, and then rose steadily. In male or female rabbits, there was no significant difference in body weight between the four groups of rabbits at each time point ($p > 0.05$, **Figure 2A,B**). The steady increase in body weight in all rabbits indicates that the animals are well tolerated for surgery and treatment.

Effects of Intravertebral Disc Injections on Food Residues in Animals

The food residues of all rabbits fluctuated with time, but there was no significant difference in the food residues between each group of animals ($p > 0.05$, **Figure 3A,B**). This shows that all rabbits can tolerate our surgery well and adapt to the relevant feeding environment.

Effects of Intravertebral Disc Injections on Clinical Blood and Urine Tests in Animals

Blood Test

Different concentrations of simvastatin injected into rabbit intervertebral discs will not affect the blood routine of rabbits of different sexes. On days 0 and 28, blood samples from all animals were collected and tested by a blood analyzer. In male animals, the contents of red blood cells, white blood cells, and hemoglobin in the four groups were all lower than those on day 0, but the differences were not statistically significant ($p > 0.05$, **Figure 4A,C,E**); There was no significant difference between platelets on day 0 and day 28 ($p > 0.05$, **Figure 4G**). In female animals, there was no significant difference in the results of red

TABLE 2 | Blood collection time points.

Grouping	Number of animals	Blood collection time	Total number of specimens
G2 (Low dose group)	3	Preoperative, postoperative 6 h, 24 h, 3 d, 7 d, 14 d, 28 d	75 (42 + 33)
G4 (High dose group)	3		
G3 (Middle dose group)	3	Preoperative, postoperative 0.5 h, 1 h, 3 h, 5 h, 8 h, 24 h, 3 d, 7 d, 14 d, 28 d	

**The low dose group was injected with hydrogel + simvastatin (0.1 mg/ml), the medium dose group was injected with hydrogel + simvastatin (1 mg/ml) and the high dose group was injected with hydrogel + simvastatin (10 mg/ml).*

blood cells, white blood cells, platelets, and hemoglobin on day 0 and day 28 ($p > 0.05$, **Figure 4B,D,F**). At day 0, there were no significant differences in the measurement results of red blood cells, white blood cells, platelets, and hemoglobin between the four groups in males and females ($p > 0.05$, **Figure 4H**). On the 28th day, in the measurement results of red blood cells, white blood cells, platelets, and hemoglobin, there was no significant difference between the four groups of male and female animals ($p > 0.05$, **Figure 4A–H**).

Blood Biochemical Examination

Different concentrations of simvastatin injected into rabbit intervertebral discs will not affect blood biochemistry of rabbits of different genders. On days 0 and 28, blood samples from all animals were collected and tested by an automatic blood biochemical analyzer. In male and female animals, there was no significant difference in serum aspartate aminotransferase, serum alanine aminotransferase, serum alkaline phosphatase, urea, and serum creatine kinase results on day 0 and day 28 ($p > 0.05$, **Figure 5A–J**). At day 0, the measurement results of serum aspartate aminotransferase, serum alanine aminotransferase, serum alkaline phosphatase, urea, and serum creatine kinase were not statistically significant between male and female animals ($p > 0.05$, **Figure 5A–J**). On the 28th day, the measurement results of serum aspartate aminotransferase, serum alanine aminotransferase, serum alkaline phosphatase, urea, and serum creatine kinase were not statistically significant between male and female animals ($p > 0.05$, **Figure 5A–J**).

Routine Urine Test

The injection of different concentrations of simvastatin into the intervertebral disc of rabbits will not affect the urine routine of rabbits of different genders. On days 0 and 28, urine samples from all animals were collected and tested by an automatic urine analyzer. All rabbits showed yellow urine on day 0 and day 28, and no white blood cells, red blood cells, urine sugar, uroketoneuria protein, and urobilinogen were detected in urine. Only one rabbit had urinary bilirubin as a +. There was no significant difference in urine specific gravity and urine pH between day 0 and day 28 in the male and female groups ($p > 0.05$, **Figure 6A–D**). At day 0, in the measurement of urine specific gravity and urine pH, there were no significant differences between the four groups in males and females ($p > 0.05$, **Figure 6A–D**). On the 28th day, in the measurement of urine specific gravity and urine pH, there was no significant difference between the four groups in males and females ($p > 0.05$, **Figure 6A–D**).

Effects of Drug Injection Into the Intervertebral Disc on Animal Pharmacokinetics

Blood was taken from different groups of animals at different time points (see the **Tables 4**, **5**, **6**) to obtain plasma, and the simvastatin content in the plasma was detected by liquid phase mass spectrometry. These results indicate that simvastatin was not detected in the blood in rabbits with different concentrations of simvastatin. ($p < 0.05$ represent statistically significant differences, $n = 3$).

Effects of Intravertebral Disc Injection of Drugs on the Morphology of Animal Tissues

Some animals show congenital abnormalities, such as no visible parathyroid tissue, large dilated cysts without fluid, and fatty tissue in the brain. No significant abnormality was observed in the organs of all animals, indicating that the experimental treatment scheme will not cause damage to various tissues and organs of the animals.

Effect of Drug Injection iInto the Disc on Animal Organ Weight

Different concentrations of simvastatin injected into rabbit intervertebral discs will not affect the organ weight of rabbits of different genders. These organs include: adrenal, brain, heart,

TABLE 3 | Histological rating scale.

Content	Grade	Grade Description
I. Annulus fibrosus	1	Normal pattern of fibrocartilage lamellae (U-shaped in the posterior aspect and slightly convex in the anterior aspect) without ruptured fibers and without a serpentine appearance anywhere within the annulus
	2	Ruptured or serpentine-patterned fibers in less than 30% of the annulus
	3	Ruptured or serpentine-patterned fibers in more than 30% of the annulus
II. Border between the annulus fibrosus and nucleus pulposus	1	Normal
	2	Minimally interrupted
	3	Moderate/severe interruption
III. Cellularity of the nucleus pulposus	1	Normal cellularity with large vacuoles in the gelatinous structure of the matrix
	2	Slight decrease in the number of cells and fewer vacuoles
	3	Moderate/severe decrease (>50%) in the number of cells and no vacuoles
IV. Matrix of the nucleus pulposus	1	Normal gelatinous appearance
	2	Slight condensation of the extracellular matrix
	3	Moderate/severe condensation of the extracellular matrix

**The histological rating scale is based on four types of degenerative changes, with scores ranging from four points for normal discs (1 point per class) to 12 points for severe disc degeneration (3 points per class).*

TABLE 4 | Simvastatin concentrations in plasma of G2 male rabbits after administration (ng/ml).

Time	Animal number			Mean	SD
	0911	0919	0921		
Pre-dose	BLQ	BLQ	BLQ	NA	NA
Post-6 h	BLQ	BLQ	BLQ	NA	NA
Post-24 h	BLQ	BLQ	BLQ	NA	NA
Post-3 D	BLQ	BLQ	BLQ	NA	NA
Post-7 D	BLQ	BLQ	BLQ	NA	NA
Post-14 D	BLQ	BLQ	BLQ	NA	NA
Post-28 D	BLQ	BLQ	BLQ	NA	NA

BLQ: Below the limit of quantitation. The data is expressed as the mean ± SD. (n = 3).

TABLE 5 | Simvastatin concentrations in plasma of G4 male rabbits after administration (ng/ml).

Time	Animal number			Mean	SD
	0907	0908	0918		
Pre-dose	BLQ	BLQ	BLQ	NA	NA
Post-6 h	BLQ	BLQ	BLQ	NA	NA
Post-24 h	BLQ	BLQ	BLQ	NA	NA
Post-3 D	BLQ	BLQ	BLQ	NA	NA
Post-7 D	BLQ	BLQ	BLQ	NA	NA
Post-14 D	BLQ	BLQ	BLQ	NA	NA
Post-28 D	BLQ	BLQ	BLQ	NA	NA

BLQ, below the limit of quantitation. The data is expressed as the mean ± SD. (n = 3).

kidney, liver, ovary, pituitary, prostate, spleen, thyroid, parathyroid, thymus, testis, and uterus.

There was no significant difference in heart weight between the four groups of male and female animals ($p > 0.05$, **Figure 7A**); there was also no significant difference in heart weight between the groups of male and female animals ($p > 0.05$, **Figure 7A**). There was no significant difference in liver weight between the four groups of male and female animals ($p > 0.05$, **Figure 7B**); there was also no significant difference in the weight of each group between male and female animals ($p > 0.05$, **Figure 7B**). There was no significant difference in spleen weight between the four groups of male and female animals ($p > 0.05$, **Figure 7C**); there was also no significant difference in the weight of each group between male and female animals ($p > 0.05$, **Figure 7C**). There was no significant difference in kidney weight between the four groups of male and female animals ($p > 0.05$, **Figure 7D**); there was also no significant difference in kidney weight between the groups of male and female animals ($p > 0.05$, **Figure 7D**).

Cerebrospinal Fluid Test After Intravertebral Disc Injection

The concentration of simvastatin in the cerebrospinal fluid increased sharply after injection, reached a peak (133.8 ng/ml, **Figure 8**) 3 h after the operation, and fell outside the detectable range 24 h after the operation. From 1 to 28 d after surgery, the concentration of simvastatin in the cerebrospinal fluid was below the detectable range (**Figure 8**).

Effects of Drugs Injected Into the Intervertebral Disc on the Intervertebral Disc

In the anulus fibrosus histological score, the score of the high-dose group was higher than that of the vehicle control group, the middle-dose group, and the low-dose group ($p = 0.0009$, $p = 0.0347$, $p = 0.0404$, **Figure 9**). In the histological score of the border between anulus fibrosus and the nucleus pulposus, the scores of the high-dose group were higher than those of the vehicle control group and the low-dose group ($p = 0.0117$, $p = 0.0347$, **Figure 9**). In the histological score of nucleus pulposus cell number and morphology, the scores of the high-dose group were higher than those of the vehicle control group and the low-dose group ($p = 0.0021$, $p = 0.0373$, **Figure 9**). In the histological score of the nucleus pulposus matrix, the scores of the high-dose group were higher than those of the vehicle control group, low-dose group, and middle-dose group ($p = 0.0002$, $p = 0.0116$, $p = 0.0330$, **Figure 9**). These results indicate that the low-dose group and the medium-dose group will not cause adverse effects on the intervertebral disc; at the same time, it also shows that the high-dose group will have a certain damaging effect on the local intervertebral disc.

DISCUSSION

In this study of pharmacokinetics and toxicology of simvastatin, we selected three drug concentrations. Choose high doses to show potential potentially adverse effects of the drug; choose low doses as the "clear" dose, which is the concentration of the drug that is cleared per unit of time; medium doses are the doses used to test the efficacy of the drug. According to the results of animal weight and animal food residues in the study, rabbits injected three doses of simvastatin can well tolerate surgery and simvastatin. The hemodynamic results show that the injected high dose of simvastatin is well metabolized and the blood concentration is below the measurable value. Observation of blood routine, blood biochemistry, urine routine, organ weight and morphology

TABLE 6 | Simvastatin concentrations in plasma of G3 male rabbits after administration (ng/ml).

Time	Animal number			Mean	SD
	0915	0916	0917		
Pre-dose	BLQ	BLQ	BLQ	NA	NA
Post-0.5 h	BLQ	BLQ	BLQ	NA	NA
Post-1 h	BLQ	BLQ	BLQ	NA	NA
Post-3 h	BLQ	BLQ	BLQ	NA	NA
Post-5 h	BLQ	BLQ	BLQ	NA	NA
Post-8 h	BLQ	BLQ	BLQ	NA	NA
Post-24 h	BLQ	BLQ	BLQ	NA	NA
Post-3 D	BLQ	BLQ	BLQ	NA	NA
Post-7 D	BLQ	BLQ	BLQ	NA	NA
Post-14 D	BLQ	BLQ	BLQ	NA	NA
Post-28 D	BLQ	BLQ	BLQ	NA	NA

BLQ, below the limit of quantitation. The data is expressed as the mean ± SD. (n = 3).

in this experiment showed that the three doses of simvastatin injected had no effect on the liver, kidney and hematopoietic system. The histological results of the intervertebral disc showed that the high-dose group would cause certain damage to the local disc tissue. The possible cause of local damage of high-dose simvastatin on intervertebral disc tissue is that local high-level simvastatin may have certain toxic effects on nucleus pulposus cells, fibroblasts and even chondrocytes. Cerebrospinal fluid is used to detect the leakage of drugs in surrounding tissues. The results of this study show that simvastatin appears in cerebrospinal fluid. The possible reason is that when simvastatin was injected, the puncture needle penetrated the entire disc and punctured the dural sac, so after the injection of the drug, the drug will enter the cerebrospinal fluid along the needle channel. Over time, the needle channel is closed, and the simvastatin content in the cerebrospinal fluid will disappear.

Simvastatin, a HMG-CoA reductase inhibitor, has been widely used clinically to regulate lipid metabolism and has great help in preventing/treating cardiovascular disease. It also has other effects: improving endothelial function, stabilizing atherosclerotic plaques, increasing nitric oxide (NO) synthesis, anti-inflammatory and anti-thrombotic effects. At present, oral simvastatin has been recognized to be very safe and reliable, but it is difficult to achieve the required drug concentration locally in the intervertebral disc when oral conventional doses of simvastatin are used. In clinical practical applications, when oral or systemic administration is used, the drug concentration required to stimulate bone and cartilage anabolic metabolism needs to be very high. Currently, the most reported adverse reactions with simvastatin are musculoskeletal reactions such as rhabdomyolysis, inflammatory myopathy, myasthenia gravis, Guillain-Barre syndrome, tendinopathy and amyotrophic lateral sclerosis (ALS) or ALS-like Syndrome has limited its clinical application (Golomb and Evans, 2008). This adverse reaction comes from the pleiotropic effects of statins and mitochondrial mechanisms. Consumption of isoprenoid compounds (the so-called "multiple action" effect of statins) results in a loss of protein isoprene and reduction of coenzyme Q-10, which promotes apoptosis, oxidation and permanent mitochondrial localization defect (Mammen and Amato, 2010). Uncommon adverse events include arthropathy, liver toxicity, insomnia, memory loss, insanity, peripheral neuropathy, erectile dysfunction, diabetes, impaired myocardial contractility, and autoimmune diseases (Godlee, 2014; Ray et al., 2014). Therefore, the method of local administration chosen in this study is to reduce the adverse effects of simvastatin on the system.

In addition, since the half-life of simvastatin is only 3 h, it is difficult to maintain the required drug concentration locally in the disc for a long time. Therefore, this study chose hydrogel triblock poly (ethylene glycol) -poly (lactic-co-glycolic acid) -poly (ethylene glycol) (PEG-PLGA-PEG) polymer as the drug carrier because it has the properties of injectability, temperature sensitivity, degradability, and biocompatibility have been proven to delay the release of drugs, thereby prolonging the action time of drugs (Chang et al., 2007; Tyagi et al., 2004; Zhang and Lin, 2008). Using PEG-PLGA-PEG hydrogel as a simvastatin transport vehicle minimizes the possibility of disc cells being exposed to transiently high concentrations of the drug during injection. This triblock polymer has been widely used as a vehicle for controlled drug or gene delivery (Jeong et al., 2000a; Li et al., 2003; Tyagi et al., 2004). Data from one study also demonstrated that the release profile of simvastatin in an *in vitro* PEG-PLGA-PEG gel was stable and sustainable. Some authors use the hydrogel formed by horseradish peroxidase (HRP) and hydrogen peroxide as a drug carrier (Than et al., 2014). In addition, polymers were selected for their sol-gel phase transition and slow degradation properties (Jeong et al., 2000b). After adding simvastatin to a liquid gel and injecting it into the disc, the compound quickly turns into a gel phase as soon as it reaches body temperature. When the gel was formed, only the IVD cells located in the center of the disc were exposed to simvastatin and it was sustained-released (Jeong et al., 1997). The gel is safer because PEG-PLGA-PEG hydrogels have been well used and validated, and a phase I clinical trial for breast cancer is currently underway (Vukelja et al., 2007).

There are some deficiencies in this experiment. First: The experimental object of this study is a New Zealand rabbit, which is still only a medium-sized animal, which is quite different from humans (different in mechanical structure and cell function), so we will choose animals that are closer to human characteristics in the next experiments or clinical trials in humans. Second: The duration of observation in this study is 28 days. It is possible that the residual toxicity or teratogenicity of some drugs has not yet appeared. Therefore, our future research will increase the observation time after injection of drugs. Third: This experiment is to observe the toxicity of simvastatin by injecting a hydrogel containing simvastatin into a normal disc. The ultimate goal of the experiment was to treat degenerative discs. The integrity, occlusion, osmotic pressure, and number of intervertebral disc cells of normal and degenerative discs are different, so they cannot truly simulate the actual clinical situation. Therefore, we will establish a disc degeneration model and then inject simvastatin to further study its toxicological effects.

CONCLUSION

This experiment planned with the purpose to examine the 28-day safety of intra-disc injected once of simvastatin and the results showed no toxic signs from the delivered three dosages to three separate groups of males and females. The evaluations by body weight, food consumption, blood chemistry, complete blood count, gross observation at necropsy and microscopy histology revealed no abnormality related to the simvastatin.

DATA AVAILABILITY STATEMENT

All data generated or analysed during this study are included in this published article.

ETHICS STATEMENT

The animal study was reviewed and approved by the Animal Ethics Committee of University of Cincinnati.

AUTHOR CONTRIBUTIONS

XH: Substantial contributions to the research design, data acquisition, statistical analysis, drafting the paper and revising it critically; WH: Data acquisition, approval of the submitted and final version; WW: Data acquisition, approval of the submitted and final version; QF: Data acquisition, approval of the submitted and final version; XY: Data acquisition, approval of the submitted and final version; ZW: Surgery supervisor, substantial contributions to the research design, data acquisition, approval of the submitted and final version; C-YL: Data acquisition, approval of the submitted and final version.

FUNDING

This project was supported by National Natural Science Foundation of China (Grant Nos. 81672178).

SUPPLEMENTARY MATERIAL

The Supplementary Material for this article can be found online at: https://www.frontiersin.org/articles/10.3389/fphar.2021.582309/full#supplementary-material

REFERENCES

Adams, M. A. (2004). Biomechanics of back pain. *Acupunct Med.* 22, 178–188. doi:10.1136/aim.22.4.178

Adams, M. A., and Roughley, P. J. (2006). What is intervertebral disc degeneration, and what causes it? *Spine* 31, 2151–2161. doi:10.1097/01.brs.0000231761.73859.2c

Andersson, G. B. (1999). Epidemiological features of chronic low-back pain. *The Lancet* 354, 581–585. doi:10.1016/s0140-6736(99)01312-4

Andersson, G. B. J. (1981). Epidemiologic aspects on low-back pain in industry. *Spine* 6, 53–60. doi:10.1097/00007632-198101000-00013

Buckwalter, J. A. (1995). Aging and degeneration of the human intervertebral disc. *Spine* 20, 1307–1314. doi:10.1097/00007632-199506000-00022

Chang, C.-W., Choi, D., Kim, W. J., Yockman, J. W., Christensen, L. V., Kim, Y.-H., et al. (2007). Non-ionic amphiphilic biodegradable PEG-PLGA-PEG copolymer enhances gene delivery efficiency in rat skeletal muscle. *J. Controlled Release.* 118, 245–253. doi:10.1016/j.jconrel.2006.11.025

Dieleman, J. L., Baral, R., Birger, M., Bui, A. L., Bulchis, A., Chapin, A., et al. (2016). US Spending on personal health care and public health. *Jama* 316, 2627–2646. doi:10.1001/jama.2016.16885

DiLeone, R. J., King, J. A., Storm, E. E., Copeland, N. G., Jenkins, N. A., and Kingsley, D. M. (1997). The Bmp8 gene is expressed in developing skeletal tissue and maps near the Achondroplasia locus on mouse chromosome 4. *Genomics.* 40, 196–198. doi:10.1006/geno.1996.4533

Godlee, F. (2014). Adverse effects of statins. *BMJ* 348, g3306. doi:10.1136/bmj.g3306

Golomb, B. A., and Evans, M. A. (2008). Statin adverse effects. *Am. J. Cardiovasc. Drugs* 8, 373–418. doi:10.2165/0129784-200808060-00004

Jeong, B., Bae, Y. H., and Kim, S. W. (2000a). Drug release from biodegradable injectable thermosensitive hydrogel of PEG-PLGA-PEG triblock copolymers. *J. Controlled Release* 63, 155–163. doi:10.1016/s0168-3659(99)00194-7

Jeong, B., Bae, Y. H., and Kim, S. W. (2000b). *In situ* gelation of PEG-PLGA-PEG triblock copolymer aqueous solutions and degradation thereof. *J. Biomed. Mater. Res.* 50, 171–177. doi:10.1002/(sici)1097-4636(200005)50:2<171:aid-jbm11>3.0.co;2-f

Jeong, B., Bae, Y. H., Lee, D. S., and Kim, S. W. (1997). Biodegradable block copolymers as injectable drug-delivery systems. *Nature.* 388, 860–862. doi:10.1038/42218

Kauppila, L. I., McAlindon, T., Evans, S., Wilson, P. W. F., Kiel, D., and Felson, D. T. (1997). Disc degeneration/back pain and calcification of the abdominal aorta. *Spine.* 22, 1642–1647. doi:10.1097/00007632-199707150-00023

Li, Z., Ning, W., Wang, J., Choi, A., Lee, P. Y., Tyagi, P., et al. (2003). Controlled gene delivery system based on thermosensitive biodegradable hydrogel. *Pharm. Res.* 20, 884–888. doi:10.1023/a:1023887203111

Mammen, A. L., and Amato, A. A. (2010). Statin myopathy: a review of recent progress. *Curr. Opin. Rheumatol.* 22, 644–650. doi:10.1097/BOR.0b013e32833f0fc7

McCann, M. R., Tamplin, O. J., Rossant, J., and Seguin, C. A. (2012). Tracing notochord-derived cells using a Noto-cre mouse: implications for intervertebral disc development. *Dis. Models Mech.* 5, 73–82. doi:10.1242/dmm.008128

Mundy, G., Garrett, R., Harris, S., Chan, J., Chen, D., Rossini, G., et al. (1999). Stimulation of bone formation *in vitro* and in rodents by statins. *Science* 286, 1946–1949. doi:10.1126/science.286.5446.1946

Murray, C. J. L., Abraham, J., Ali, M. K., Alvarado, M., Atkinson, C., Baddour, L. M., et al. (2013). The state of US health, 1990-2010. *Jama* 310, 591–608. doi:10.1001/jama.2013.13805

Oryan, A., Kamali, A., and Moshiri, A. (2015). Potential mechanisms and applications of statins on osteogenesis: current modalities, conflicts and future directions. *J. Controlled Release* 215, 12–24. doi:10.1016/j.jconrel.2015.07.022

Ray, S., Jindal, A. K., Sengupta, S., and Sinha, S. (2014). Statins: can we advocate them for primary prevention of heart disease? *Med. J. Armed Forces India.* 70, 270–273. doi:10.1016/j.mjafi.2013.05.008

Reddi, A. H. (1994). Bone and cartilage differentiation. *Curr. Opin. Genet. Dev.* 4, 737–744. doi:10.1016/0959-437x(94)90141-o

Rickert, M. (2008). BMP-14 gene therapy increases tendon tensile strength in a rat model of achilles tendon injury. *J. Bone Jt. Surg AmAmerican* 90, 445–446. doi:10.1016/s0276-1092(08)79297-6

Ringwalt, C., Gugelmann, H., Garrettson, M., Dasgupta, N., Chung, A. E., Proescholdbell, S. K., et al. (2014). Differential prescribing of opioid analgesics according to physician specialty for Medicaid patients with chronic noncancer pain diagnoses. *Pain Res. Manag.* 19, 179–185. doi:10.1155/2014/857952

Risbud, M. V., and Shapiro, I. M. (2014). Role of cytokines in intervertebral disc degeneration: pain and disc content. *Nat. Rev. Rheumatol.* 10, 44–56. doi:10.1038/nrrheum.2013.160

Roberts, S., Urban, J. P. G., Evans, H., and Eisenstein, S. M. (1996). Transport properties of the human cartilage endplate in relation to its composition and calcification. *Spine.* 21, 415–420. doi:10.1097/00007632-199602150-00003

Salmon, S. J. B., Hulley, P. A., and Loughlin, J. (2010). BMP5 activates multiple signaling pathways and promotes chondrogenic differentiation in the ATDC5 growth plate model. *Growth Factors* 28, 268–279. doi:10.3109/08977191003752296

Sekiya, I., Colter, D. C., and Prockop, D. J. (2001). BMP-6 enhances chondrogenesis in a subpopulation of human marrow stromal cells. *Biochem. biophysical Res. Commun.* 284, 411–418. doi:10.1006/bbrc.2001.4898

Silveira, J. W., Issy, A. C., Castania, V. A., Salmon, C. E. G., Nogueira-Barbosa, M. H., Guimarães, F. S., et al. (2014). Protective effects of cannabidiol on lesion-induced intervertebral disc degeneration. *PLoS One.* 9, e113161. doi:10.1371/journal.pone.0113161

Than, K. D., Rahman, S. U., Wang, L., Khan, A., Kyere, K. A., Than, T. T., et al. (2014). Intradiscal injection of simvastatin results in radiologic, histologic, and

genetic evidence of disc regeneration in a rat model of degenerative disc disease. *Spine J.* 14, 1017–1028. doi:10.1016/j.spinee.2013.11.034

Tyagi, P., Li, Z., Chancellor, M., De Groat, W. C., Yoshimura, N., and Huang, L. (2004). Sustained intravesical drug delivery using thermosensitive hydrogel. *Pharm. Res.* 21, 832–837. doi:10.1023/b:pham.0000026436.62869.9c

Urban, J. P., and Roberts, S. (2003). Degeneration of the intervertebral disc. *Arthritis Res. Ther.* 5, 120–130. doi:10.1186/ar629

Vukelja, S. J., Anthony, S. P., Arseneau, J. C., Berman, B. S., Casey Cunningham, C., Nemunaitis, J. J., et al. (2007). Phase 1 study of escalating-dose OncoGel (ReGel/paclitaxel) depot injection, a controlled-release formulation of paclitaxel, for local management of superficial solid tumor lesions. *Anti-Cancer Drugs* 18, 283–289. doi:10.1097/CAD.0b013e328011a51d

Zhang, H., and Lin, C.-Y. (2008). Simvastatin stimulates chondrogenic phenotype of intervertebral disc cells partially through BMP-2 pathway. *Spine* 33, E525–E531. doi:10.1097/BRS.0b013e31817c561b

Conflict of Interest: The authors declare that the research was conducted in the absence of any commercial or financial relationships that could be construed as a potential conflict of interest.

Advantages of publishing in Frontiers

OPEN ACCESS
Articles are free to read for greatest visibility and readership

FAST PUBLICATION
Around 90 days from submission to decision

HIGH QUALITY PEER-REVIEW
Rigorous, collaborative, and constructive peer-review

TRANSPARENT PEER-REVIEW
Editors and reviewers acknowledged by name on published articles

Frontiers
Avenue du Tribunal-Fédéral 34
1005 Lausanne | Switzerland

Visit us: www.frontiersin.org
Contact us: frontiersin.org/about/contact

REPRODUCIBILITY OF RESEARCH
Support open data and methods to enhance research reproducibility

DIGITAL PUBLISHING
Articles designed for optimal readership across devices

FOLLOW US
@frontiersin

IMPACT METRICS
Advanced article metrics track visibility across digital media

EXTENSIVE PROMOTION
Marketing and promotion of impactful research

LOOP RESEARCH NETWORK
Our network increases your article's readership